# Instituto Politécnico Nacional

Centro de Investigación en Ciencia Aplicada y Tecnología Avanzada

Sección de Estudios de Posgrado

## Feasibility of Hydrogen Integration with Renewable Energy in Mexico: A Geospatial and Computational Analysis.

A THESIS SUBMITTED IN PARTIAL FULFILLMENT OF

THE REQUIREMENTS FOR THE DEGREE OF

Ph.D. in Energy

BY

## M.Sc. Valeria Juárez Casildo

Supervisors:
Prof. Ilse Cervantes Camacho
Prof. Rosa de Guadalupe González Huerta

Querétaro, 2024

# Resumen

Esta tesis evalúa la viabilidad técnico económica de integrar la producción de hidrógeno con fuentes de energía renovable utilizando Modelado Energético y Sistemas de Información Geográfica (SIG). El objetivo de este trabajo es proporcionar evidencia que respalde la inclusión del hidrógeno como vector energético en México y sentar las bases para el desarrollo del Mapa de ruta de hidrógeno. Se estimó que, aunque el potencial solar es el más abundante en México, este, junto con el potencial eólico terrestre y marino, puede satisfacer adecuadamente la demanda de hidrógeno en sectores que son difíciles de descarbonizar.

Los resultados indican que México puede reutilizar su infraestructura existente de petróleo y gas para implementar la producción de hidrógeno en alta mar. Además, se identificó que, aunque actualmente hay nueve proyectos de producción de hidrógeno en México, aún falta la implementación de políticas públicas decisivas que favorezcan la importación y adquisición de tecnología, lo que afecta los valores del Costo Nivelado del Hidrógeno (LCOH), que se encontraron tres veces más altos en comparación con el mercado internacional.

Este estudio presenta una propuesta para la estructura del mapa de ruta del hidrógeno en México, considerando cuatro aspectos esenciales: eficiencia energética, reducción de emisiones, desarrollo de infraestructura y adaptación y educación de la sociedad. Los conocimientos proporcionados en este trabajo no solo refuerzan la viabilidad del hidrógeno como vector de energía limpia, sino que también ofrecen orientación práctica para que los formuladores de políticas y las partes interesadas alineen los esfuerzos nacionales con las tendencias globales. Al abordar las lagunas políticas actuales y optimizar los marcos económicos, México podría posicionarse como un líder en el mercado global del hidrógeno, contribuyendo así a un futuro energético más sostenible y resiliente.

# Abstract

This thesis evaluates the technical and economic feasibility of integrating hydrogen production with renewable energy sources using Energy modelling and Geographic Information Systems (GIS). The aim of this work to provide evidence supporting the inclusion of hydrogen as an energy vector in Mexico and to lay the foundation for the development of a hydrogen roadmap. It was estimated that, while solar potential is the most abundant in Mexico, it, together with onshore and offshore wind potential, can adequately meet hydrogen demands in hard-to-decarbonize sectors.

The results indicate that Mexico can repurpose its existing oil and gas infrastructure to implement offshore hydrogen production. Moreover, it was identified that although there are currently nine hydrogen production projects in Mexico, there is still a lack of decisive public policies that favor the importation and acquisition of technology affecting the Levelized Cost of Hydrogen (LCOH) values which were found there times higher in comparison the international market.

This study presents a proposed structure for the hydrogen roadmap in Mexico, considering four essential aspects: energy efficiency, emission reduction, infrastructure development, and societal adaptation and education. The insights provided herein not only reinforce the viability of hydrogen as a clean energy vector but also offer actionable guidance for policymakers and stakeholders to align national efforts with global trends. By addressing current policy gaps and optimizing economic frameworks, Mexico can position itself as a leader in the global hydrogen market, thus contributing to a more sustainable and resilient energy future.

# Peer Reviewed Contributions

1. Journal Papers

   (a) Valeria Juárez-Casildo, Ilse Cervantes, R. de G. González-Huerta, Harnessing offshore wind for decarbonization: A geospatial study of hydrogen production and heavy industry utilization in Mexico, International Journal of Hydrogen Energy, Volume 83, 2024, Pages 701-716, ISSN 0360-3199, https://doi.org/10.1016/j.ijhydene.2024.08.142.

   (b) Valeria Juárez-Casildo, Ilse Cervantes, R. de G. González-Huerta. Strategic Pathways for Offshore Wind in Mexico: Geospatial Insights and Economic Viability Towards Energy Sustainability. **Submitted and under review**.

   (c) Valeria Juárez-Casildo, Ilse Cervantes, Carlos A. Cervantes-Ortiz, R. de G. González-Huerta, Key aspects in quantifying massive solar hydrogen production: Energy intermittence, water availability and electrolyzer technology, Journal of Cleaner Production, Volume 371, 2022, 133550, ISSN 0959-6526, https://doi.org/10.1016/j.jclepro.2022.133550.

   (d) Valeria Juárez-Casildo, Ilse Cervantes, R. de G. González-Huerta, Solar hydrogen production in urban areas of Mexico: towards hydrogen cities, International Journal of Hydrogen Energy, Volume 47, Issue 70, 2022, Pages 30012-30026, ISSN 0360-3199, https://doi.org/10.1016/j.ijhydene.2022.06.137.

   (e) Valeria Juárez-Casildo, Ilse Cervantes, Marco Antonio Hernández-Nochebuena, R. de G. González Huerta. "Current Status, Challenges and Opportunities for Transport Electrification Deployment in Mexico: The importance of Low-emissions

sources of electricity". Renewable and Sustainable Energy Reviews, 2024. **Submitted and Under review**

2. Science Outreach Articles

   (a) Valeria Juárez-Casildo and Ilse Cervantes. "Mapas de Ruta internacionales y la importance de su creación en México". Revista del Fideicomiso para el ahorro de la energía eléctrica, 33, 2022.

   (b) Valeria Juárez-Casildo, R. de G. González Huerta and Ilse Cervantes. "Desmitificando los Colores del Hidrógeno: Un Enfoque en la Intensidad de Emisiones para la Sostenibilidad". Revista del Fideicomiso para el ahorro de la energía eléctrica, 33, 2024.

3. Conference Proceedings

   (a) Valeria Juárez-Casildo, Ilse Cervantes and R. de G. González Huerta. "Assessment of massive solar hydrogen production in urban areas of México" XXI International Congress of the Mexican Hydrogen Society, 2021.

   (b) R. de G. González Huerta, Valeria Juárez-Casildo, Ernesto ntonio Hernández Medel, and Juan Manuel Sandoval Pineda. International Congress of the Mexican Hydrogen Society, 2021.

   (c) "The importance of accurate hydrogen research to build a hydrogen road map in Mexico" XXII International Congress of the Mexican Hydrogen Society, Tabasco, México, 2022.

   (d) "Comparison of the techno-economic competitiveness of hydrogen in different energy storage sectors". XXII International Congress of the Mexican Hydrogen Society, Tabasco, México, 2022.

   (e) Valeria Juárez-Casildo and Ilse Cervantes."Evaluation of hydrogen production from wind energy in Mexico". World Congress of Chemical Engineering, Buenos Aires Argentina, 2023

(f) Valeria Juárez-Casildo, Marco Hernández-Nochebuena, Ilse Cervantes, R. de G. González-Huerta. "GIS-Multicriteria Decision Analysis Approach for Optimal Wind-Solar Hydrogen Production Sites Selection in Mexico". World Hydrogen Energy Conference, Cancún, México, 2024.

(g) Valeria Juárez-Casildo, Anindita Golder, Chandan Chetri, Ruvini De Seram, Marco Hernández-Nochebuena, Ilse Cervantes, and Sheldon Wiliamson. "Design and Control of a Maximum Power Point Tracking System for a Fuel-Cell-Battery Hybrid Electric Vehicle". Transportation Electrification Conference & Expo, Illinois, USA, 2024.

(h) Valeria Juárez-Casildo, Anindita Golder, Ilse Cervantes, R. de G. González Huerta and Sheldon Williamson. "Techno-Economic Considerations for Optimal Sizing of Isolated Hydrogen-Battery-Solar Powered Microgrids". Annual Conference of the IEEE Industrial Electronics Society, Chicago, USA, 2024.

# Acknowledgment

- **Institutions**

  - I would like to extend my gratitude to the Instituto Politécnico Nacional for providing the facilities and space for my development in the Doctoral Program in Energy.

  - I am also grateful to CONAHCYT for the doctoral scholarship granted during the four years of study.

  - My thanks to the Secretariat of Research and Graduate Studies (SIP-IPN) for the financial support for attending scientific and academic events both nationally and internationally.

  - I appreciate the Dirección de Relaciones Internacionales (DRI-IPN) for the 2023 mobility scholarship that allowed me to undertake a research stay at the University of Ontario Institute of Technology in Canada.

  - Additionally, I am grateful to SIP-IPN for the financial support provided within the framework of the Innovation Projects for Students (2021-2022) call. This support was crucial for acquiring the equipment required for the completion of this thesis.

  - My thanks to COFAA-IPN and Fundación Politécnico for the scholarship awarded under the Activities with Queen Mary University of London during 2024, which enabled me to attend the Intensive English Course.

# Introduction

This study was conducted to evaluate the technical and economic feasibility of producing and using Hydrogen ($H_2$) in Mexico. In 2020, the Ministry of Energy began to show interest in integrating $H_2$ to generate 1.3 % of the electrical energy in Combined Cycle power plants, as cited in PRODESEN. This would imply conducting studies to evaluate hydrogen production from large-scale renewable sources. However, to date, such studies are basic and very scarce. Therefore, it is urgent to answer three key questions for Mexico: Where can hydrogen be produced? How much can be produced? And how much does it cost to produce it? The availability of this information will set the guidelines for the development of public energy policies.

The development of this research was divided into three stages. The first focuses on processing solar and wind resource data to estimate the available energy and thereby the mass of hydrogen that can be produced through water electrolysis at each point in the country. Subsequently, using Geographic Information Systems (GIS), data on hydrogen demand, and current energy infrastructure, the optimal areas of the country for producing $H_2$ will be determined. Finally, all the generated information will be integrated into databases and can be consulted in software designed for the visualization of information on interactive maps, as well as the integration of a roadmap proposal for hydrogen development in Mexico.

This document is organized into eight chapters. The first chapter provides the preliminary aspects of the research such as the problem statement, specific objectives, hypotheses, and the justification that motivated this research, among others. The second chapter focuses on describing the theoretical framework needed for the development of the technical

and background aspects of this project, addressing specific aspects of renewable energies, economic parameters for evaluating energy projects, and the theoretical aspect of geographic information systems.

Chapter three deals with everything related to the determination of the potential for solar hydrogen production on a macro scale (the entire country is evaluated). It also includes an analysis of precipitation water, aiming to demonstrate how much rainwater would be required to transform all the solar potential into hydrogen.

The explanation of solar hydrogen production in the scenario of Mexican cities is presented in Chapter four. This section presents results on the potential for hydrogen production in all urban settlements and its application in transportation.

The main results about onshore and offshore wind energy potential are reported in Chapters 5 and 6, showcasing all the mathematical and statistical techniques used for wind characterization and the corresponding energy harvesting for hydrogen production.

Chapter seven details the production and integration of hydrogen on a micro-scale, addressing issues of solar and wind energy management at the residential level considering the effect of climate conditions on hydrogen production.

Finally, chapter eight is a special section that presents the foundations for a possible hydrogen road map for Mexico, compiling and assembling all the previously obtained results.

# Contents

# List of Tables

# List of Figures

# Chapter 1

# Research Context

## 1.1 Problem Statement

Achieving the 1.5 °C targets outlined in the Paris Agreement for 2050 to revert climate change is a major challenge since it necessitates significant advancements, particularly in the energy transition. Under the 1.5 °C scenario, 70 % of $CO_2$ emission reductions are expected through electrification, energy efficiency, and renewable sources [12]. However, hydrogen will unquestionably be needed to achieve full decarbonization covering approximately 11 % of the emission abatement with a required global production of 523 MTon/year and 373 MTon/year have to be produced by G20 countries [5].

Mexico, as a member of the G20 and signatory to the Paris Agreement, stands at a critical juncture where its current actions fall lamentably short of aligning with the established commitments limiting its Nationally Determined Contribution (NDC). Prevailing public policies prioritize petroleum refineries and fossil fuel subsidies, undermining progress towards emission reduction goals. Projections indicate that Mexico's emissions are on track to reach 750 MTon $CO_{2_{eq}}$ by 2030, far exceeding 1.5 °C the target of 399 MTon $CO_{2_{eq}}$ (Figure 1.1) [13].

Transparency Climate Report rankings designate Mexico as "highly insufficient" in taking actions toward 2050 targets, underscoring the glaring absence of robust public policies conducive to the development of decarbonization strategies, particularly in the realm of hy-
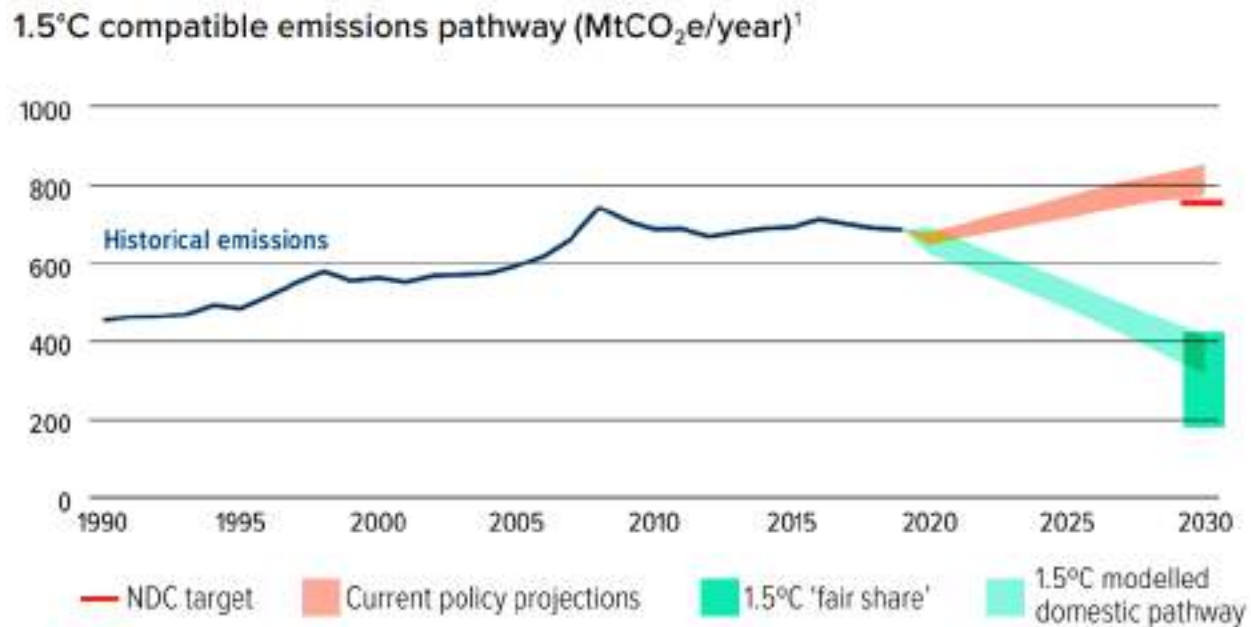
Figure 1.1: Mexico's emissions projections based on current public policies [5].

drogen, which holds paramount importance in the climate agenda [13]. Therefore there is an urgency to address Mexico's deficient action on hydrogen deployment within the framework of the Paris Agreement.

Although Mexico considers hydrogen as a clean energy source in at least 22 laws and has established certain guidelines for promoting hydrogen use [14], these remain mere statements that do not set a specific goal or provide a concrete action. This reflects the lack of accurate and objective information for developing strong policies, the creation of a Road Map, and a National Strategy.

Institutions such as the Hydrogen Mexican Association, Gesellschaft fur Internationale Zusammenarbeit (GIZ), and HINICIO, have made a great effort to generate this information, however, its results tend to be unrealistic and may be viewed with a sense of sensationalist political narratives, especially in terms of cost projections. The real state of Mexico and issues regarding technology importation, which may generate erroneous expectations about the direction of hydrogen in Mexico, are not considered. Moreover, these efforts are isolated; the government must have sufficient tools to unify them and construct a Hydrogen Road Map.

This underlines the imperative necessity for comprehensive, realistic, and objective information that contextualizes the current state and envisions the future of hydrogen in the country. It is crucial for careful integration into the energy matrix, aligned with decarbonization goals. Therefore, this thesis generates, processes, and compiles the requisite information to formulate a Hydrogen Roadmap proposal for Mexico. This proposal will provide accurate and objective analyzed data, enabling the government, academia, industry, and society to make informed decisions on this critical matter.

## 1.2 Hypotesis

This thesis aims to verify the following hypotheses:

1. It is feasible to establish a methodology enabling the assessment of the technical and economic viability of integrating hydrogen with renewable energies. This can be achieved by incorporating optimization tools, GIS techniques, energy management models, and information regarding energy resources, energy consumption, and geographical constraints.

2. The utilization of hydrogen as a storage system has the potential to address the electrification challenges Mexico faces into the integration of renewable energy in the energy networks.

## 1.3 Objectives

### 1.3.1 General Objective

To estimate the technical and economic feasibility of using hydrogen integrated with renewable energies using GIS and other computing tools, in order to provide evidence supporting the inclusion of hydrogen as an energy vector in Mexico and to lay the foundations for developing a hydrogen roadmap.

### 1.3.2 Specific objectives

1. To calculate the quantity of electrical energy generated from solar power, utilizing data obtained from meteorological stations

2. To ascertain the technical and economic viability of harnessing renewable resources, the cost of electricity production will be diagnosed to establish it as a benchmark parameter for reference and comparison.

3. To evaluate the impact of integrating hydrogen energy storage on the technical and economic viability of harnessing renewable resources, the costs associated with hydrogen technology will be included to analyze the economic implications of utilizing it as a storage system.

4. To determine which renewable energy sources are the most promising for utilization in Mexico, as well as evaluate production scenarios in relation to the time of year and national technology production

5. To size a micro-level hydrogen storage system in order to establish the limitations of renewable energy utilization in relation to consumption profiles.

6. To outline a preliminary, non-exhaustive roadmap for hydrogen based on the results obtained in this thesis.

## 1.4 Motivation

Hydrogen is a key complement to achieving complete decarbonization within the energy sector. It can address the challenges posed by industrial processes that are hard to electrify, such as heavy industries including refineries, ammonia production, and raw material processing. Its versatility as an energy carrier extends the reach of renewable energy sources to sectors traditionally reliant on fossil fuels. It presents a viable solution for seasonal energy storage, surpassing the limitations of conventional battery technologies. Consequently, Mexico urgently needs to implement measures to integrate hydrogen within its energy framework.

The period between 2020 and 2030 was declared as the "Decade of Hydrogen," high-lighting the global recognition of hydrogen's pivotal role in driving the transition toward a sustainable energy future. The proliferation of hydrogen-related initiatives and investments worldwide underscores the momentum behind this transformative energy vector. However, Mexico's initial absence from the International Energy Agency's radar in terms of hydrogen-related actions highlights the need for accelerated efforts to position the nation as a proactive player in the hydrogen economy.

During the past four years, Mexico has made significant strides in identifying and advancing low-carbon hydrogen projects, with more than five such projects already announced and under feasibility assessment. These developments underscore Mexico's growing recognition of the strategic importance of hydrogen in its energy transition agenda. Nevertheless, the absence of robust policy frameworks tailored to support hydrogen deployment poses a significant risk to the successful realization of these projects.

Therefore, it is time for Mexico to harness the opportunities presented by hydrogen to drive forward its energy transition agenda. By establishing a clear and ambitious roadmap for hydrogen integration, Mexico could position itself as a good player in the global hydrogen economy while simultaneously advancing its climate and energy goals. The window of opportunity is open, and decisive action is needed to ensure a sustainable and prosperous future for generations to come.

## 1.5   Literature Review

Hydrogen exhibits the highest calorific value (141.86 MJ/kgH$_2$) among all currently existing fuels, capable of storing 33.3 kWh/kgH$_2$ of chemical energy. Furthermore, it demonstrates efficient combustion, yielding only water vapour as a byproduct without the greenhouse gases characteristic of fossil fuels. However, given its unavailability in its isolated form in nature, transformation processes are requisite to obtain and utilize it as an energy carrier [15].

Substances or devices possessing the capacity to store energy in various forms for subsequent controlled release are termed energy vectors or carriers. Hydrogen, one of the most abundant elements on the planet, is globally recognized as an exceptional energy vector.

Utilizing hydrogen as an energy vector sustainably involves sourcing the requisite energy for its production exclusively from renewable resources, such as solar, wind, marine, geothermal, among others. This process entails generating gaseous hydrogen through the electrolysis of water, employing electrical energy derived solely from these renewable sources.

The integration of hydrogen with renewable energy sources presents significant advantages across two primary dimensions. Firstly, it facilitates the increased utilization of renewable energy sources, thereby contributing to the transition towards a more sustainable energy paradigm. Additionally, hydrogen can find versatile applications beyond energy storage, including but not limited to hydrocarbon refining, ammonia production, or serving as synthesis gas in chemical processes. Moreover, the utilization of hydrogen ensures a substantial reduction in greenhouse gas emissions throughout its entire production to utilization chain, thereby contributing to mitigating climate change effects.

The significance of hydrogen as an option for reducing carbon emissions has gained importance in numerous countries[16], [17], [18]. Among the possibilities for producing "green" hydrogen, solar and wind energies perhaps stand out as the most popular, owing to their global availability and scalability, making them suitable for large-scale production.

## 1.5.1   Solar hydrogen production

The availability of renewable sources is specific to particular regions and contingent upon geographic conditions. Therefore, the initial step toward generating a road map involves quantifying Mexico's hydrogen production capacity from wind and solar photovoltaic energy.

Several studies report methodologies and results regarding the quantification of hydrogen at the continent, country, or specific region levels, such as [19], [20], [21], [22], [23], [24], [25],

[26], [27], [28], among others. The primary objective of these studies is to assess the technical potential for producing green hydrogen and substituting grey or black hydrogen to reduce carbon footprint.

In particular, the amount of carbon-intensive hydrogen that could be replaced in Europe using renewable energy taking into account land-use limitations and techno-economic restrictions was evaluated in [19]. The authors found the existence of regions with an excess of potential (from 50 % to 81 %) after satisfying their electricity demand.

The carbon dioxide emissions from electricity production in Algeria were computed in [21] in order to use geothermal heat extraction to generate electricity. The objective is to identify locations where geothermic electricity could produce electricity and hydrogen and to estimate the corresponding costs.

Algeria's solar and wind potential to produce hydrogen has been evaluated in [23], [24]. In particular, [24] hourly production of hydrogen is used to reveal the solar hydrogen potential, which is found to vary from 0.10 to 0.14 $Nm^3/m^2$-day, they also found that the minimum amount of hydrogen that could be produced in isolated systems varies between 0.07 and 0.13 $Nm^3/m^2$-day.

The wind-hydrogen production in Ukraine was assessed in [25] taking into account wind farms of 688 GW, the authors concluded that it is possible to produce 43 MTon/year. The production of hydrogen using hydro-power was studied in [26] for Nepal. The authors first forecast the hydroelectric energy for 8 years and then compute the corresponding hydrogen production. Using different amounts of energy surplus, the authors found that hydrogen production could vary from 0.06 to 3.15 MTon/year.

The production of hydrogen using seawater, lakes, and rivers was evaluated in Turkey [28]. The authors found that hydrogen production has a high sensitivity to the water pH and salinity values and that other factors such as water temperature and sunshine duration

should be considered in the assessment. Their analysis arose that the Mediterranean Sea would have higher potential than some lakes during May and June.

In [29], the authors provide an estimation of the hydrogen consumption for transportation purposes in Algeria by 2045. They also provided an economical analysis of the production of green hydrogen using two different scenarios. They found that the levelized cost of solar hydrogen may be between 5 \$/kg to 0.9 \$/kg, while the production using geothermic energy would vary between 4.66 \$/kg to 3.54 \$/kg by 2045.

The mass production of hydrogen opens up a plethora of hydrogen applications such as the chemical industry, electric transportation [30], [31], [32], and as an energy storage system in electrical grids [33]. Consequently, it is worthwhile to undertake a formal and detailed study on the production potential of hydrogen in Mexico as a foundational step in creating a roadmap.

## 1.5.2   Wind hydrogen potential

Wind potential has been extensively studied for large-scale hydrogen production. Several authors have focused on developing methodologies for estimating wind potential. For instance, [34] calculated the resource, geographic, and technical wind potential across the African continent, considering air density variation, the impact of slopes, and the required spacing between turbines. They concluded that Africa could harness up to 30,000 $\text{MWh/km}^2$ from wind.

The analysis conducted by Dejan Doljak et al. [35] presents a methodology that combines multicriteria methods, GIS techniques, and geographic constraints (such as slopes, elevation, water bodies, rivers, urban areas, airports, roads, highways, and transmission lines) to select suitable zones for harnessing wind energy.

Within methodologies developed by some authors, the interpolation of data measured by meteorological stations serves as a key factor in describing the hydrogen production po-

tential in a given area. However, these studies face limitations in the number of elements available for calculations. For instance, [36] utilized only 34 meteorological stations to assess the wind potential in Venezuela, while in determining hydrogen production capacities in Iran, [37] conducted interpolation with only 150 meteorological stations. Due to the nature of interpolation, the reported results in such cases are highly likely to be erroneous.

Additionally, in a study conducted for Ukraine [25], the wind-driven hydrogen production potential was evaluated, considering wind farms of 688 GW. The authors concluded that it is feasible to produce 43 million tons per year of hydrogen. However, the methodology only took into account 40 meteorological stations.

Adicionalmente, en un estudio realizado para ucrania [25], se evalúa la producción eólica de hidrógeno en Ucrania teniendo en cuenta parques eólicos de 688 GW, los autores concluyen que es posible producir 43 MTon/año de hidrógeno. Sin embargo en la meteodología solo consideraron 40 estaciones meteorológicas.

Despite wind energy being extensively studied in Mexico, research on wind-driven hydrogen production capacities is nearly nonexistent. Morales Ruvalcaba, et al. [38] utilized the data reanalysis technique via the MERRA-2 model to describe wind speed in 24 meteorological stations across the country, using data from 2004 to 2008. They concluded that using reanalysis in Mexico is not a suitable tool for characterizing wind potential on a large scale. Pearson correlation coefficients ranged between 0.2 and 0.8.

In [39] authors determined the monthly and annual energy complementarity in Mexico by analyzing the correlation between solar and wind energy using the Pearson correlation coefficient with data from 2018. Through geospatial analysis and statistical methods, they found that the highest energy complementarity for harvesting solar and wind energy exists from central to northern Mexico.

### 1.5.3 Structure of a Road Map

Many countries already have plans and projects to develop the infrastructure that enables the integration of $H_2$ across all sectors. IRENA recognizes four stages for the development of hydrogen policy [40]:
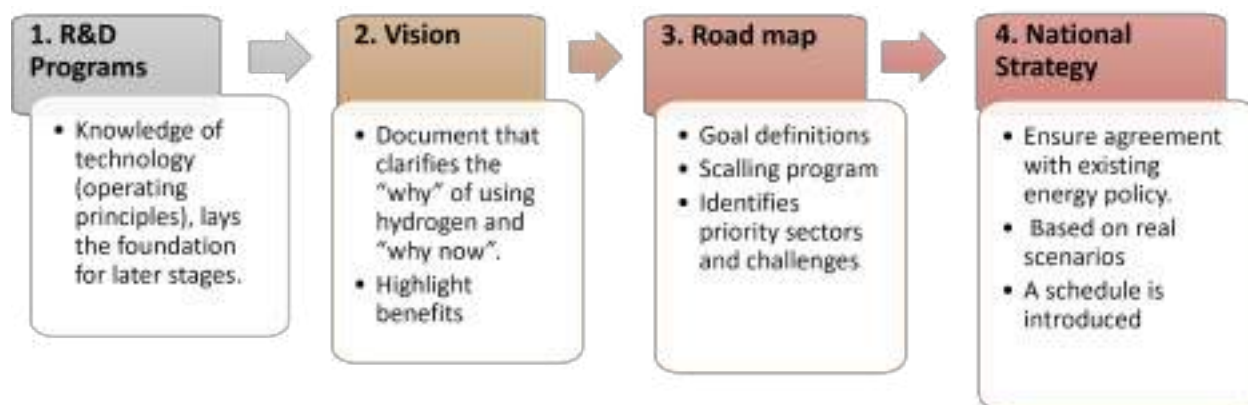


Figure 1.2: Stages in the development of a National Hydrogen Strategy

The roadmap (MR) is essential in planning green hydrogen projects, as it delineates the path between mere intentions and tangible realities within a specific context. As an example, several international roadmaps are presented.

Six documents were selected from existing roadmaps to represent different geographical regions of significance. These include Europe [41], North America (United States) [42], Australia [43], the United Kingdom [44], Chile [16], and Colombia [45] (Figure 1.3).

In general, four pillars were identified in which hydrogen roadmap structures were organized (Figure 1.4). Two of these pillars set goals for 2030 and 2050 related to decarbonization objectives, while the other two pillars address development plans and challenges to overcome. The latter typically include aspects related to legal frameworks (public policies), economic and social considerations, as well as research and development, and are necessarily specific to each country or geographical region.

Figure 1.3: Geographical regions and countries chosen as examples for having a hydrogen roadmap
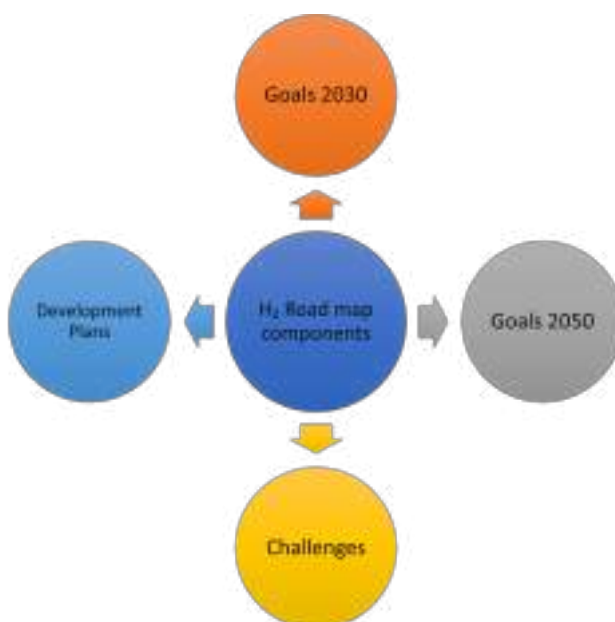


Figure 1.4: Main pillars of hydrogen roadmaps.

Based on the wealth of information found in the road maps, a summary was constructed to facilitate the identification of the topics addressed. This summary is presented in Table 1.1. In addition to the aforementioned main axes, technical aspects such as the potential for green hydrogen generation, generation costs, and the planned use of fuel cell electric vehicles (FCEVs) were considered important, as these are common themes across most roadmaps.

Table 1.1: Relevant topics addressed in Hydrogen Road Maps

| Development Indicators | Europe | United Kingdom | United States | Australia | Chile | Colombia |
|:---:|:---:|:---:|:---:|:---:|:---:|:---:|
| Goals 2030 | ✓ | ✓ | ✓ | ✓ | ✓ | ✓ |
| Goals 2050 | ✓ | ✓ | | | | ✓ |
| Production Potential | | | ✓ | ✓ | ✓ | |
| Light Vehicles | ✓ | | ✓ | | | ✓ |
| Heavy Vehicles | ✓ | | ✓ | | | ✓ |
| Exportation | | ✓ | | | ✓ | |
| Production Cost (LCOH) | | ✓ | | ✓ | ✓ | ✓ |
| Invesment | ✓ | ✓ | ✓ | | ✓ | ✓ |
| Development Plans | ✓ | ✓ | ✓ | ✓ | ✓ | ✓ |
| Challenges | ✓ | ✓ | ✓ | | ✓ | |

Two themes stand out in all the reviewed roadmaps: goals for 2030 and development plans. The year 2030 represents the nearest future in common planning due to the Paris Agreement, which is expected to be a turning point in the hydrogen trajectory. Once the objectives for this date are achieved, widespread use of hydrogen in various production and transportation contexts is envisioned.

An example of this is seen in the roadmaps of Colombia and Chile. Colombia's roadmap suggests a transition from blue hydrogen to green hydrogen during the 2020-2030 decade, with initial applications in refineries, buses, trucks, cars, and the chemical industry. By the period of 2030-2050, green hydrogen is expected to be fully established, enabling its exportation and utilization in electricity generation, industry, and heavy transportation.

On the other hand, Chile's main goal is to dominate exports worldwide by 2030-2050, having previously activated the domestic industry to produce hydrogen at more competitive costs in the future. According to their projections, Chile aims to achieve a LCOH of 0.8 USD/kg by 2050.

The period 2020-2030 is considered the decade of hydrogen, as this timeframe is crucial for laying the foundations of the infrastructure necessary to achieve decarbonization goals and, consequently, economic goals. The 2030 goals for the studied locations are shown in Table 1.2.

Table 1.2: Main Goals established for 2030

| Geographic Zones | Electrolysis Installed Capacity | LCOH | Transport | $CO_{2e}$ Emissions | Exportations | Investments |
|---|---|---|---|---|---|---|
| Europe | 40 GW | —— | 3.7 Millones vehículos ligeros 45,000 Truks 570 Trains | 400 MTon | $70 \times 10^9$ € | $8 \times 10^9$ € |
| United Kingdom | 5 GW | 2 USD/kg | ——- | 41 MTon | 96 TWh de hydrogen | $4 \times 10^9$ £ /año |
| United States | 40 GW | —— | 4300 hydrogen stations 1.2 M light vehicles 300,000 heavy vehicles | —— | —— | $8 \times 10^9$ USD/año |
| Australia | 100 MW | 2.3-2.8 USD/kg | | 315 MTon | —— | —— |
| Chile | 25 GW | 1.8 USD/kg | —— | —- | $2.5 \times 10^{12}$ USD/año | $5 \times 10^{12}$ USD |
| Colombia | 1-3 GW | 1.7-2 USD/kg | 1500-200 light vehicles 1000-1500 heavy vehicles 50-100 hydrogen stations | 2.5-3 Mton | —— | $2500 \times 10^6$-$5500 \times 10^6$ |

Europe aims to achieve an installed electrolysis capacity of 40 GW and utilize the hydrogen produced to power 3.7 million light vehicles, 45,000 trucks, and 570 trains, thereby enabling a reduction of up to 400 MTon $CO_{2e}$. However, to reach the 2°C target by 2050, more than 800 MTon of $CO_{2e}$ must be reduced. Given that Europe's maximum hydrogen production capacity is estimated at 560 MTon $CO_{2e}$, this implies that Europe might be a hydrogen importer.

The goals of the United States are centred on transportation and investments. The roadmap indicates that by 2030, 4,300 hydrogen refuelling stations should be installed to supply 1.2 million light vehicles and 300,000 heavy-duty vehicles. Furthermore, it is proposed that the objective of this country is to export technology and raw materials.

The goals outlined in these roadmaps are strongly influenced by two essential factors:

1. The legal framework.

2. Research and technological development.

The legal framework is responsible for establishing public policies primarily in two directions: facilitating the utilization and distribution of hydrogen for multiple applications; and reducing costs in both technology and electricity. Overcoming economic challenges is crucial in achieving the objectives.

On the other hand, research and technological development play a significant role in formulating public policies and laying the groundwork for projecting the future of hydrogen. Only through these efforts can the feasibility of the goals be established.

As observed in Table 1.2, in most geographical regions, it is expected that by 2030, the levelized cost of hydrogen production will be around 2 USD/kg, with projections indicating a decrease in the LCOH to 1 USD/kg by 2050. To achieve this, IRENA stipulates that electrolysis technology costs must decrease by 80 %, followed by a reduction in the costs of renewable electricity from 0.053 USD/kWh to less than 0.02 USD/kWh.

The roadmaps have revealed that the costs of hydrogen production, rather than technological barriers, constitute the primary bottleneck hindering the adoption of green hydrogen to combat decarbonization. Therefore, the road maps have established the cost production targets as the starting point for planning, while the planning of public policies and scientific and technological research are contingent upon these targets. This observation is crucial, as it implies that the first step for any planning, including that of our country, should be to conduct a cost analysis so that technological development goals can be stratified based on this analysis.

Due to the aforementioned factors, each country will face particular challenges in achieving the proposed cost targets, as they all start from different states of technological development, as well as varying degrees of conviction that will enable or hinder the generation and implementation of favourable public policies.

The hydrogen cost projections of Latin America are similar to those of Europe or Australia (countries that have demonstrated a determined adoption of decarbonization goals) and contemplate becoming global hydrogen suppliers. This could be a good guide for Mexico, given its significant renewable potential. However, how much of the global projections can be considered for our country remains uncertain until the necessary efforts to meet the projected hydrogen production costs worldwide are first assessed.

## 1.5.4 Public policy status for hydrogen in Mexico

According to [46], before 2021, Mexican legislation regarding hydrogen already considered it as a clean energy source. This legislation can be classified as described in Figure 1.5.
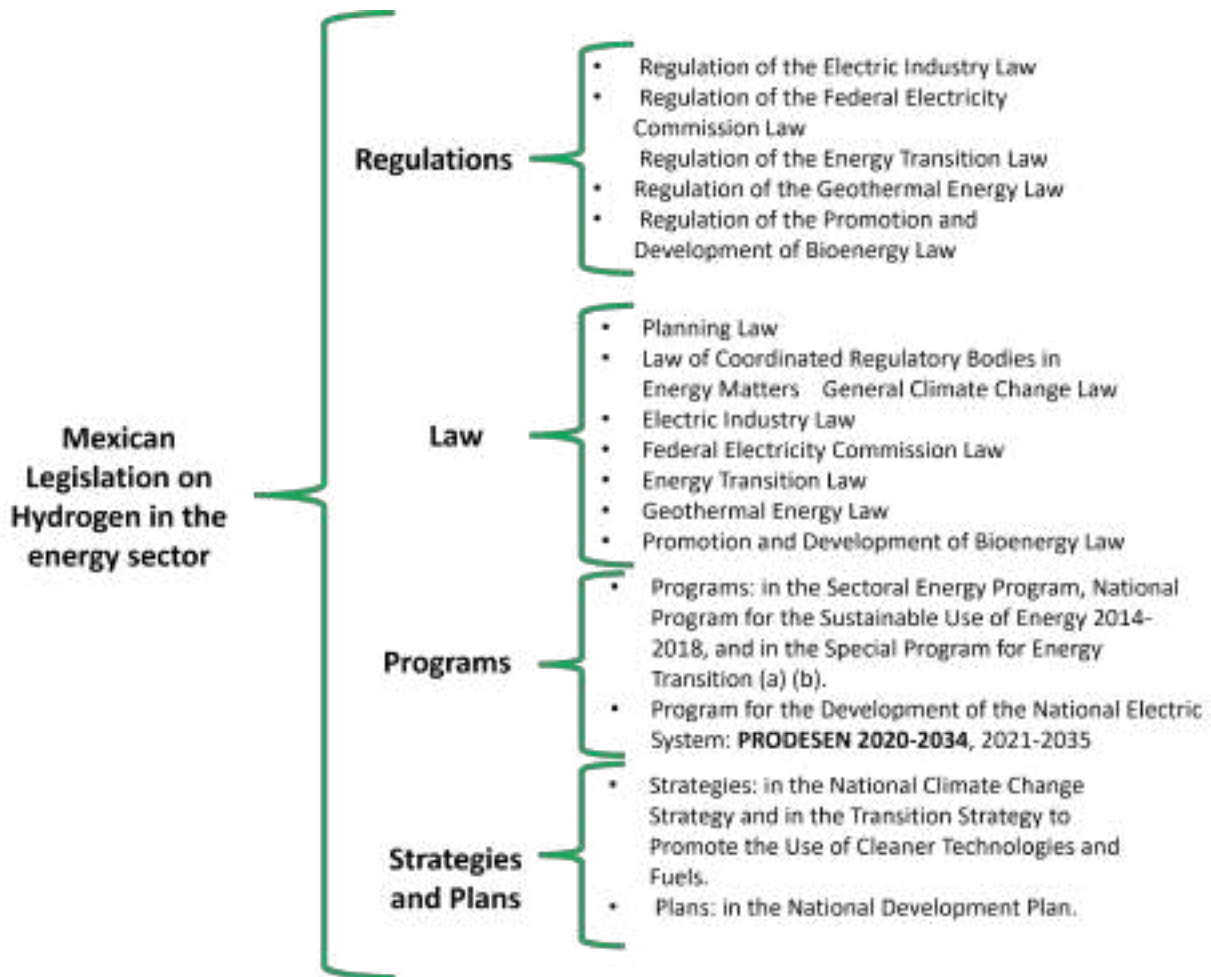


Figure 1.5: Mexican Legislation where hydrogen was considered a clean energy source before 2021

Regarding hydrogen handling and utilization, there exists a legal framework of regulations, wherein it is notable that to produce it, a permit from the Energy Regulatory Commission (CRE) is required, particularly when natural gas is used as a raw material. Regarding conditioning, ASME B31.12 standards are employed for the use of specific pipelines and ducts for hydrogen. Transport necessitates a permit from the Secretariat of Communications and Transport (STC) and compliance with the regulations for the terrestrial transport

of hazardous and explosive materials. In the chemical industry, attention must be paid to the technical specifications of equipment that will utilize hydrogen, such as reactors and burners. Given the expanding applications of hydrogen in mobility, adherence to the NOM-194-SCFI-2015 standard, which applies to any motorized vehicle, is imperative. Finally, as a source of electrical energy, compliance with regulations established by the National Center for Energy Control (CENACE) and the Electrical Industry Law must be considered [46].

Despite the existence of certain legislation regarding hydrogen in Mexico, one sector lacking such regulations is the market. In [47], the current state of laws to regulate the hydrogen market in Mexico was analyzed, revealing their nonexistence and highlighting a dire need for their development. This is because current policies pose commercial, ecological, human, economic, and technological challenges that may run counter to international agreements and challenge energy governance by discouraging the hydrogen market and hindering expected decarbonization efforts.

## 1.5.5 Potential for renewable energy production in Mexico

The potential for photovoltaic and wind energy production in Mexico has previously been assessed in [48], where the primary objective was to evaluate, from a techno-economic perspective, four VRES (Variable Renewable Energy Sources) technologies: onshore wind, offshore wind, utility-scale photovoltaic, and rooftop photovoltaic, up to the year 2050.

The results revealed the feasibility of generating up to 54 PWh of renewable electricity at a levelized cost of electricity of less than 0.07 €/kWh. Approximately 91 % (49 PWh) of this electricity would originate from utility-scale photovoltaic parks totalling 23 TW of capacity, capable of occupying up to 578,000 km$^2$ of eligible land throughout the country. 1.9 TW of onshore wind installations could produce the remaining 9 % (4.8 PWh) allocated to approximately 68,500 km$^2$ of subsidizable land, predominantly adjacent to three mountainous regions. The combination of offshore photovoltaic and wind turbines represents a very small fraction, less than 0.03 %, of the total techno-economic potential.

## 1.5.6 Hydrogen Production Potential in Mexico

Despite the recent establishment in the PRODESEN 2021 that by 2025, 1.3 % of the installed capacity for electricity generation in the country must come from the use of green hydrogen in combined cycle plants, there is indeed limited information available on hydrogen-related topics to justify such proposals holistically.

The energy partnership Mexico-Germany supported by HINICIO [49] have made estimations based on models suggesting that the energy that could be produced in Mexico considering solar and wind technology amounts to 39.8 PWh. Furthermore, they estimate that by 2050, the LCOE for both technologies will range between 0.015 and 0.03 USD/kWh and that achieving a LCOH of 1 USD/kg is feasible. They also mention that Mexico possesses the necessary human and technological resources to produce electrolyzers, fuel cells, and venture into hydrogen storage [50].

The aforementioned suggests that Mexico holds promising prospects in the realm of hydrogen development. While the methodology justifying these figures lacks clarity, this study does underscore the need for Mexico to embark on the four stages (R&D, Vision, road map, and National Strategy) to facilitate the implementation of green hydrogen technologies in the country.

HINICIO [49] estimated that by 2050, Mexico could achieve hydrogen production at 1 USD/kg. This estimation would need to consider a realistic starting point, acknowledging that as of 2022, Mexico is poised to enter Stage 1 (R&D Programs) and is not a technology producer, thus necessitating initial technology imports ( the proposed international price target can only be attainable in a context involving the use of domestic technology).

# Chapter 2

# Theoretical Framework

## 2.1 Renewable Energy Sources

### 2.1.1 Overview of Photovoltaic Solar Energy

The photovoltaic effect is a physical process whereby a photovoltaic cell converts sunlight into electricity. Sunlight consists of packets of solar energy known as photons. These photons carry varying amounts of energy corresponding to different wavelengths across the electromagnetic spectrum [51].

Solar cells are composed of two different types of semiconductors, namely, a p-type and an n-type, which are joined together to form a p-n junction. This junction creates an electric field, causing electrons to move towards the positive p-side and holes to move towards the negative n-side. This field induces negatively charged particles to move in one direction and positively charged particles in another direction [52].

When light of an appropriate wavelength strikes these cells, the photon's energy is transferred to an atom in the semiconductor material at the p-n junction. Specifically, the energy is transferred to the material's electrons, causing them to jump to a higher energy state known as the conduction band. This leaves a hole in the valence band from which the electron jumped. With its newfound energy, the electron can escape its normal position

associated with a single atom in the semiconductor to become part of the current in an electrical circuit. The special electrical properties of the electric field provide the necessary voltage to drive the current through an external load. Figure 2.1 illustrates the photovoltaic effect.

Solar energy is vital for life on Earth; it releases 95 % of its energy in the form of visible light, which represents only a fraction of the total radiation spectrum. Infrared and ultraviolet rays are also important parts of the solar spectrum. Each portion of the solar spectrum is associated with a different energy level. In the visible fraction of the spectrum, red is at the low-energy end, and violet is at the high-energy end [51].
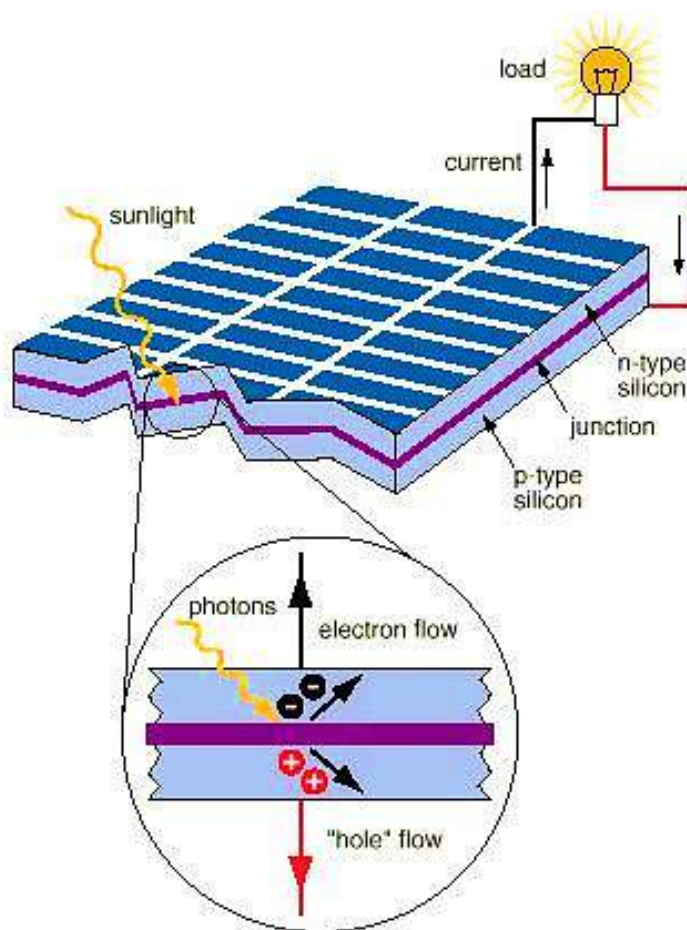


Figure 2.1: Photovoltaic Effect

Table 2.1: Characteristics of commercially ready and nearly ready solar cell material designs.

| Cell type | Materials properties | Absortion | Band Gap | Costs |
|---|---|---|---|---|
| Single junction designs | | | | |
| Monocrystalline silicon | Excellent | Bad | Regular | Hight |
| Polycrystalline silicon | Regular | Bad | Regular | Regular |
| Amorphous silicon | Bad | Excellent | Regular | Low |
| Polycrystalline thin films (CdTe) | Regular | Hight | Regular-Excellent | Low |
| Monocrystalline thin films | Excellent | Excellent | Excellent | Hight |
| Multiple junction designs | Bad-excellent | Excellent | Excellent | Low-Hight |

The solar cell is the fundamental unit of a solar panel or module. This component is responsible for transforming solar radiation into energy. Although many semiconductor materials are available, polycrystalline silicon is currently the most popular option for commercial cells (Table 2.1). Solar cells can be classified according to the type of junction as either single-junction or multi-junction designs [53].

It is important to mention that the band gap, or energy gap, is a characteristic parameter for materials used in the development of solar cells. It represents the energy difference between the top of the valence band and the bottom of the conduction band. This quantity is present in insulators and semiconductors. The electrical conductivity of an intrinsic (pure) semiconductor depends largely on the width of the gap [54]. Table 2.1 illustrates the different solar cell technologies and their main characteristics.

The basic unit or photovoltaic cell typically produces only a small amount of energy. To generate more energy, cells can be interconnected to form modules, which can then be connected in arrays to produce even more energy, and so forth (see Figure 2.2). Due to this modularity, photovoltaic systems can be designed to meet any electrical requirement, regardless of size [51]. Photovoltaic arrays can be installed in two configurations: standalone and grid-connected, depending on users' conditions and needs. Figure 2.3 illustrates the two types of systems.
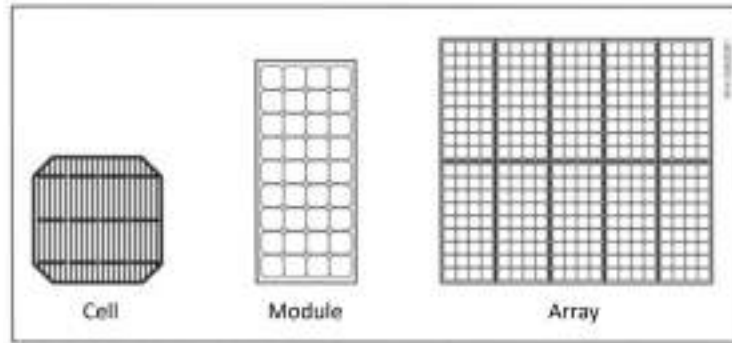
Figure 2.2: Arrangements of solar cells to form high capacity systems.
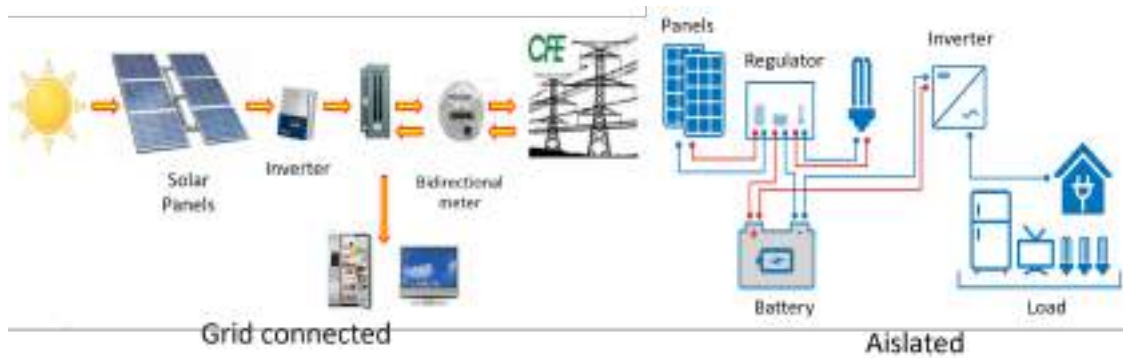


Figure 2.3: PV panels integration systems.

Grid-connected photovoltaic systems offer benefits to electricity consumers such as access to renewable energy, economic savings, and energy efficiency. Standalone systems are frequently used in remote locations to generate electricity in areas inaccessible to the electrical grid.

Regarding the ecological aspect and the lifespan of photovoltaic technology, life cycle assessments are known to determine the carbon footprint "from cradle to grave." In a study conducted by NREL, different stages of the life cycle and proportions of greenhouse gas emissions (GHG) for photovoltaic and coal energy were compared. It was found that for coal-fired power plants, fuel combustion during operation emits the vast majority of GHGs, whereas for photovoltaic power plants, most GHG emissions occur during material and module manufacturing (see Figure 2.4) [55].
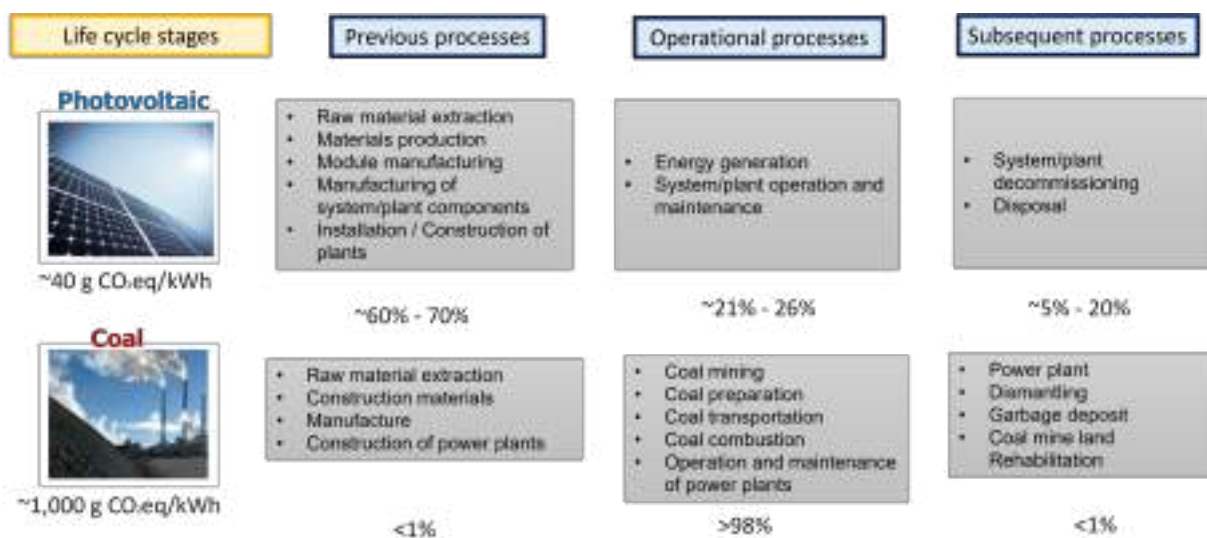
Figure 2.4: GHG emissions for photovoltaics and coal

## 2.1.2 Overview of Wind Energy

Wind energy is a byproduct of the sun; electromagnetic radiation heats the Earth's surface unevenly, being stronger in the tropics and weaker at higher latitudes. Additionally, as a result of differential absorption of sunlight by soil, rocks, water, and vegetation, the air in different regions is heated to varying intensities. This heating generates convective processes in the air, which are adjusted by the rotation of the Earth. Convective processes disrupt the hydrostatic equilibrium, causing stagnant air masses to move and react to forces induced by changes in air density and buoyancy due to temperature differences. Air is pushed from high to low-pressure regions, balancing friction and inertia forces due to the Earth's rotation [56].

Differential heating patterns of the Earth's surface, along with other thermal processes such as evaporation, precipitation, clouds, shading, and variations in surface radiation absorption, occur at different spatial and temporal scales. These combine with dynamic forces due to the Earth's rotation and the redistribution of flow momentum to generate a variety of wind generation processes, leading to the existence of a wide range of wind phenomena.

Wind power density (WPD) is used to compare wind resources regardless of wind turbine size and serves as the quantitative basis for standard wind resource classification at NBREL[57]. WPD offers advantages over average wind speed for comparing sites with different probability distribution asymmetries due to the nonlinear cubic dependence of wind energy on wind speed. Typical values for wind power classes with corresponding power densities and average wind speeds are presented in Table 2.2.

When selecting a site for the installation of a wind system, it is important to consider several criteria. The main factors that guide site selection include [58]:

1. Wind availability: Since wind speed is not constant, the average speed must be calculated hourly, daily, weekly, and monthly from readings taken over a period of 1 year. The site should have a satisfactory and uniform average wind speed throughout the year. The useful operating range for wind speed is 4-30 m/s.

2. Land availability: The installation of a 1 MW wind turbine plant requires approximately 10 hectares. The actual land directly used for wind turbine installation is only 10 % of this value. The remaining land can be used for low-height vegetation agriculture.

3. Land access: The land should be connected to roads for the transportation of machinery and construction materials.

4. Grid stability: Wind systems typically feed into the grid; therefore, the grid should be free from voltage and frequency fluctuations as much as possible.

**Operating principle of a wind generator**

A wind turbine is a generic term for a wind energy system that collectively converts the kinetic energy of the wind into electrical energy. Wind turbines are available in a variety of designs and power ratings, but the most familiar design is the horizontal-axis propeller-type wind turbine, as depicted in Figure 2.5 in a simplified form. The basic components of a wind turbine are [59]:

Table 2.2: Types of wind power measured at 50 meters above ground level according to the classification based on NREL's wind power density.

| Potential type | Resource Potential | Wind Density Power [W/m$^2$] | Wind speed [m/s] |
|:---:|:---:|:---:|:---:|
| 1 | Pooor | 0-200 | 0.0-5.9 |
| 2 | Limited | 200-300 | 5.9-6.7 |
| 3 | Regular | 300-400 | 6.7-7.4 |
| 4 | Good | 500-600 | 7.4-7.9 |
| 5 | Excellent | 500-600 | 7.9-8.4 |
| 6 | Exceptional | 600-800 | 8.4-9.3 |
| 7 | Outstanding | >800 | >9.3 |

1. Support tower: The tower allows the rotor blades to be elevated to a satisfactory height to increase their exposure to the wind. Large wind turbines (in the MW range) have towers reaching up to 250 meters above the bas

2. Rotor: This is the fundamental element of the turbine, as it intercepts the kinetic energy of the wind with its blades, converting it into mechanical energy. Rotor blades are typically made of materials such as fiberglass-reinforced polyester or epoxy-bonded wood. The length of the rotor blades ranges from 5 meters to over 60 meters.

3. Gearbox: A gearbox is used to connect the low-speed rotating blades to the high-speed generator. It also serves as a clutch.

4. Generator: A generator is connected to the high-speed shaft of the gearbox to transform the mechanical energy from the rotating blades into electrical energy.

5. Controller: A controller connects the wind generator system to the utility grid and locks the blades when the wind speed falls below the minimum generation limit or exceeds the design constraints of the system

Electricity is obtained as follows: when the wind reaches the blades of the wind turbine, it transfers its kinetic energy to them, converting it into mechanical energy, which in turn is transformed into electrical energy with the help of an electric generator. Generators have a rotor that rotates inside a stationary housing called a stator. Electricity is generated when

conductors move through a magnetic field, cutting through lines of flux and producing voltage and current.

The operating principle of all electrical machines is based on Faraday's law of electromagnetic induction and the interaction of magnetic flux and electric current. There are three main prerequisites for electrical generation: a coil or set of conductors, a magnetic field system, and relative motion between the conductors and the field [59].
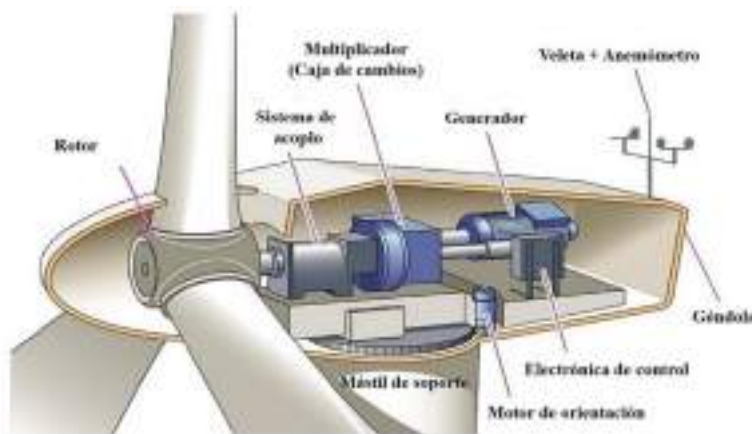


Figure 2.5: Basic components of a wind turbine.

Depending on the axis of rotation, wind turbines can be classified as horizontal-axis wind turbines (HAWT) and vertical-axis wind turbines (VAWT). HAWTs are the most commonly used today. In vertical-axis devices, the axis of rotation of the turbine blades (rotor) is horizontal or parallel to the ground; whereas in VAWTs, the axis of rotation of the blades is vertical to the ground. Figure 2.6 illustrates the two types of technologies.

## 2.2   Hydrogen Technologies

### 2.2.1   Water Electrolysis Classification

Many hydrogen production technologies can be integrated with renewable systems; however, the most developed and anticipated for large-scale implementation are water electrolysis processes, which can be classified into low-temperature processes including alkaline and
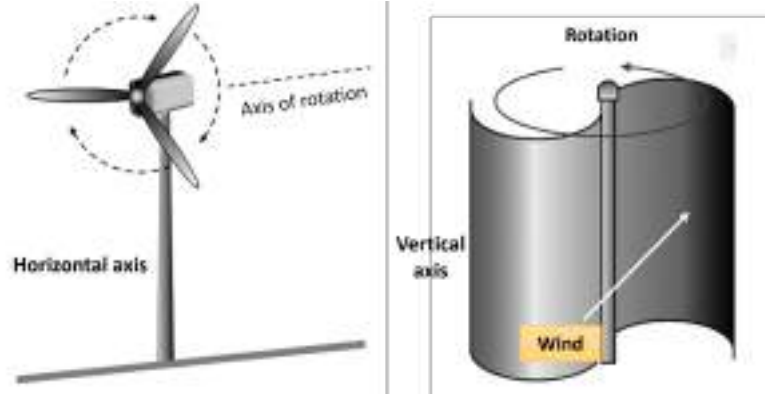
Figure 2.6: Horizontal-axis and vertical-axis wind turbines.

acidic electrolysis (PEM) (T<120 °C), medium-temperature (200 °C<T<600 °C), and high-temperature (T>600 °C) processes where electrolysis with a solid oxide electrolyte takes place [60], [61]. It is worth noting that low-temperature technologies have been the most developed, studied, and applied. Figure 2.7 summarizes the characteristics of these technologies.

## 2.2.2   Hydrogen storage technologies

Hydrogen is one of the primary options for storing renewable energy. $H_2$ energy is considered one of the most important energy sources for the near future [62]. It can be obtained cleanly from water and transformed into useful energy with high efficiency and without negative environmental impact, as its combustion only produces water vapour [63]. Additionally, it has applications in gas turbines to enhance the flexibility of the energy system. $H_2$ is the primary source of ammonia, which could also be used in coal power plants to reduce emissions.

In grids and microgrids, determining the optimal size of components is necessary for the system to be safe and reliable while minimizing costs [64]. Proper sizing and the best grid operation strategy must take into account the location's characteristics and needs, as well as the properties of distributed energy resources. Considering hydrogen as a storage system involves evaluating different production and storage technologies to make an efficient selection, as well as an optimal operational strategy.
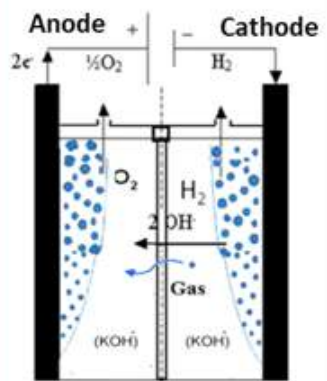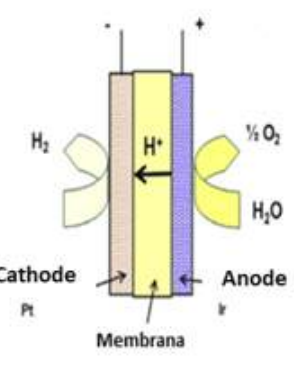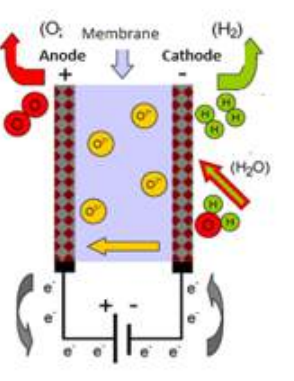
| ELECTROLYSIS TYPES | | | |
| --- | --- | --- | --- |
| **PROPERTIES** | **ALKALINE** | **ACID (PEM)** | **SOLID OXIDE** |
| **Half reactions** | $2H_2O + 2e^- \rightarrow H_2 + 2OH^-$ <br> $2OH^- \rightarrow \frac{1}{2}O_2 + H_2O + 2e^-$ | $H_2O \rightarrow \frac{1}{2}O_2 + 2H^+ + 2e^-$ <br> $2H^+ + 2e^- \rightarrow H_2$ | $2H_2O + 4e^- \rightarrow 2O_2^- + 2H_2$ <br> $2O_2^- \rightarrow O_2 + 4e^-$ |
| **Process** | | | |
| **Electrodes/ Catalyst** | Anode: Ni, Fe/Alloys Ni, metallic oxides <br> Cathode: Steel +Ni/Ni-Co | Anode: Graphite-PTFE+Ti/RuO$_2$, IrO$_2$ <br> Cathode: Steel + Pt/Pt | Anode: Ceramics (Mn, La, Cr) /Ni <br> Cathode: Zr+Ni/CeOx |
| **Electrolyte** | NaOH(15-20%w) <br> KOH (30-35%w) | Polymeric solid <br> Usually, Nafion® | $Y_2O_3 - ZrO_2, Sc_2O_3ZrO_2$ <br> $MgO - ZrO_2, CaO - ZrO_2$ |
| **Separator** | Anion exchange membrane, Zirfon, NiO | Proton exchange electrolytic membrane | Electrolytic ion exchange membrane |
| **Ion** | **OH⁻** | **H⁺** | **O⁻²** |
| **Temperature and pressure** | (60-80) °C <br> Up to 30 bar | (50-80) °C <br> Up to 700 bar | (600-1000) °C <br> Up to 5 bar |
| **Energy Consumption** | **4.3-5 kWh/Nm³ de H$_2$** | **4.2-4.6 kWh/Nm³ de H$_2$** | **2.8-3 kWh/Nm³ de H$_2$** |
| **Efficiency** | 50-70% | 40-80% | 90-95% |
| **Capacity** | **1-500 Nm³/h** | **1-230 Nm³/h** | **1 Nm³/h** |
| **Lifetime** | 20-30 years | 10-20 years | 1-12 years |
| **Current density** | 0.2-0.8 A/cm² | 0-2 A/cm² | 0-2 A/cm² |
| **Advantages** | Has more commercial development <br> Implies lower investment costs. <br> Does not require noble metals as catalysts | Solid electrolyte (non-corrosive) <br> Operates at high current densities. <br> High pressures (300 bar) | Solid electrolyte (non-corrosive) <br> Increases thermal contribution to reduce electrical consumption. <br> Withstands high pressures |
| **Disadvantages** | Low hydrogen purity <br> Slow response time <br> Low current densities <br> Operates at low pressure | Use of noble metals as catalysts <br> The water must be ultra-pure <br> Small scales | High temperatures limit the useful life of materials. <br> Only laboratory scale equipment is available. |

Figure 2.7: Electrolysis Process and its characteristics.

The main challenge for the widespread use of hydrogen is storage, as it is the lightest gas of all (densidad= 0.089 kg/$m^3$). Therefore, different methods have been developed to address this characteristic. The diagram in Figure 2.8 presents the various hydrogen storage technologies.
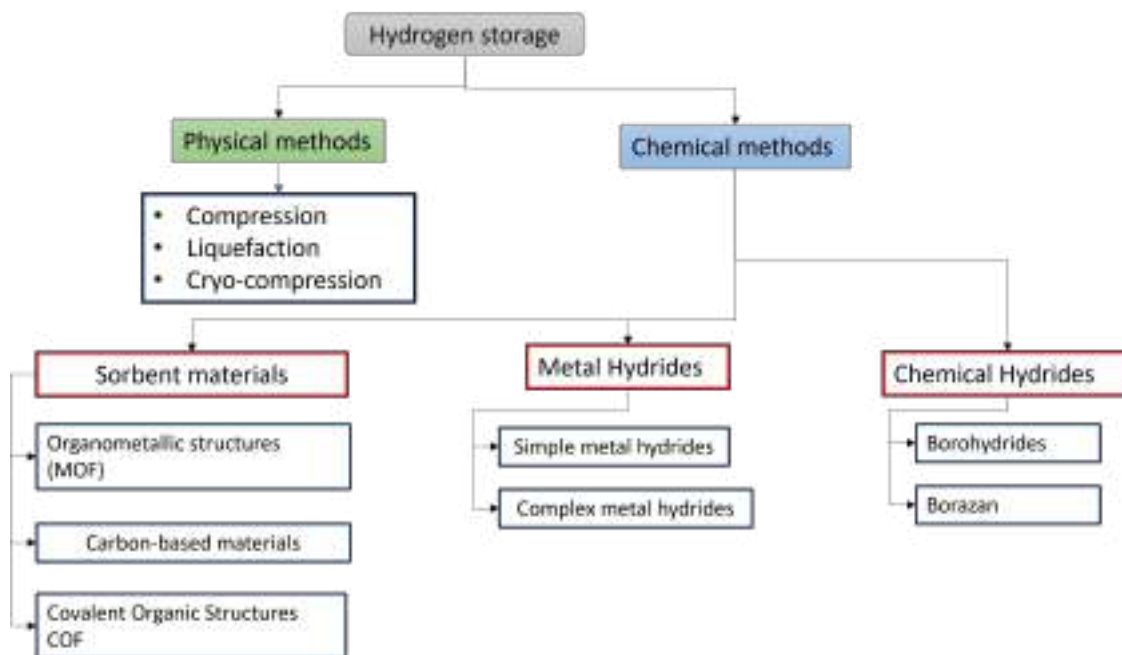
Figure 2.8: Hydrogen Storage Technologies.

## 2.2.3   Hydrogen Applications

Hydrogen has multiple applications across various sectors. In construction, it is considered for enriching natural gas lines for use in residential and commercial units in large cities. In the industry, $H_2$ plays a significant role in petroleum refining, ammonia production, methanol production, and steel manufacturing. In the transportation sector, both maritime and aviation industries have limited options for low-carbon fuels, making hydrogen a promising alternative. However, the competitiveness of hydrogen depends on the costs of fuel cells (see Figure 2.9) [15].

## 2.2.4   Hydrogen Production Cost

In Figure 2.10, a projection is presented regarding the cost reduction required to achieve a future hydrogen production cost of 1 USD/kg [7].

Currently, the global average cost of hydrogen production, according to the IEA [15], ranges between 3.5 and 7 USD/kg. However, by focusing on certain aspects, it may be

possible for hydrogen generation to compete with fossil fuel prices. In general, for the electrolysis process, if the cost of the electrolyzer were reduced by 80 %, the production cost would range from 3 to 5 USD/kg. Another significant reduction needed is in electricity costs; if electricity could be obtained at 20 USD/MWh, hydrogen generation would cost between 1.5 and 3 USD/kg. Hence, achieving operational advantages is crucial to increase demand and regulate the market.
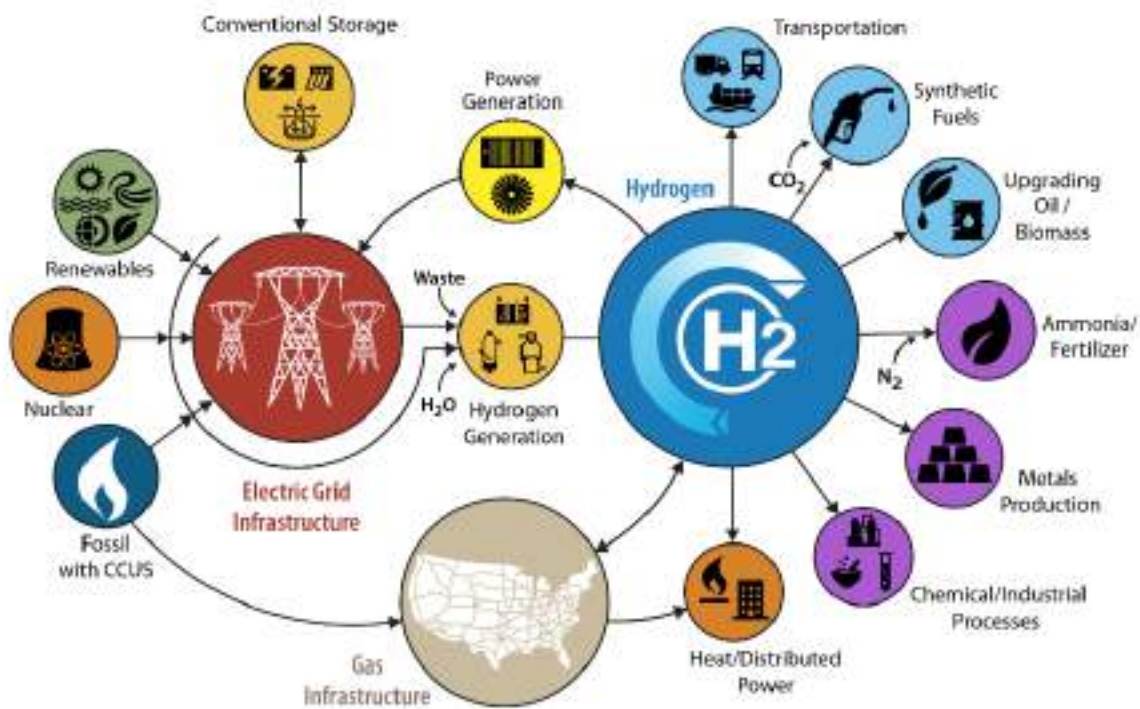


Figure 2.9: Hydrogen application options [6].

## 2.3   Geographic Information System

There are several definitions of what a Geographic Information System (GIS) is. One of them states that a GIS "is a tool that allows for the analysis, presentation, and interpretation of facts related to the Earth's surface" [65]. A GIS is indeed a tool that enables us to understand the spatial behaviour of various variables, such as temperature, precipitation, solar radiation, wind, etc. Therefore, it is widely used in assessing the potential of renewable energy.
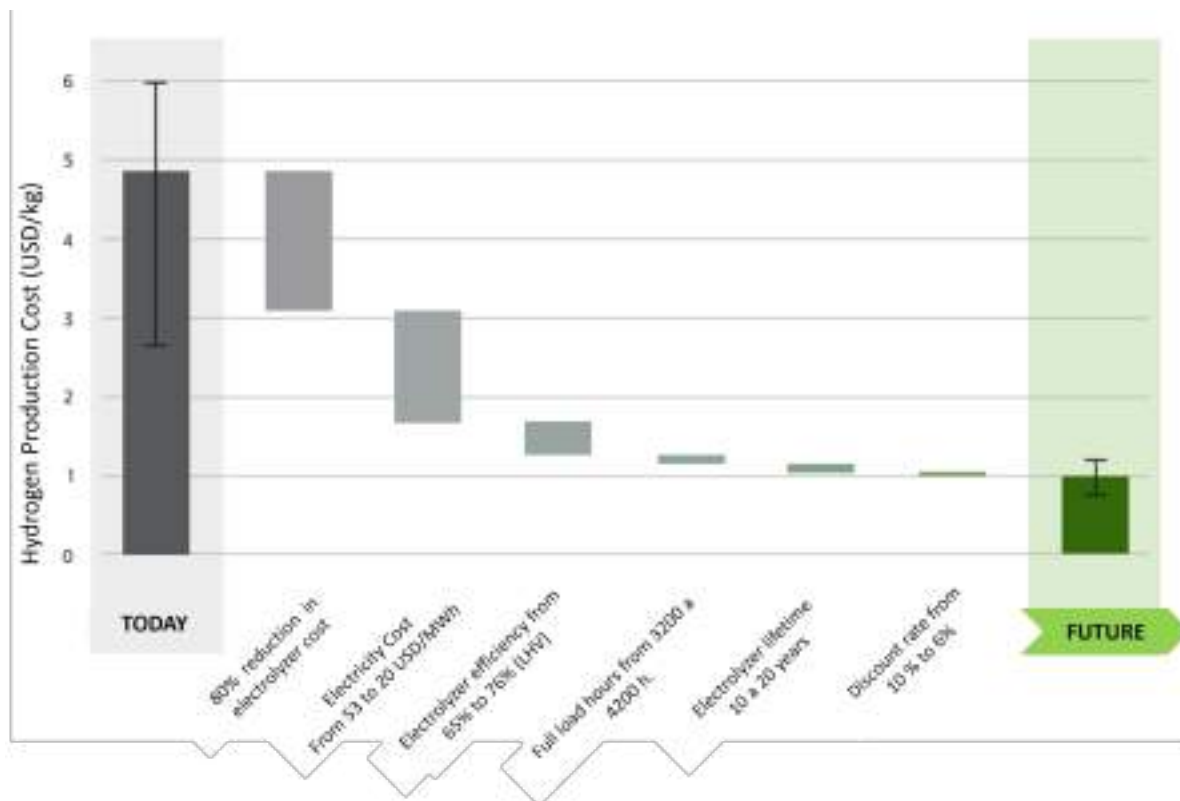
Figure 2.10: Reduction in the costs of hydrogen technology components [7].

### 2.3.1  Gesopatial data types

a) Vector Model.

Vector data (Figure 2.11) enables the digital representation of spatial objects in a GIS environment through geometries, which can be points, lines, or polygons. For example, a river or a road is represented by lines, while cities are represented by polygons. Point data only provide location information, without shape, length, or area [66].

The computational tools that enable the analysis of this type of data do so through layers, which are a set of points, lines, or polygons, depending on the type of representation being used. These data contain integrated information that allows us to know the position of the variable under analysis, and this information is called coordinates.
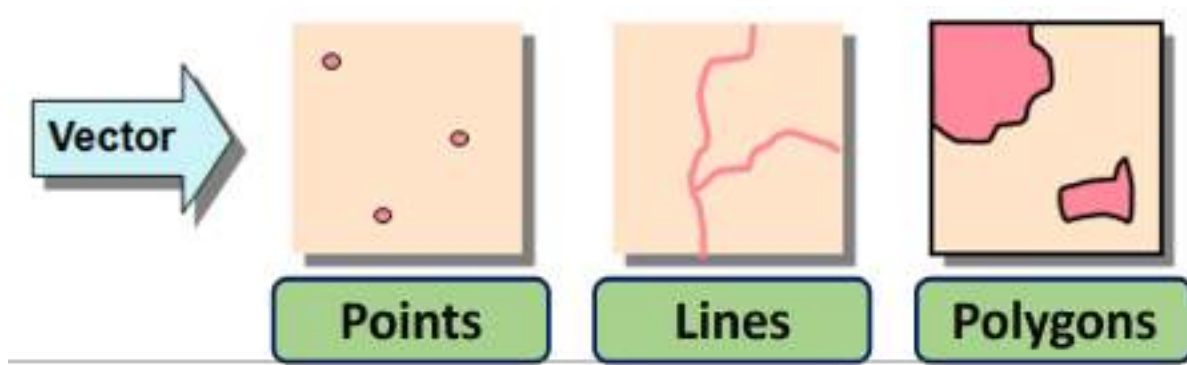
Figure 2.11: Vector data type.

b) Raster Model.

Rasters (Figure 2.12) consist of a matrix of pixels (also called cells), each with a specific value, representing the variable of interest at that particular position. A straightforward way to interpret them is through a matrix. A raster is composed of rows (running from side to side) and columns (running from top to bottom) of pixels (also known as cells). Each pixel represents a geographic region, and the value in that pixel represents some characteristic of that region [67].

Raster data can be obtained in various ways. Two of the most common methods are aerial photography and satellite imagery. In aerial photography, an aircraft flies over the area with a camera mounted underneath it. The photographs are then imported into a computer and georeferenced. Satellite imagery is created when satellites orbiting the Earth, equipped with special digital cameras aimed at the Earth's surface, capture images of the areas they pass over.

## 2.3.2   Gesospatial Analysis Tools

GIS tools (Figure 2.13) are designed to process spatially integrated information, there are software programs that facilitate the management of such data, some of which are open-source while others are proprietary. QGIS is an open-source software that enables various operations on both vector and raster files, including database connectivity, online querying, interpolation methods, etc. [68].
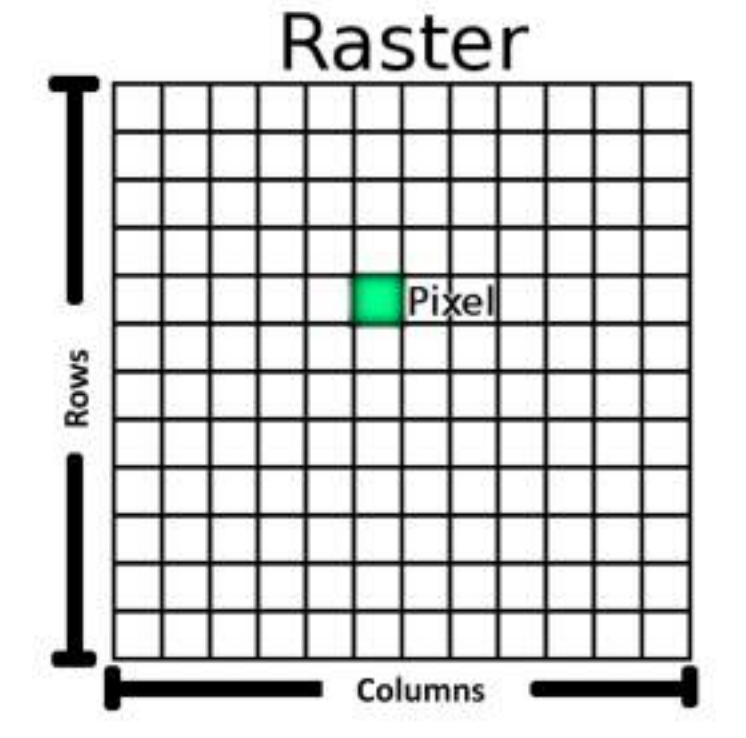
Figure 2.12: Raster model

On the other hand, ArcGIS is proprietary software owned by ESRI, offering substantial capabilities as a GIS tool. This program, along with its Geostatistical Analyst Tools extension, is specifically designed for conducting interpolation methods and geostatistical analyses [69].



Figure 2.13: Common Geospatial Analysis Tools

# Chapter 3

# Solar H$_2$ Production. Part A: Centralized Scenario

This chapter aims to elucidate the solar hydrogen production potential in Mexico using geospatial analysis methodologies. It delineates the water requisites across various states and examines the influence of electrolyzer efficiency and costs, energy accessibility, and operational hours on the Levelized Cost of Hydrogen (LCOH).

The formulation of effective public policies for the deployment of hydrogen necessitates a thorough evaluation of generation capacities derived from renewable sources. This analysis plays a pivotal role in identifying suitable locations for implementing hydrogen production infrastructure, estimating production potential, and considering operational and environmental limitations. Such assessments facilitate strategic and efficient planning, ensuring the long-term sustainability and feasibility of hydrogen production initiatives, thereby fostering an effective transition towards a cleaner and more sustainable energy paradigm.

There are significant efforts to assess hydrogen production in many countries or regions using renewable energies [70], [19], [25], [26], [27], [28], [71], among many others. In these works, the main objectives are to evaluate the technical potential for producing green hydrogen and substituting grey hydrogen to reduce the carbon footprint. However, most of these works do not address the limitations imposed by water availability for hydrogen pro-

duction at each location, in addition to the lack of analysis on the effects of variables such as energy intermittency, technology import costs, and electrolyzer efficiency on the LCOH. This study addresses those gaps to generate the necessary information to identify locations for harnessing solar resources in hydrogen production.
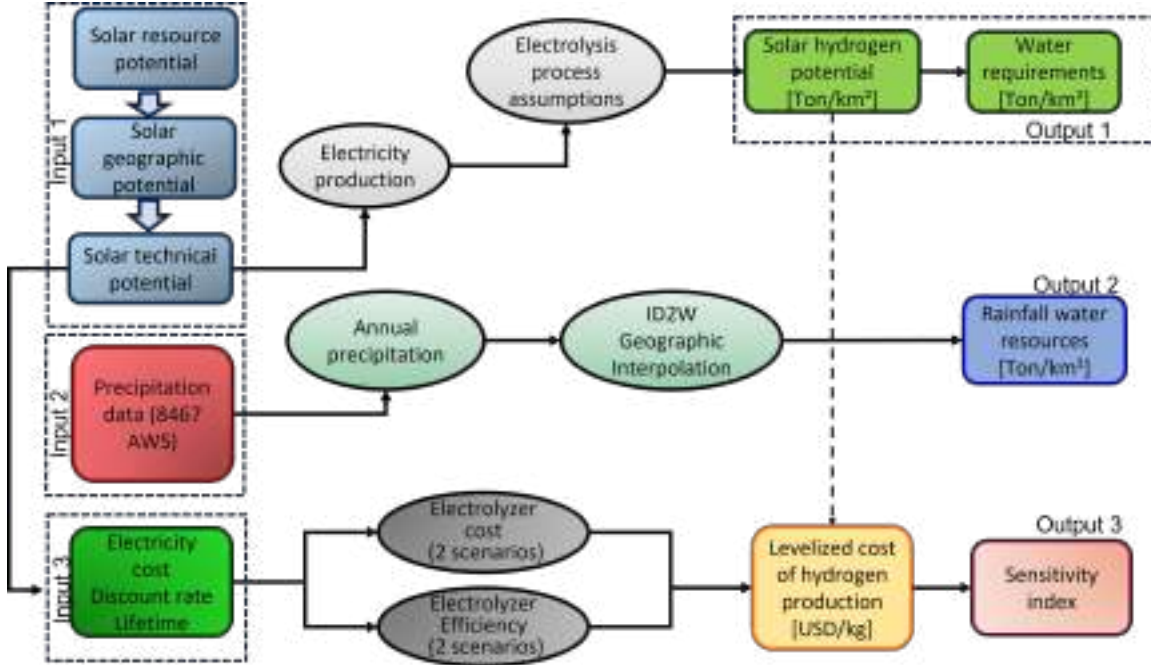


Figure 3.1: General methodology.

# 3.1 Methodology

## 3.1.1 Study area

In this study, 8,467 automatic weather stations were utilized to obtain three key variables: duration of insolation, global horizontal irradiance, and precipitation. Additionally, temperature measurements were considered to calculate variations in photovoltaic panel efficiency as described below. All measured data adhered to the daily, monthly, and annual data integrity criteria set forth by the World Meteorological Organization (WMO) [72], ensuring the time-dependent representativeness of the measurements. The methodology developed to assess the solar hydrogen production potential is depicted in Figure 3.1.

For the computation of the technical potential of solar resources, some constraints were used to exclude territories with more than 4 % inclination or land use categorized as forest, jungles, agricultural terrain, water bodies, as well as urban areas. Additionally, protected areas, archaeological sites, gas stations, recreational areas, entertainment venues, airports, volcanoes, ports, industrial zones, and oil and gas pipelines were also eliminated. The remaining land was designated as the Land Available Area (LAA) for solar energy and hydrogen collection, and it was found to be significant when represented as a percentage of the total area per state. The land estimation was calculated using GIS, employing spatial resolution cells of 500 m x 500 m. If $A_i$ represents the area of the cell capable of collecting solar energy (as described earlier), the available land area is given by:

$$LAA = \sum A_i \tag{3.1}$$

Having 90 % of $LAA$ would imply that 90 % of the surface area of a state is suitable for capturing solar energy and producing hydrogen. It is important to highlight that, for consistency, water availability is reported considering only the $LAA$ for hydrogen collection. In other words, no additional area was considered.

For the hydrogen potential assessment, the total of the 32 states of the Mexican Republic were considered: Aguascalientes (Ags), Morelos (Mor), Baja California (BC), Nayarit (Nay), Baja California Sur (BCS), Nuevo León (NL), Campeche (Camp), Oaxaca (Oax), Chihuahua (Chih), Puebla (Pue), Chiapas (Chis), Querétaro (Qro), Coahuila (Coah), Quintana Roo (Qroo), Colima (Col), Sinaloa (Sin) , Ciudad de México (CdMx), San Luis Potosí (SLP), Durango (Dgo), Sonora (Son), Guerrero (Gro), Tabasco (Tab), Guanajuato (Gto), Tamaulipas (Tamps), Hidalgo (Hgo), Tlaxcala (Tlax), Jalisco (Jal), Veracruz (Ver), México (Mex), Yucatán (Yuc), Michoacán (Mich), Zacatecas (Zac).

The Si-PV technology with a global nominal efficiency of 17 % was considered. For the derivation of solar potential, the nominal efficiency was multiplied by losses due to dust and shadows, power electronic circuits, and cable losses, as considered in [73]. Overall, photo-

voltaic efficiency accounted for two contributions: the first one encompassing all electrical losses and sunlight blocking, and the second one considering efficiency changes due to temperature variations, as described in [73].

Finally, the technical potential of solar resources was utilized to calculate hydrogen production and the required water, following the methodology described in the subsequent section.

### 3.1.2 Hydrogen Production Potential

The amount of hydrogen produced in a year $(\overline{M_{H_2,i}})$ in Ton/km$^2$ was calculated using Equation 3.2 [74].

$$\overline{M_{H_2,i}} = \frac{\eta_{elec}\overline{E_{pvs,i}}}{HHV_{H_2}} \tag{3.2}$$

where $HHV_{H_2}$ is the hydrogen Higher Heating Value (39.4 kWh/kg), $\eta_{elec}$ is the electrolyzer efficiency, and $\overline{E_{pvs}}$ is the technical potential of energy released by the photovoltaic system in kWh/km$^2$year.

The quantity of H$_2$ per unit area for the entire Mexican territory was computed through map algebra in Q-GIS, employing geospatial raster data utilizing cell area (A$i$) in km$^2$. Additionally, the total mass of hydrogen production (M$H_2$) in MTon/year was calculated according to Equation 3.3.

$$M_{H_2} = \sum \overline{M_{H_2,i}} A_i \tag{3.3}$$

*Rainfall water resourses*

Due to the significance of water as a raw material in the electrolysis process, the evaluation of rainfall as a potential water source for hydrogen production was proposed.

The required water mass $(\overline{W_{req,i}})$ in Ton/km$^2$ was calculated using Equation 3.4:

$$\overline{W_{req,i}} = \overline{M_{H_2,i}} \cdot E_r \tag{3.4}$$

where $E_r$ is the stoichiometric ratio of the overall electrolysis reaction. 10 kg of water are required per kilogram of hydrogen produced, considering a water density of 1000 kg/m³ for simplicity. The total water mass required was calculated using the cell area. Then, the average annual rainfall was calculated for each measurement point, and finally, the technique of inverse distance squared weighting (ID2W) interpolation was used to obtain the distribution of rainfall across the entire country.

The required water was also expressed as a percentage of the annual precipitation, subsequently, referred to as the percentage of required rainfall water (PWreq); a PWreq value of 20 % would imply that the water required for hydrogen production (corresponding to the total solar technical potential of the location) is 20 % of the total rainfall water in that territory.

Three scenarios of water availability were studied. The first is at the national level, the second at the state level, and the third at the local level. Our motivation is based on the fact that precipitation is a local phenomenon, so differences in hydrogen production would not be generally evident. This also motivates the analysis at the state level and the use of density variables (i.e., variables per unit area).

### 3.1.3   LCOH Assessment

A hydrogen Road Map integration, in addition to requiring technical data, also necessitates economic indicators. Therefore, in this study, the Levelized Cost of Hydrogen (LCOH) was evaluated. It is a measure of the average cost of hydrogen produced per unit mass (USD/kg). This cost takes into account not only the initial investment due to plant construction but also management throughout the entire lifespan, enabling comparison of production costs among different technologies. The LCOH was calculated based on [75] and [76], as shown below:

$$\text{LCOH} = \frac{\sum_{j=0}^{N}((\text{CAPEX} + \text{OPEX})(1 + I)^{-j})}{\sum_{j=0}^{N}((M_{H_2}[j])(1 + I)^{-j})} \tag{3.5}$$

where I is the discount rate (i.e., the interest rate on the project cost, considered as 10 % in this study), N is the project's lifespan, and CAPEX represents the capital expenditures to acquire the electrolysis technology and is given by:

$$\text{CAPEX} = \text{UCE} \times \frac{M_{H_2} R_{en}}{\text{Top}} \tag{3.6}$$

Where UCE represents the unit cost of the electrolyzer in USD/kW, $R_{en}$ denotes the theoretical energy required to produce 1 kg of hydrogen (52.5 kWh/kg), while Top refers to the operating hours in a year. Typically, Top is considered as 8,760 hours (see for example [74], [76], and [22]), indicating that the electrolyzer operates 24 hours a day, 7 days a week. In this study, the LCOH results from this standard assumption were compared with the case where Top considers only the duration of sunlight (where hydrogen production is possible), as analyzed in the following section. And OPEX represents operational expenses and is given by Equation 3.7:

$$\text{OPEX} = \text{CIE} + \text{COM} + \text{CORP} \tag{3.7}$$

where COM is the cost of operation and maintenance, and CORP is the replacement cost, considered here as 2 % and 25 % of the CAPEX respectively according to [15], [74]). CIE is the investment cost in electricity in USD given by:

$$\text{CIE} = Egc \cdot E_{pvs} \tag{3.8}$$

*Egc* represents the electricity generation cost in USD/kWh, and $E_{pvs}$ is the energy delivered by the photovoltaic system in kWh.

**Operating time and sunlight duration**

As mentioned earlier, typically when calculating the LCOH, a standard assumption of 8760 operating hours is considered. However, since the electrolyzer is only capable of producing

hydrogen during the day and, more precisely, during sunlight hours, this consideration must be taken into account.

The duration of sunlight primarily depends on the latitude of a given location; theoretical radiation can be reasonably estimated using only location data. However, the actual duration of insolation is more complex to model as it depends on climatological aspects such as cloud cover, which varies with temperature, relative humidity, and wind conditions, among other variables. In this study, the duration of sunlight was derived using daily measurements of global horizontal irradiance following the procedures of the World Meteorological Organization (WMO) in [72], and then average annual values were calculated for the years with available data.

The duration of sunlight not only accounted for the bright hours of the day but also considered the times when solar energy could be sufficiently strong to provide measurable and processable power according to [72].

It is worth mentioning that the hydrogen potential is not affected by the consideration of operating times in the electrolyzer, as this potential was computed with actual solar radiation measurements and implicitly considers the total operating time. However, the LCOH is affected because it considers management costs throughout the entire lifespan of the electrolyzer.

**Sensitivity Index**

To reveal the effect of certain parameters in the LCOH and hydrogen production, the sensitivity index (SI) was employed, which is given by:

$$\text{SI} = [max_\gamma - min_\gamma(x)]/max_\gamma(x) \tag{3.9}$$

where $\gamma$ represents the varied parameter and $x$ the output variable under evaluation. In this study, sensitivity indices were calculated for the cost of the electrolyzer (considering

importation), electrolyzer efficiency, available energy, energy cost, and operating time.

**Production cost scenarios**

Different production and cost scenarios were analyzed to calculate the sensitivity index. The first one corresponded to different electrolyzer technologies and hence electrolyzer efficiency. In this study, efficiencies of 75 % and 65 % were considered as these values constitute typical extreme values for new and used PEM and Alkaline electrolyzers [77].

The second scenario involved production costs that are related to the lifetime and type of electrolyzer. According to IEA [15], the current costs of electrolyzers in 2021 were 1,000 USD/kW and 600 USD/kW for PEM and Alkaline respectively. The lifespan of electrolyzer plants was considered to be 10 and 20 years for PEM and Alkaline electrolyzers respectively, according to [77]. Additionally, the scenario of electrolyzer importation was analyzed by adding a 60 % surcharge on the unit cost. In summary, two electrolyzer cost scenarios for each type of technology were evaluated, as shown in Table 3.1.

Table 3.1: Considered scenarios in this study

| Technology | Alkaline | PEM | Acronym |
|---|---|---|---|
| Base cost [15] | 600 | 1000 | SC1A / SC1P |
| Base cost + 60% Importation costs | 960 | 1600 | SC3A / SC3P |

Finally, the effect of electricity production costs was also analyzed to compare different energy production technologies. In particular, two different scenarios were considered. The first one estimated prices according to energy availability as in [73]. These prices are inversely dependent on energy production, so states with more capacity to produce solar energy have lower electricity production costs.

A second scenario utilized information from the Energy Regulatory Commission (CRE) of Mexico, which reports real average electricity production prices for the entire country.

The CRE reports electricity production costs from five sources: nuclear, hydroelectric, wind, solar, and geothermal. The reported prices are not differentiated geographically and are valid only for the amount of energy produced during the considered period, but they were used to reveal the corresponding hydrogen production costs as a point of comparison.

## 3.2   Results: Centralized Hydrogen Potential

In general, the obtained results showed that:

1. The hydrogen potential was estimated between 2,366.33 MTon/year and 2,050.82 MTon/year depending on the electrolyzer efficiency ($\eta_{elect}$= 75 % and 65 % respectively), which constitutes over 26 times the global hydrogen consumption in 2020.

2. The water needed to produce hydrogen can be obtained from precipitation. At the national level, less than 6 % of rainfall water is required; however, the local analysis proved essential to derive the exact conditions of hydrogen production viability.

3. From the local analysis of water requirements, it was found that:

   (a) Most states require less than 10 % of the annual rainfall water.

   (b) 90 % of the total territory capable of producing hydrogen requires less than 20 % of the rainfall water.

   (c) 1 % of the evaluated territory requires between 50 and 100 % of the rainfall water, and 0.002 % requires more than 100 %.

4. The LCOH for the alkaline electrolyzer ranged from 3.15 to 5.27 USD/kg, with the most expensive scenario being associated with import costs, whereas the LCOH for the PEM electrolyzer ranged from 4.41 to 7.48 USD/kg.

5. Sensitivity indices of up to 52 % were found for Top (electrolyzer operation time) , indicating it as the most significant factor influencing the LCOH, followed by electricity cost (up to 39 %), energy availability (up to 27 %), electrolyzer cost (up to 27.43 %), and electrolyzer efficiency (13.36 %).

6. The LCOH utilizing various renewable energy sources, including hydroelectric, solar, wind, and geothermal, exhibited comparable values in Mexico according to electricity prices reported by the CRE in 2019, 2020, and 2021. However, the price trend proved to be significantly different.

## 3.2.1   Hydrogen Production Potential

The initial investigation pertained to a designated scenario wherein the sensitivity to a range of factors was examined, with its formulation predicated upon the computation of hydrogen potential as an initial step. The execution of a comprehensive non-geographic analysis is unattainable due to several factors influencing the potential, including but not limited to solar radiation, precipitation, and the spatial extent available for energy extraction. These determinants inherently exhibit locality-specific attributes depending on climatic conditions, latitude, local legislation, and land management practices within respective countries. Consequently, the objective of this study was to elucidate how these factors impact the predefined conditions and, by extension, the overall assessment of the technical and economic viability of hydrogen potential.

As previously indicated, the determination of hydrogen potential comes from the solar technical potential, derived through the analysis of data obtained from Atmospheric Water Stations (AWS) meeting the completeness criteria stipulated by the World Meteorological Organization (WMO). Additionally, this assessment incorporates constraints imposed by terrain inclination and land usage.

The findings revealed that with an electrolysis efficiency of 75 %, Mexico could potentially produce 2,366.33 MTon/year of hydrogen. According to IEA (IEA, 2020), the global hydrogen demand stood at 88.48 MTon/year in 2020, with an estimated increase to 230.86 MTon/year by 2030. A comparative analysis between this demand and the identified hydrogen potential indicates that Mexico's potential production could range from approximately 26 times the demand for 2020 to 10 times the demand for 2030.

The results revealed that several states possess significant potential for hydrogen production, each with capacities exceeding 100 MTon/year. Specifically, the states of Chihuahua (443.15 MTon/year), Coahuila (322.73 MTon/year), Sonora (316.04 MTon/year), Durango (186.29 MTon/year), Zacatecas (130.23 MTon/year), Baja California Sur (118.80 MTon/year), and Nuevo León (102.57 MTon/year) were identified as notable contributors to this potential. These seven states could collectively generate up to 68.45 % of the country's total hydrogen production. Situated in northern Mexico, they share an arid climate, thereby necessitating the computation of water availability to ascertain the feasibility of production. Conversely, the states located in southern regions and those with limited territorial extents exhibited the lowest hydrogen production potential. Notably, Mexico City, serving both as a state and a city, demonstrated the lowest potential with 0.69 million metric tons (MTon) per year. This was followed by Tabasco with 1.98 MTon/year, Tlaxcala with 2.10 MTon/year, Morelos with 3.39 MTon/year, and Colima with 4.36 MTon/year.

Figure 3.2 presents the hydrogen potential distribution, assuming an electrolyzer efficiency of 75 %. It is evident from the figure that the highest potential is concentrated in the northern regions. In these areas, hydrogen production density reaches up to 4,933 Ton/km$^2$. Conversely, regions where the density falls below 2,265 tons per square kilometer per year comprise only 0.01 % of the assessed territory.

In order to evaluate the impact of efficiency due to electrolyzer aging, a secondary computation was conducted assuming an efficiency of 65 %. The outcomes are presented in Table 3.2, juxtaposed with those obtained under nominal conditions. The analysis revealed a 13 % reduction in the total hydrogen output. Nevertheless, even under these circumstances, the hydrogen potential for the regions under study exceeded the 2020 demand by a factor of 23 and the 2030 demand by a factor of 9.

To calculate the effect of electrolyzer efficiency due to the ageing of the electrolyzer, a second calculation was performed with an efficiency of 65 %. The results are shown in Table 3.2 along with their comparison to nominal conditions. A 13 % reduction in the total amount

Table 3.2: Hydrogen production per state

| State | Technical Potential [TWh/year] | $\eta_{elec}$=75 % M$_{H_2}$ [MTon/year] | $\eta_{elec}$= 65 % M$_{H_2}$ [MTon/year] |
|---|---|---|---|
| Ags | 269 | 5.12 | 4.44 |
| BC | 3,336 | 63.51 | 55.04 |
| BCS | 6,241 | 118.80 | 102.96 |
| Camp | 658 | 12.53 | 10.86 |
| Chih | 23,280 | 443.15 | 384.06 |
| Chis | 1,949 | 37.10 | 32.15 |
| Coah | 16,954 | 322.73 | 279.70 |
| Col | 229 | 4.36 | 3.78 |
| CDMX | 37 | 0.69 | 0.60 |
| Dgo | 9,786 | 186.29 | 161.45 |
| Gro | 3,929 | 74.79 | 64.82 |
| Gto | 1,664 | 31.68 | 27.45 |
| Hgo | 948 | 18.05 | 15.64 |
| Jal | 3,929 | 74.79 | 64.81 |
| Mex | 811 | 15.44 | 13.39 |
| Mich | 2,599 | 49.47 | 42.87 |
| Mor | 178 | 3.39 | 2.94 |
| Nay | 541 | 10.29 | 8.92 |
| NL | 5,388 | 102.57 | 88.89 |
| Oax | 4,285 | 81.56 | 70.69 |
| Pue | 1,468 | 27.95 | 24.22 |
| Qro | 553 | 10.53 | 9.13 |
| Qroo | 621 | 11.83 | 10.25 |
| Sin | 1,033 | 19.67 | 17.05 |
| SLP | 4,969 | 94.60 | 81.98 |
| Son | 16,603 | 316.04 | 273.90 |
| Tab | 104 | 1.98 | 1.72 |
| Tamps | 3,366 | 64.08 | 55.54 |
| Tlax | 110 | 2.10 | 1.82 |
| Ver | 918 | 17.48 | 15.15 |
| Yuc | 710 | 13.52 | 11.72 |
| Zac | 6,841 | 130.23 | 112.86 |
| Ntn'l | 124,311 | 2,366.33 | 2,050.82 |

of hydrogen was found, but even in this case, there was 23 times the demand for 2020 and 9 times the demand for 2030 in the territories studied.

The impressively high potential found leads to a detailed analysis of water availability, in order to verify the feasibility of its exploitation, given the diversity of climates (arid, tropical, and temperate) in the territory studied.
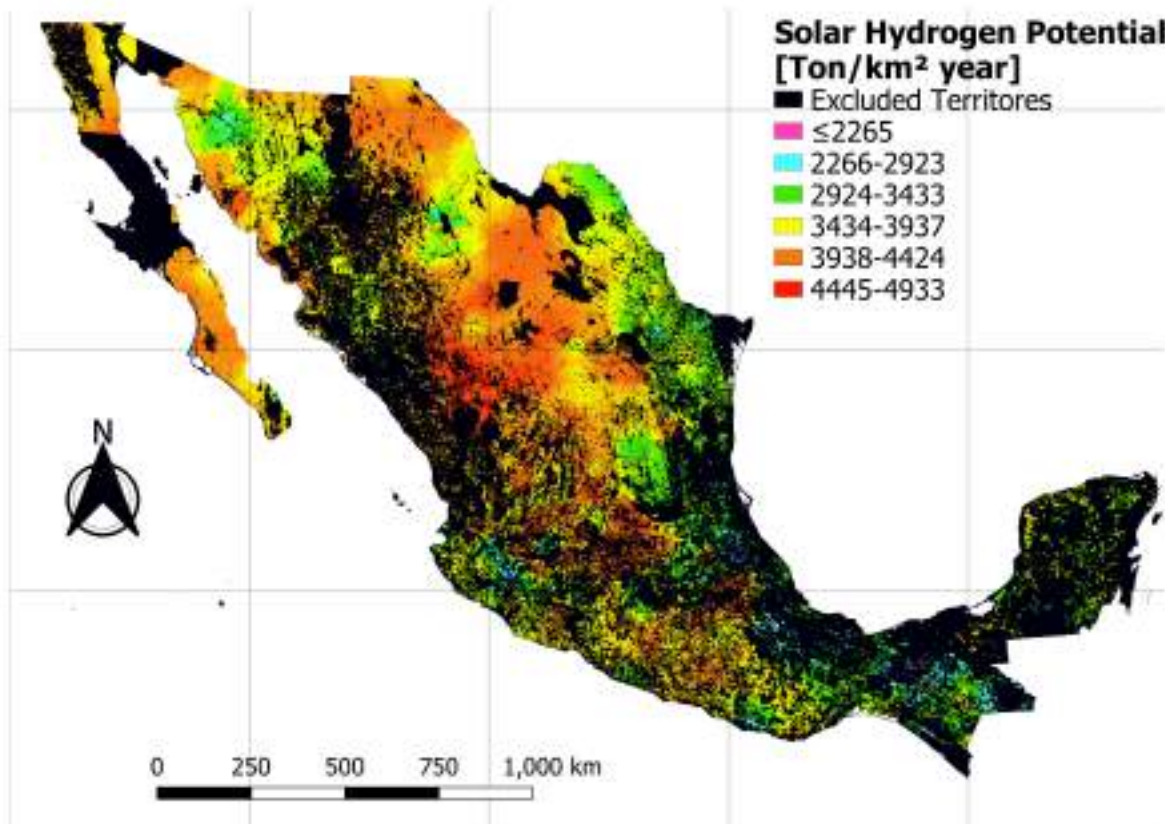


Figure 3.2: Solar hydrogen potential considering a nominal efficiency of 75 %.

### 3.2.2 Water requirements

*Country level*

As an initial step towards assessing water availability for hydrogen production, the country's annual average water precipitation was computed. It was determined that the available rainfall amounted to 445,472.23 MTon/year, calculated using 69 years of data to establish the mean. Conversely, the water required to fully exploit the hydrogen potential was deter-
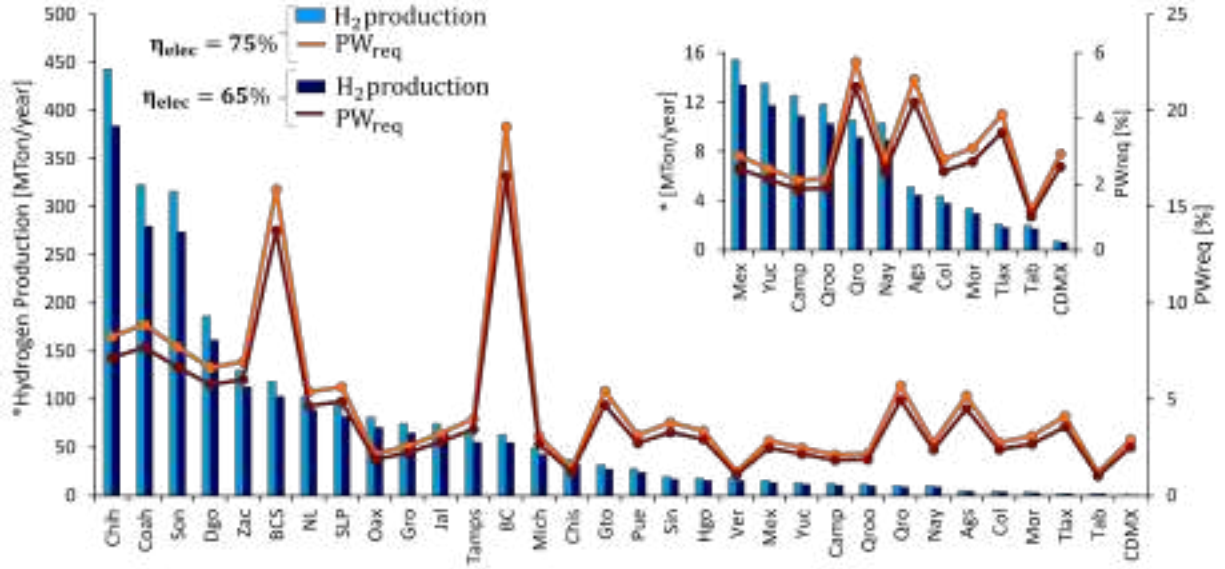
Figure 3.3: Percentage of rainfall required for total hydrogen production by federal entity.

mined to be 23,663.29 Mton/year for an electrolyzer efficiency ($\eta_{elec}$) of 75 %, and 20,508.19 Mton/year for $\eta_{elec}$ of 65 %. Thus, the water demand accounted for between 5.3 % and 4.6 % of the total available water resources.

Out of the entire area under investigation, only 38.77 % demonstrated the capacity for hydrogen production. Within this territory, a subset of 3.67 % necessitated less than 2.5 % of the available rainfall water to realize 100 % of its hydrogen potential, encompassing an area of 30,414 km$^2$, under nominal conditions of electrolyzer efficiency (75 %). Additionally, it was observed that 0.7 % of the hydrogen-producing territory demanded over 50 % of the available rainfall water, equivalent to approximately 5,869.25 square kilometers.

*State Level*

Given the intricate and site-specific nature of rainfall patterns, it is imperative to assess water availability at the local level. Consequently, the requisite and average rainfall water were computed at the state level. The outcomes of this analysis are depicted in Figure 3.3.Eleven states were identified to exceed the national average (5.3 % = PW$req$) where of water requirement for hydrogen production, with a majority located in Northern Mexico (with $\eta elec$ = 0.75 %). These states include Baja California (19.2 %), Baja California Sur

Table 3.3: Hydrogen production as function of PWreq.

| State | PWreq≤19.83 % | | | 19.83 %<Pwreq≤ 50 % | | | 50 %< Pwreq≤100 % | | |
|---|---|---|---|---|---|---|---|---|---|
| | MH$_2$ $\eta_{elec}=75\%$ [MTon/year] | MH$_2$ $\eta_{elec}=65\%$ [MTon/year] | % de LAA | MH$_2$ $\eta_{elec}=75\%$ [MTon/year] | MH$_2$ $\eta_{elec}=65\%$ [MTon/year] | % de LAA | MH$_2$ $\eta_{elec}=75\%$ [MTon/year] | MH$_2$ $\eta_{elec}=65\%$ [MTon/year] | % de LAA |
| Ags | 5.1 | 4.4 | 100 | 0.0 | 0.0 | 0 | 0.0 | 0.0 | 0 |
| BC | 14.6 | 12.6 | 23 | 41.6 | 36.1 | 65 | 7.3 | 6.4 | 12 |
| BCS | 26.9 | 23.3 | 23 | 91.1 | 78.9 | 77 | 0.8 | 0.7 | 1 |
| Camp | 12.5 | 10.9 | 100 | 0.0 | 0.0 | 0 | 0.0 | 0.0 | 0 |
| Chih | 431.3 | 373.8 | 97 | 11.6 | 10.0 | 3 | 0.3 | 0.3 | 0 |
| Chis | 37.1 | 32.2 | 100 | 0.0 | 0.0 | 0 | 0.0 | 0.0 | 0 |
| Coah | 290.6 | 251.9 | 90 | 31.9 | 27.7 | 10 | 0.2 | 0.2 | 0 |
| Col | 4.4 | 3.8 | 100 | 0.0 | 0.0 | 0 | 0.0 | 0.0 | 0 |
| CDMX | 0.7 | 0.6 | 100 | 0.0 | 0.0 | 0 | 0.0 | 0.0 | 0 |
| Dgo | 185.8 | 161.0 | 100 | 0.5 | 0.5 | 0 | 0.0 | 0.0 | 0 |
| Gro | 74.7 | 64.7 | 100 | 0.0 | 0.0 | 0 | 0.0 | 0.0 | 0 |
| Gto | 31.6 | 27.4 | 100 | 0.0 | 0.0 | 0 | 0.0 | 0.0 | 0 |
| Hgo | 18.0 | 15.6 | 100 | 0.0 | 0.0 | 0 | 0.0 | 0.0 | 0 |
| Jal | 74.8 | 64.8 | 100 | 0.0 | 0.0 | 0 | 0.0 | 0.0 | 0 |
| Mex | 15.4 | 13.4 | 100 | 0.0 | 0.0 | 0 | 0.0 | 0.0 | 0 |
| Mich | 49.5 | 42.9 | 100 | 0.0 | 0.0 | 0 | 0.0 | 0.0 | 0 |
| Mor | 3.4 | 2.9 | 100 | 0.0 | 0.0 | 0 | 0.0 | 0.0 | 0 |
| Nay | 10.3 | 8.9 | 100 | 0.0 | 0.0 | 0 | 0.0 | 0.0 | 0 |
| NL | 102.6 | 88.9 | 100 | 0.0 | 0.0 | 0 | 0.0 | 0.0 | 0 |
| Oax | 81.6 | 70.7 | 100 | 0.0 | 0.0 | 0 | 0.0 | 0.0 | 0 |
| Pue | 28.0 | 24.2 | 100 | 0.0 | 0.0 | 0 | 0.0 | 0.0 | 0 |
| Qro | 10.5 | 9.1 | 100 | 0.0 | 0.0 | 0 | 0.0 | 0.0 | 0 |
| Qroo | 11.8 | 10.3 | 100 | 0.0 | 0.0 | 0 | 0.0 | 0.0 | 0 |
| Sin | 19.7 | 17.0 | 100 | 0.0 | 0.0 | 0 | 0.0 | 0.0 | 0 |
| SLP | 94.5 | 81.9 | 100 | 0.1 | 0.1 | 0 | 0.0 | 0.0 | 0 |
| Son | 270.2 | 234.2 | 85 | 37.7 | 32.7 | 12 | 8.2 | 7.1 | 3 |
| Tab | 2.0 | 1.7 | 100 | 0.0 | 0.0 | 0 | 0.0 | 0.0 | 0 |
| Tamps | 64.1 | 55.5 | 100 | 0.0 | 0.0 | 0 | 0.0 | 0.0 | 0 |
| Tlax | 2.1 | 1.8 | 100 | 0.0 | 0.0 | 0 | 0.0 | 0.0 | 0 |
| Ver | 17.5 | 15.2 | 100 | 0.0 | 0.0 | 0 | 0.0 | 0.0 | 0 |
| Yuc | 13.5 | 11.7 | 100 | 0.0 | 0.0 | 0 | 0.0 | 0.0 | 0 |
| Zac | 130.2 | 112.9 | 100 | 0.0 | 0.0 | 0 | 0.0 | 0.0 | 0 |
| National | **2140.7** | **1855.2** | **90** | **208.8** | **181.0** | **9** | **16.8** | **14.5** | **1** |

(15.9 %), Coahuila (8.9 %), Chihuahua (8.3 %), Sonora (7.7 %), Zacatecas (7.0 %), Durango (6.7 %), Querétaro (5.7 %), San Luis Potosí (5.7 %), Guanajuato (5.4 %), and Nuevo León (5.4 %).

To elucidate water limitations at the state level, the hydrogen potential was categorized into three groups based on the percentage of rainfall water required (PW$req$). The first category comprises hydrogen potential necessitating less than 19.83 % of rainfall water (PW$req \leq$ 19.83 %). The second category encompasses potential requiring between 19.83 %

and 50 % of rainfall water (19.83 % < PW$req$ ≤ 50 %). Lastly, the third category consists of potential necessitating between 50 % and 100 % of rainfall water (50 % < PW$req$ ≤ 100 %).

90 % of the territories were found to necessitate PW$req$ ≤ 19.83 %, while 9 % required 19.83 % < PW$req$ ≤ 50 %, and only 1 % necessitated 50 % < PW$req$ ≤ 100 %. The results for each state are presented in Table 2. Additionally, a comparison between the nominal conditions ($\eta elec$ = 75 %) and the scenario with $\eta_{elec}$ = 65 % was conducted.

Indeed, only 90 % of the total hydrogen production potential was deemed feasible for exploitation while requiring less than 20 % of the total rainfall water. Any further production beyond this threshold would either significantly impact the groundwater table or necessitate additional costs for water transportation. In either scenario, a more intricate analysis involving the potential desalination of seawater and water treatment would be imperative.
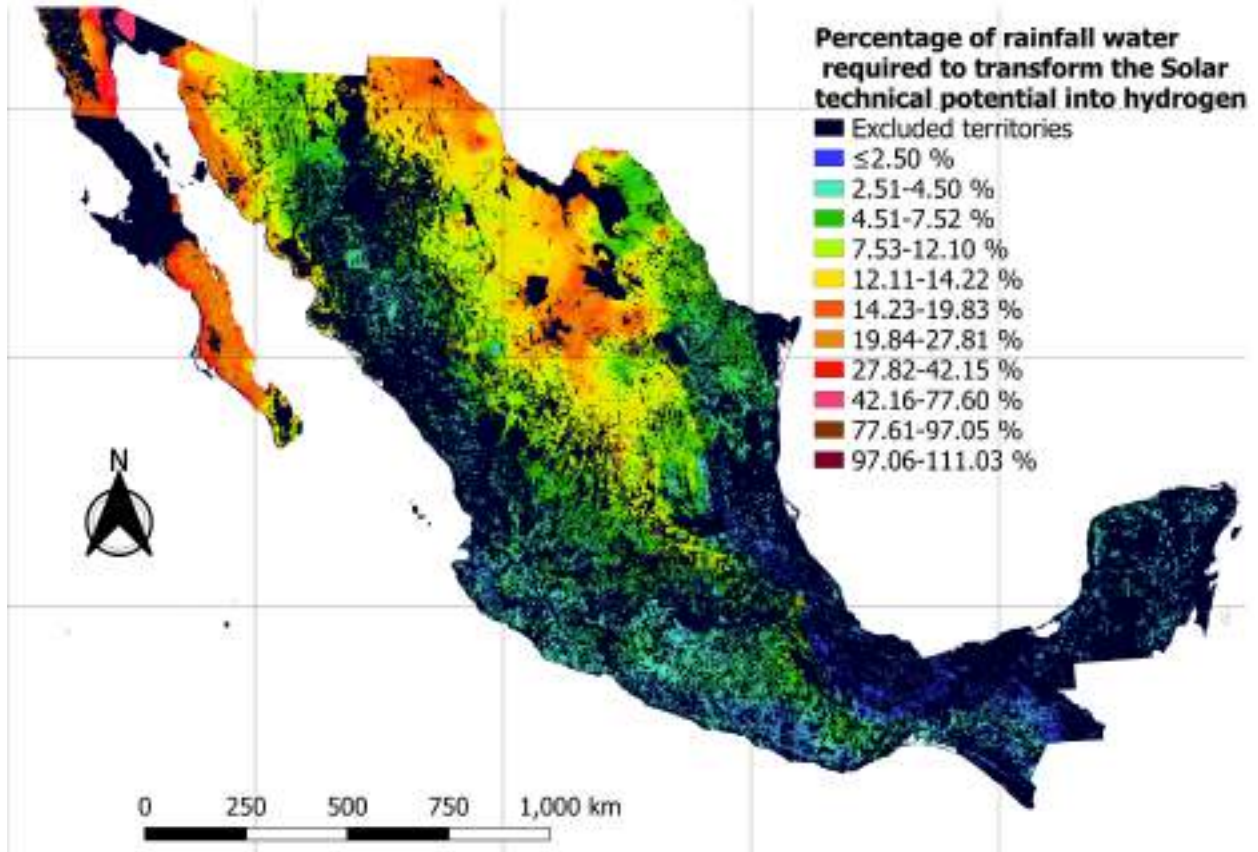


Figure 3.4: Percentage of rainfall water required for total hydrogen production. (PW$_{req}$)

*Cell level*

Local water demands were also calculated using a grid resolution of 500m × 500m. These findings are visualized in Figure 3.4, enabling the examination of regional water availability across the geographical landscape. Notably, the California Peninsula and certain regions of northern Mexico, specifically the states of Coahuila and Chihuahua, experienced constrained precipitation levels. Of particular concern, certain areas within Sonora state required more than 42.15 % of the annual precipitation.

It was also found that a community in Chih state (El Carrizo located in the province of Coyame del Sotol) requires more than 100 % of the annual precipitation to produce hydrogen that constitutes less than 0.001 % of the territory. Finally, certain areas characterized by minimal solar and hydrogen production potential exhibited significant water availability. Specifically, regions with tropical climates demonstrated low potential not attributable to solar radiation but rather to the presence of jungle areas and reserved zones.

## 3.2.3   LCOH and Sensitivity Index

The LCOH evaluation was conducted for large-scale hydrogen production across the scenarios outlined in Table 3.1, encompassing diverse electrolyzer technologies and associated costs (inclusive or exclusive of import expenses). The outcomes are depicted in Figure 3.5, considering an electrolyzer efficiency of 75 %. Two distinct operational durations were considered: i) continuous operation throughout the year and ii) operation during daylight hours.

**a) The Effect of Alkaline and PEM Electrolyzer Technology.**

In the current scenario, the most cost-effective option for large-scale hydrogen production would be the alkaline technology, with an average price of 3.37 USD/kg. Conversely, adopting PEM technology would result in a higher cost, averaging at 4.57 USD/kg. Nonetheless, both price points fall within the range proposed by the Hydrogen Council in 2021 for global prices. The transition between electrolyzer technologies precipitated an increase of up to 26.26 % in production costs. This escalation can be attributed to the reduced lifespan of PEM electrolyzers and their higher initial investment compared to alkaline counterparts.
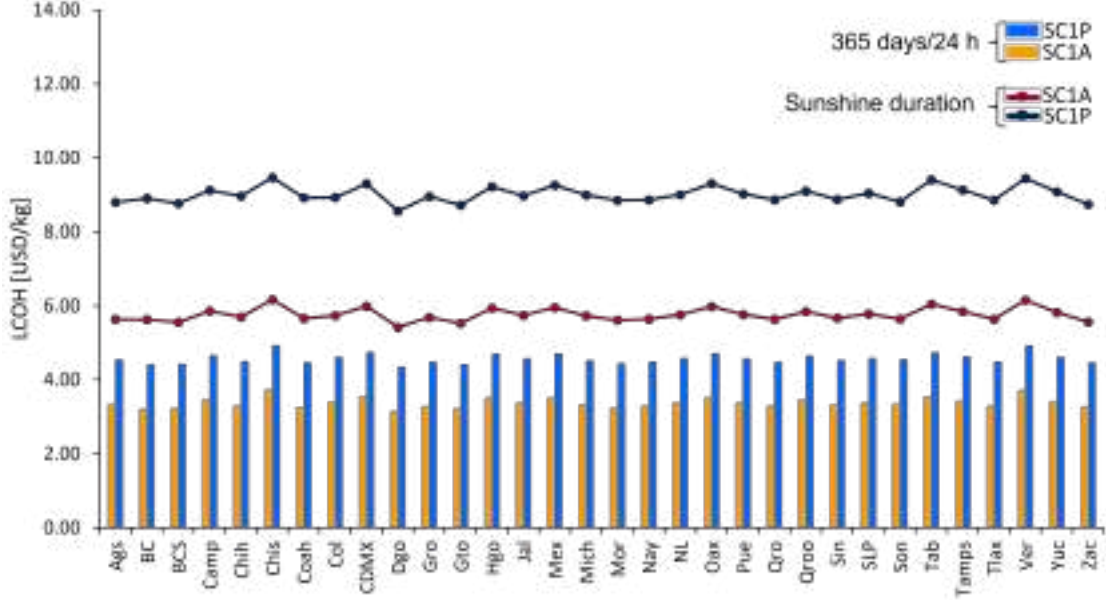
Figure 3.5: LCOH @ $\eta_{elec} = 0.75$ for the SC1A/SC1P scenarios as function of the operation.

**b)The effect of the Electrolyzer Top and energy availabilty.**

Following the computation of operation times aligned with sunshine duration, a substantial reduction in time, amounting to 63.96 % compared to continuous operation, was observed. The ten states exhibiting the highest sunshine duration annually were identified as Durango (3,338.9h), Aguascalientes (3,319.4 h), Sonora (3,314.0 h), Zacatecas (3,308.4 h), Guanajuato (3,296.6 h), Colima (3,290.3 h), Baja California Sur (3,278.2 h), Sinaloa (3,276.1 h), Tlaxcala (3,262.0 h), and Nayarit (3,261.9 h).

Despite a notable increase in production costs induced by the transition to advanced electrolyzer technology, the impact of operation times was even more pronounced. This led to a 45 % increase in price for alkaline electrolyzers and a 52 % increase for PEM electrolyzers. Consequently, prices surged to as high as 5.5 USD/kg for alkaline electrolysis and 9 USD/kg for PEM electrolysis, surpassing the international price range proposed by the Hydrogen Council.

These findings underscore the importance of incorporating complementary energy sources at production sites to extend operation times. Such measures are vital for achieving global

production prices of hydrogen and mitigating the impact of increased costs associated with prolonged operation durations.

### c) Effect of energy availability

The impact of energy availability on the LCOH was also assessed, considering variations in solar panel efficiency. Commercial silicon photovoltaic (Si-PV) modules exhibit a range of efficiencies, typically ranging from 15 % to 21 %. Our analysis revealed that employing higher efficiency modules (21 %) could result in a reduction of up to 28 % in price compared to conservative scenarios employing modules with 15 % efficiency.
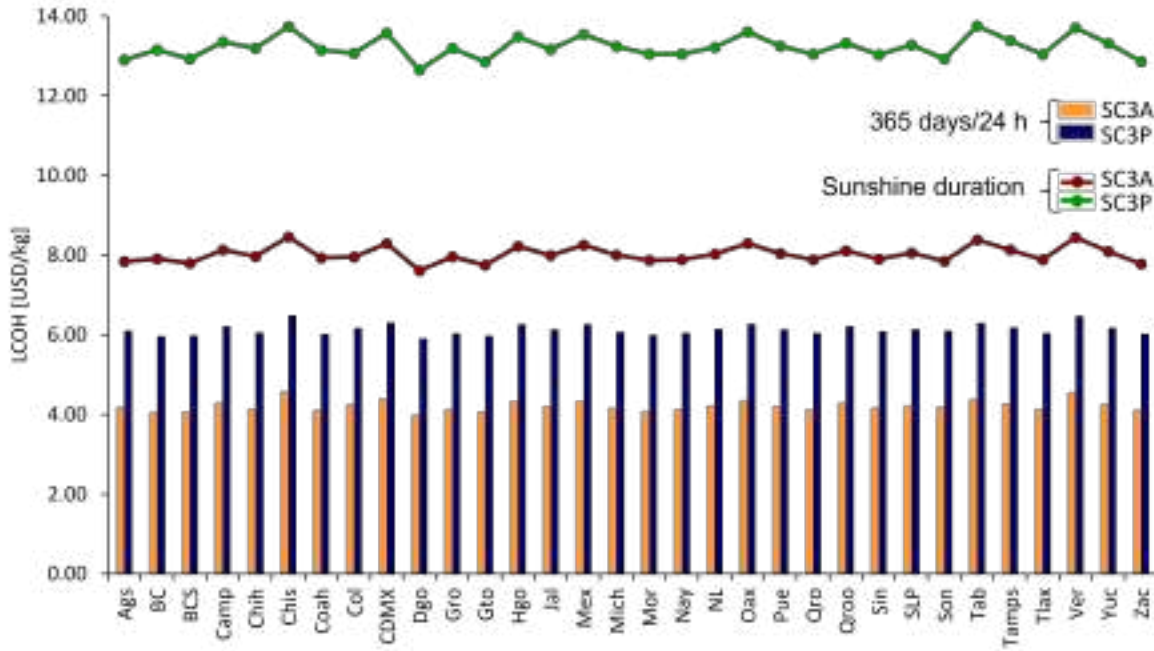


Figure 3.6: LCOH @ $\eta_{elec} = 0.75$ for the SC3A/SC3P scenaries as function of operation time.

### d) The effect of the Electrolyzer importing and transportation costs.

The analysis scenario becomes more intricate when importing costs are factored in. Up to 60 % of the increase in electrolyzer costs can be attributed to importing and transportation fees. The outcomes of this scenario are depicted in Figure 3.6. The impact of importing and transportation costs on the LCOH was found to be significant. An increase of up to 27 % was observed in the national production price for PEM technology, while a 22 % increase

was noted for alkaline electrolyzers. These cost escalations underscore the importance of ensuring access to low-duty prices or implementing suitable technology development policies to ensure the sustainability of hydrogen.

### e) Effect of the electricity cost

The analysis of the solar technical potential across the investigated locations yielded electricity costs ranging from 0.03 to 0.05 USD/kWh. Notably, the ten states exhibiting the most economically favourable electricity prices were identified as follows: Dgo (0.033 USD/kWh), BC (0.035 USD/kWh), BCS (0.035 USD/kWh), Gto (0.035 USD/kWh), Mor (0.035 USD/kWh), Chih (0.036 USD/kWh), Coah (0.036 USD/kWh), Gro (0.036 USD/kWh), Nay (0.036 USD/kWh), and Qro (0.036 USD/kWh).

These disparities in electricity costs resulted in a national-level sensitivity index of up to 28 % for alkaline electrolyzers and 20 % for PEME systems. Such variations can be attributed to discrepancies in electrolyzer acquisition and operational expenses, which are contingent upon the specific electrolyzer technology utilized.

It was observed that states characterized by lower LCOH values were influenced by a confluence of three primary factors: reduced electricity expenditures, heightened energy availability, and prolonged operational durations. Specifically, the ten states exhibiting lower hydrogen prices for SC1A (alkaline electrolyzers) were identified as: Dgo (3.15-5.40 USD/kg), BC (3.21-5.60 USD/kg), Gto (3.22-5.72 USD/kg), BCS (3.23-5.80 USD/kg), Mor (3.24-5.71 USD/kg), Zac (3.27-5.74 USD/kg), Coah (3.27-85.85 USD/kg), Gro (3.28-5.72 USD/kg), Tlax (3.29-5.76 USD/kg), and Nay (3.29-5.80 USD/kg).

In the case of PEM technology (SC1P), analogous trends in LCOH were observed, wherein states with lower prices remained the same but experienced escalated costs: Dgo (4.35-8.48 USD/kg), BC (4.41-8.89 USD/kg), Gto (4.42 - 8.70 USD/kg), BCS (4.43 - 8.75 USD/kg), Mor (4.44 - 8.80 USD/kg), Zac (4.47 - 8.95 USD/kg), Coah (4.47- 8.95 USD/kg), Gro (4.48 - 8.97 USD/kg), Tlax (4.49 - 6.98 USD/kg), and Nay (4.49 - 8.98 USD/kg).
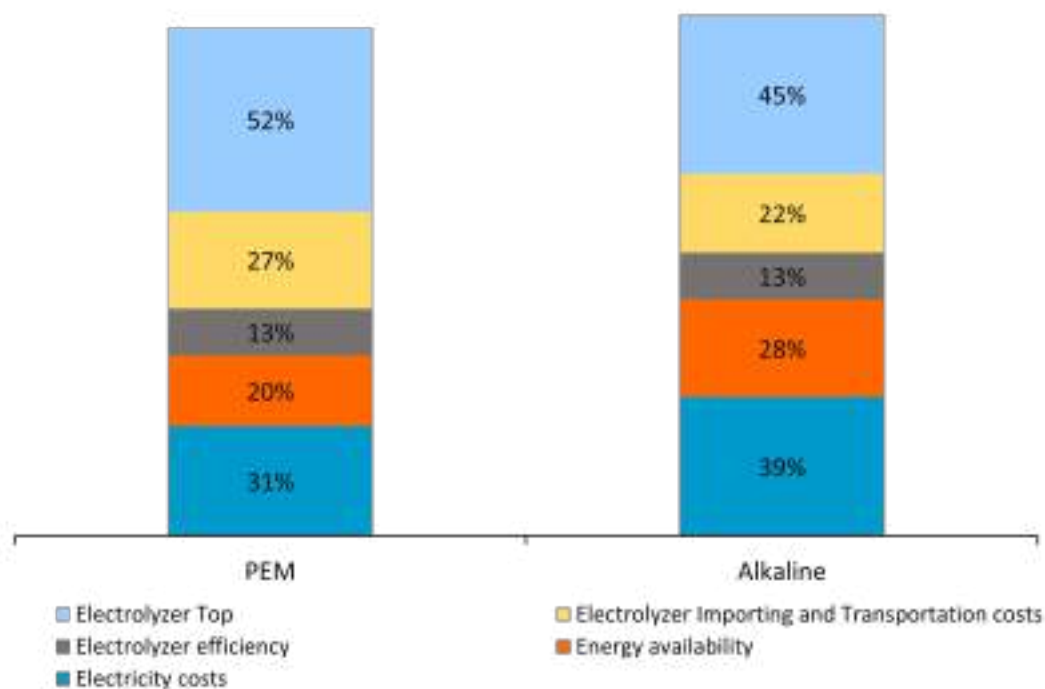
Figure 3.7: Índice de sensibilidad para parámetros involucrados en LCOH considerando horas de sol

The consideration of importing costs notably augmented the LCOH, leading to a significant increase. The ten states exhibiting lower hydrogen prices under this revised assessment were: Dgo (3.95-7.40 USD/kg), BC (4.00-7.95 USD/kg), Gto (4.00-7.90 USD/kg), BCS (4.05-7.90 USD/kg), Mor (4.10-7.90 USD/kg), Zac (3.27-5.74 USD/kg), Coah (3.27-85.85 USD/kg), Gro (3.28-5.72 USD/kg), Tlax (4.15-7.85 USD/kg), and Nay (4.12-7.90 USD/kg), with respect to alkaline electrolysis.

For PEM electrolyzers, incorporating transportation and importation costs resulted in the lowest LCOH values observed in the following states: Dgo (5.85-12.85 USD/kg), BC (6.00-13.30 USD/kg), Gto (6.00-12.65 USD/kg), BCS (7.90-12.95 USD/kg), Mor (5.90-13.00 USD/kg), Zac (5.90-12.70 USD/kg), Coah (6.00-13.00 USD/kg), Gro (6.00-13.07 USD/kg), Tlax (6.00-12.85 USD/kg), and Nay (4.12-7.90 USD/kg).

To elucidate the discerned patterns in the LCOH, a sensitivity analysis encompassing five variables—namely, Electricity costs, energy availability, electrolyzer efficiency, electrolyzer Top, and electrolyzer Importing and Transportation costs—was conducted. The outcomes of this analysis are depicted in Figure 3.7, delineating their dependencies relative to the type of electrolyzer employed.

## 3.2.4 Summary and Highlights

The findings showed notable disparities in the proportion of rainfall water requisite at various geographical scales, spanning national, state, and local levels. While the national average indicates a demand for less than 5.3 % of annual rainfall water, certain states, encompassing 9 % of the country, necessitate up to 50 %, with approximately 1 % of Mexican territory earmarked for hydrogen production requiring more than 50 % of annual rainfall water. This underscores the imperative of localized assessments for large-scale hydrogen production endeavours, as national hydrogen production initiatives may necessitate the establishment of water transportation infrastructure, a factor pivotal in production cost considerations.

Through a sensitivity analysis, we discerned that hydrogen production costs are primarily influenced by electricity costs, energy availability, and notably, electrolyzer operation time, constituting up to 52 % of total costs. These findings underscore the significance of integrating solar hydrogen production with other energy sources to mitigate overall production expenses.

Additionally, our findings underscored the growing significance of electrolyzer importing and transportation costs, particularly evident in scenarios featuring lower electrolyzer operation times. In such contexts, the relative impact of energy availability and electricity costs diminishes in comparison. This underscores the pivotal role of importing and transportation costs as a significant bottleneck in production, necessitating careful consideration in realistic estimations. Given that countries with high solar hydrogen potential may not necessarily be technology producers, it becomes imperative for international agencies to devise policies supporting scientific advancement and technology development to achieve global hydrogen

price targets.

Production prices as low as 3.15 USD/kg and 4.41 USD/kg for alkaline and PEM electrolysis, respectively, were identified under a 24-hour operation regime. Consequently, alkaline technology emerges as economically more viable due to its lower investment costs and longer lifespan. Notably, utilizing alkaline technology could lead to prices within the range projected by the IEA for 2021 and the IRENA for 2020. However, if hydrogen production is confined solely to daylight hours, the reduced prices were calculated as 5.41 USD/kg for alkaline electrolysis and 8.56 USD/kg for PEM electrolysis.

# Chapter 4

# Solar $H_2$ Production. Part B: Decentralized Scenario

This section showcases the potential for solar hydrogen production in a decentralized scenario, specifically focusing on urban settlements within the country. Additionally, production costs are assessed through the utilization of the LCOH, water requirements are evaluated, and capacities to meet energy demand in the transportation sector are analyzed.

The utilization of geospatial analysis techniques in assessing the potential for hydrogen production from renewable resources constitutes a fundamental tool in energy projects. However, it is common to observe a systematic exclusion of urban settlements from analysis within the established geographical constraints in many of these studies [74]. This exclusion arises from various methodological and practical considerations. On one hand, it stems from the interest in centralized, large-scale hydrogen and energy production. On the other hand, it is influenced by the intrinsic complexity of urban environments, characterized by dense networks of infrastructure and human activities, which could impede the deployment of renewable sources. Nevertheless, excluding urban settlements presents a significant limitation in the comprehensive understanding of energy and hydrogen production potential. Rather than transporting them from remote locations to consumption centres, energy and hydrogen could be generated and consumed locally. Therefore, it is crucial to study urban settlements
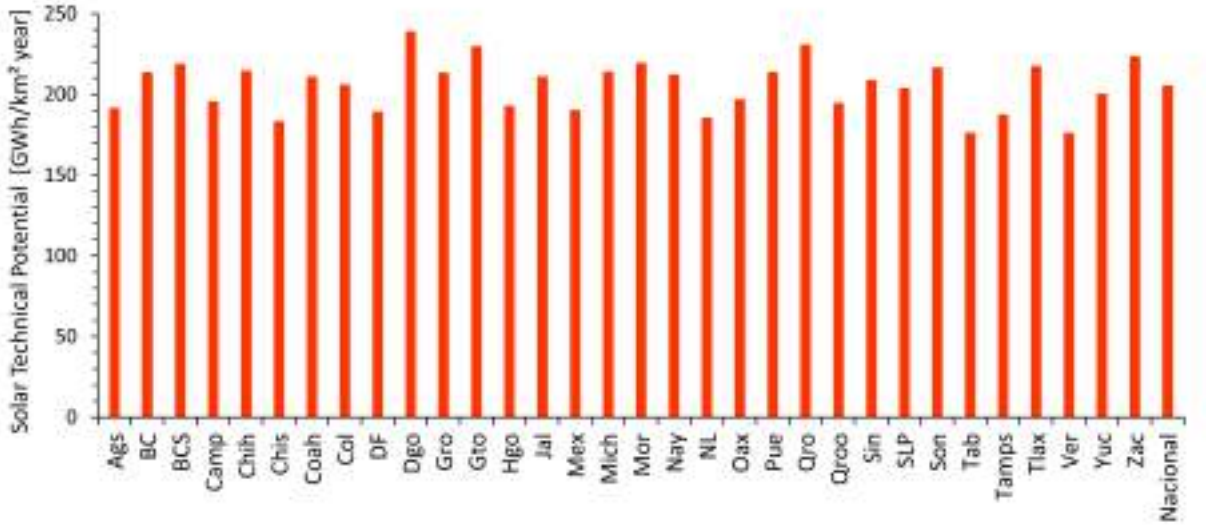
Figure 4.1: Technical Solar Potential in Urban Settlements of Mexico.

separately to fully grasp their potential contribution to energy and hydrogen production.

Several authors ([78], [79], [80], [81]) have demonstrated that urban areas present significant opportunities and capabilities for energy harvesting and subsequent hydrogen production. Therefore, this study evaluates the technical and economic potential of $H_2$ production in Mexican cities, analyzing its impact on transportation.

## 4.1 Cities and Solar Technical Potential

It is well-known that Mexico boasts abundant renewable energy resources owing to its geographical location, notably rich solar radiation. The assessment of solar potential was conducted according to [73] utilizing data from 1242 automatic weather stations for horizontal global irradiance, following the data integrity criteria of the World Meteorological Organization (WMO) at daily, monthly, and annual levels [72].

The geographical locations for solar energy capture (urban settlements) were selected in accordance with the Territorial Ordinance established by INEGI [82], taking into account an effective available area factor of the city. In other words, this study analyzes a scenario
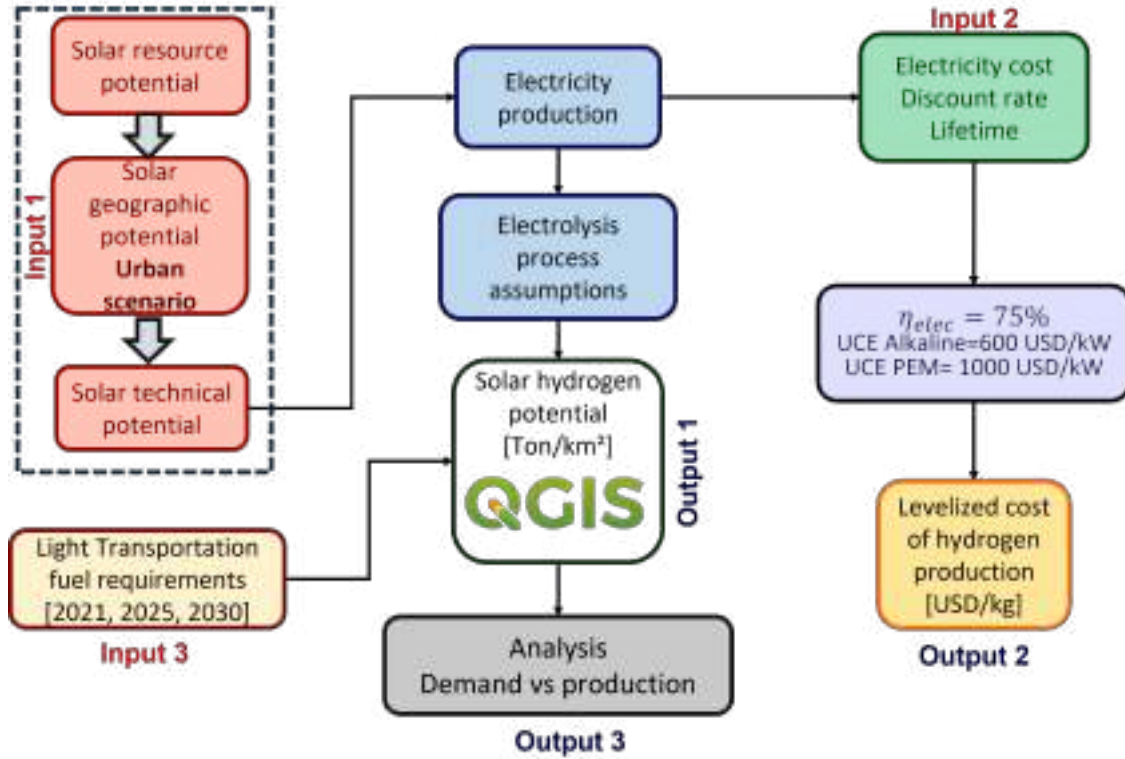
Figure 4.2: General Methodology

of distributed generation, assuming the installation of photovoltaic panels on the roofs of houses and buildings. Protected areas, archaeological sites, gas stations, recreational areas, water parks, entertainment facilities, airports, ports, industrial areas, oil pipelines, and gas pipelines that may intersect with some cities were not considered suitable areas for the installation of photovoltaic panels. Additionally, only 10 % of the resulting area was considered as the Effective Available Area (EAA) for energy collection, according to [73].

For the computation of the technical potential, Silicon solar panels with a nominal efficiency of 17 % were considered. For the assessment of solar potential, the nominal efficiency of the panels was multiplied by various losses due to power electronics, shading, dust accumulation at connection points, and losses in cables according to [73]. The technical potential of the solar resource was used to calculate hydrogen production. The data were processed in raster format with a spatial resolution of 500 m × 500 m.
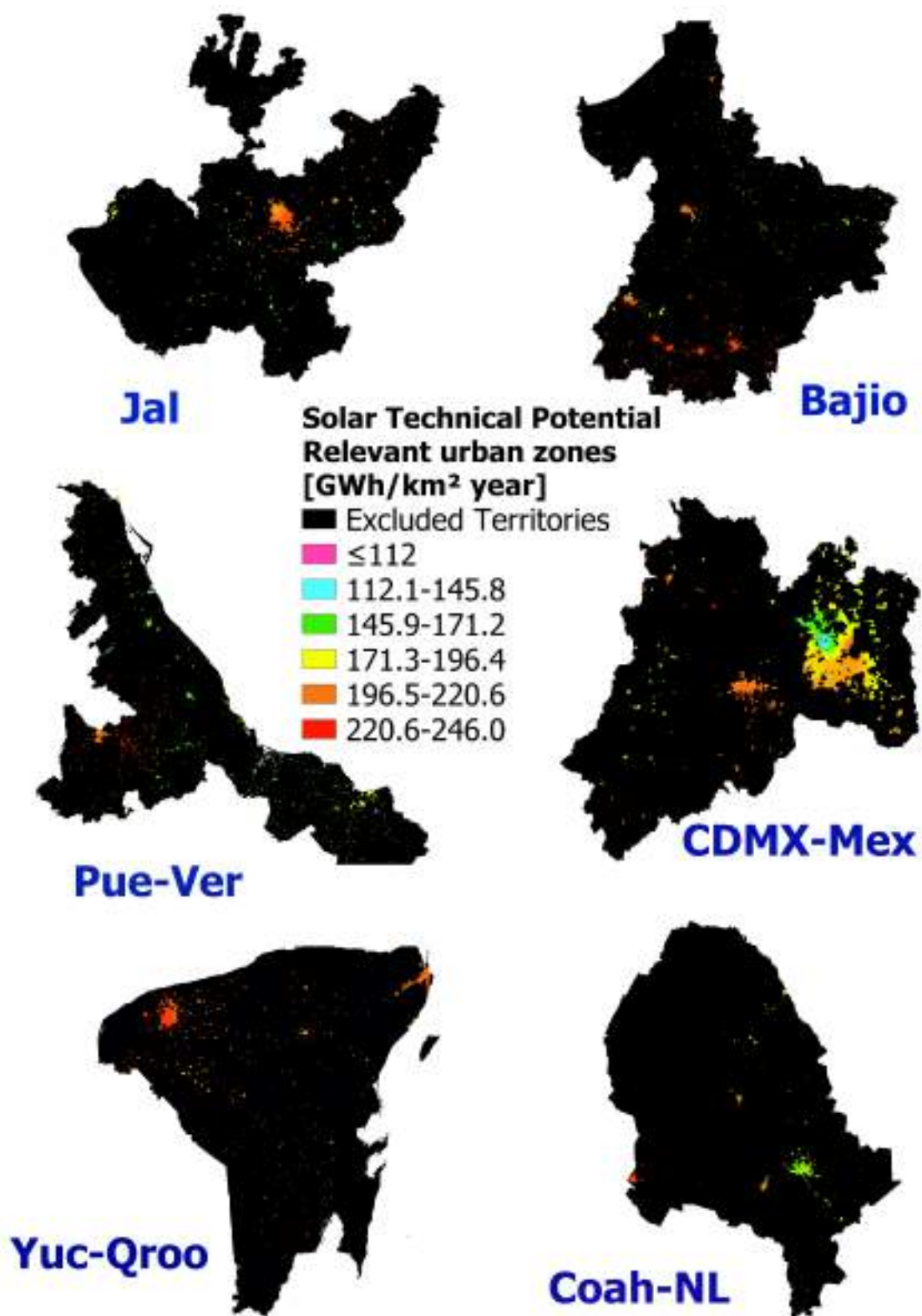
Figure 4.3: Solar Technical Potential of six significant urban areas of Mexico

The analysis of this study considers urban settlements within the 32 federal entities of Mexico mentioned in the previous chapter. As depicted in Figure 4.1, the available energy at the state level varies between 180 GWh/km$^2$ and 240 GWh/km$^2$ depending on the region. Additionally, to examine the geographical distribution of solar hydrogen potential, six significant zones were identified for illustrative purposes, coinciding with the regions of highest economic activity in the country according to INEGI (Figure 4.3) [83]. This allows for a detailed understanding of the amount of energy available at the local level (cell).

### 4.1.1 Urban Hydrogen Production Potential

The assessment of the hydrogen production potential was conducted following the methodology outlined in Figure 4.2. The mass of hydrogen ($M_{H_2}$) in Ton/km$^2$ year was calculated based on the solar technical potential using Equation 4.1 [74].

$$M_{H_2} = \frac{\eta_{elec} E_{pvs}}{HHV_{H_2}} \tag{4.1}$$

where $HHV_{H_2}$ represents the Higher Heating Value of hydrogen (39.4 kWh/kg), $\eta_{elec}$ denotes the electrolyzer efficiency, and $E_{pvs}$ signifies the technical potential or the energy supplied by the photovoltaic system in kWh/km$^2$ year. The quantity of H$_2$ per unit area was calculated for the selected territory using map algebra in QGIS, which is an open-source software useful for processing geospatial data.

### 4.1.2 Toward the substitution of gasoline with Hydrogen

The Crude Oil and Petroleum Products Prospective outlined in [84] estimates that from 2021 to 2030, the energy demand for light transportation will increase by approximately 20 % due to a growing population and the sustained expansion of the vehicle fleet. In contrast, gasoline production in Mexico has been declining [84]. In 2018, approximately 8/9 parts of gasoline were imported. These facts underscore the significance of considering alternative options, such as the utilization of hydrogen in vehicles.

The hydrogen demand stemming from transportation was estimated based on the total gasoline consumption in Mexico by light vehicles, which are predominantly utilized in urban areas. The gasoline consumption ($G_c$) for the years 2021, 2025, and 2030 was estimated as 876.5, 979.4, and 1039.5 million barrels per day (Mbd), respectively. The total chemical energy (TCE) obtained from the fuel is given by:

$$\text{TCE} = G_c \cdot LHV_g \tag{4.2}$$

where LHV$g$ represents the lower heating value of gasoline (5269 MJ/bl) [85]. Additionally, considering an engine efficiency ($\eta engine_{ci}$) of 25 %, the mechanical energy (ME) required in the vehicle is given by:

$$\text{ME} = TCE \cdot \eta_{mot_{ci}} \tag{4.3}$$

If the mechanical energy were to be supplied by an electric motor, the required energy (EE$v$) in MWh/year would be described according to Equation 4.4, where the motor ($\eta mot_{elec}$) and power electronics ($\eta_{conv}$) efficiencies are assumed to be 90 %.

$$EE_v = \frac{ME}{\eta_{mot_{elec}} \eta_{conv}} \tag{4.4}$$

Subsequently, the amount of hydrogen demanded to meet the energy requirements of the light transport sector was obtained through the relationship between EE$v$ and the $LHV_{H_2}$, utilizing the equation below:

$$MD_{H_2} = \frac{EE_v}{LHV_{H_2}} \tag{4.5}$$

In Equation 4.5, $LHV_{H_2}$ represents the lower heating value of hydrogen (33.33 kWh/kg).

## 4.2 Results: Urban hydrogen potential

The results demonstrated that:

1. The solar hydrogen potential across all urban regions in Mexico was assessed to be 9.39 MTon/year, a capacity capable of meeting the 2021 hydrogen demand in Mexico up to 42.6 times.

2. Roughly 46.1 %, 51.6 %, and 54.7 % of urban hydrogen production could potentially replace the gasoline needed for light transportation in 2021, 2025, and 2030, respectively. This substitution could result in the avoidance of approximately 124.38 million tons per year (MTon/year) of $CO_2$ emissions, accounting for approximately 23 % of the total transportation-related emissions in Mexico.

3. Spring and summer emerged as the seasons characterized by the most notable solar hydrogen production, with monthly production ranging between 0.52 and 0.81 MTon.

4. The LCOH was estimated to range between 6.25 USD/kg and 9.50 USD/kg for Alkaline and PEM technologies, respectively.

5. The water footprint associated with hydrogen production in urban areas is negligible.

### 4.2.1 Annual hydrogen production

As per the proposed methodology, the hydrogen potential in urban areas of Mexico was evaluated considering an electrolyzer efficiency of 75 %. The mass of hydrogen production per state is presented in Table 4.1.

It was determined that all urban areas in Mexico could potentially generate 9.39 MTon/year of solar hydrogen, assuming an EAA of 10 % from the total urban settlement surface. According to [86], in 2021, Mexico required approximately 0.2 MTon of hydrogen, the majority of which, 98.6 %, was provided by PEMEX through oil and gas reforming processes. Therefore, by harnessing hydrogen in urban areas, it would be feasible to meet this demand 42.6
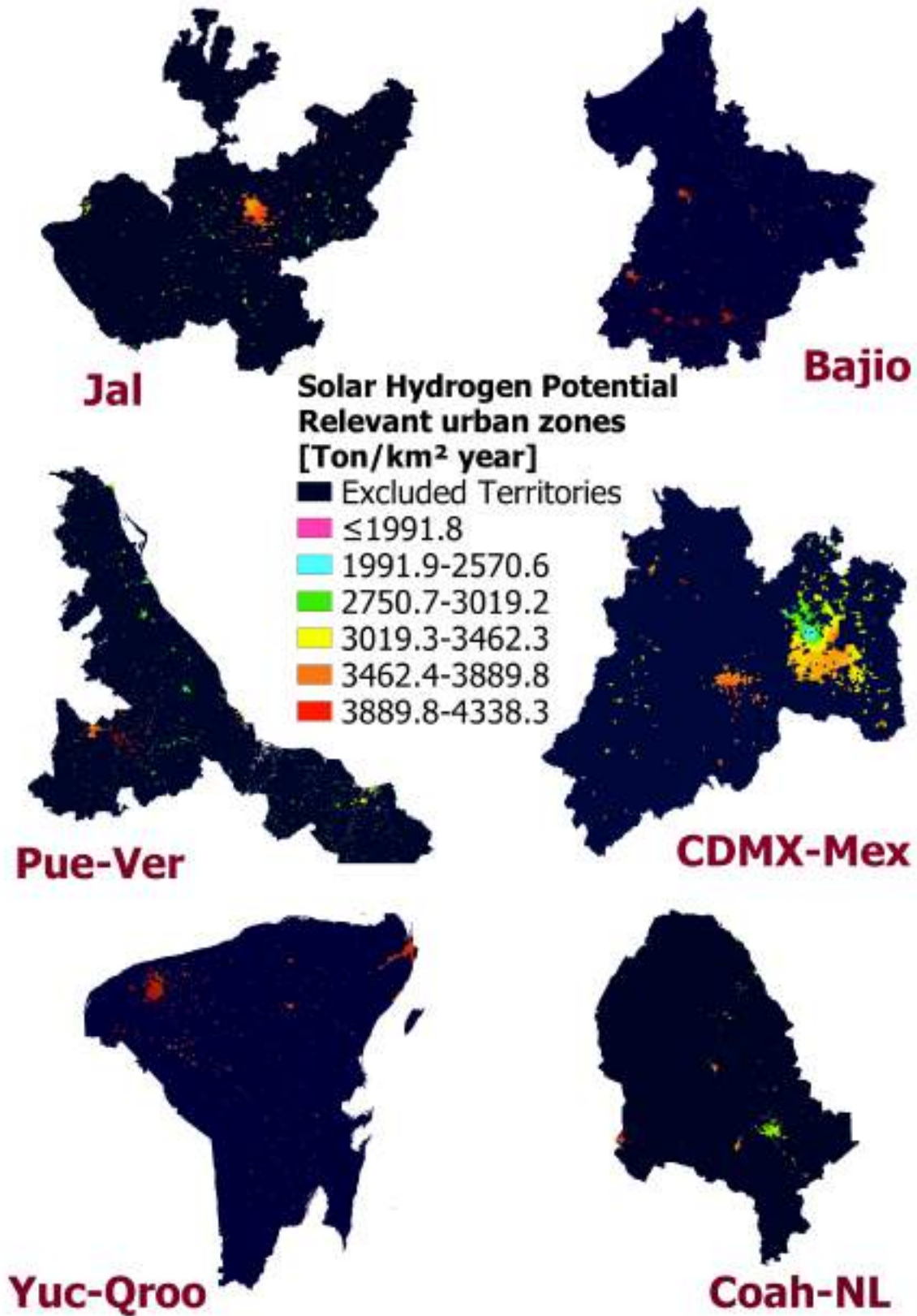
Figure 4.4: The Hydrogen Production Potential of Six Major Urban Areas in Mexico $\eta_{elec}$=75 %

times, resulting in a reduction in the utilization of gray hydrogen. Table 4.1 displays the states with the highest hydrogen production potential, namely Chih (0.65 MTon/year), Jal (0.64 MTon/year), Sin (0.49 MTon/year), BC (0.47 MTon/year), and Ver (0.47 MTon/year).

Conversely, the states with the lowest production potential (less than 0.13 MTon/year) included Col (0.08 MTon/year), Ags (0.09 MTon/year), Tab (0.10 MTon/year), Qro (0.12 MTon/year), and BCS (0.12 MTon/year).

Table 4.1: Urban hydrogen production per federal entity and the corresponding LCOH

| | | | | | Sunshine duration effect | | | |
| | | | | | Min | | Mean | |
| State | Urban Technical Potential [TWh/año] | H$_2$ Potencial M$_{H_2}$ [MTon/año] | Electricity cost [USD/kWh] | Sunshine duration (min) [h/año] | Sunshine duration (mean) [h/año] | LCOH Alkaline [USD/kg] | LCOH PEM [USD/kq] | LCOH Alkaline [USD/kg] | LCOH PEM [USD/kg] |
|---|---|---|---|---|---|---|---|---|---|
| Ags | 4.79 | 0.09 | 0.052 | 3,133.7 | 3,319.4 | 6.62 | 9.97 | 6.40 | 9.57 |
| BC | 24.84 | 0.47 | 0.046 | 3,054.2 | 3,207.7 | 6.42 | 9.86 | 6.23 | 9.51 |
| BCS | 6.23 | 0.12 | 0.044 | 3,074.1 | 3,278.2 | 6.27 | 9.69 | 6.02 | 9.23 |
| Camp | 7.63 | 0.15 | 0.048 | 2,875.5 | 3,220.3 | 6.79 | 10.44 | 6.33 | 9.60 |
| Chih | 34.40 | 0.65 | 0.046 | 2,969.6 | 3,220.4 | 6.52 | 10.06 | 6.20 | 9.46 |
| Chis | 13.64 | 0.26 | 0.052 | 2,891.7 | 3,188.8 | 6.97 | 10.60 | 6.57 | 9.87 |
| Coah | 16.96 | 0.32 | 0.046 | 2,871.3 | 3,225.1 | 6.67 | 10.34 | 6.21 | 9.47 |
| Col | 4.40 | 0.08 | 0.046 | 3,182.5 | 3,290.3 | 6.25 | 9.55 | 6.13 | 9.32 |
| CDMX | 10.70 | 0.20 | 0.053 | 3,068.7 | 3,182.0 | 6.74 | 10.17 | 6.60 | 9.91 |
| Dgo | 9.97 | 0.19 | 0.041 | 3,018.2 | 3,338.9 | 6.20 | 9.68 | 5.81 | 8.96 |
| Gro | 12.39 | 0.24 | 0.045 | 3,041.4 | 3,214.8 | 6.36 | 9.82 | 6.14 | 9.42 |
| Gto | 20.97 | 0.40 | 0.043 | 3,124.3 | 3,296.6 | 6.14 | 9.51 | 5.94 | 9.13 |
| Hgo | 8.55 | 0.16 | 0.051 | 2,998.5 | 3,197.7 | 6.73 | 10.23 | 6.47 | 9.76 |
| Jal | 33.77 | 0.64 | 0.046 | 3,018.5 | 3,251.5 | 6.48 | 9.96 | 6.19 | 9.42 |
| Mex | 21.96 | 0.42 | 0.053 | 2,943.8 | 3,181.1 | 6.92 | 10.49 | 6.61 | 9.91 |
| Mich | 23.22 | 0.44 | 0.046 | 2,932.5 | 3,214.5 | 6.56 | 10.15 | 6.20 | 9.47 |
| Mor | 6.62 | 0.13 | 0.044 | 3,083.6 | 3,245.8 | 6.29 | 9.70 | 6.09 | 9.33 |
| Nay | 11.61 | 0.22 | 0.045 | 2,942.3 | 3,261.9 | 6.50 | 10.08 | 6.10 | 9.32 |
| NL | 20.79 | 0.40 | 0.052 | 3,020.5 | 3,238.6 | 6.75 | 10.24 | 6.48 | 9.73 |
| Oax | 17.07 | 0.32 | 0.050 | 2,824.5 | 3,164.7 | 6.95 | 10.68 | 6.49 | 9.81 |
| Pue | 17.63 | 0.34 | 0.046 | 2,894.4 | 3,228.1 | 6.64 | 10.27 | 6.21 | 9.46 |
| Qro | 6.38 | 0.12 | 0.042 | 3,228.1 | 3,259.9 | 6.00 | 9.26 | 5.96 | 9.19 |
| Qroo | 9.84 | 0.19 | 0.048 | 2,939.6 | 3,228.7 | 6.68 | 10.26 | 6.31 | 9.57 |
| Sin | 25.93 | 0.49 | 0.046 | 3,048.2 | 3,276.1 | 6.42 | 9.87 | 6.14 | 9.35 |
| SLP | 12.16 | 0.23 | 0.047 | 2,996.1 | 3,219.2 | 6.54 | 10.05 | 6.26 | 9.53 |
| Son | 21.71 | 0.41 | 0.044 | 3,053.7 | 3,314.0 | 6.33 | 9.77 | 6.02 | 9.19 |
| Tab | 5.13 | 0.10 | 0.053 | 2,811.9 | 3,131.1 | 7.11 | 10.85 | 6.66 | 10.02 |
| Tamps | 23.01 | 0.44 | 0.050 | 2,868.6 | 3,204.0 | 6.88 | 10.54 | 6.43 | 9.71 |
| Tlax | 1.97 | 0.04 | 0.046 | 3,000.4 | 3,262.0 | 6.51 | 10.01 | 6.18 | 9.40 |
| Ver | 24.74 | 0.47 | 0.054 | 2,969.0 | 3,194.1 | 6.97 | 10.51 | 6.68 | 9.97 |
| Yuc | 20.52 | 0.39 | 0.047 | 3,026.7 | 3,219.2 | 6.53 | 10.00 | 6.28 | 9.55 |
| Zac | 13.76 | 0.26 | 0.044 | 3,164.9 | 3,308.4 | 6.18 | 9.50 | 6.01 | 9.19 |
| Ntn'l | 493 | 9.39 | 0.047 | 3,002.2 | 3,237.0 | 6.54 | 10.04 | 6.25 | 9.50 |

It is crucial to highlight that these potentials are strongly influenced by the size of the total urban areas in each state. For instance, despite its abundant solar resource (220 GWh/km$^2$), BCS is among the states with the lowest potential due to its cities' small total surface area of 228 km$^2$. In contrast, Ver exhibits one of the lowest solar potentials (180 GWh/km$^2$); however, it boasts one of the highest hydrogen production figures owing to its large urban area surface of 1,385 km$^2$.

Table 4.2: Solar Hydrogen Production in Selected Mexican Cities.

| City | Solar Technical Potential [GWh/km$_2$] | Energy Production [TWh/year] | Hydrogen Production [Mton/year] |
|---|---|---|---|
| Aguascalientes | 187.6 | 5.57 | 0.05 |
| Cancún | 198.7 | 8.22 | 0.06 |
| Ciudad de México | 188.2 | 23.99 | 0.20 |
| Ciudad Juárez | 210.4 | 13.39 | 0.12 |
| Guadalajara | 224.6 | 8.54 | 0.08 |
| Guanajuato | 188.9 | 1.40 | 0.01 |
| Mérida | 207.9 | 14.19 | 0.13 |
| Monterrey | 178.8 | 8.76 | 0.07 |
| Playa del Carmen | 181.9 | 2.35 | 0.01 |
| Puebla | 218.9 | 6.81 | 0.06 |
| Querétaro | 233.2 | 6.50 | 0.06 |
| Saltillo | 211.6 | 5.98 | 0.06 |
| San Luis Potosí | 219.7 | 7.00 | 0.07 |
| Tijuana | 211.4 | 17.34 | 0.16 |
| Toluca | 209.4 | 4.90 | 0.05 |
| Xalapa | 177.0 | 2.88 | 0.03 |

Figure 4.4 illustrates the geographical distribution of hydrogen production. It is observed that regions with the highest energy availability yield the most substantial hydrogen production per unit of area (Figure 4.3). This elucidates why Bajio, Yuc-Qroo, and Jal exhibit the highest production levels (ranging from 3,889.8 to 4,338.3 Ton/km$^2$ year) in areas where energy production exceeds 200 GWh/km$^2$.

According to INEGI [87], the most significant cities in Mexico, based on their population, are listed in Table 4.2. CDMX stands as the largest city in the country and, consequently, possesses the most considerable potential for hydrogen production (0.20 MTon/year), followed by Tijuana (0.16 MTon/year) and Mérida (0.13 MTon/year). The production capacity of these cities represents 100 %, 34 %, and 33.3 %, respectively, of what all urban settlements in CDMX, BC, and Yucatan could generate (ver Tabla 4.2).

These cities hold critical significance due to their dense population and economic activities. They have the potential to serve as primary energy sources for their respective states; for instance, the city of Queretaro could meet 50 % of all the energy requirements of urban

settlements in Qro. These findings hold significant implications for governmental decision-making, providing guidance on identifying cities that could potentially evolve into "hydrogen cities".

These results are noteworthy as the aforementioned cities harbour significant industrial, residential, and service activities. The adoption of solar hydrogen could prove beneficial in mitigating $CO_2$ emissions, as the industrial hydrogen demand of the country could potentially be met by just one state with a production capacity of at least 0.3 MTon/year. The substantial potential identified suggests the feasibility of exploring other hydrogen applications in the near future, such as light mobility, which is the predominant mode of transportation in urban areas.

Additionally, we assessed the hydrogen potential with and without gas stations considered as solar harvesting areas to underscore the importance of including these locations. It was found that the inclusion of gas stations resulted in a mere 0.1 % increase in hydrogen production; thus, their contribution is marginal. The decision to include or exclude gas stations may be subject to debate. However, given that most assessments in the literature have omitted such areas, we opted to exclude them to ensure the comparability of our results.

## 4.2.2   Solar hydrogen for transportation in Mexico

The quantity of hydrogen necessary to replace all gasoline consumption in Mexico was calculated using Eq. 4.5 and is presented in Table 4.3. By 2025, it is estimated that hydrogen requirements will amount to approximately 4.84 MTon/year, while by 2030, this figure could increase to 5.14 MTon/year. Notably, the total H$_2$ produced by urban settlements in Mexico could meet such demands, as only 40 % and 52 % of the total generated hydrogen would be necessary to cover these requirements.

The potential reduction in $CO_2$ emissions resulting from gasoline substitution is delineated in Table 4.3. Up to 124.38 MTon/year of $CO_2$ emissions could be mitigated by 2021, with this figure potentially escalating to 147.52 MTon/year by 2030. This implies the potential elimination of emissions stemming from light vehicles, a significant contributor to
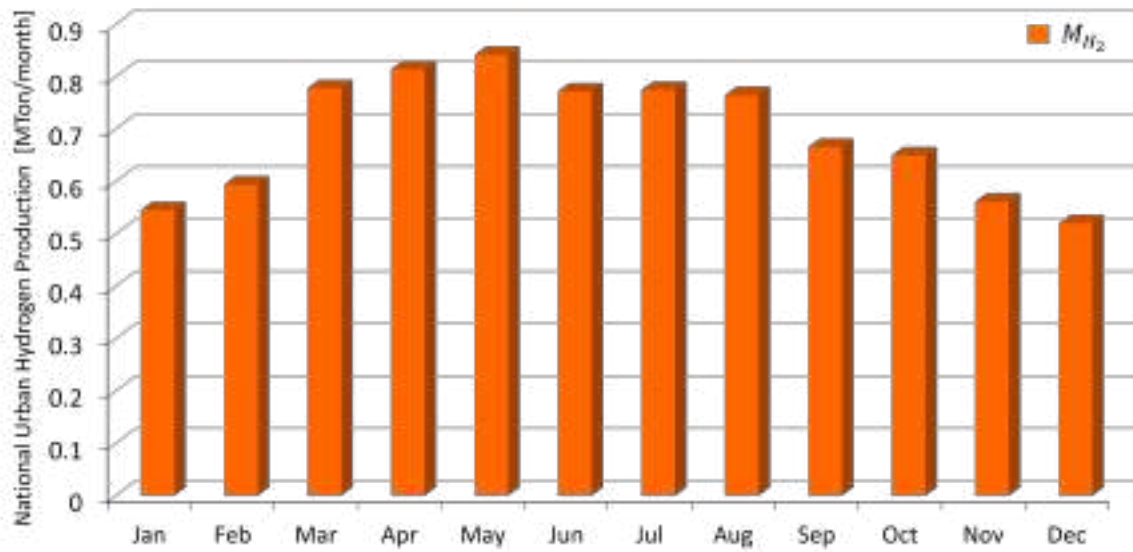
Figure 4.5: Monthly Profile of National Hydrogen Production in Urban Settlements.

greenhouse gas emissions in Mexico, accounting for 23 % of the total emissions [88].
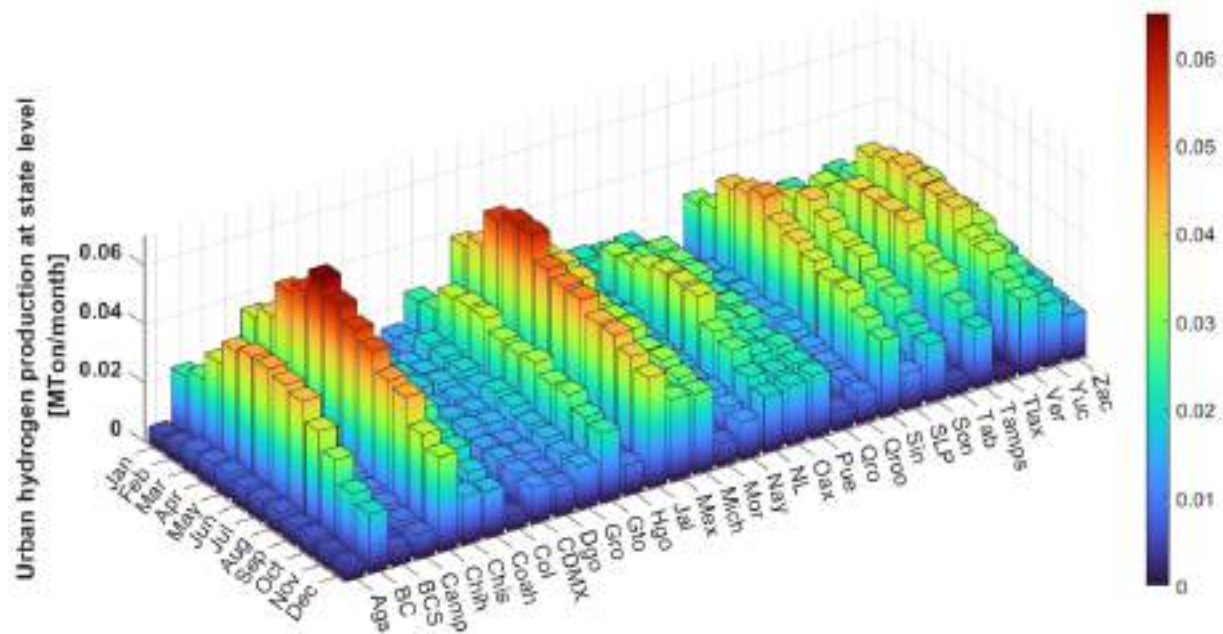


Figure 4.6: Monthly Urban Hydrogen Production by Federal Entity ($\eta_{elec}$=75 %).

Table 4.3: Amount of Hydrogen Demand for Light Transportation in Mexico

| Year analyzed | Mechanical Energy required [TWh/year] | Hydrogen demand [Mton/year] | CO$_2$ Avoided emissions [Mton/year] |
|---|---|---|---|
| 2021 | 144.519 | 4.336 | 124.388 |
| 2025 | 161.486 | 4.845 | 138.991 |
| 2030 | 171.395 | 5.142 | 147.520 |

## 4.2.3 Monthly profile of hydrogen production

Figure 4.5 illustrates the monthly national average of hydrogen production, ranging from 0.52 MTon/month to 0.81 MTon/month over the year. It was observed that the highest hydrogen yields were obtained during the spring months, with May exhibiting the peak production. Conversely, a decline in hydrogen production was observed during the winter months, with December registering a 35.8 % decrease in production compared to May.

Figure 4.6 depicts hydrogen production across states and months. It was observed that monthly production per state fluctuated between 0.005 MTon/month and 0.06 MTon/month. States with consistently lower production throughout the year included Ags, Col, Tab, Tlax, and BCS, with production values not surpassing 0.01 MTon/month.

Six states consistently maintained production levels above 0.025 MTon/month throughout the year: BC, Chih, Jal, Sin, Tamps, and Ver. Among these, Jal exhibited continuous high production exceeding 0.04 MTon/month consistently. This substantial production capacity opens avenues for considering alternative applications beyond transportation, particularly in industries such as the chemical sector.

As per data from the National Association of the Chemical Industry of Mexico, the apparent national consumption of hydrogen by this sector amounted to 0.081 MTon in 2020 [89]. This suggests that even states with a production capacity of 0.01 MTon/month could feasibly meet such demand.

Our findings emphasize the significant hydrogen production potential inherent in Mexican urban settlements. Nonetheless, it is imperative to conduct assessments of production feasibility and associated costs to gain a realistic understanding of the prospects for large-scale hydrogen utilization in Mexico.

## 4.2.4   Urban LCOH

LCOH was calculated using Equation 3.5 for two electrolysis technologies, with national averages presented in Table 4.1.

Given that E$_{gc}$ was derived from [73], the total cost of energy production was contingent upon both the energy generated and factors such as initial investment, installation expenses, maintenance costs, and operational expenses of PV modules. The price of electricity was notably influenced by solar energy availability, with higher production correlating with lower energy costs (refer to [73] for comprehensive insights). Electricity costs ranging from 0.041 to 0.052 USD/kWh were factored in, contingent upon the geographical location.

The analysis revealed that sunshine duration played a pivotal role in determining LCOH. When the minimum sunshine duration was employed as the operational time for electrolyzers instead of the average, hydrogen production costs escalated by approximately 0.2 USD/kg for Alkaline electrolyzers and 0.4 USD/kg for PEME. Particularly pronounced impacts were observed in states where the minimum hours of sunshine fell below 2,900 hours per year, with cost escalations of 0.8 USD/kg observed in states such as Chis and Tab.

The Levelized Cost of Hydrogen (LCOH) for urban areas exhibited variability, ranging from 5.81 USD/kg to 6.68 USD/kg for alkaline electrolyzers and from 9.13 USD/kg to 10.02 USD/kg for PEM technology. LCOH disparities across states ranged from approximately 0.1 to 1 USD/kg, contingent upon solar potential per unit area, with greater energy availability correlating with reduced LCOH.

Among alkaline technology, the ten states boasting the lowest LCOH were identified as Dgo (5.81 USD/kg), Gto (5.94 USD/kg), BCS (6.02 USD/kg), Zac (6.01 USD/kg), Son (6.02
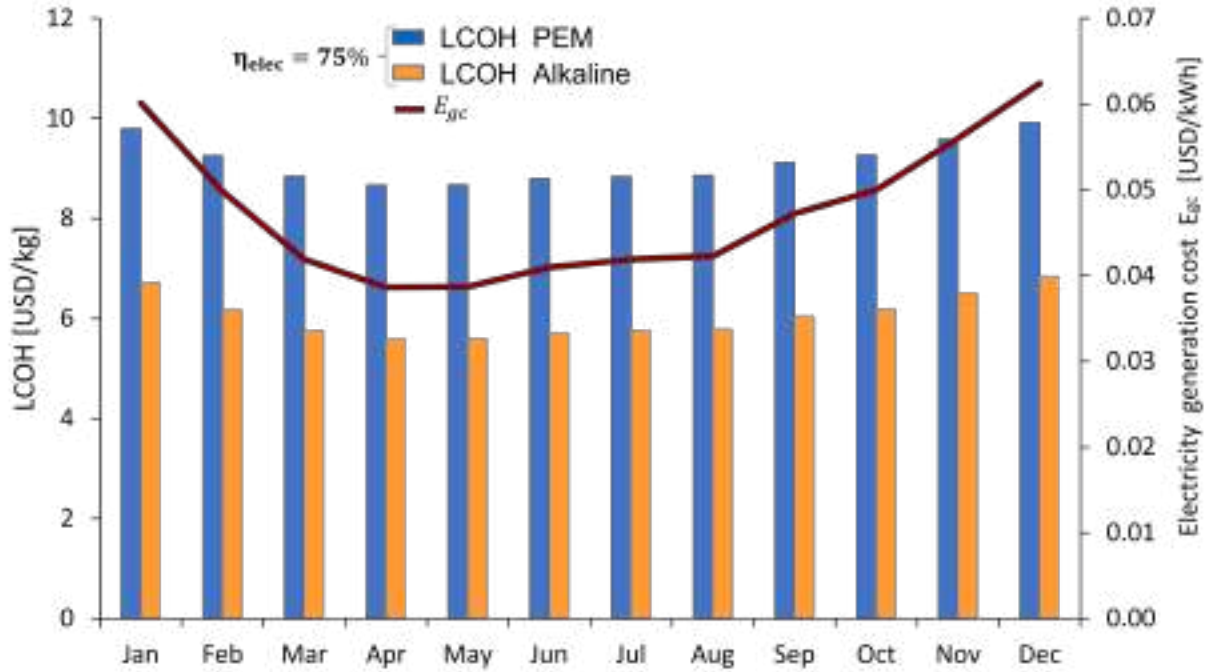
Figure 4.7: National average of LCOH and electricity generation costs throughout the year (monthly profile).

USD/kg), Qro (5.96 USD/kg), Mor (6.09 USD/kg), Nay (6.10 USD/kg), Sin (6.14 USD/kg), and Col (6.14 USD/kg).

The ten states with the lowest production costs for PEM electrolysis differed from those identified previously due to the intrinsic cost of the technology, which contributed to an increase in price by approximately 3 USD/kg. These states included Dgo (8.96 USD/kg), Gto (9.13 USD/kg), BCS (9.23 USD/kg), Zac (9.19 USD/kg), Son (9.19 USD/kg), Qro (9.19 USD/kg), Nay (9.32 USD/kg), Coah (9.32 USD/kg), Mor (9.33 USD/kg), and Sin (9.35 USD/kg). Urban areas within these states are situated in the northern and Bajio regions, characterized by a solar potential close to 240 GWh/km$^2$ (see Figure 4.1).

The ten states with the highest production costs for alkaline electrolyzers were Ver (6.68 USD/kg), Tab (6.66 USD/kg), Chis (6.57 USD/kg), CDMX (6.60 USD/kg), Mex (6.61 USD/kg), Oax (6.49 USD/kg), NL (6.48 USD/kg), Hgo (6.47 USD/kg), Tamps (6.43 USD/kg), and Ags (6.40 USD/kg). Conversely, for PEM electrolyzers, these states were
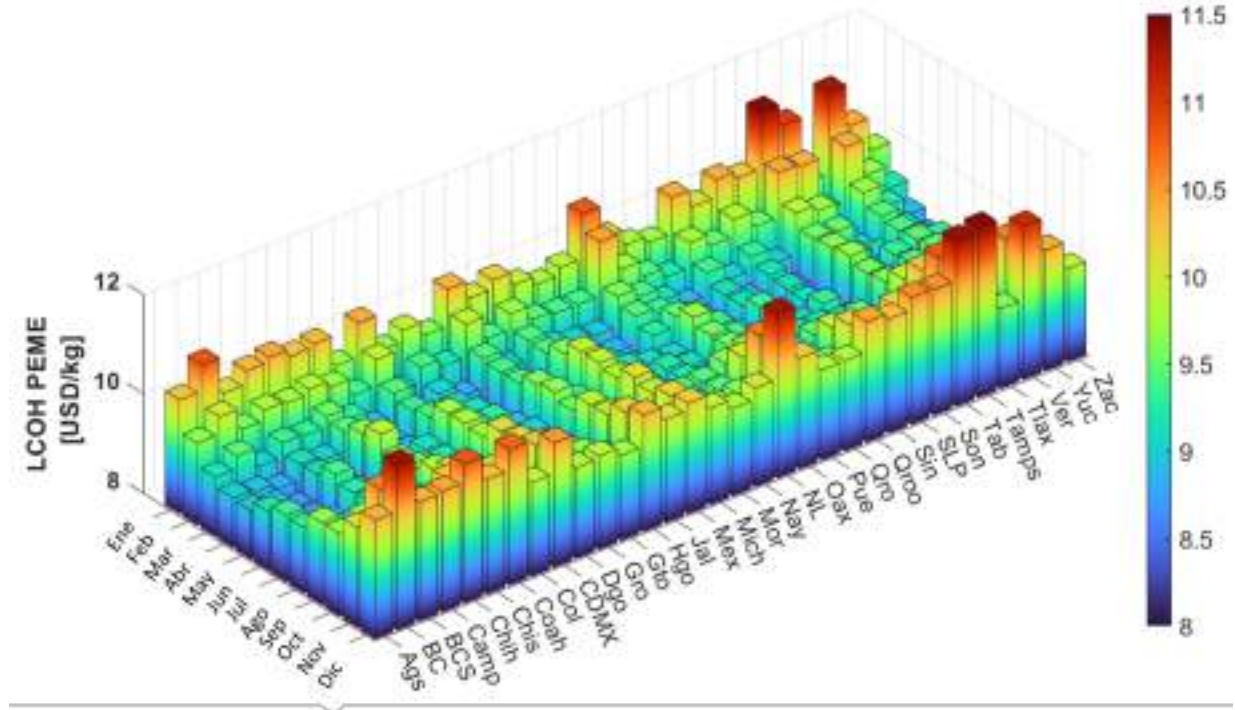
Figure 4.8: LCOH Monthly profile per Federal Entity ($\eta_{elec}$=75 %) for PEM Electrolyzer.

Ver (9.97 USD/kg), Tab (10.02 USD/kg), Chis (9.87 USD/kg), CDMX (9.91 USD/kg), Mex (9.91 USD/kg), Oax (9.81 USD/kg), NL (9.73 USD/kg), Hgo (9.76 USD/kg), Tamps (9.71 USD/kg), and Camp (9.60 USD/kg). These states are situated in the southern and central regions of Mexico, where the solar energy potential is approximately 180 GWh/km$^2$.

The identified cost intervals underscore the significance of implementing public policies aimed at reducing electricity and electrolyzer costs to achieve feasible hydrogen production as a sustainable energy source. In the short term, Mexico could leverage alkaline electrolyzers, given their substantial production potential and the resultant lower production costs.

**LCOH as a function of the month of the year.**

The national average of LCOH over the year is depicted for two technologies, contingent on the electricity cost, as illustrated in Figure 4.7. As elucidated previously, lower electricity costs correlate with reduced hydrogen production costs. Furthermore, it was determined that hydrogen could be produced economically for six months, capitalizing on periods of
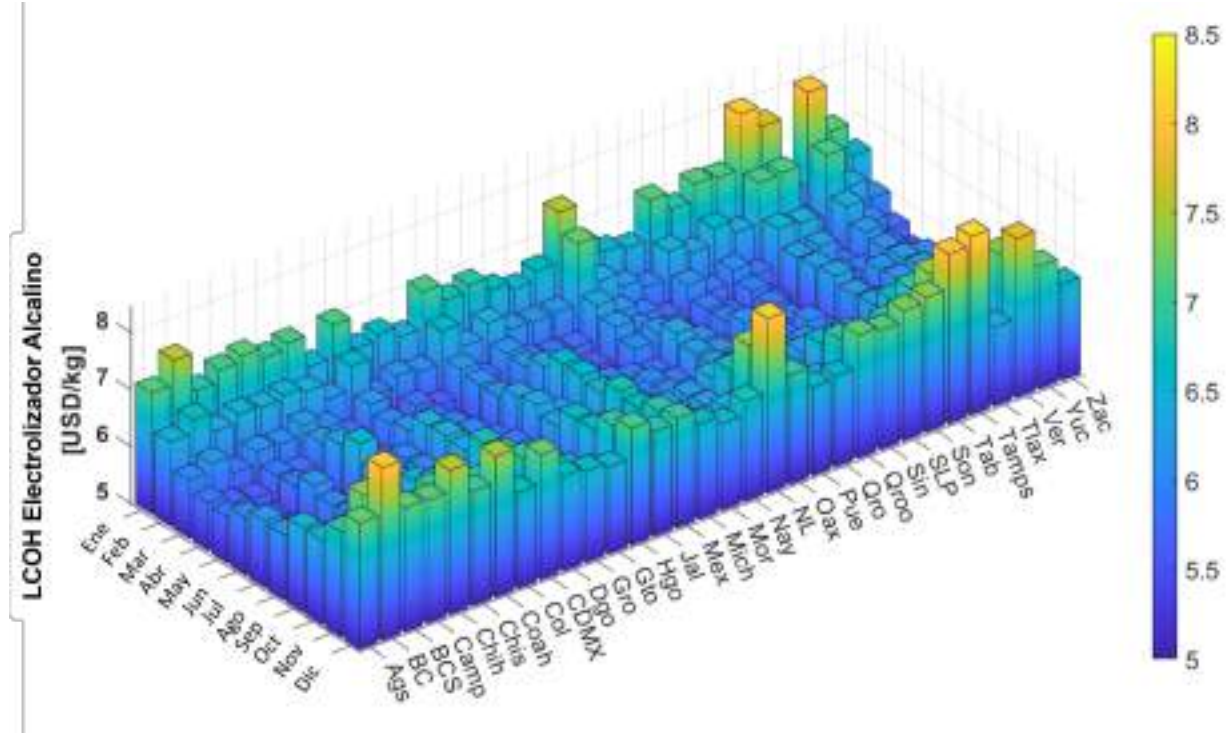
Figure 4.9: LCOH Monthly profile per Federal Entity, ($\eta_{elec}$=75 %), for Alkaline Electrolyzer.

heightened hydrogen availability, where the LCOH is approximately 13 % lower than during winter months.

Figures 4.8 and 4.9 illustrate the variation in LCOH throughout the year for each state. It is observed that LCOH exhibits an inverse relationship with hydrogen production, with peak production occurring during the spring and summer seasons, resulting in lower LCOH values. States with higher hydrogen generation potential, such as BC, Chih, Jal, NL, Sin, Son, Tamps, and Ver, would be more economically viable for hydrogen production in urban settlements. This information may facilitate the development of production plans tailored to each month, optimizing production during periods of peak availability and lower costs.

## 4.2.5 Water Requirements

Several researchers have investigated the water requirements for large-scale hydrogen production, with conclusions indicating that the water footprint associated with generating hydrogen remains minimal, even over the long term ([90], [91], and [92]).

Table 4.4: Hydrogen production considering $\eta_{elec}$=98 %

| Variable | Value (National) |
|---|---|
| H$_2$ National Production | 12.2 Mton/year |
| $PW_{RW}$ (renewable) | 0.08 % |
| $PW_{RH}$ (rainfall water) | 7.27 % |
| % of total H$_2$ required for transportation in 2030 | 41.89 % |
| Reduction in LCOH | 23.44 % |

These findings are consistent with the results. It was observed that the proportion of renewable water required for urban areas was notably low. The top 10 states with the highest consumption of renewable water were identified as follows: CDMX ($PW_{RW}$=0.32 %), Ags ($PW_{RW}$=0.17 %), BC ($PW_{RW}$=0.16 %), Qroo ($PW_{RW}$=0.11 %), Gto ($PW_{RW}$=0.1 %), BCS ($PW_{RW}$=0.1 %), NL ($PW_{RW}$=0.09 %), Mex ($PW_{RW}$=0.09 %), Coah ($PW_{RW}$=0.09 %), and Mor ($PW_{RW}$=0.07 %).

Considering that renewable water may still entail costs related to pumping and pipeline infrastructure, the analysis also incorporated rainfall water, which can be collected on-site. It was observed that reasonable percentages of rainfall water were necessary, with the highest proportions observed in states characterized by arid climates. The top 10 states with the highest consumption of rainfall water were identified as follows: BC ($PW_{RH}$=26.5 %), BCS ($PW_{RH}$=21.44 %), Son ($PW_{RH}$=15.23 %), Coah ($PW_{RH}$=13.07 %), Chih ($PW_{RH}$=12.31 %), Dgo ($PW_{RH}$=11.58 %), Zac ($PW_{RH}$=10.29 %), Qro ($PW_{RH}$=9.78 %), Gto ($PW_{RH}$=8.42 %), and Sin ($PW_{RH}$=8 %); while Mexico City (which functions as both a state and a city) required $PW_{RH}$=6.09 %.

Figure 4.10 provides a visual summary of the findings, illustrating the necessary rainwater and renewable water to achieve the hydrogen potential relative to the urban settlements in each state.
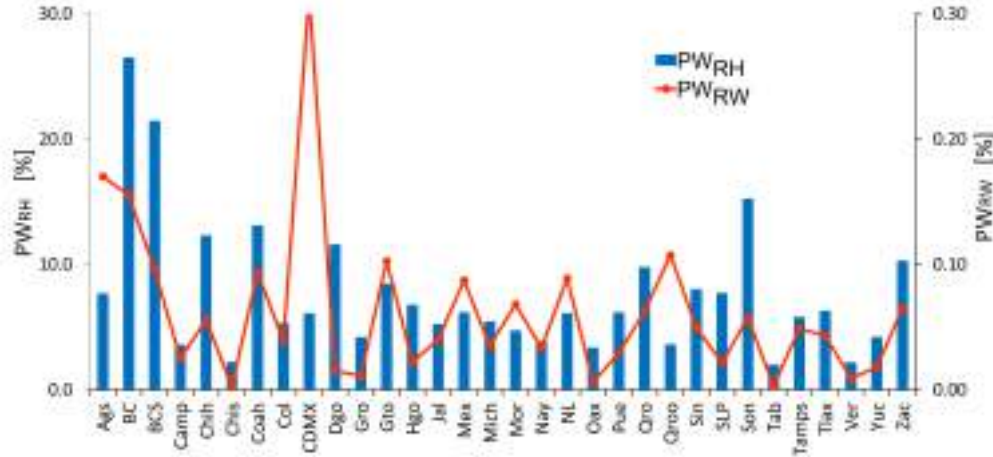
Figure 4.10: Comparison of water requirements by state. Blue: required Water as a percentage of annual rainfall water. Red: required Water as a percentage of renewable water.
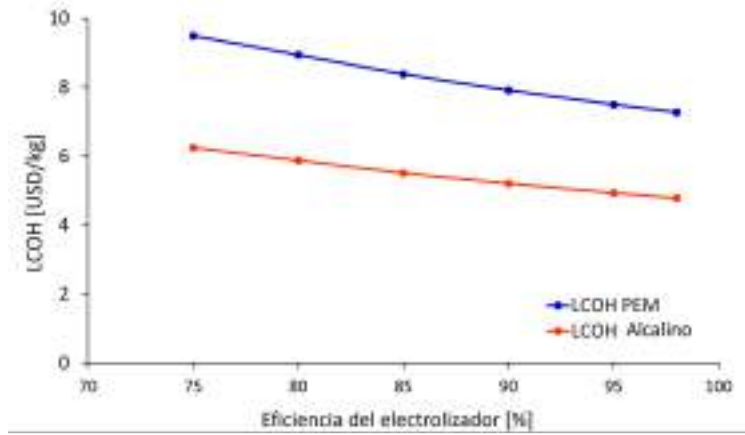


Figure 4.11: LCOH Values for Different Electrolyzer Efficiencies [75 %-98 %].

## 4.2.6 High efficiency electrolysis

The hydrogen production potential was estimated using an electrolyzer efficiency of 75 %; however, recent findings in [7], [93] indicate that such efficiency could potentially increase up to 98 % in the long term (by 2050). Therefore, it is essential to understand the technical implications of assessing the hydrogen potential considering an efficiency ($\eta_{elec}$) of 98 %. Table 4.4 presents the outcomes of such an evaluation.

Utilizing such a high efficiency could augment hydrogen production by 29.93 %, leading to reduced water requirements, both in terms of rainwater and renewable water, along

with savings of approximately 23.44 % in production costs. Given the expected gradual introduction of this technology, we computed the gradual increase in efficiency and its corresponding impact on the LCOH, as depicted in Figure 4.11. As anticipated, the rise in efficiency substantially decreased production costs.

## 4.3    Summary and Chapter Highlights

The hydrogen demand for transportation in 2021, 2025, and 2030 was found to be achievable using 46.1 %, 51.6 %, and 54.7 % of the potential of urban areas, respectively. Additionally, the entire annual hydrogen demand for 2020 could theoretically be met by just one month of production in urban areas of Jal. The solar hydrogen potential of all urban areas in Mexico was estimated at 9.39 MTon/year, capable of satisfying up to 42.6 times the current hydrogen demand in the country. Significant variations in the LCOH production were observed throughout the year, with the lowest LCOH recorded at 6.25 USD/kg for alkaline electrolyzers and 9.50 USD/kg for PEM technology in urban settlements.

In contrast to prior research, a pragmatic perspective was adopted for LCOH calculations, incorporating importation costs and actual sunshine measurements for electrolyzer operation times. Despite slightly higher LCOH values compared to those reported by the IEA, the feasibility of large-scale hydrogen production in Mexico's urban settlements using alkaline technology is emphasized, given its favourable outcomes. This underscores the necessity for collaborative efforts between government and academia to position Mexican hydrogen competitively on the global stage, leveraging the nation's significant potential.

This study also examined the water requirements for electrolysis, affirming that urban hydrogen production entails minimal water demands and a negligible water footprint. Finally, the paper delved into production costs for current and high-efficiency long-term technologies. Future research avenues should explore infrastructure planning for hydrogen management, encompassing compression and distribution aspects.

# Chapter 5

# Wind H$_2$ Production. Part A: Onshore

In this section, we outline the procedures and results obtained from the assessment of the potential for hydrogen production from wind resources in the Mexican territory.

## 5.1  Wind Energy Assessment for Mexico

The onshore wind energy generation potential in Mexico has been previously analyzed by several authors. However, certain deficiencies have been identified due to the origin of the data. Some studies use meteorological station datasets, but very few stations were considered for interpolation across the entire Mexican territory. In other cases, just a specific geographic region is analyzed due to the lack of measured data [94]. For instance, eight years of wind speed data from 131 weather stations were used in [95] to describe the energy potential across the entire Mexican territory. The results showed that the maximum annual average wind speed was 4.7 m/s.

In [96], the wind energy resource in five northern states of Mexico was evaluated using data from 221 weather stations and 21 specific points derived from satellite data. The results indicated that power densities of 1000 W/m² can be found in the state of Tamaulipas. The periodicity of wind was analyzed in [97], using an eight-year wind speed series. The authors determined that wind behaviour in Mexico is highly periodic, with lower speeds in

the morning and higher speeds at night.  It was also highlighted that this information is crucial for identifying the optimal times for energy harvesting.

On the other hand, MERRA-2 has been shown to inadequately represent wind behaviour in the Mexican territory.  In [38], the wind energy capacity factors for Mexico were calculated using the MERRA-2 dataset and contrasted with measurements from meteorological stations.  The authors demonstrated that MERRA-2 does not uniformly represent wind behaviour in Mexico. It overestimates wind speed values by 18 % in areas with high topographic variability, resulting in correlation coefficients below 0.5.

According to [98], ERA5 could be the most reliable climatological data set for wind power modelling, however, its resolution is one of the biggest disadvantages, Giovanni Gualtieri [99] demonstrated this by comparing ERA5's wind speed values with measurements at specific locations.  The results showed that ERA5 (31 km × 31 km) underestimates wind speed values by 48 % in highly complex terrain, consequently, the use of ERA5 should be avoided in high variation topography.

Great efforts have been made to increase the resolution through a downscaling process considering medium and high-resolution topography, an example of this is the well-known Global Wind Atlas (GWA) that offers a 250 m × 250 m resolution data set of the annual average wind speed for the entire world [100].

In Mexico, there have been collaborative projects such as "Wind Atlas of Mexico" where several institutions tried to adapt the ERA5 dataset and enhance its high-resolution representation through a downscaling process considering Mexico's orography.  However, according to a 2016 report, mesoscale modelling had not been successful, resulting in data severely overestimated in zones with high wind resources [101]. Subsequently, in 2021, a report from the same project did not present a final result on the model's predictions for the entire Mexican territory [102].

Many studies attempting to quantify harvestable wind energy have relied on the Global Wind Atlas dataset; however, this dataset has not been validated. In [103], it has been compared with datasets provided by NREL, yet discrepancies between datasets were calculated to exceed 40 %. This highlights the significant discrepancies in the existing information. The GWA has also been used to determine the hydrogen production potential in Mexico [49]; however, the lack of information validating these data raises questions about their usage.

An adequate characterization of Mexico's wind potential has not been conducted so far. Indeed, SENER in the "Atlas Nacional de Zonas con alto potencial de energías limpias" [104] reports wind potential maps based on previously mentioned studies that do not accurately represent the wind resource. This highlights the importance of conducting an accurate evaluation using measurements from meteorological stations, which can serve as a reference for validating data calculated through modelling. Precise assessment of wind potential is crucial for the effective utilization and development of this renewable resource.

## 5.2 Methods

This study evaluates the potential for onshore wind hydrogen production in Mexico by processing wind speed data recorded in the historical databases of the National Meteorological System. The process begins with data depuration, adhering to the completeness criteria established by the World Meteorological Organization. Daily, monthly and annual averages are then obtained, and the best interpolation method is determined by cross-validation, to finally calculate the harvestable energy.

### 5.2.1 Data handling

The general methodology is depicted in Figure 5.1. For this analysis, over 103 million wind speed data points were processed, sourced from the CONAGUA database with resolutions ranging from 10, 15, 20, 30 minutes, and 1 hour depending on the meteorological station. The initial step in analyzing the available wind energy from climatological measurements involves data depuration. In this case, the standards set by the World Meteorological Organization

were employed to establish quality parameters. For climatological variables, meteorological stations with at least 8/9 of the data available for a given year, month, and day are considered [72]. This study utilized monthly and daily metrics, leading to the processing of approximately 850 weather stations to calculate the available wind energy.
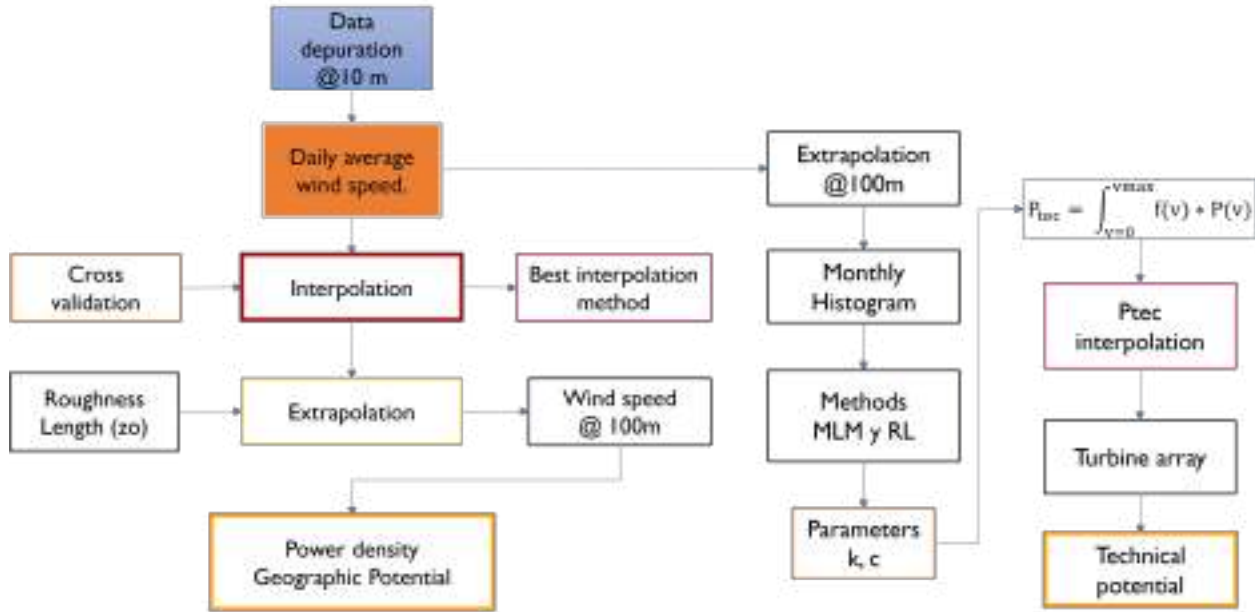


Figure 5.1: Onshore Wind Energy Analysis using data from Weather stations.

Utilizing the annual or monthly average wind speed values, it becomes feasible to assess the wind energy potential in Mexico:

1. Resource potential: Theoretical potential that encompasses the entire territory.

2. Geographical potential: The available land suitable for the installation of wind turbines, taking into account geographical constraints.

3. Technical potential: The energy generated within the available territory, considering energy losses inherent to the technology.

The resource potential can be described based on the wind power density (WPD) in W/m$^2$ (Equation 5.1), where the air density ($\rho$) can be approximated as a function of temperature using an equation of state or as a function of altitude.

$$WPD = \frac{1}{2}\rho v^3 \tag{5.1}$$

According to [34], the wind density can be approximated using a height correlation, following Equation 5.2.

$$\rho = 1.225 - (1.194 \times 10^{-4}) \times z \tag{5.2}$$

Where $z$ represents the variation in height relative to the ground.

By employing the digital elevation model (DEM) for Mexico, the value of air density was determined based on altitude (Figure 5.2).
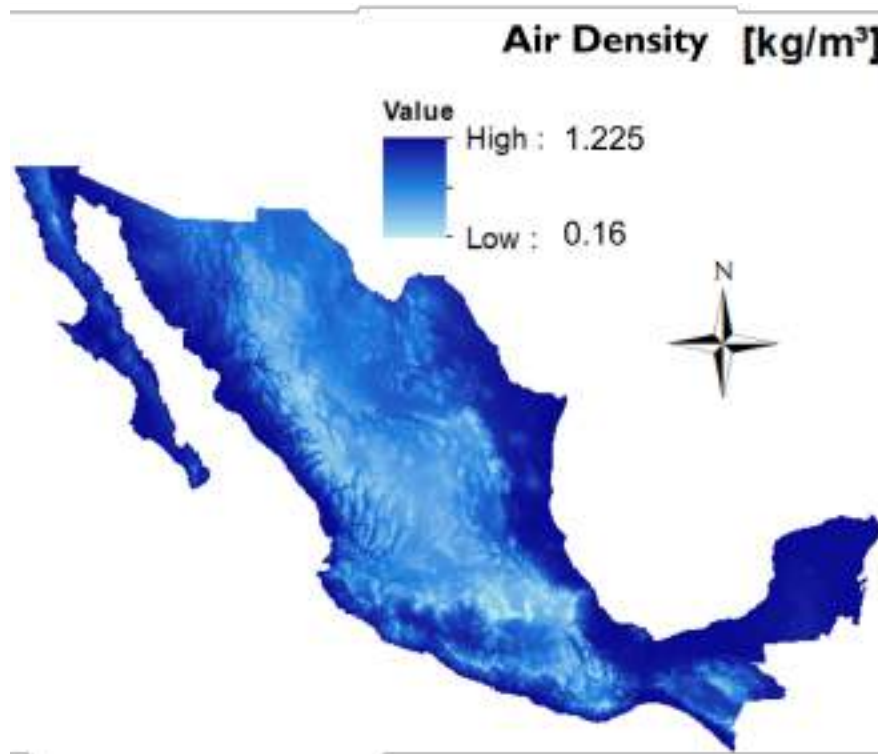


Figure 5.2: Air density, resolution 500 x 500 m.

Regarding meteorological stations, the standard wind measurement height relative to the ground is 10 m. However, wind turbine heights exceed 80 m, necessitating wind speed extrapolation to obtain accurate values. Various methods exist for conducting extrapolation, with the most commonly used being the power law and logarithmic methods. The latter

relies on terrain roughness values, as this value strongly influences the vertical wind profile. Figure 5.3 displays the classification of Mexican terrain types and their respective roughness values.
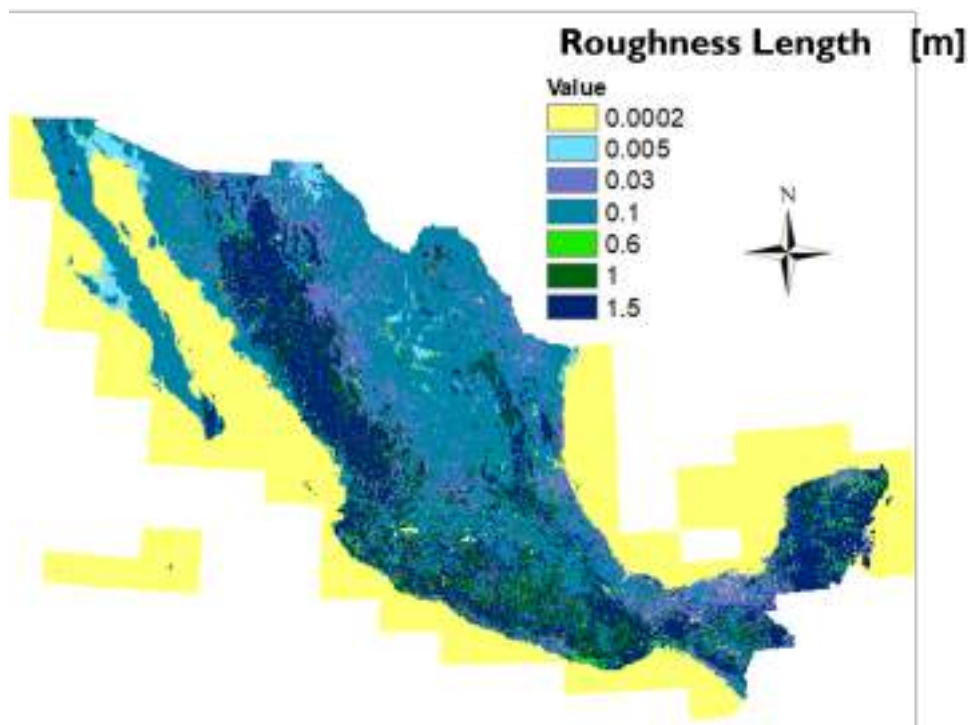


Figure 5.3: Roughness Length.

The geographical potential of wind is delimited by areas where it is not possible to install wind turbines, such as protected areas, forests, jungles, etc. Table 5.1 lists the restrictions considered for this analysis.

Table 5.1: Geographic constraints

| Constraints | Buffer |
|---|---|
| Road | 200 m |
| Airports | 2500 m |
| Urban settlements | 1000 m |
| Protected Zones | - |
| Waster bodies | 200 m |
| Jungles | - |
| Pipelines | 100 m |
| Archaeological zones | - |

## 5.2.2 Wind speed Interpolation

The measurements from the meteorological stations were interpolated to create a surface of wind speed values across the Mexican territory. Although wind speed is a complex variable to predict, several studies have reported that kriging and IDW methods yield the best results [105]. The effectiveness of IDW strongly depends on the coefficient used; some studies have reported that a power of 3 (ID3W) produces accurate results [106], while in others, a power of 2 is sufficient (ID2W) [107]. In this study, the IDW method with a power of 2 was used to interpolate wind speed, and the selection of the number of neighbours was determined by measuring the root mean square error (RMSE) by cross-validation, using a random sample of 3 % of the stations (Figure 5.4). The results indicated that a higher number of neighbours (12) led to more successful interpolation, reducing the RMSE value. A study conducted by NREL also found that for wind speed interpolation, IDW performs better with more neighbours [108].
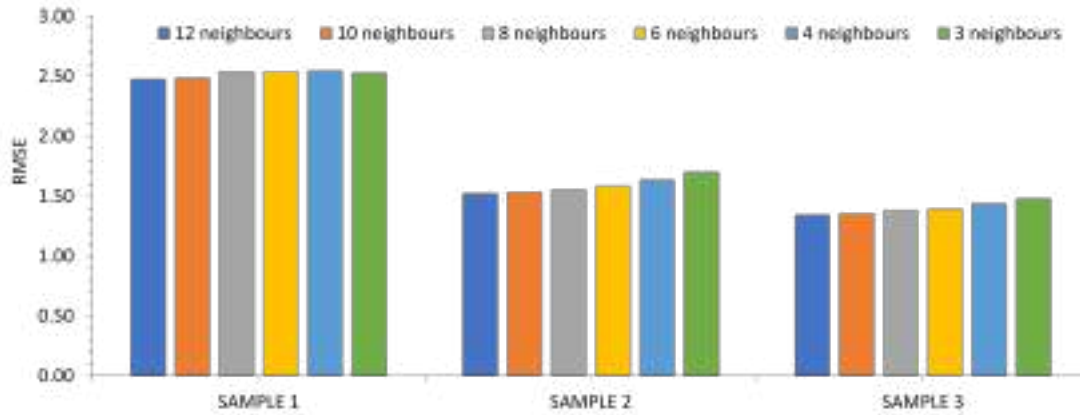


Figure 5.4: Neighbors number for Interpolation Using the IDW Method with Power 2.

## 5.2.3 Technical Potential of Onshore Wind Energy

The evaluation of technical potential is determined by the energy output of a wind turbine, which is defined by the characteristic power curve (P(v)) and the probability density function of wind speed (f(v)) over a specified period of time, for example, 1 year (Equation 5.3).

$$PT = \int_{vcut_{in}}^{vcut_{out}} P(v)f(v)\,dv = \sum_{vcut_{in}}^{vcut_{out}} P(v)f(v) \tag{5.3}$$

Where PT is the power delivered by the turbine over the year considering its characteristics such as $vcut_{in}$, which refers to the minimum speed for the wind turbine to start producing energy, and $vcut_{out}$, which is the maximum permissible speed during turbine operation.

The probability of a certain wind speed value can be described using the Weibull distribution (Equation 5.4), which is a statistical model whose shape (k) and scale (c) parameters need to be determined.

$$f(v) = \frac{k}{c}\left(\frac{v}{v}\right)^{k-1} exp\left[-\left(\frac{v}{c}\right)^{k}\right] \tag{5.4}$$

There are many methods to determine the k and c values, and various authors have compared the effectiveness of each. Among the most commonly used methods are Maximum Likelihood (MLM), Linear Regression or Graphical Method (LR), Moments, Standard Deviation, Power Density, etc. In this study, the MLM and LR methods were utilized to approximate the parameter values for each meteorological station under investigation [109, 110, 111, 112, 113].

*Linear Regression Method*

The linear regression method is based on the Cumulative Weibull Distribution Function (Equation 5.5), which can be transformed into a linear function according to Equations 5.6 - 5.8.

$$F(v) = 1 - exp\left[-\left(\frac{v}{c}\right)^{k}\right] \tag{5.5}$$

$$1 - F(v) = exp\left[-\left(\frac{v}{c}\right)^{k}\right] \tag{5.6}$$

$$\frac{1}{1 - F(v)} = exp\left[-\left(\frac{v}{c}\right)^{k}\right] \tag{5.7}$$

$$ln-ln[1-F(v)] = kln(v) - kln(c) \tag{5.8}$$

1. Using wind speed data, calculate the cumulative frequency distribution, or first evaluate the frequency distribution, which requires classifying the wind speed data, and then, using the frequency distribution, obtain the cumulative frequency distribution.

2. Calculate the values $(\ln(v_i)\ \ln\text{-}\ln[1\text{-}F(v_i)])$

3. To solve the least squares problem and find the shape and scale parameters using Equations 5.9 and 5.10.

$$k = a \tag{5.9}$$

$$c = exp(\frac{-b}{a}) \tag{5.10}$$

*Maximum Likelihood Method*

On the other hand, the Maximum Likelihood Method requires extensive iterative calculations using algorithms such as Newton-Raphson. The shape and scale parameters of the Weibull distribution are estimated using Equations 5.11 and 5.12.

$$k = \left( \frac{\sum_{i=1}^{n} v_i^k ln(v_i)}{\sum_{i=1}^{n} v_i^k} - \frac{\sum_{i=1}^{n} ln(v_i)}{n} \right)^{-1} \tag{5.11}$$

$$c = \left( \frac{\sum_{i=1}^{n} (v_i)^k}{n} \right)^{\frac{1}{k}} \tag{5.12}$$

Where $n$ is the number of wind speed data points. This method is implemented in two stages

1. Using wind speed data, calculate the sums in Equations 5.11 and 5.12, taking into account wind speeds of zero, which make the logarithm undefined. Then, calculate the shape parameter using Equation 5.12.

2. To find the scale parameter using a numerical technique to find the root of Equation 5.11.
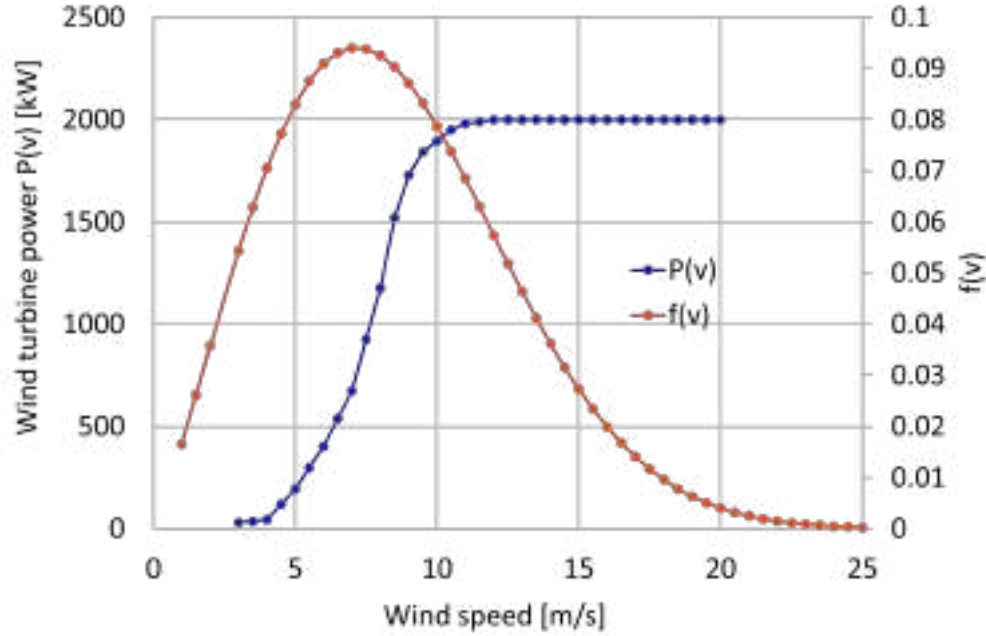


Figure 5.5: Roughness Length.

*Standard Deviation Method*

In certain investigations, the Standard Deviation Method has been employed to estimate these parameters with commendable accuracy ([113], [114]). The $k$ parameter exhibits a relationship with the standard deviation ($\alpha$), as delineated in Eq. (5.13), whereas the $c$ parameter is correlated with the mean wind velocity and its determination is facilitated through the application of Eq. (5.14). Herein, $\bar{v}$ symbolizes the average wind speed, and $\Gamma$ denotes the gamma function.

$$k = \left(\frac{\alpha}{\bar{v}}\right)^{-1.086} \tag{5.13}$$

$$c = \frac{\bar{v}}{\Gamma\left(1 + \frac{1}{k}\right)} \tag{5.14}$$

The annual wind energy production ($E_{expected}$) of a single grid cell was calculated as follows (3) considering the total number of effective hours ($h_{eff}$) of a year.
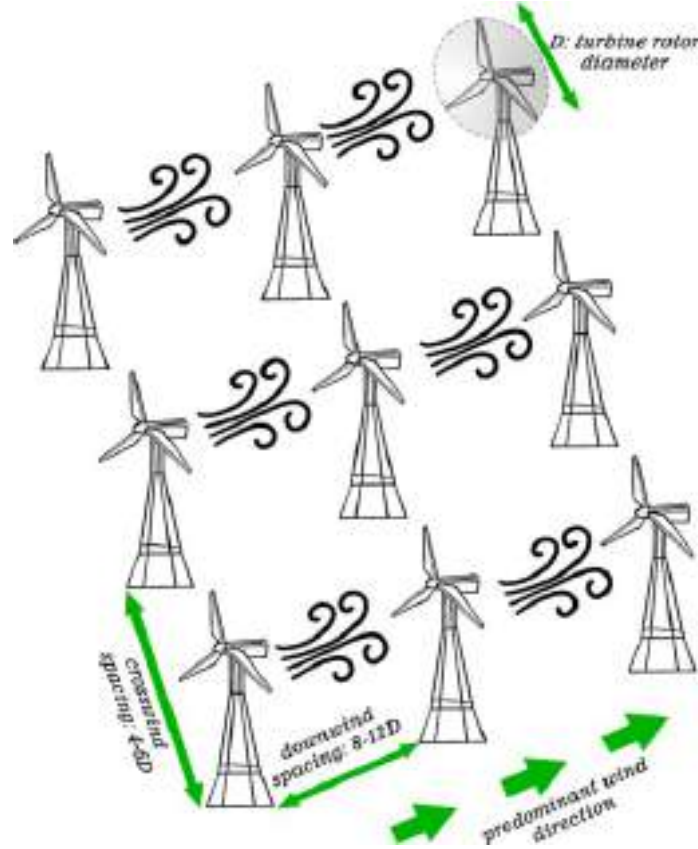
Figure 5.6: Roughness Length.

$$E_{expected} = h_{eff} \times PT \tag{5.15}$$

In this work, we used the 2 MW Vestas wind turbine (V110-2.0) with a rotor diameter of 110 m, the power curve is shown in Figure 5.5. Five and eight rotor diameters in the crosswind and downwind direction were considered as inter-turbine spacing, respectively as presented in Figure 5.6.

A pivotal metric in the evaluation of renewable energy potential is the Capacity Factor (CF), which quantifies the actual electrical output of a power facility relative to its maximum possible generation under continuous full-capacity operation over a specific period of time. In this work, CF is assessed annually and monthly following Eq. (5.16) where $E_{\text{nom}}$ is the amount of energy a wind turbine would generate assuming it operated at its maximum capacity for a delineated time frame.

$$CF = \frac{ET}{E_{nom}} \tag{5.16}$$

### 5.2.4 Wind hydrogen production

The potential for hydrogen production was derived from the generated wind energy. The hydrogen mass ($M_{H_2}$) in Ton/km$^2$ year was computed as per Equation 5.17, based on guidelines from [115].

$$M_{H_2} = \frac{\eta_{converter} E_{Expected}}{R_{en}} \tag{5.17}$$

where $R_{en}$ represents the energy needed for the electrolyzer to produce hydrogen (52.5 kWh/kg) at 75 % efficiency, and $\eta_{converter}$ is the converter efficiency set at 97 %. The hydrogen output per unit area for the selected regions was calculated using map algebra in ArcGIS Pro$^{TM}$.

## 5.3 Results

### 5.3.1 Resource Potential

Based on the methodology explained, the ID2W interpolation method was used to obtain the wind speed distribution using approximately 800 meteorological stations. Figure 5.7b shows the annual average wind speed for the entire Mexican territory, where values range from 1.14 to 12.52 m/s. Areas with high wind speed values (>5 m/s) are mainly located along the coasts of Tamaulipas, Oaxaca, Baja California, and Baja California Sur.

The annual average wind speed values from the meteorological stations were compared with those reported by GWA, revealing significant discrepancies. GWA severely overestimates the annual average wind speed, especially in mountainous regions, where differences
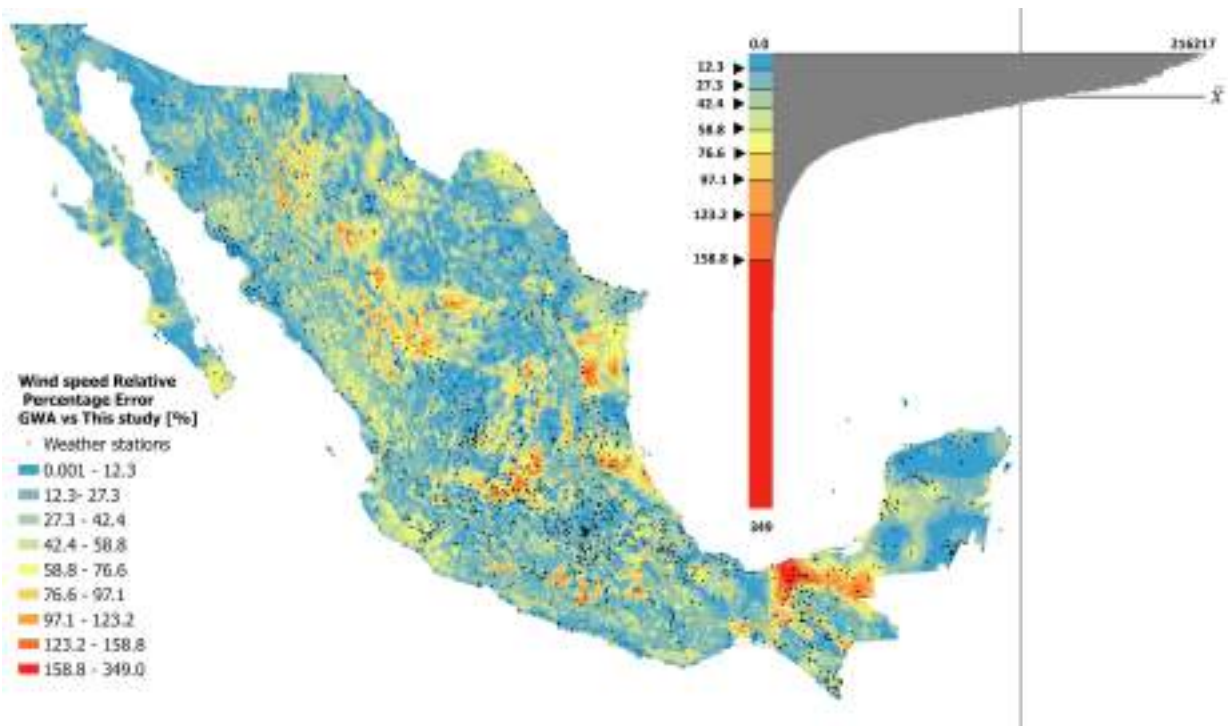
(a)
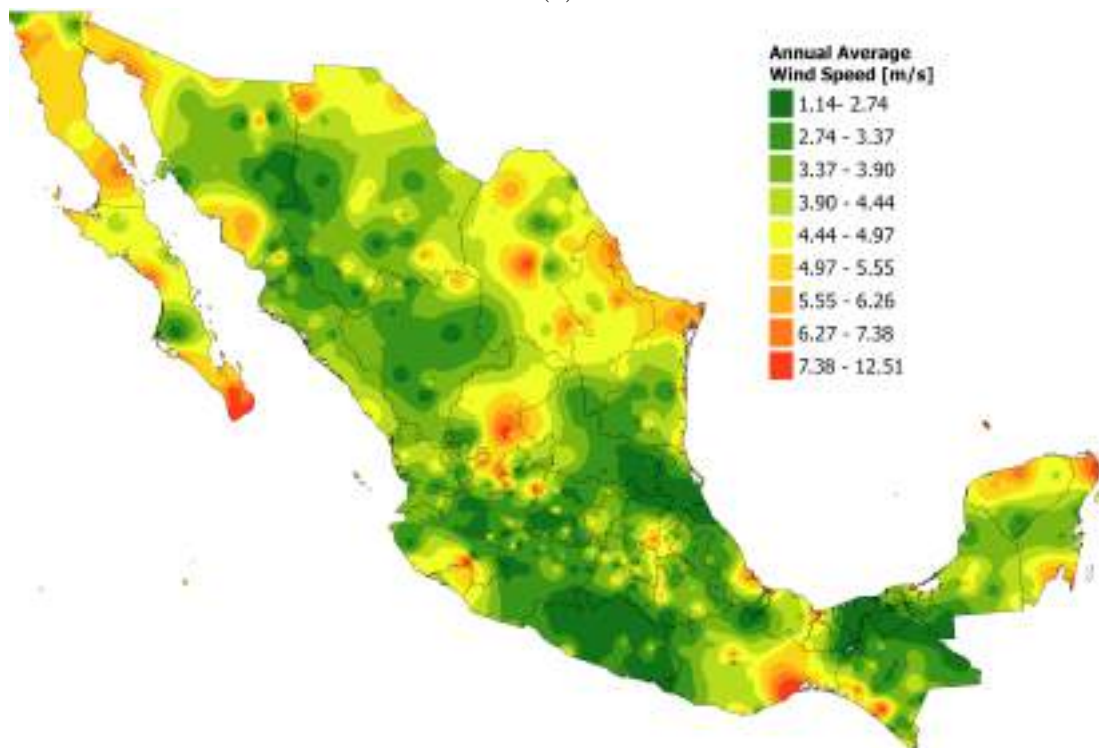


(b)

Figure 5.7: a) Wind Speed Relative Percentage Error of GWA vs This study. b) ID2W Wind speed interpolation (Annual average).
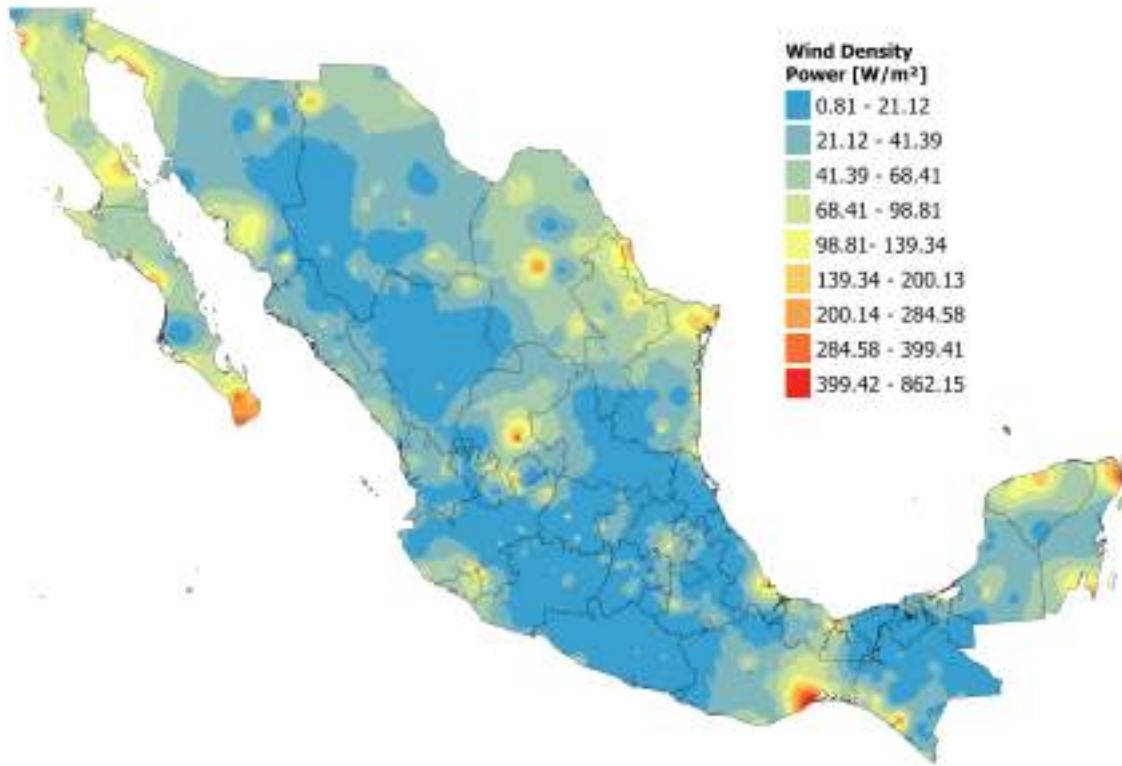
Figure 5.8: Wind Power Density Distribution (Resource Potential).

can reach up to 7 m/s, resulting in relative errors exceeding 158 % in just 3 % of the territory. Conversely, relative errors below 2 % were found in 10 % of the territory, corresponding to an approximate difference of 0.2 m/s (Figure 5.7a).

These results do not completely reject the utility of GWA, as it provides good approximations in areas with uncomplicated orography. Therefore, it may only be valid for such areas, and caution is recommended when using it for potential wind energy assessments since it inaccurately describes wind speed values in 90 % of the territory.

The wind power density (WPD) distribution is shown in Figure 5.8. According to [116], WPD is the primary indicator for determining wind resource potential in a given geographical region. Installing wind turbines for energy harvesting starting from 200 W/m$^2$ is highly feasible. In the case of Mexico, it was found that, based on this metric, only 1.35 % of the territory would be strictly viable for wind energy harvesting.

## 5.3.2 Technical Potential

Based on the geographic constraints considered in this study and after excluding areas where the annual average wind speed is less than 4.3 m/s, the technically available area for wind energy harvesting was determined. This area is shown in Figure 5.9. It represents only 20.8 % of the Mexican surface, meaning that only 393,110 km$^2$ are suitable to host an installed capacity of 297 GW dedicated to large-scale electricity generation. Mexico has an installed wind energy capacity of 7,691 MW [117], implying that only 2.6 % of all available wind potential has been used so far.

The technical potential of wind energy was calculated using Equation 5.3. This required determining the parameters k and c through the Weibull distribution. Data fitting was performed for each available station. The k and c parameters estimation per month in one wheater station is depicted as an example in Figure 5.10. The method that best described the wind speed behaviour was MLM, generally yielding values less than 0.25. Conversely, LR exhibited RMSE above 0.3 at certain stations.

The results indicated that in the areas available for the installation of wind farms, up to 17.34 GWh/km$^2$ could be generated (Figure 5.11), which implies that it could be possible to generate 2,153.76 TWh annually. In 2022, the electrical energy consumption in Mexico was 322.54 TWh [117], which means that the wind energy potential could cover that demand 6.67 times. Wind energy would be enough to supply the country's electrical power, and the remainder could lead to other applications such as hydrogen production.

Additionally, a comparison of the technical potential of energy obtained using GWA data was conducted, the results are shown in Table 5.2. It was observed that using the GWA dataset, the available area for wind harvesting is 1.8 percentage points larger. Furthermore, the capacity for the installation of wind farms was calculated to be 1027.74 GW, which is 3.45 times greater than that obtained in this study. Consequently, the potential energy that could be generated is proportionally larger compared to the results derived from meteorological

station data. Therefore, these findings highlight the importance of data quality. While it is true that GWA overestimates wind speed values, the impact on energy potential assessment is significant, potentially influencing decision-making in the energy transition process.
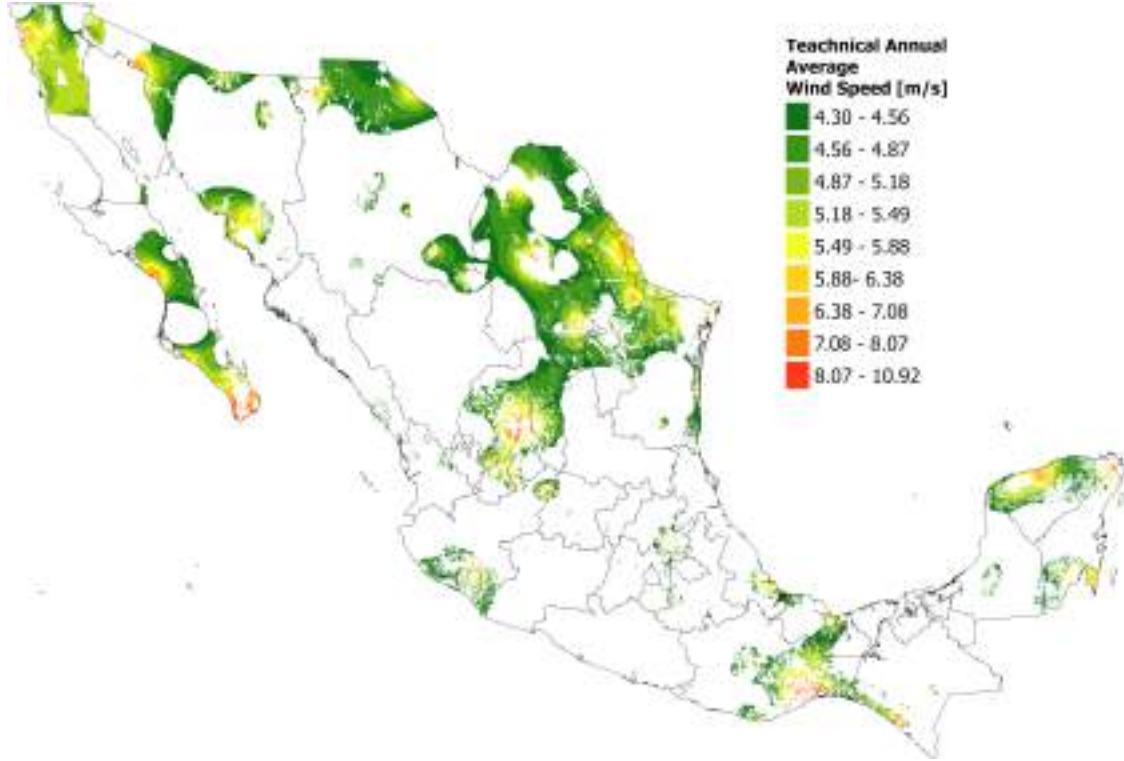


Figure 5.9: Available area for wind energy harvesting).

## 5.3.3 Onshore Wind Hydrogen Production

Figure 5.12 shows the distribution of hydrogen production per unit area. Mexico has a hydrogen mass density of up to 151.86 Ton/km$^2$ year, while the national generation potential is 38.97 MTon/year. This capacity could cover 158 times the current Mexican demand for hydrogen (0.25 MTon/year) so it can be thought that this potential can cover current and future hydrogen requirements (vehicles, industry, refinery, natural gas).

Table 5.2 shows the state's total hydrogen production The top five states with the highest potential for hydrogen production are Coah (7.87 MTon/year), Son (4.59 MTon/year), BC (4.54 MTon/year), BCS (4.00 MTon/year), and NL (3.73 MTon/year). This is attributed to
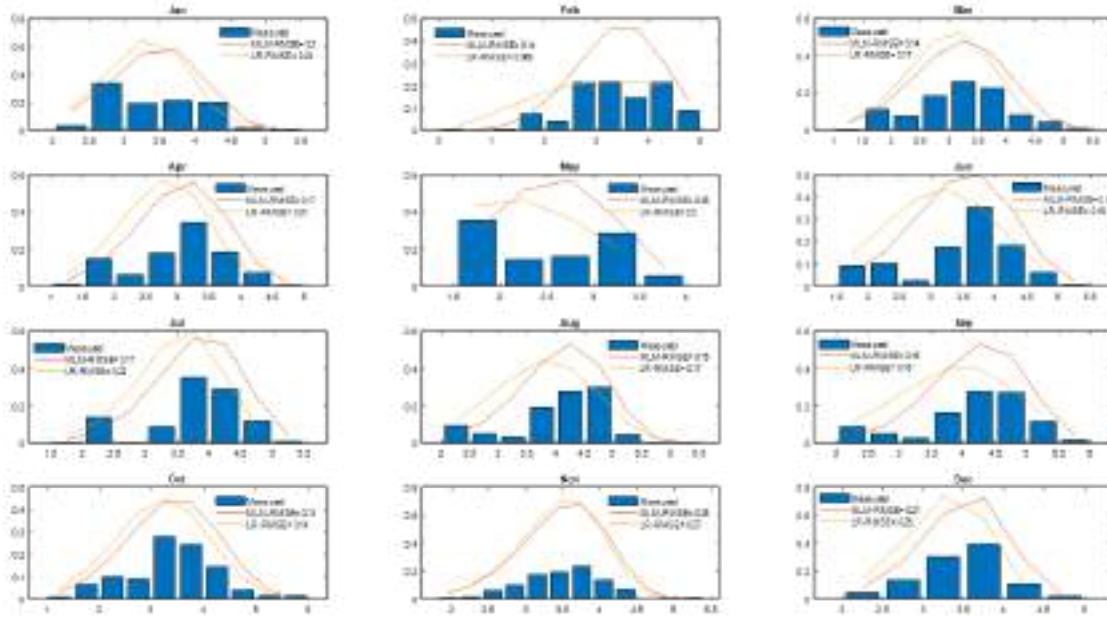
Figure 5.10: Weilbull Functions approximated by MLM and LR methods and Histogram wind Speeds Observed.

the fact that in these states, the average annual wind speed exceeds 5 m/s, and the available area for energy harvesting is considerably large relative to the surface area of each state, being 54.91 %, 24.28 %, 45.73 %, 41.87 %, and 58.66 %, respectively. On the other hand, regarding the comparison made with the potential according to GWA, significant differences are found in states where production capacity is low. For example, according to GWA, it would be possible to harvest hydrogen in CDMX using 0.49 % of the surface area. However, in this study, it was determined that large-scale hydrogen production is not feasible in CDMX due to wind speed constraints.

According to [118], Mexico's potential for solar hydrogen production is 2,366.33 MTon/year, which is 60 times greater than that of wind hydrogen. Nevertheless, wind energy's contribution to hydrogen generation could serve as an excellent supplement in regions where flat terrain is not available for photovoltaic technology installation. This information is of utmost importance as it enables stakeholders to make informed decisions and devise strategies for the integration of hydrogen into the energy matrix.
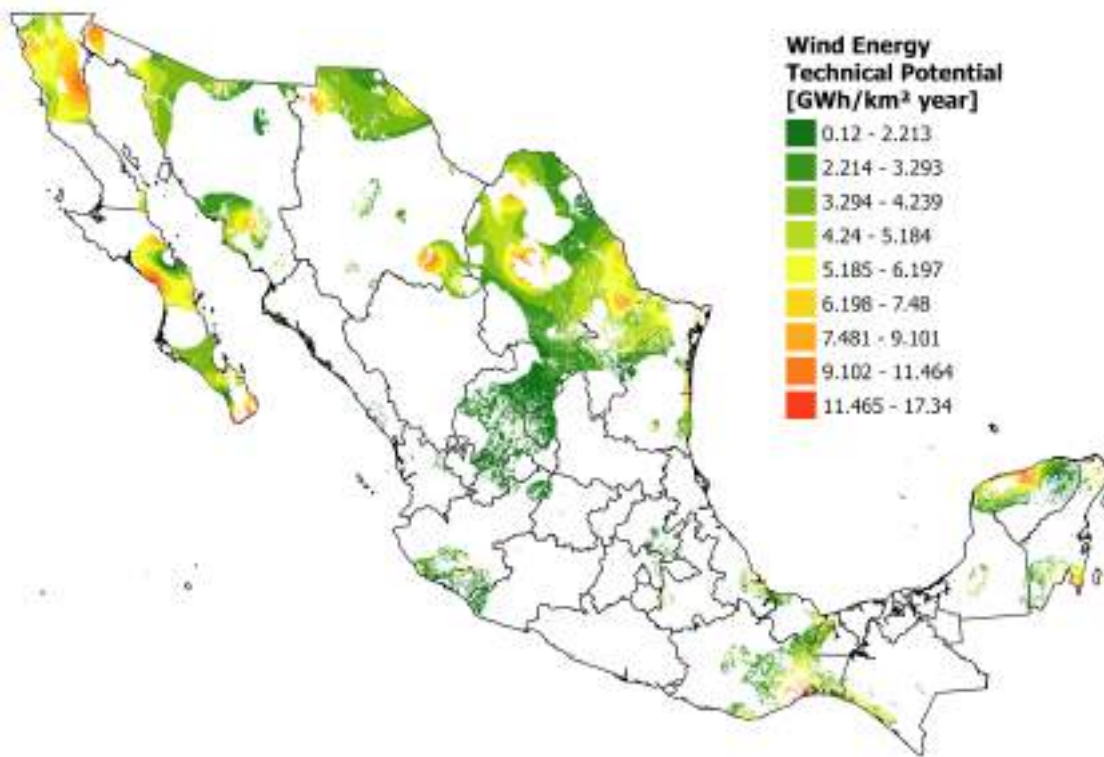
Figure 5.11: Wind energy technical potential.

### 5.3.4 Economic assessment

Figure 5.13 presents the distribution of the LCOE, demonstrating that in areas with low wind resources (<6 m/s), the LCOE can reach values up to 406.87 USD/MWh. Conversely, seven zones are identified where the LCOE ranges from 9 USD/MWh to 111.98 USD/MWh.

Currently, wind energy is one of the most cost-effective energy sources. In Mexico, it was reported at 45 USD/MWh in 2023, as wind farms are installed in or close to areas identified as high-potential zones. Therefore, these results align with the current behaviour of the wind energy market in our country. Furthermore, there remains untapped potential to be integrated into the energy matrix, contributing to a cleaner national electrical system.

Figures 5.14a and 5.14b show the distribution of the LCOH over the available area for
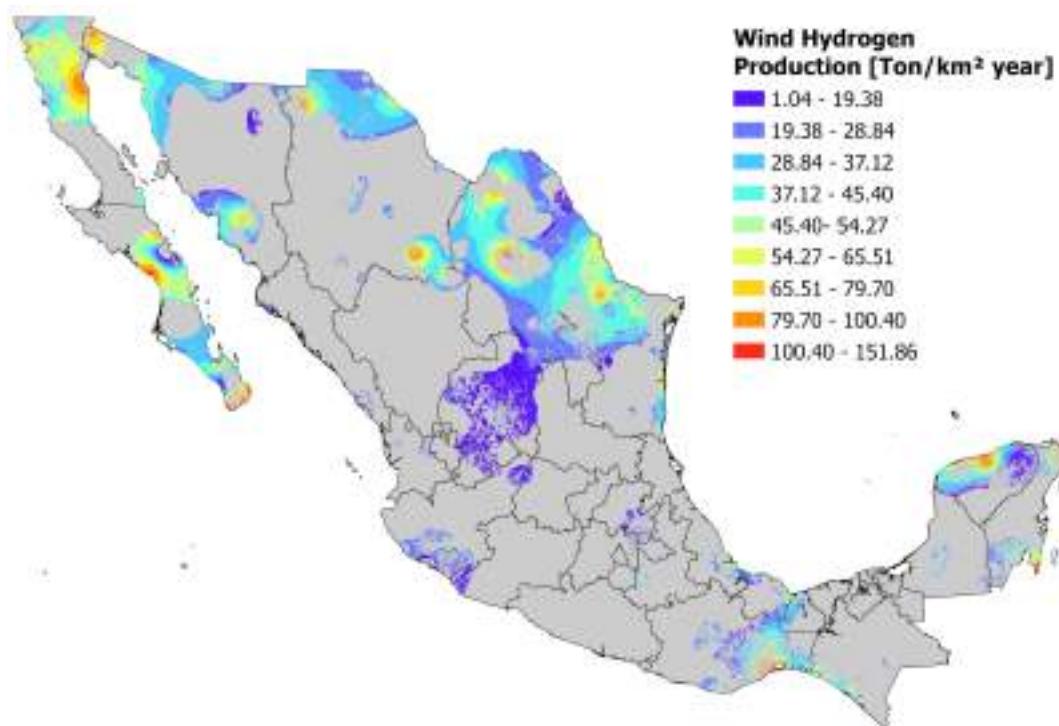
Figure 5.12: Anuual wind hydrogen production per unit of area.
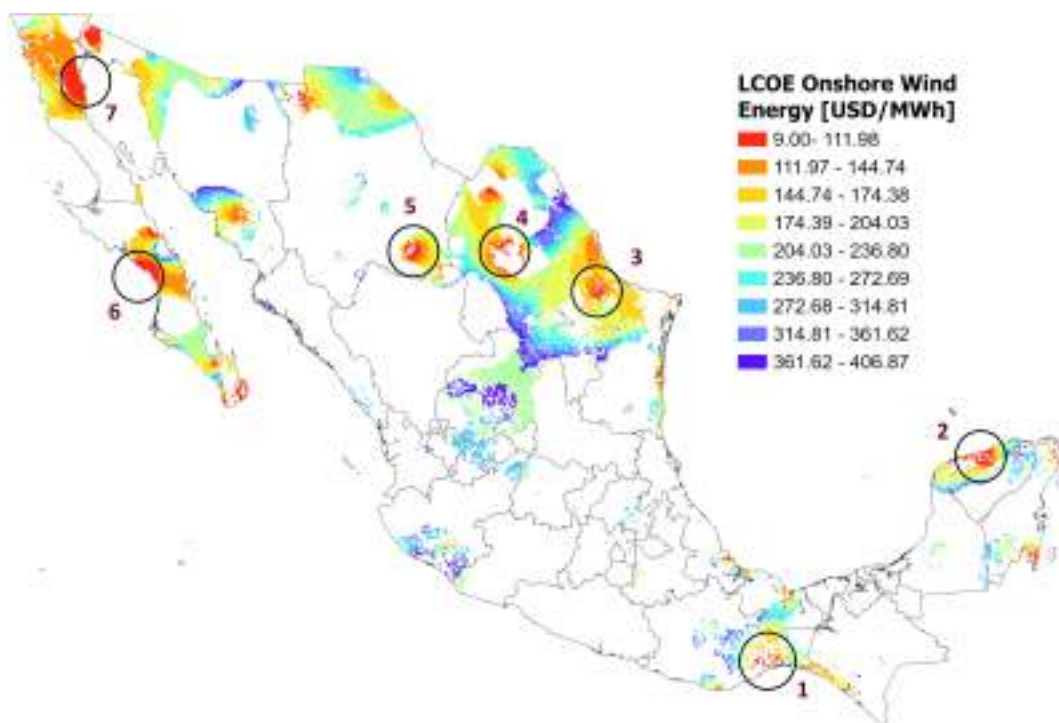


Figure 5.13: Onshore Wind LCOE.

Table 5.2: Wind Hydrogen Production Potential based on the annual average of wind speed of the GWA and the calculated in this study.

| State | Available Area [ %] | | Power Capacity [GW] | | Energy Generation Potential [TWh/year] | | Hydrogen Production [MTon/year] | |
|---|---|---|---|---|---|---|---|---|
| | GWA | This study | GWA | This study | GWA | This study | GWA | This study |
| Ags | 12.35 | 10.37 | 1.567 | 0.165 | 10.433 | 1.10 | 0.189 | 0.020 |
| BC | 17.90 | 45.73 | 33.790 | 33.464 | 253.730 | 251.27 | 4.591 | 4.547 |
| BCS | 19.25 | 41.87 | 30.282 | 29.134 | 229.866 | 221.15 | 4.159 | 4.002 |
| Camp | 12.31 | 2.81 | 12.601 | 1.158 | 100.058 | 9.20 | 1.811 | 0.166 |
| Chis | 8.58 | 3.66 | 15.871 | 2.407 | 118.436 | 17.96 | 2.143 | 0.325 |
| Chih | 40.55 | 20.28 | 245.249 | 37.659 | 1774.800 | 272.53 | 32.115 | 4.931 |
| CDMX | 0.49 | — | 0.014 | – | 0.066 | — | 0.001 | – |
| Coah | 49.34 | 54.94 | 204.994 | 57.931 | 1540.491 | 435.35 | 27.876 | 7.878 |
| Col | 0.08 | 26.26 | 0.009 | 0.890 | 0.064 | 6.67 | 0.001 | 0.121 |
| Dgo | 23.50 | 2.19 | 69.315 | 1.833 | 512.853 | 13.56 | 9.280 | 0.245 |
| Gto | 17.49 | 1.48 | 13.855 | 0.217 | 103.498 | 1.62 | 1.873 | 0.029 |
| Gro | 1.58 | 0.19 | 2.219 | 0.080 | 15.389 | 0.55 | 0.278 | 0.010 |
| Hgo | 7.26 | 5.75 | 3.529 | 0.406 | 25.066 | 2.88 | 0.454 | 0.052 |
| Jal | 4.18 | 9.90 | 8.109 | 3.510 | 54.703 | 23.68 | 0.990 | 0.428 |
| Mex | 1.26 | 1.88 | 0.592 | 0.254 | 4.210 | 1.81 | 0.076 | 0.033 |
| Mich | 0.96 | 2.67 | 1.239 | 0.700 | 7.839 | 4.43 | 0.142 | 0.080 |
| Mor | 0.01 | 0.34 | 0.001 | 0.009 | 0.004 | 0.07 | 0.000 | 0.001 |
| Nay | 0.12 | 1.78 | 0.071 | 0.223 | 0.513 | 1.62 | 0.009 | 0.029 |
| NL | 53.21 | 58.66 | 99.153 | 31.166 | 657.426 | 206.64 | 11.896 | 3.739 |
| Oax | 12.84 | 15.92 | 34.639 | 10.965 | 267.640 | 84.72 | 4.843 | 1.533 |
| Pue | 6.31 | 1.81 | 5.661 | 0.457 | 44.492 | 3.59 | 0.805 | 0.065 |
| Qro | 14.73 | 0.45 | 4.349 | 0.024 | 28.359 | 0.16 | 0.513 | 0.003 |
| Qroo | 1.65 | 13.22 | 1.548 | 5.279 | 10.986 | 37.46 | 0.199 | 0.678 |
| SLP | 27.28 | 8.58 | 45.153 | 2.603 | 217.503 | 12.54 | 3.936 | 0.227 |
| Sin | 0.45 | 1.59 | 0.468 | 0.253 | 3.137 | 1.70 | 0.057 | 0.031 |
| Son | 16.88 | 24.58 | 67.892 | 34.060 | 505.778 | 253.74 | 9.152 | 4.591 |
| Tab | 28.96 | — | 14.620 | — | 56.795 | — | 1.028 | – |
| Tamps | 36.54 | 21.71 | 93.656 | 13.151 | 675.891 | 94.91 | 12.230 | 1.717 |
| Tlax | 2.56 | 0.94 | 0.219 | 0.036 | 1.184 | 0.20 | 0.021 | 0.004 |
| Ver | 13.38 | 10.91 | 21.625 | 5.994 | 139.522 | 38.68 | 2.525 | 0.700 |
| Yuc | 25.20 | 37.25 | 19.971 | 10.201 | 158.735 | 81.08 | 2.872 | 1.467 |
| Zac | 35.74 | 37.48 | 67.470 | 13.0206 | 377.797 | 72.91 | 6.836 | 1.319 |
| **Ntn'l** | **22.38** | **20.51** | **1,027.74** | **297.25** | **7,897.26** | **2,153.76** | **142.903** | **38.973** |

energy harvesting for alkaline and PEM electrolyzers, respectively. This calculation was developed considering an efficiency of 75 %, and it was found that the LCOH ranges from 7.4 to 34.9 USD/kg for alkaline electrolyzers and from 8.9 to 39.4 USD/kg for PEM electrolyzers. It is observed that in the seven zones identified with the highest economic potential, the LCOH is the lowest, with costs that could be internationally competitive, given a CAPEX of 1,800 and 2,000 USD/kW for electrolyzers.

It is important to emphasize that when evaluating the economic potential for hydrogen production, the real conditions of the technology in the Mexican context must be considered. Especially in terms of costs, inaccurate information could be generated, which would have significant repercussions on decision-making. Through quotations obtained for the importation of electrolyzers to Mexico, it was found that the CAPEX for electrolyzers would be 8,000 USD/kW and 12,000 USD/kW for alkaline and PEM electrolyzers, respectively. These costs have a strong impact on the LCOH, as shown in Figure 5.15.

The effect of the electrolyzer's CAPEX on the LCOH across the seven regions with high economic potential is shown in Figure 5.15. If the cost of importing an electrolyzer to Mexico does not decrease in the coming years, it will be difficult for wind hydrogen production to be attractive, as the LCOH increases by 3 to 5 times. This is exemplified in zones 1 and 5, where the LCOH has values of 29.5 and 32.3 USD/kg for zone 1, while for zone 5, the LCOH would be 33.6 and 51.2 USD/kg for alkaline, and PEM electrolyzer, respectively.

These production costs would definitively render the development of hydrogen in the country unfeasible, as the electrolyzer CAPEX reported by the IEA pertains to countries where already exist a mature market for the technology. This underscores the urgent need to develop international alliances and public policies that enable cost reductions in technology imports. Although Mexico possesses regions with high wind potential, the cost of the technology would not allow for harnessing this resource.

## 5.4   Summary and Highlights

In summary, assessing hydrogen generation potential from wind resources has shed light on crucial facets of Mexico's renewable energy landscape. The findings reveal that 20.5 % of Mexican territory holds the promise for wind technology deployment, with a capacity reaching up to 297 GW. However, as of 2022, only 7,691 MW had been installed, representing a utilization of merely 2.6 % of this potential capacity. Such statistics highlight Mexico's substantial shortfall in meeting its decarbonization objectives by 2024.
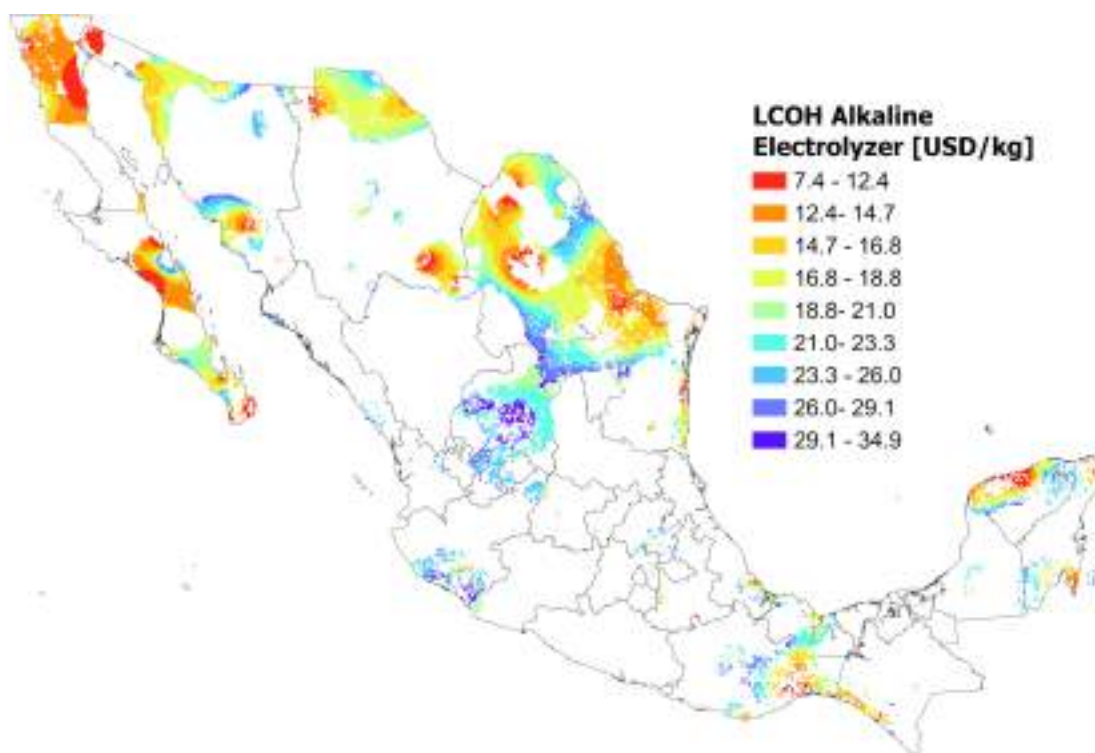
(a)
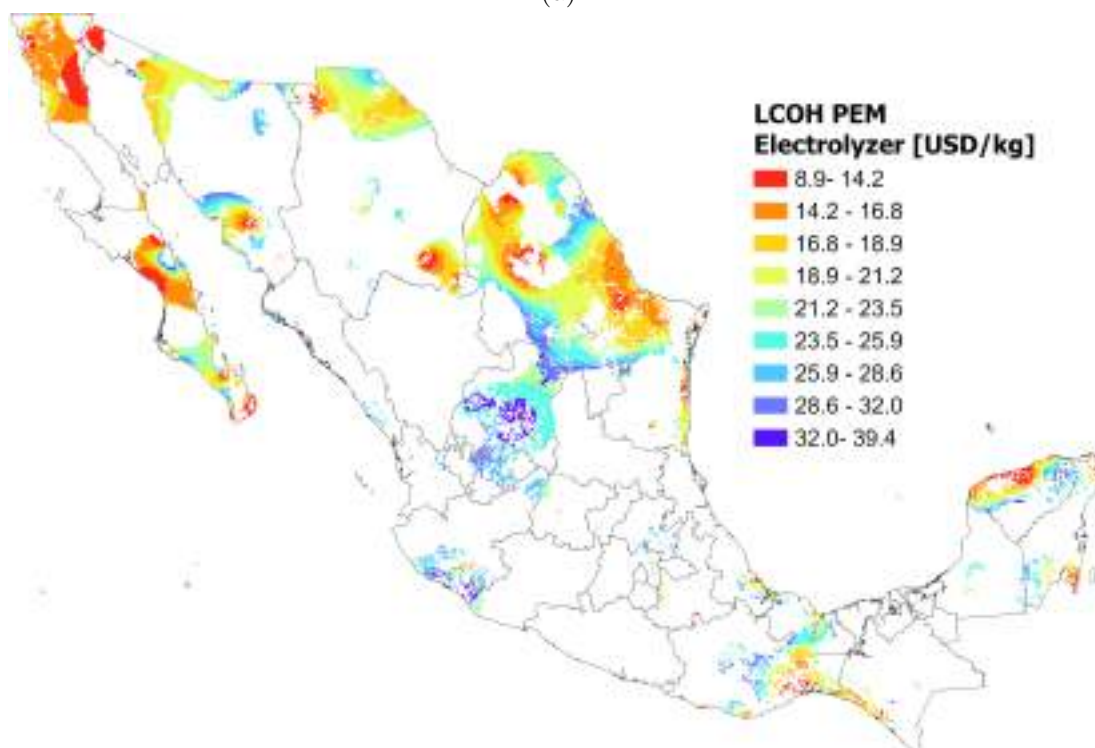


(b)

Figure 5.14: Onshore Wind LCOH distribution.
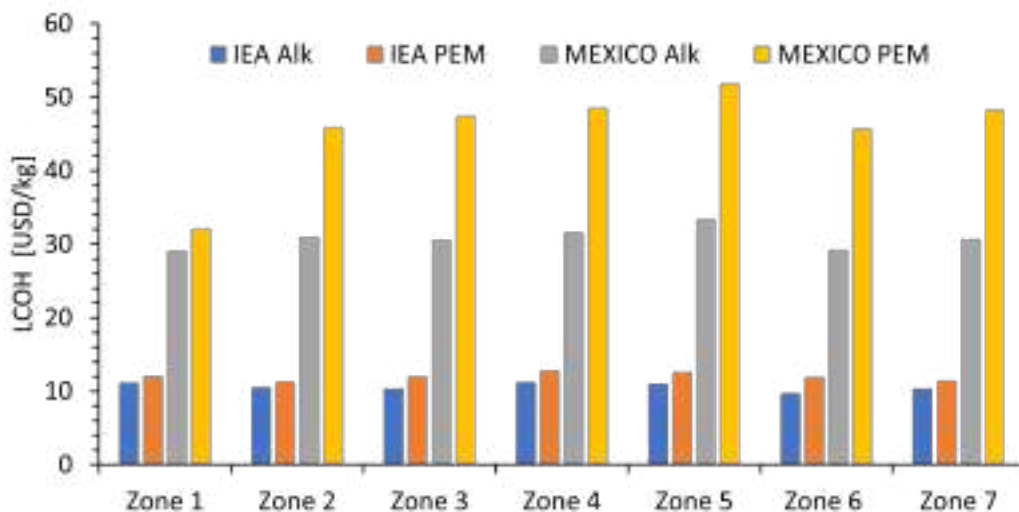
Figure 5.15: Impact of the Electrolyzer CAPEX on the LCOH per zone of high economic potential.

Despite the competitive nature of wind energy compared to conventional sources, the lack of comprehensive policy frameworks impedes its full integration into the national energy portfolio. Consequently, the envisioned scenario for leveraging renewable energies, particularly wind power, to facilitate sectoral decarbonization through hydrogen remains fraught with challenges. Addressing these obstacles necessitates a concerted effort to enact robust public policies that foster the widespread adoption of wind energy technologies, thereby fostering a more sustainable and environmentally conscious energy landscape in Mexico.

# Chapter 6

# Wind H$_2$ Production. Part B: Offshore

> In this section, we outline the procedures and results obtained from the assessment of the potential for hydrogen production from wind resources in the Mexican seas.

## 6.1 Methods

### 6.1.1 Wind Speed data and Study area

In the present study, utilization was made of the ERA 5 atmospheric reanalysis dataset, which was provided by the European Centre for Medium-Range Weather Forecasts (ECMWF). This dataset facilitates the provision of hourly estimations for various atmospheric parameters, including wind speed, at a spatial resolution of 0.25 × 0.25 degrees, situated at an altitude of 100 meters [119]. The applicability of this dataset in assessing the wind energy potential across diverse geographical regions has been affirmed by numerous researchers [8, 120, 114]. Additionally, its comparative effectiveness in relation to alternative datasets, such as MERRA-2, has been examined in [98]. The ERA 5 dataset served as the foundation for the development of the Global Wind Atlas (GWA) [100], wherein subsequent endeavours in mesoscale and microscale modelling contributed to an enhancement in spatial resolution to 250 × 250 meters.

The resolution enhancement procedure in the current investigation was executed using the bilinear interpolation functionality embedded within ArcGIS Pro®. This process was guided by the foundational reference of the Global Wind Atlas (GWA). Subsequently, meticulous comparisons were conducted on velocity distributions, maintaining an identical resolution of $250 \times 250$ meters. This comparative analysis revealed Root Square Error (RSE) values ranging from 0.5 % to 3 %, with the most notable deviations observed in coastal regions. Moreover, this inquiry encompassed the processing of wind speed values at an augmented resolution of $500 \times 500$ meters within the Exclusive Economic Zone (EEZ) of Mexico, spanning an area of 3,177,210 km$^2$ [121] (Fig. 6.1).
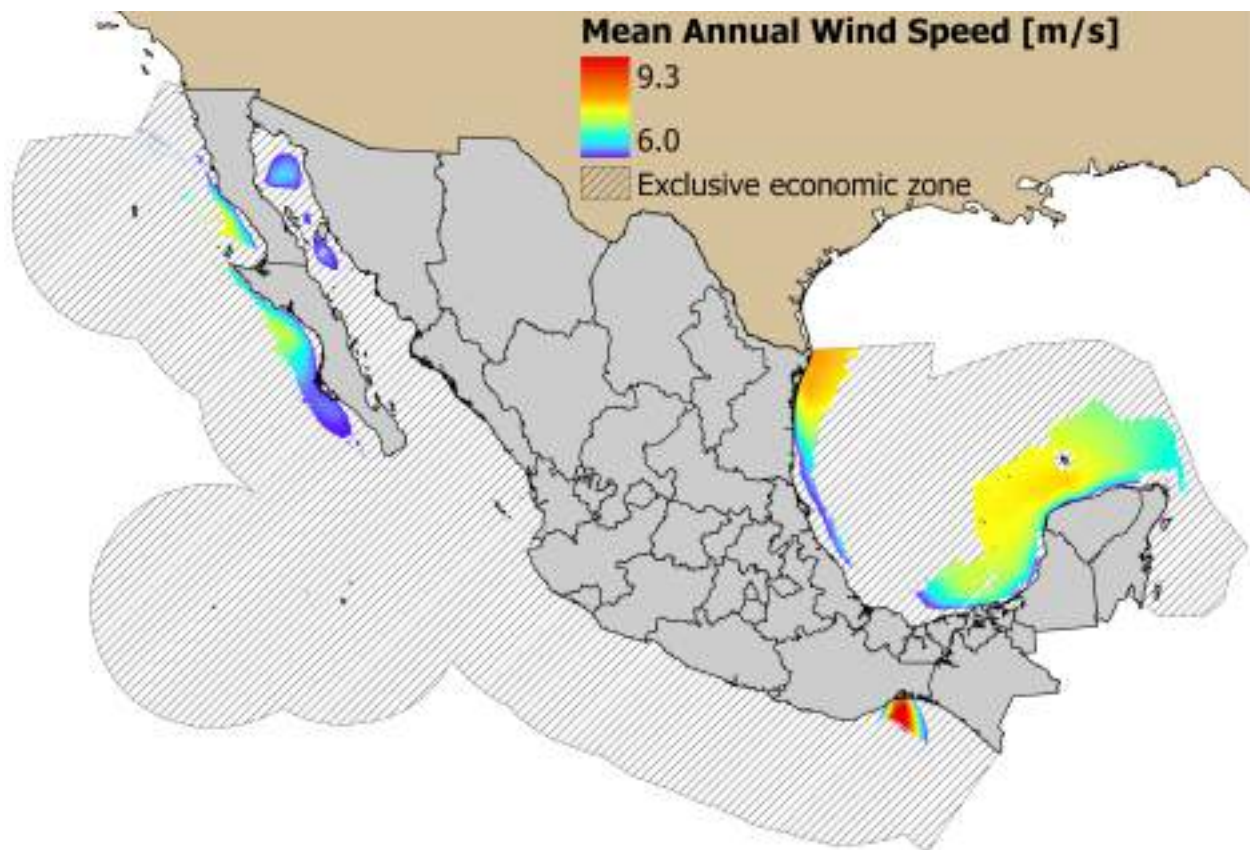


Figure 6.1: Annualized Mean Wind Velocity in the Eligible Territories of the Exclusive Economic Zone Post-Implementation of Geographic and Technical Harvesting Constraints.

### 6.1.2 Offshore Wind Hydrogen Potential Assessment

The assessment of the technical and economic potential for offshore hydrogen production was conducted following the methodology outlined in Figure 6.2. Within this methodology, economic factors such as LCOE and LCOH play important roles. The offshore energy output and the LCOE assessment involve several steps detailed in Figure 6.3.

The assessment of wind energy extraction involves various dimensions, including the resource or theoretical potential, which encompasses the global energy content; the geographic potential, indicating the available area for turbine installation; and the technical potential, which considers limitations imposed by current technology. The constraints considered in this study are enumerated in Table 6.1.

The equations involved in wind energy extraction calculation have been previously outlined in the preceding chapter. The power density describes the resource potential according to Equation 5.1, while the technical potential relies on turbine capacities (Power Curve) and velocity distribution is described by the Probability Density Function, as elucidated in Equation 5.4. Equations 5.3 and 5.15 delineate the expected energy ($E_{Expected}$), and the capacity factor was computed using Equation 5.16.

In the present analysis, emphasis is placed on the Vestas V164-9.5 MW turbine, a model previously utilized in various offshore projects [8]. The power curve and notable characteristics of this turbine are depicted in Figure 6.4. Turbine spacing was set at 7 rotor diameters along the dominant wind direction and 5 diameters perpendicularly. This setup facilitated the calculation of monthly and annual technical potential for offshore wind energy generation.

The potential for hydrogen production was derived from the generated wind energy. The hydrogen mass ($M_{H_2}$) in Ton/km$^2$ year was computed according Equation 5.17 as explained in the previous chapter.
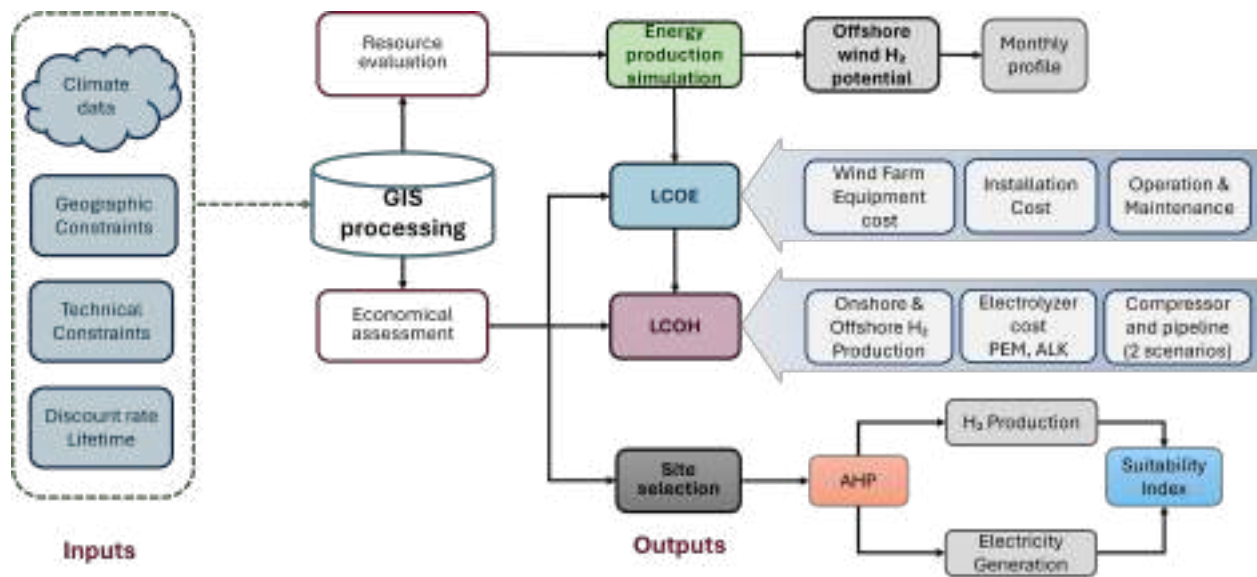
Figure 6.2: Research methodology.
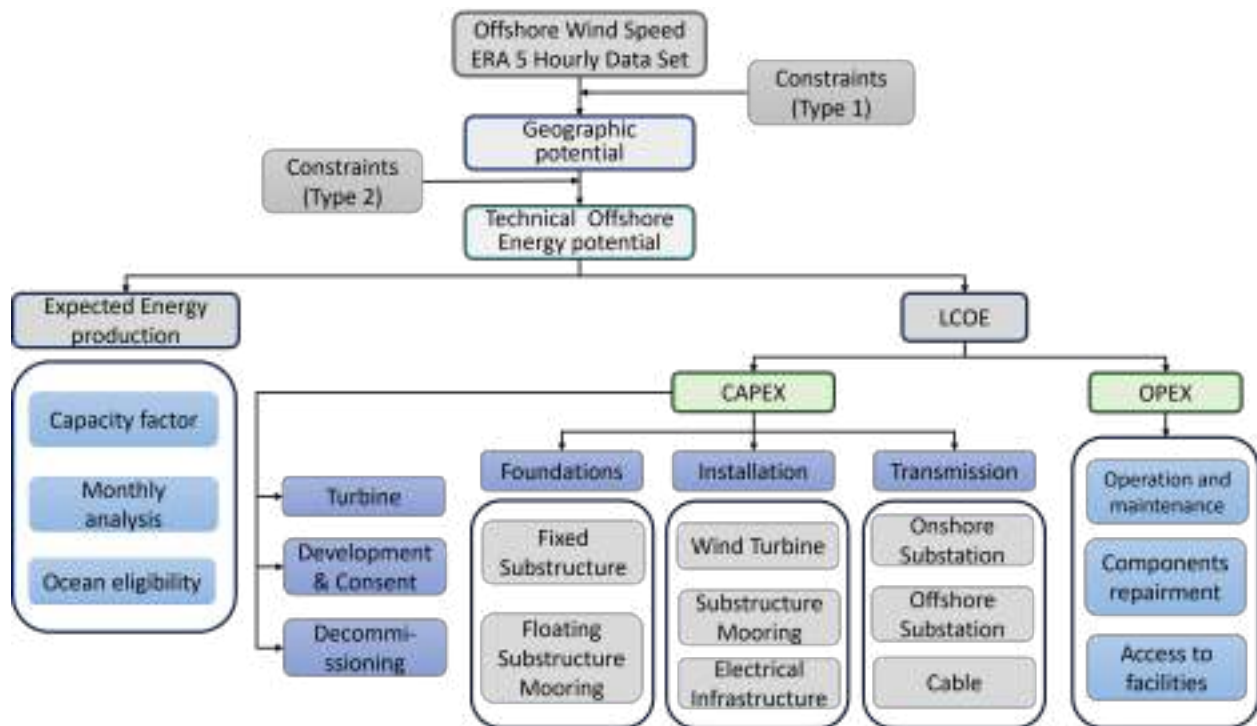


Figure 6.3: Detailed Offshore Wind Energy and LCOE Assessment procedure.

Table 6.1: Constraints considerations in assessing offshore energy potential

| Geographic Potential (Type 1) | | |
|---|---|---|
| Constraint | Excludes | Value |
| Protected zones | Below | 1000 m |
| Distance from shore | Above | 200 km |
| Pipelines | Below | 500 m |
| Technical Potential (Type 2) | | |
| Water depth (d) | Above | 1000 m |
| Wind speed (annual average) | Bellow | 6 m/s |
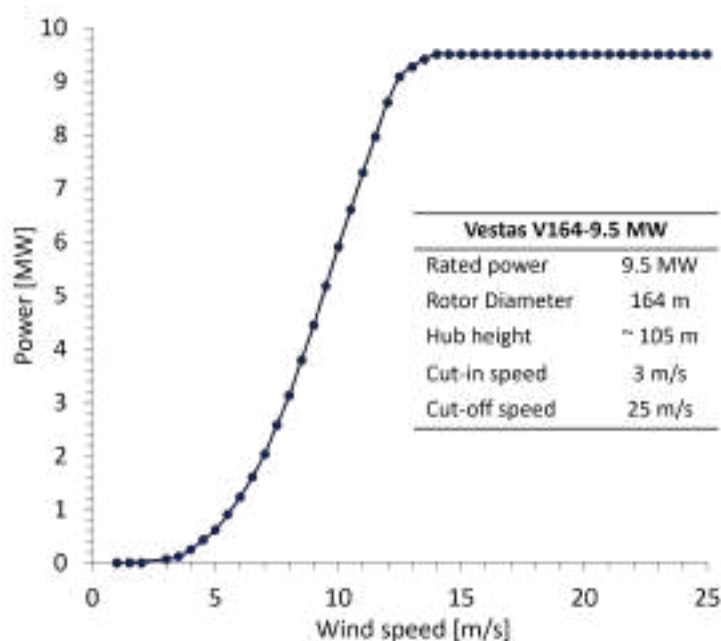


Figure 6.4: Vestas V164-9.5 turbine power curve [8].

## 6.1.3   Economic assessment

1. A 1 GW offshore wind generation plant.

2. Two foundation technologies: Fixed bottom and Floating, selected based on depth.

3. 90 % of energy is used for hydrogen production and 10 % for compression and desalination.

4. As described in Table 6.2, offshore wind hydrogen (OWH) production is analyzed using three integration schemes. Only OnEL and COfEL are considered, as DOfEL, a more complex system, is deemed feasible post-2050 according to [122].

5. For COfEL, electricity cost includes inter-array cable costs only since export cable costs are null.

6. Hydrogen transport infrastructure in COfEL is evaluated in two scenarios: using new equipment (COfEL-New) and repurposing existing assets (COfEL-Rep).

### LCOH Offshore

LCOH is calculated using Equation 6.1, where CAPEX$_{H_2}$ represents the capital expenditures and OPEX$_{H_2}$ denotes the operational expenses. The required parameters are detailed in Table 6.3.

$$\text{LCOH} = \frac{\sum_{j=0}^{N}((\text{CAPEX}_{H_2} + \text{OPEX}_{H_2})(1+I)^{-j})}{\sum_{j=0}^{N}((M_{H_2}[j])(1+i)^{-j})} \tag{6.1}$$

where CAPEX$_{H_2}$ and OPEX$_{H_2}$ are calculated using Equations 6.2 and 6.3, respectively. The hydrogen infrastructure plant includes the electrolyzer and balance of plant components (*Elec*), compressor and pipeline systems (*Comp&pipe*), and the desalination unit (*Desal*).

$$\text{CAPEX}_{H_2} = \text{CAPEX}_{Elec} + \text{CAPEX}_{Comp\&pipe} + \text{CAPEX}_{Desal} \tag{6.2}$$

$$\text{OPEX}_{H_2} = \text{OPEX}_{Elec} + \text{OPEX}_{Comp\&pipe} + \text{OPEX}_{Desal} \tag{6.3}$$

*Electrolyzer*

The calculation of CAPEX$_{Elec}$ is accomplished utilizing Equation 6.4, which incorporates the electrolyzer cost (EC) for both PEM and Alkaline (ALK) technologies, as outlined in Table 6.3. EC is examined under two scenarios: the international market, following the specifications of IEA [123], and the Mexican market, based on received quotations.

$$\text{CAPEX}_{Elec} = \text{EC} \times \left(\frac{M_{H_2} R_{en}}{h_{eff}}\right) \tag{6.4}$$

Table 6.2: Integrating schemes for offshore wind energy and hydrogen production ([1],[2]).

| Connection Schemes | Energy Vector to shore | Characteristics | Advantages | Disadvantages |
|---|---|---|---|---|
| Onshore electrolysis (OnEL) | Electricity | Electricity is produced, and transmitted to shore, then H$_2$ is produced | *The electrolyzer operation and efficiency is ensured for onshore conditions. *Easier installation | *Energy losses by electrical transmission. * High cost of submarine cables |
| Centralized Offshore electrolysis (COfEL) | Hydrogen | H2 is directly produced with a central electrolyzer then, is compressed and carried to shore using pipelines. | *H$_2$ pipelines are only feasible for large WF and long distances. * Maintenance reduction | *Electrolyzer operation require verification. * Extra cost in vessels to install electrolyzers |
| Offshore electrolysis decentralized (DOfEL) | Hydrogen | The electrolyzer, co-located with desalination facilities, is situated proximate to the wind turbine. The generated H$_2$ is compressed and carried with pipelines | *The wind turbine substructure is used to install the electrolyzer. *As modular system offers greater manageability in the event of failures. | *System complexity * Electrolyzer require verification *Difficulty in O&M |

$$\text{OPEX}_{Elec} = \text{CIE} + \text{COM} + \text{CORP} \qquad (6.5)$$

$$\text{CIE} = \text{LCOE} \cdot ET \qquad (6.6)$$

OPEX$_{Elec}$ encompasses the electricity investment (CIE), operation and maintenance costs (COM), and replacement costs (CORP), with COM and CORP constituting 2 % and 25 % of CAPEX$_{Elec}$, respectively, as delineated in Equation 6.5. CIE is defined according to Equation 6.6.

### Compressor and pipeline

Compressor and pipeline costs are considered together. According to [124], these costs are given in M€/km and updated to 2023 MUSD/km. In some studies, the cost of each component has been obtained independently ([125], [126]). Table 6.3 shows all the parameters employed in LCOH calculation.

### Desalinisation Unit

Hydrogen production from offshore wind necessitates using seawater, incorporating desalination units. Stoichiometrically, 10 kg of water is needed per kg of H$_2$, though typical requirements are 15-17 kgH$_2$O/kgH$_2$ due to losses [127]. Based on the annual hydrogen output of a 1GW plant, the water flow rate (V$_{H_2}O$) in m$^3$/h can be approximated. Desalination

costs, set according to daily processing capacity, range from 1,000 to 10,000 m$^3$/day, fitting this study's scale. Here, the desalination cost (D$_c$) is 1000 USD/m$^3$/day, and the capital expenditure for desalination (CAPEX$_{Desal}$) follows Equation 6.7 ([2], [122]).

$$\text{CAPEX}_{Desal} = V_{H_2O} \times D_c \tag{6.7}$$

Table 6.3: Value of parameters required in LCOH calculation.

| Variable | Long name | Values |
|---|---|---|
| | Electrolyzer | |
| N | Lifetime [years] | ALK= 20 yeas PEM=10 |
| I | Discount rate [%] | 10 |
| EC | Electrolizer cost [USD/kW] | ALK=1,700 PEM=2,000 ALK$_{MEX}$= 8,000 PEM$_{MEX}$= 12,000 |
| | Pipeline & Compressor [124] | |
| CAPEX$_{Comp\&pipe}$ | Repurposing Infrastructure | 0.6 [MUSD/km] |
| OPEX$_{Comp\&pipe}$ | Repurposing infrastructure | 0.74 [MUSD/km] |
| CAPEX$_{Comp\&pipe}$ | New infrastructure | 3.36 [MUSD/km] |
| OPEX$_{Comp\&pipe}$ | New infrastructure | 0.74 [MUSD/km] |

**Offshore Wind Energy Cost**

The LCOE of offshore wind farms has been thoroughly examined in numerous research efforts ([125], [128], [129], [4]). The computation of capital expenses is recognized as a significantly intricate task, owing to the complex nature of the involved components, as well as dependencies on technological advancements and geographical specifications.

The LCOE, represented as the average cost per megawatt-hour ($/MWh), serves as a crucial economic indicator, encompassing the cumulative initial investment necessary for plant establishment and subsequent operational management throughout the project's lifetime. This metric facilitates comparative analyses across various energy generation technologies by delineating the equilibrium price required for electricity production throughout a project's existence. The methodology for computing this parameter is as follows [130]:

$$\text{LCOE} = \frac{\sum_{j=0}^{N} \left( (\text{CAPEX} + \text{OPEX})(1+I)^{-j} \right)}{\sum_{j=0}^{N} \left( (ET[j])(1+i)^{-j} \right)} \tag{6.8}$$

where $N$ signifies the lifespan of the project. CAPEX (in USD) embodies the initial capital expenditures, and OPEX encompasses the ongoing operation and maintenance costs.

Figure 6.5: Foundation Type and Ocean Suitability by Depth for the Five Designated Zones of Offshore Wind Energy Deployment.

In the current analysis, the LCOE is evaluated within areas identified as technically feasible for the installation of offshore wind farms (Fig. 6.5), following the methodologies delineated in [9], [131], and [3]. These methodologies incorporate the initial criteria established by IRENA for the geospatial assessment of LCOE. A power plant with a capacity of 1 GW was selected for this assessment, necessitating the utilization of raster data characterized by a cell dimension of 10 x 10 km. Given the variable seabed depths within Mexican maritime boundaries, evaluations were conducted for Fixed-bottom and Floating foundation technologies. The analysis was conducted using a discount rate of 10 % and a projected operational period of 20 years.

*CAPEX Calculation*

The estimation of investment costs is bifurcated into two distinct categories. The first category includes expenses that are contingent upon factors such as water depth and the distance to the coastline, encompassing Foundation ($C_{\text{found}}$), Electricity Transmission ($C_{\text{Trans}}$), Installation ($C_{\text{Inst}}$), and Decommissioning costs ($C_{\text{Decom}}$), the latter being a proportion of $C_{\text{Inst}}$. Conversely, the second category comprises costs that are solely influenced by the capacity of the plant, including the Turbine ($C_{\text{Turbine}}$) and Development and Consent procedures ($C_{\text{DevC}}$).

CAPEX was calculated according to [9], following Eq. (6.9). This calculation was performed for each cell ($i$), representing the necessary surface area for a 1 GW offshore wind farm:

$$\begin{aligned} CAPEX_i &= C_{DevC,i} + C_{Turbine,i} + C_{found,i} + C_{Trans,i} \\ &\quad + C_{Inst,i} + C_{Decom,i} \end{aligned} \tag{6.9}$$

*Development and Consent Costs*

Development and consent costs encompass environmental assessments, services, project management, and investigations into seabed and climatological conditions. As per the National Renewable Energy Laboratory (NREL), these costs constitute 2.1 % of the total Capital Expenditure (CAPEX) for fixed-bottom projects and 1.6 % for projects utilizing floating technology, with an applied rate of 98 USD/kW [132].

*Turbine Costs*

Wind turbine expenses constitute a significant portion of CAPEX, alongside foundations and substructures. Variations in offshore turbine cost estimations stem from various sources, resulting in a range of reported figures. NREL has documented costs of 1,301 USD/kW for the period 2021-2022 [132] and 1,700 USD/kW for 2022-2023 [133]. A median value of 1,600 USD/kW was utilized in [130], whereas BVG Associates suggests a baseline of 1,000 USD/kW [134]. This analysis adopts a turbine cost of 1,700 USD/kW, which represents the latest and most accurate value available.

*Foundation Costs*

The substructure selection is significantly influenced by water depth, directly impacting costs. The industry distinguishes between Fixed-bottom and Floating substructure technologies [135]. Fixed-bottom technologies commonly include Monopile and Fixed Jacket structures, while Floating technologies encompass Wind Float, Tension Leg Buoy (TLB), Hywind, SWAY, and Semisubmersible platforms, among others [136]. The deployment depth ranges for these technologies are detailed in Table 6.4 and Fig. 6.5, delineating five prospective zones for offshore wind farm installation: Northwest (Cortes Sea), BC-BCS (Baja California and South Baja California coasts), Northeast (northern Gulf of Mexico), Oriental (Oaxaca coasts), and Peninsular (north and west of the Yucatan Peninsula).

Cost evaluations for substructures incorporate material and manufacturing expenses, with specific studies on floating technology estimating 8 million euros per turbine [131]. The dynamic nature of this technology and the scarcity of detailed cost information pose challenges for precise cost determination. NREL has reported 609 USD/kW for fixed-bottom and 1,708 USD/kW for floating technologies [133].

Research by [9], [137], and [138] establishes cost correlations for substructures and foundations based on water depth for turbines around 8 MW. This methodology is advantageous for mapping the LCOE across specific geographic regions. The current study maps LCOE for offshore energy in Mexico, underscoring the importance of water depth as a cost determinant.

In [9] the foundation costs were correlated as a function of depth ($d$) for Monopile, Fixed Jacket, and Tension Leg Buoy (TLB) technologies in 2016 USD and it was initially proposed by Anders Myhr et al. [4]. The data were updated to 2023 USD values to account for annual inflation. Fig. 6.6 illustrates the resultant cost curves, with the associated parameters detailed in Table 6.4.

Floating technology require the utilization of mooring lines and anchors, which are essential for maintaining the positional integrity of the substructure. The financial investment
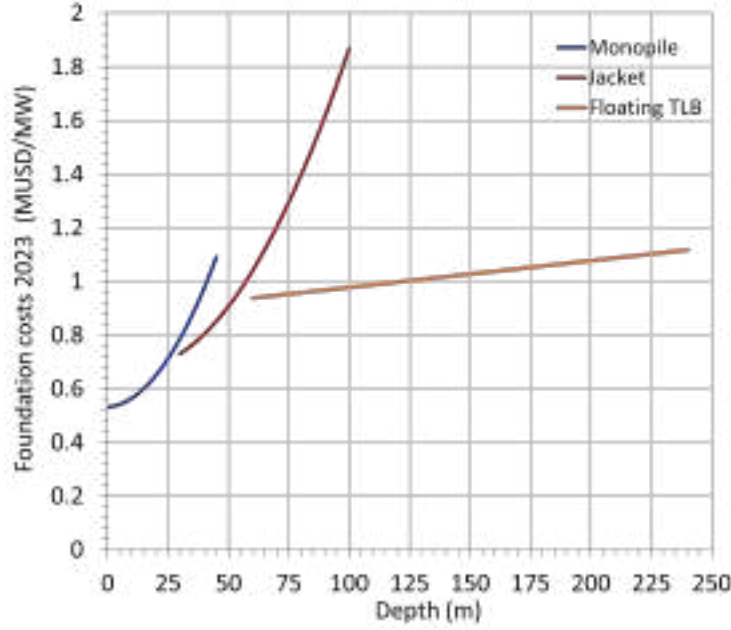
Figure 6.6: Foundation Cost as a Function of Depth, Updated to 2023 Based on the Model Initially Proposed in [4].

in this apparatus depends on the extent of line utilization, which is influenced by water depth and the specific anchor technology employed [130]. In Tension Leg Buoy (TLB) configurations, mooring lines are anchored at two elevations: the seabed, 50 meters below the water's surface, and approximately 25 meters above it. The upper segment of the mooring line descends to the seabed at a 45° inclination, with the mooring radius extended by an additional 25 meters beyond the water depth [136]. The overall mooring expenditure for the typical plant was determined using Equation. (6.10), which represents an adaptation of the framework proposed in [130], tailored to the requirements of TLB technology.

Table 6.4: Foundation Costs as a function of depth for three different technologies.

| Foundation Techology | Depth interval [m] | Cost as function of the depth $(d)$ [USD/MW] |
|---|---|---|
| Monopile | 0-30 | $259.26\mathrm{dd}d^2 + 790.59d + 530{,}727$ |
| Jacket | 30-60 | $147.35d^2\text{-}2928d + 685{,}862$ |
| TLB | >60 | $998.15d + 877{,}937$ |

$$C_{mooring} = n_{tur}n_{lines}\left[C_{anchor} + (L_1 + L_2)\,C_{line}\right] \qquad (6.10)$$

where $n_{\text{tur}}$ denotes the total count of turbines, $n_{\text{lines}}$ refers to the requisite mooring lines per turbine (three pairs), $C_{\text{anchor}}$ represents the cost per anchor (476,909 USD) with a requirement of three per turbine. $L_1$ and $L_2$ indicate the lengths of the mooring lines, while $C_{\text{line}}$ is the price per kilometre of line (1,032 USD/km). The values for $C_{\text{anchor}}$ and $C_{\text{line}}$ were adjusted to 2023 USD based on [136].

*Transmission cost (Electrical infrastructure)*

Determining the costs of submarine transmission cables relies on several crucial factors, notably the distance to shore ($D$) [131]. For projects with capacities in the hundreds of megawatts, the "break-even" analysis is employed to determine at what distance High Voltage Direct Current (HVDC) becomes more economically viable than High Voltage Alternating Current (HVAC), taking into account energy losses and infrastructure requirements. This analysis evaluates both transmission types (Fig. 6.7), considering the necessary substation, cable length relative to distance, and the inter-array cabling as described in Eq. (6.11), with costs obtained from [3] and detailed in Table 6.5.

$$
\begin{aligned}
C_{Trans} &= Dn_{ex\_cab}C_{ex\_cab} + n_{off\_sub}C_{off\_sub} \\
&+ n_{on\_sub}C_{on\_sub} + dc_{in}C_{in}
\end{aligned}
\tag{6.11}
$$

where $D$ is the distance to shore, $n$ represents the number of subsea and exportation cables ($ex$) and substations required that can be onshore ($on\_sub$) or offshore ($off\_sub$).$C$ quantifies the cost. Following [131], the inter-array cabling is anticipated to necessitate 20 strands, each capable of supporting 5 turbines. The aggregate length of the inter-array cables is forecasted at 201.8 km, with an ensuing expenditure of 0.39 MUSD/km.

Table 6.5: Parameters for Transmission Cost of a 1 GW Offshore Wind Plant [3].

| Element | HVAC | HVDC |
|---|---|---|
| $n_{ex\_cab}$ | 3 | 3 |
| $C_{ex\_cab}$ [MUSD/km] | 2.45 | 1.22 |
| $n_{off\_sub}$ | 3 | 2 |
| $C_{off\_sub}$ [MUSD] | 40.95 | 149.89 |
| $n_{on\_sub}$ | | 1 |
| $C_{on\_sub}$ [MUSD] | | 88.57 |
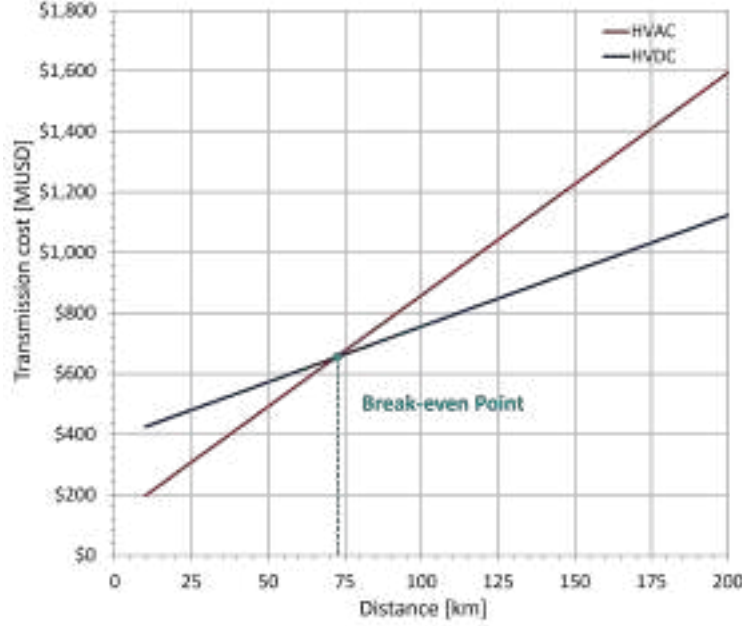
Figure 6.7: Transmission costs as a function of the distance to shore [9]. Values are updated to 2023 USD.

*Installation Cost*

Ascertainment of installation expenditures poses challenges due to the scarcity of large-scale projects providing precise cost insights. According to NREL, installation costs may vary between 229 USD/kW and 279 USD/kW. These costs encompass the installation of turbines and substructures ($C_{\text{Itur-subs}}$), as well as electrical infrastructure ($C_{\text{Iinfelec}}$), which includes export cables, inter-array cables, and substations as outlined in Eq. (6.12). Additionally, the cost of installing mooring systems must be accounted for when utilizing floating technology.

$$C_{Inst} = C_{Itur-subs} + C_{Iinfelec} \tag{6.12}$$

In [136], costs were reported that include the installation of the turbine and substructure. These updated values for 2023 are 1.92 MUSD/Turbine and 2.46 MUSD/Turbine for Monopile and Jacket technologies, respectively. For the floating modality, an algorithm is presented in [131] that enables the calculation of installation costs for the turbine and substructure based on distance and installation time. This procedure is given by Equation 6.13, where $n_{tur}$ is the number of turbines for a 1 GW plant, $t_{inst}$ is the installation time,

Table 6.6: Values of parameters used in calculating installation costs.

| Electrical Installation | |
|---|---|
| Cable | Cost [USD/km] |
| Export cable | 680.2057 |
| Inter-array cable | 226.7352 |
| Substation Technology | Cost 2023 KUSD |
| Fixed | 63,050 |
| Float | 49,090 |
| Floating Installation parameters | |
| Element | Value |
| ntur trip | 5 |
| tinst | 2 |
| Vvessel [km/h] | 20 |
| Cvessel [2023 USD/h] | 1,4415.66 |

Table 6.7: Parameters for Decommissioning Cost Calculation [4]

| Factor | Floating [%] | Fixed-Bottom [%] |
|---|---|---|
| Complete wind turbine | 70 | 80 |
| Subsea cables | 10 | 10 |
| Substation | 90 | 90 |
| Mooring system | 90 | — |

$C_{vessel}$ is the cost of the jack-up vessel, $V_{Vessel}$ is the velocity, and $n_{tur_trip}$ are the carried turbines per trip. All the involved parameters in the installation costs are shown in Table 6.6 [3].

$$C_{Itur} = n_{tur} \left[ t_{inst} + \frac{2D}{V_{Vessel}} \right] \frac{C_{vessel}}{n_{tur_trip}} \tag{6.13}$$

*Decommissioning cost*

The decommissioning costs exhibit an inverse relationship with installation costs, wherein a common practice involves treating them as a percentage of the $C_{Inst,i}$ and therefore, they depend on the technological framework. The percentages considered are presented in Table 6.7 for floating and fixed technologies, respectively.

*OPEX Calculation*

OPEX is also spatially variable depending on the accessibility of the site from a suitable port, local cost of labour, vessel, and the project site type and conditions mainly the distance to shore. In some studies, OPEX is reported as a constant value for a specific distance, for
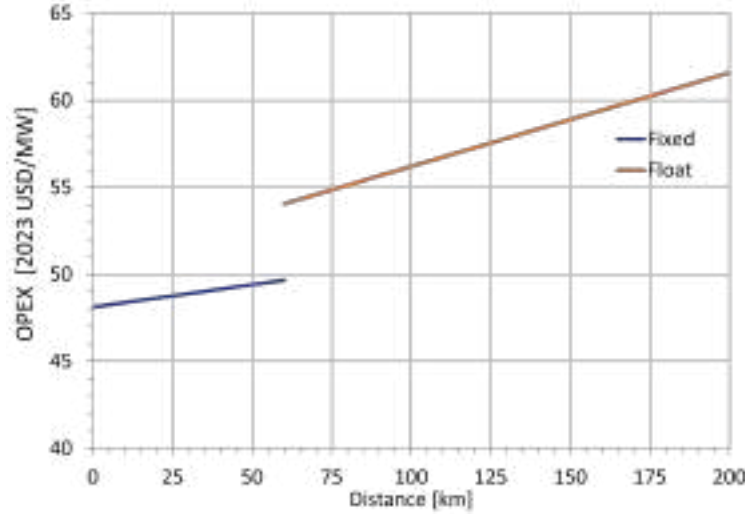
Figure 6.8: Operation and maintenance costs as a function of the distance to shore [9].

example in [131], a value of 138 k€/MW/year was considered and 40 €/MW/km/year was added to include travelling expenses. NREL reported that the total OPEX can be approximated to 87 USD/kW/year. In [9] the OPEX is reported in 2016 USD/MW/year as a function of the distance from shore and for each technology, this approach was originally addressed by Myhr et al [4], and in this work, it is used, these costs were actualized to 2023 USD considering the inflation. In Figure 6.8 OPEX is presented as a function of the distance.

## 6.1.4  GIS-MCDM Analysis for suitable site selection

In techno-economic assessments of offshore wind energy, the calculation of LCOE and LCOH entails site selection governed by specific constraints. This study compares sites for electricity generation and hydrogen production utilizing the Multi-Criteria Decision-Making (MCDM) framework, a method previously utilized by some researchers ([139], [140], [141]).

Among MCDM methods, the Analytic Hierarchy Process (AHP), developed by Thomas L. Saaty in 1970 [142], holds particular popularity. When combined with Geographic Information Systems (GIS), AHP efficiently categorizes geographical areas for energy harvesting. The AHP framework arranges objectives, criteria, sub-criteria, and decision alternatives into a hierarchical structure. The implementation of AHP involves several steps, as outlined by [143], [144], [145]:

Table 6.8: Techno-economic criteria and suitability reclassification for electricity generation

| Criteria/Suitability class | Poor | Limited | Fair | Good | Excellent | Outstanding |
|---|---|---|---|---|---|---|
| Wind speed [m/s] | 6-6.5 | 6.5-7 | 7-7.5 | 7.5-8 | 8-8.5 | 8.5-9 |
| Water Depth [m] | 300-1,000 | 200-300 | 100-200 | 60-100 | 30-60 | 0-30 |
| Distance to shore [km] | 170-200 | 130-170 | 100-130 | 70-100 | 35-70 | 0-35 |
| Distance to grid [km] | 80-100 | 60-80 | 50-60 | 30-50 | 20-30 | 0-20 |
| Distance to ports [km] | 125-150 | 100-125 | 75-100 | 50-75 | 25-50 | 0-25 |

Table 6.9: Techno-economic criteria and suitability reclassification for hydrogen generation

| Criteria/H₂ Suitability class | Poor | Limited | Fair | Good | Excellent | Outstanding |
|---|---|---|---|---|---|---|
| Wind speed [m/s] | 6-6.5 | 6.5-7 | 7-7.5 | 7.5-8 | 8-8.5 | 8.5-9 |
| Water Depth [m] | 300-1000 | 200-300 | 100-200 | 60-100 | 30-60 | 0-30 |
| Distance to Petrochemical Plants [km] | 170-200 | 130-170 | 100-130 | 70-100 | 35-70 | 0-35 |
| Distance to Refineries [km] | 80-100 | 60-80 | 50-60 | 30-50 | 20-30 | 0-20 |
| Distance to Gas pipelines [km] | 125-150 | 100-125 | 75-100 | 50-75 | 25-50 | 0-25 |
| Distance to Refinery pipelines [km] | 80-100 | 60-80 | 50-60 | 30-50 | 20-30 | 0-20 |

1. *Problem decomposition into a hierarchy.* A hierarchical structure is built to govern the decision-making process and the goal is established. In this case, the objective is to find the locations with the lowest cost for offshore energy harvesting and hydrogen production. These are different optimization problems since the criteria involve specific techno-economic factors.

2. *Suitability reclassification, setting a normalized scale.* The values of the criteria taken into account in this study are classified according to six categories (Tables 6.8 y 6.9). According to [146], hydrogen transportation through pipelines would necessitate the placement of a compressor every 250 km. Therefore, this study establishes a slightly more restrictive scenario, whereby the maximum distance from a generation point to petrochemical plants is set at 200 km, and 100 km for gas-oil facilities (pipelines and refineries).

3. *Pairwise comparison.* All decision criteria must be paired against all others according to the level of importance related to the main goal and arranged in a comparison matrix 6.10. The criteria $A_i$ in the first column is compared to each criterion $A_j$ in the top row producing an $a_{ij}$ element arranged in a square matrix. To quantify the importance of one criterion over another, a special scale established by Satty is used [143]. It is

important to point out that in the matrix $a_{ij}$=1 when $i$=$j$ and $a_{ji}$=1/$a_{ij}$. The pairwise comparison matrixes for the cases analyzed in this study are shown in Table 6.11 and 6.12.

4. *Relative weights and normalization matrix.* The normalized matrix is built by dividing each element by the respective column sum. Then, the impact of each criterion on the objective is measured by the relative weight and it is computed by calculating the average of the values in each row of the normalization matrix, these values form the priority vector (W) (Tables 6.13).

5. *Robustness verification.* The consistency of the pairwise comparisons is evaluated by calculating the Consistency Ratio (CR) through the correlation between the Consistency Index (CI) and the Random Index (RI) (Equation 6.14). CI is computed as in Equation 6.15, where $\lambda_{max}$ is the maximum eigenvalue (AXw=$\lambda_{max}$X w), n is the number of criteria and RI is the random index and has been evaluated according to the number of criteria [147]. According to Saaty, if CR is larger than 0.1 the comparisons are inconsistent and therefore they have to be revised and repeated. In this case, the CR values are 0.049 and 0.075 for the electricity and hydrogen cases, respectively. Therefore, the comparison matrixes are correct.

$$CR = \frac{CI}{RI} \tag{6.14}$$

$$CI = \frac{\lambda_{max} - n}{n - 1} \tag{6.15}$$

6. Suitability Index: Finally the Suitability Index is computed through equation 6.16 where $x_i$ is the normalized variable value of each economic criteria and $W_i$ are the respective criteria weight. This step was applied to each pixel of the raster layer of study using GIS software producing a Site suitability map.

$$LSI = \sum_{i}^{n} x_i W_i \tag{6.16}$$

Table 6.10: Comparison matrix

| C/SubC | $A_1$ | $A_2$ | $A_3$ | ... | $A_n$ |
|--------|-------|-------|-------|-----|-------|
| $A_1$ | 1 | $a_{12}$ | $a_{13}$ | ... | $a_{1n}$ |
| $A_2$ | $a_{21}$ | 1 | $a_{23}$ | ... | $a_{2n}$ |
| $A_3$ | $a_{31}$ | $a_{32}$ | 1 | ... | $a_{3n}$ |
| $\vdots$ | $\vdots$ | $\vdots$ | $\vdots$ | $\ddots$ | $\vdots$ |
| $A_n$ | $a_{n1}$ | $a_{n2}$ | $a_{n3}$ | ... | 1 |

Table 6.11: Pairwise comparison matrix for electricity

| Criteria | Wind speed | Water Depth | Distance to shore | Distance to grid |
|----------|-----------|-------------|-------------------|------------------|
| Wind speed | 1.00 | 2.00 | 4.00 | 5.00 |
| Water depth | 1/2 | 1.00 | 4.00 | 4.00 |
| Distance to shore | 1/4 | 1/4 | 1.00 | 2.00 |
| Distance to grid | 1/5 | 1/3 | 1/2 | 1.00 |
| Distance to ports | 1/7 | 1/5 | 1/3 | 0.33 |
| Sum | 2.09 | 3.78 | 9.83 | 12.33 |

## 6.2   Results

1. Mexico harbors a significant offshore wind energy capacity estimated at 1609.7 GW.

2. Analysis of the designated area for turbine installation reveals that 58 % supports floating technology implementation, whereas 42 % is amenable to fixed-bottom structures.

3. The utilization of offshore wind power for transportation electrification is viable, requiring merely 2.3 % of the ascertainable energy to satisfy demand.

4. Computed LCOE suggests competitiveness within the Mexican energy sector, with values spanning from 63 to 241 USD/MWh.

Table 6.12: Pairwise comparison matrix for hydrogen

| Criteria | Wind speed | Water Depth | Distance to Petrochemical Plants | Distance to Refineries | Distance to Gas pipelines | Distance to Refinery pipelines |
|----------|-----------|-------------|----------------------------------|------------------------|---------------------------|--------------------------------|
| Wind speed | 1.00 | 3.00 | 4.00 | 5.00 | 7.00 | 7.00 |
| Water Depth | 1/3 | 1.00 | 3.00 | 4.00 | 7.00 | 7.00 |
| Distance to Petrochemical Plants | 1/4 | 1/3 | 1.00 | 4.00 | 5.00 | 6.00 |
| Distance to Refineries | 1/5 | 1/4 | 1/4 | 1.00 | 3.00 | 2.00 |
| Distance to Gas pipelines | 1/7 | 1/7 | 1/5 | 1/3 | 1.00 | 3.00 |
| Distance to Refinery pipelines | 1/7 | 1/7 | 1/6 | 1/2 | 1/3 | 1.00 |
| Sum | 2.07 | 4.87 | 8.62 | 14.83 | 23.33 | 26.00 |

Table 6.13: Significance weights of the criteria considered

| Electricity | | Hydrogen | |
| --- | --- | --- | --- |
| Criteria | Weight | Criteria | Weight |
| Wind speed | 0.44 | Wind speed | 0.41 |
| Water Depth | 0.30 | Water Depth | 0.26 |
| Distance to shore | 0.12 | Distance to Petrochemical Plants | 0.17 |
| Distance to grid | 0.09 | Distance to Refineries | 0.07 |
| Distance to ports | 0.05 | Distance to Gas pipelines | 0.05 |
| —- | — | Distance to Refinery pipelines | 0.03 |

5. Mexico can produce up to 217.33 MTon/year of hydrogen, with the Gulf of Mexico contributing 78.8 % of this capacity.

6. Centralized offshore hydrogen production shows LCOE reductions of up to 27.9 % beyond 100 km from shore, making it more feasible than offshore electricity generation.

7. In the centralized offshore configuration (COfEL), hydrogen production is 0.92 USD/kg and 0.84 USD/kg cheaper than onshore (OnEL) for alkaline and PEM technologies, respectively.

8. Utilizing existing oil and gas infrastructure for offshore hydrogen transport reduces LCOH by 11 % and 8.5 % compared to acquiring new technology (COfEL-New) and onshore production (OnEL), respectively.

9. 40 % of the assessed offshore wind area is highly suitable for hydrogen production due to its proximity to oil piping infrastructure.

## 6.2.1   Offshore Wind Energy Assessment

Geographic constraints indicate that the exploitable area for wind energy extraction encompasses 300,342 km$^2$, constituting 10 % of the national exclusive economic zone. Employing the mean wind power density (WPD) derived from Eq. (5.1), the gross wind resource potential was identified, with WPD values ranging from 132 to 490 W/m$^2$. Notably, the regions of Oriental, Northeast, and Peninsular emerge as the most prolific in terms of energy yield per unit area (Fig. 6.9).

The anticipated energy yield from offshore wind technology varies from 25.2 to 61.3 GWh/km$^2$ annually, as depicted in Fig. 6.10. If the entire technical potential for offshore wind were realized, the annual energy production could achieve 12,688 TWh, surpassing Mexico's 2022 electricity consumption of 333.66 TWh by approximately 33 times (Table 6.14). Furthermore, the global capacity for offshore wind farm development is estimated at 1609.74 GW, a scale comparable to the potentials of Japan (392 GW), England (2,125 GW) [128], Brazil (700 GW), and Colombia (50 GW). Despite the current lack of installed capacity in Latin American countries compared to England and Japan, strategic roadmaps are being developed to facilitate the integration of offshore wind energy into their respective energy matrices [148], highlighting Mexico's substantial offshore wind potential.

Table 6.14 outlines the energy potential across different oceanic zones, emphasizing the superior performance of the turbine V164-9.5 in the Oriental zone with a technical power density (TPD) of 6.3 MW/km$^2$, followed by the Peninsular and Northeast zones at 5.3 and 5.2 MW/km$^2$, respectively. Despite the Oriental zone's optimal TPD, the Peninsular (1,011.3 GW), Northeast (240.63 GW), and BC-BCS (224.56 GW) regions exhibit the largest capacities for wind farm deployment due to available ocean space, rendering them the primary zones for annual energy production with 8,083.7, 1,913.0, and 1,769.4 TWh/year respectively.

In this study, fixed bottom and floating turbine foundations were employed based on ocean depth (Table 6.4). Floating technology could be applied to 58 % of the available area, while fixed foundations were suitable for 42 %. The potential deployment of 904 GW with floating foundations and 703.72 GW with fixed bottom in Mexico was determined. These findings are crucial for informing public policy development and providing initial insights into feasible offshore wind energy harvesting areas and suitable technologies.

The Capacity Factor (CF) was assessed annually and monthly across the oceanic zones employing the Vestas V164-9.5 turbine. For the annual average, CFs ranged from 30.5 % in the BC-BCS zones to 60 % in parts of the Oriental region (Fig. 6.11). CF has also been evaluated using other commercial turbines; in [120], the CF in the Gulf of Mexico was ana-

Figure 6.9: Gross Wind Power Density in the available zones.
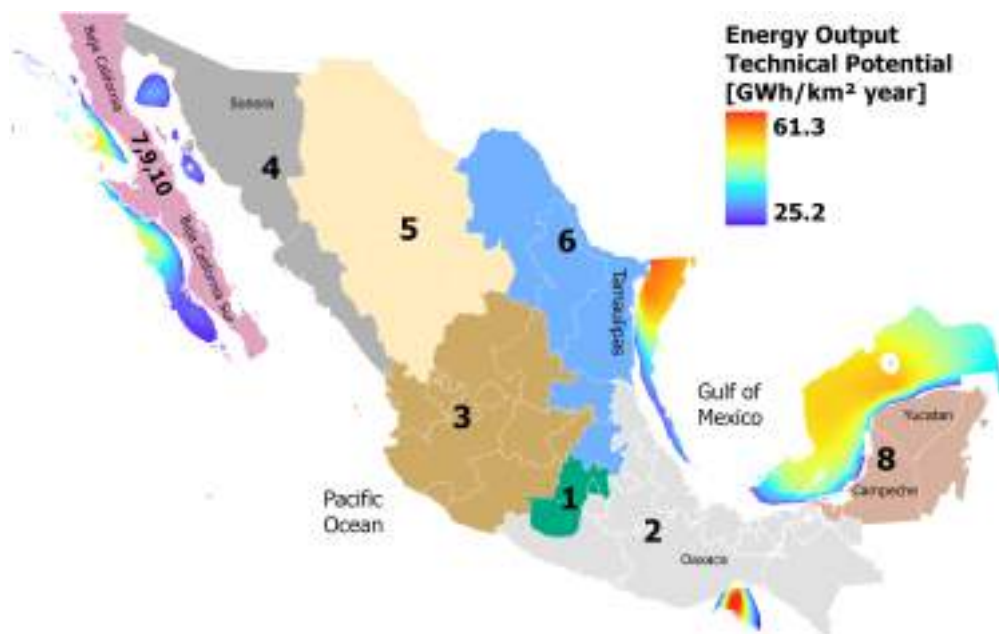


Figure 6.10: Technical potential of wind energy in Mexican oceans. Numbers 1-10 correspond to the energy demand regions of the Mexican National Electric System.

lyzed considering NREL (5 MW) and DTU (10 MW) turbine models, revealing CF values ranging from 20 % to 55 %. Conversely, [149] reported CFs exceeding 42 % in certain locales with commercial turbines like the Gamesa G128-5.0 and Siemens Gamesa SG 8.0–167 DD. Given the congruence in reported CF ranges, the commercial turbines examined herein are deemed suitable for Mexico's renewable energy context.

The monthly capacity factor (CF) is illustrated in Fig. 6.12, with December recording the lowest CF across all zones, ranging from 15 % to 30 %. Conversely, the Oriental and Peninsular regions exhibited significantly higher CF values during January, April, August, and October. The Northwest zone maintained the lowest CFs in the second half of the year, while the BC-BCS zone reached its highest CF in September.

Table 6.14: Offshore Wind Energy Technical Potential per Oceanic Zone.

| Oceanic Zone | Total Area [km] | TDP [MW/km$^2$] | Capacity Factor [%] | Power availability [GW] | Number of turbines | Technical Energy Potential [MWh/year] | Power availability [%] | | Fraction of Area [%] | |
|---|---|---|---|---|---|---|---|---|---|---|
| | | | | | | | floating | fixed | floating | fixed |
| Oriental | 10,875 | 6.3 | 50.1 | 241.43 | 11,568 | 482.8 | 69.19 | 30.81 | 70.52 | 29.48 |
| Peninsular | 183,613 | 5.3 | 48.4 | 1015.22 | 195,327 | 8,083.70 | 41.35 | 58.65 | 41.88 | 58.12 |
| Northeast | 41,918 | 5.2 | 51.5 | 72.27 | 44,592 | 1,913.00 | 83.13 | 16.87 | 82.47 | 17.53 |
| Northwest | 14,088 | 4.2 | 33.9 | 61.34 | 14,987 | 431.4 | 94.17 | 5.83 | 93.87 | 6.13 |
| BC-BCS | 49,849 | 4.7 | 42 | 224.91 | 53,030 | 1,769.40 | 91.92 | 8.08 | 91.42 | 8.58 |
| **Ntn'l** | **300,342** | | | 1615.17 | **319,504** | **12,680.2** | **56.43** | **43.57** | **58.00** | **42.00** |

Fig. 6.12 additionally depicts the monthly profile of wind energy generation. The Peninsular zone consistently displayed the highest energy production due to the availability of oceanic areas, where it could potentially generate up to 1,079 TWh in August, followed by the Northeast zone with 225 TWh. Analyzing the monthly CF and energy generation profiles offers initial insights into optimal energy utilization from offshore plants, thereby facilitating strategic planning for their integration with the electrical grid.

*Potential applications*

The comparison between the generation capacity of oceanic zones and the energy demand of regions within the Mexican National Electric System (NES) was conducted (refer to Fig. 6.10 for the definition of such regions). Relationships between oceanic zones and electrical

regions were established based on geographical proximity, as delineated in Table 6.15. It was determined that meeting the energy demand of Regions 1 and 2 (with the highest population density) would necessitate approximately 23 % of the generation capacity of the Oriental zone. Additionally, the Northeast area could satisfy the energy demand of Regions 3 and 6 using 6.95 % of its capacity. These findings highlight the significant potential for integrating offshore wind energy into the electrical grid.
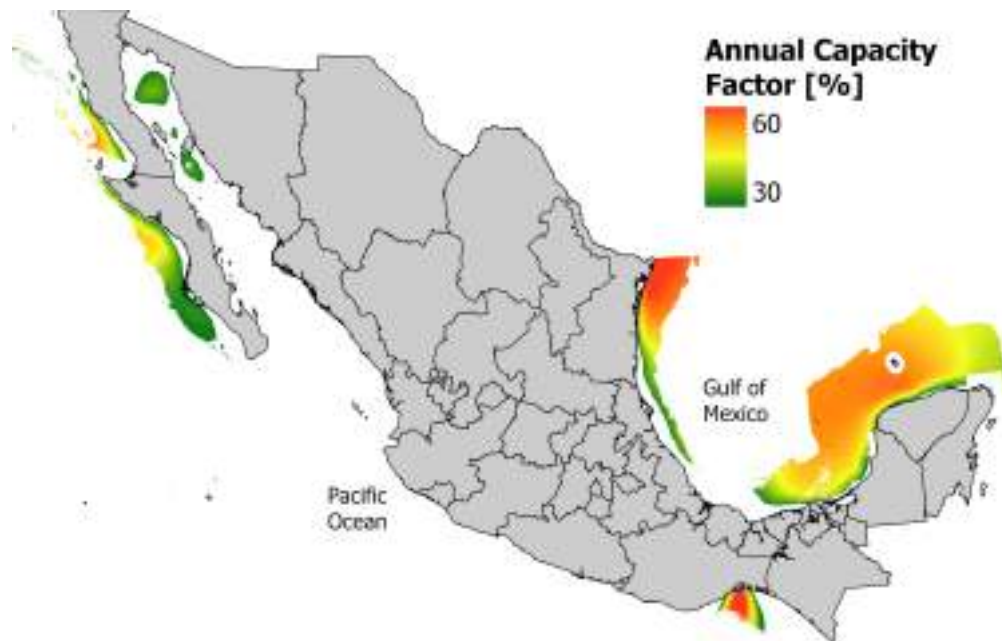


Figure 6.11: Annual Capacity Factor distribution.

Given the capacity of Mexico's offshore wind potential to meet current energy demands, exploring alternative applications, such as transportation electrification, becomes compelling. An analysis of the current energy demand of internal combustion engine vehicles in states adjacent to oceanic zones (Tamaulipas, Campeche, Yucatan, Oaxaca, Baja California, and Baja California Sur) was conducted (refer to Fig. 6.10). Results indicated that covering this demand for all oceanic zones required less than 1 % of their energy potential (refer to Table 6.16). By 2030, the projected national energy demand for light transport was 171.4 TWh/year, necessitating only 35.5 % of the Oriental zone's energy potential in that scenario.
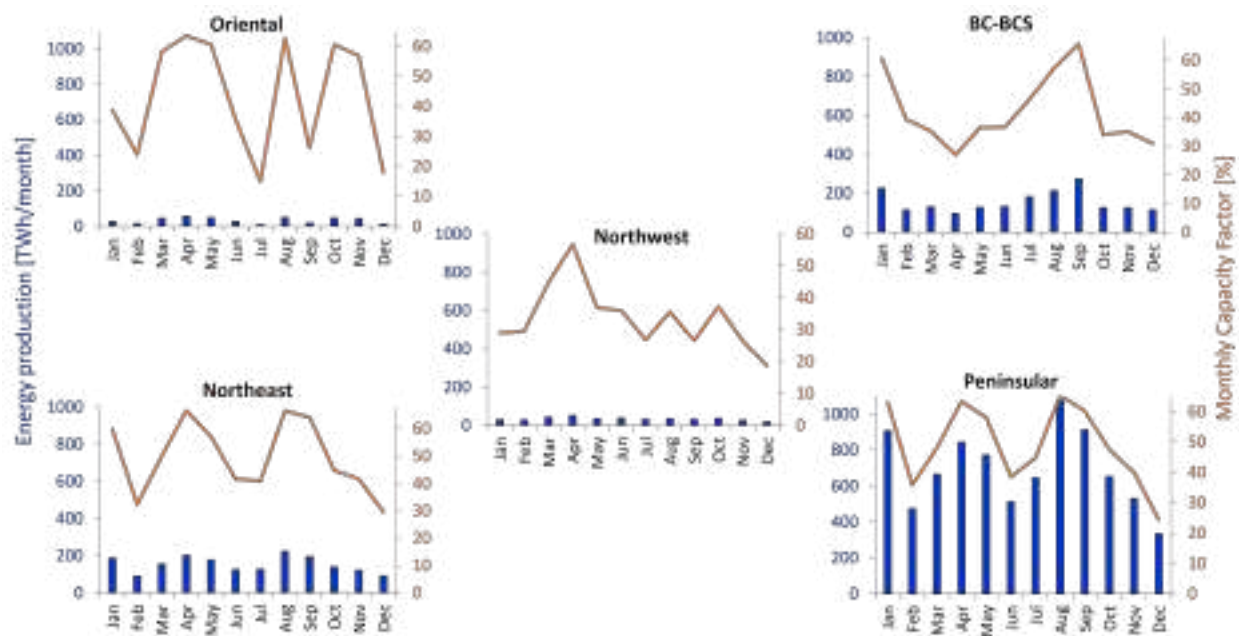
Figure 6.12: Month profile of Wind energy production and CF per oceanic zone. Blue (Energy Production [TWh/month]), orange (Capacity Factor [%])

Table 6.15: Proportion of energy needed to satisfy the demands of the regions within the NES.

| Oceanic Zone | NES Region | 2022 NES Region Demand [TWh] | Energy Required to Cover NES Region Demand [%] | Energy Required to Cover Mexico Total Demand [%] |
|---|---|---|---|---|
| Oriental | 1,2 | 110.198 | 22.83 | 69.11 |
| Peninsular | 8 | 14.47 | 0.18 | 4.13 |
| Northeast | 6,3 | 132.956 | 6.95 | 17.44 |
| Norweast | 4,5 | 55.47 | 12.86 | 77.34 |
| BC-BCS | 7,9, 10 | 19.345 | 1.10 | 18.86 |

Table 6.16: Proportion of energy needed to meet transportation energy demand.

| Oceanic Zone | Adjacent States | Transportation Energy Demand [TWh/year] | Energy required [%] |
|---|---|---|---|
| Oriental | Oaxaca | 2.67 | 0.55 |
| Peninsular | Yucatan-Campeche | 4.46 | 0.055 |
| Northeast | Tamaulipas | 6.36 | 0.33 |
| Norweast | Sonora | 4.28 | 0.99 |
| BC-BCS | Baja California, Baja California Sur | 8.19 | 0.46 |

## 6.2.2   Economic assessment (LCOE)

In this techno-economic characterization, the maximum allowable limits for distance to shore and water depth were established at 200 km and 1000 m, respectively. It is noteworthy that cost estimations under extreme scenarios, where these limits are reached, entail inherent uncertainties since real projects have been deployed at maximum depths of 200 m and distances to shore of 80 km. Nevertheless, these estimations offer valuable approximations for such scenarios.

The CAPEX for 1 GW wind farm was determined using Eq. (6.9) and subsequently spatially mapped across the available oceanic zones (Fig. 6.13). Factors such as transmission, decommissioning, and installation costs are primarily influenced by proximity to shore, while foundation costs are contingent upon water depth, thereby dictating the choice of technology. In shallower zones (< 60 m), CAPEX ranges from 2,695 to 3,095 MUSD, corresponding to closer distances to the coastline. Conversely, depths exceeding 60 meters result in CAPEX ranging from 3,438 to 5,612 MUSD. The Peninsular and Northeastern zones exhibit the lowest CAPEX values. It is worth emphasizing that areas farther from shore, across all oceanic zones, tend to exhibit greater depths, necessitating the deployment of floating-type technology. In such cases, the mooring system's CAPEX is heavily influenced by water depth, ranging from 109 to 709 MUSD.

Installation costs are influenced by both the distance to shore and the type of technology, as depicted in Fig. 6.14. The number of trips required for equipment transportation contributes to the cost variation with proximity to shore. Additionally, the choice of technology significantly impacts installation expenses, with Floating TLB exhibiting the highest values due to the inclusion of mooring infrastructure.

OPEX is influenced by the type of technology and the distance to shore. The proximity to ports is crucial in maintenance costs, as longer journeys involve more resources. OPEX ranges from 0.05 MUSD to 0.08 MUSD, reflecting the variability between different scenarios.
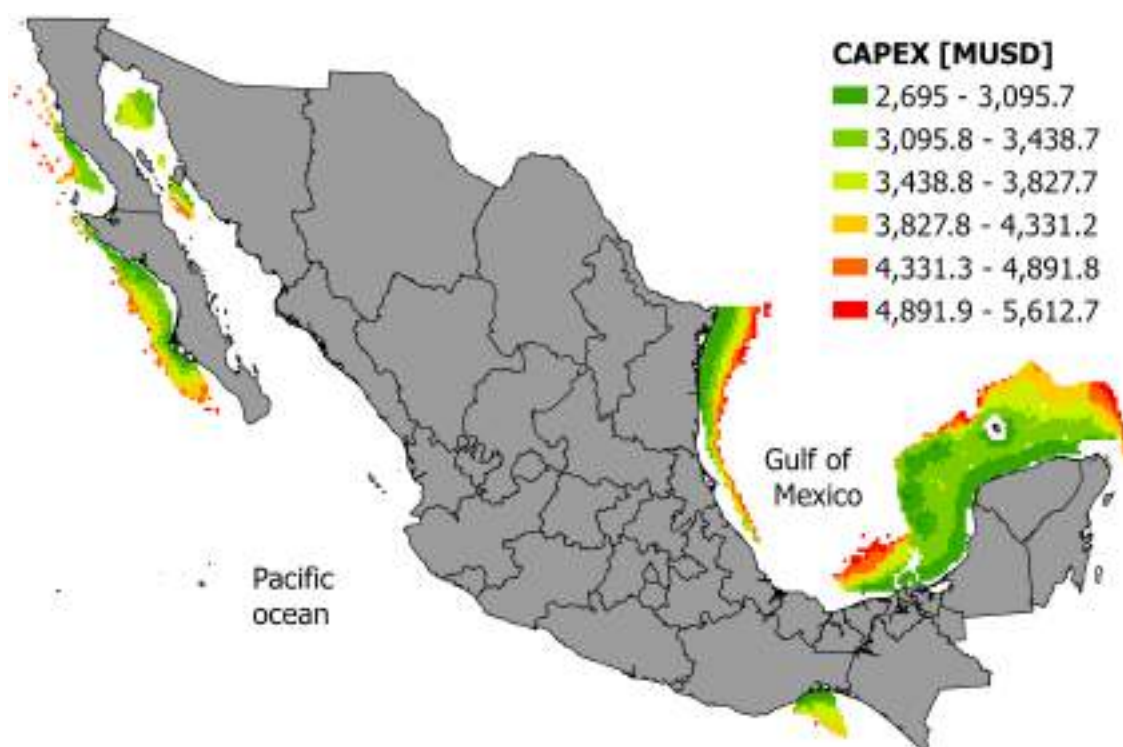
Figure 6.13: CAPEX for the studied 1GW Wind Farm.
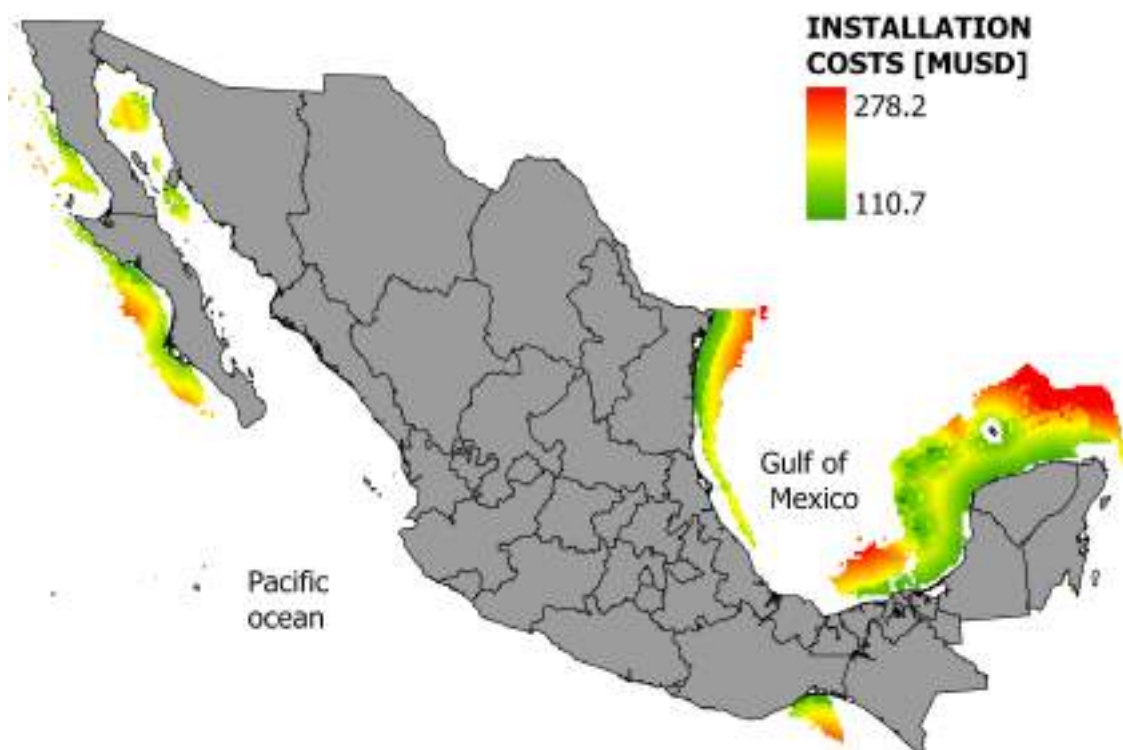


Figure 6.14: Installation cost.
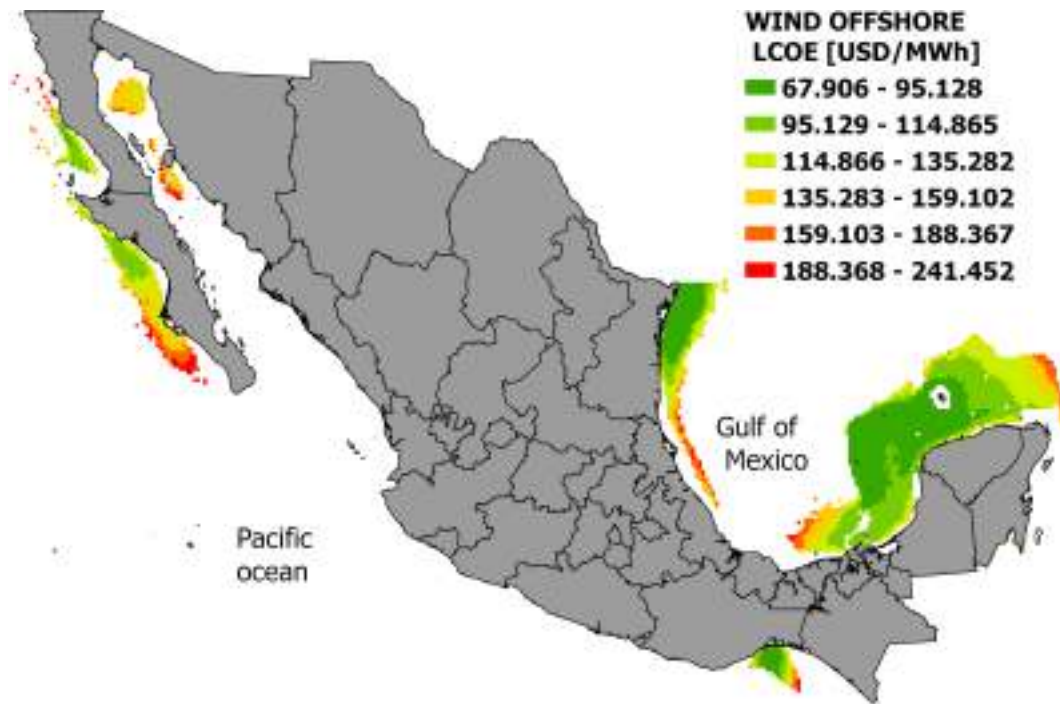
Figure 6.15: Offshore wind Levelized Cost of Energy.

The LCOE of the offshore plant under examination spans from 67.9 to 241.45 USD/MWh across the available energy harvesting zones (Fig. 6.15). Areas with greater energy production capacity, notably the Northeastern, Eastern, and Peninsular sectors, exhibit predominantly lower LCOE values ranging from 67.9 to 95.12 USD/MWh. These regions are characterized by shallower depths (typically less than 60 meters) and relatively closer proximity to shorelines.

Conversely, zones such as Sonora and Baja California Sur (BCS) demonstrate LCOE values surpassing 114.8 USD/MWh. The heightened costs in these locales arise from significant water depths necessitating the adoption of floating technologies for energy generation. Consequently, the augmented capital and operational expenditures associated with such technologies contribute to the elevated LCOE observed in these regions.

The variability in LCOE among different offshore zones underscores the impact of geographical and technological factors on the economic viability of electricity generation. Lower

LCOE values observed in shallower, nearshore regions emphasize the critical role of site selection and technology deployment strategies in optimizing offshore energy projects.
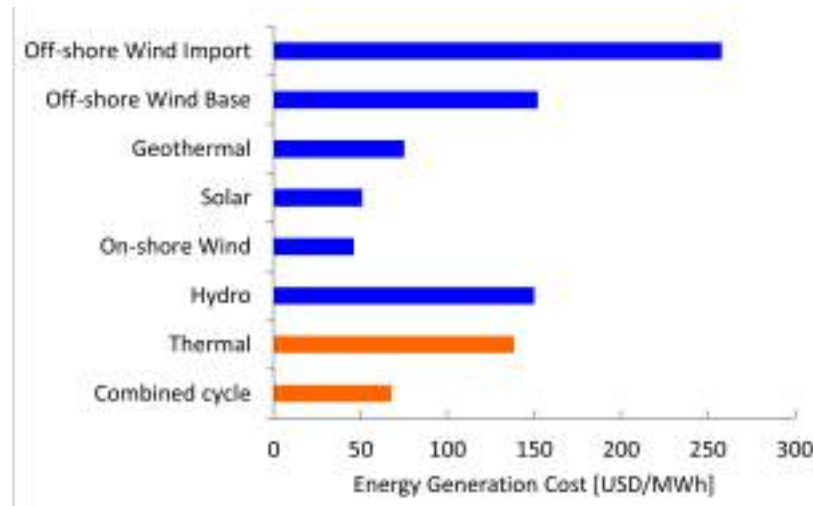


Figure 6.16: Energy generation Cost for different sources for the Mexican energy market in 2023.

Traditionally focused on non-renewable energy sources, Mexico encounters obstacles in the development of renewable energy technologies, often resorting to imports. Consequently, the computation of LCOE considered the influence of importation costs, resulting in a 60 % increase in CAPEX. Within this context, LCOE ranges from 107 to 410 USD/MWh, highlighting the challenges associated with implementing offshore technology and emphasizing the significance of international trade dynamics in Mexico's energy transition.

The internal competitiveness of offshore wind energy was evaluated through a comparative analysis of electricity generation costs across various energy sources (refer to Fig. 6.16). Offshore wind demonstrated competitive prospects with hydro generation, averaging around 150 USD/MWh. In contrast, conventional energy sources ranged between 60 and 140 USD/MWh in 2023, while solar and onshore wind energy were the least expensive at 55 USD/MWh ([150]). Although offshore generation is relatively more costly, particularly considering import scenarios, it presents an opportunity for Mexico to stimulate technological advancement and mitigate high costs.

Moreover, offshore wind energy holds potential for international competitiveness, as evidenced in regions with significant wind potential such as the European Atlantic and Mediterranean Sea, where LCOE values range from 90 to 250 €/MWh with floating technology [131]. Given the applicability of both fixed and floating technologies in Mexico, there exists the potential for competitive engagement in the global market, even under import scenarios, thereby highlighting the benefits of offshore wind energy deployment and positioning Mexico advantageously on the international stage.
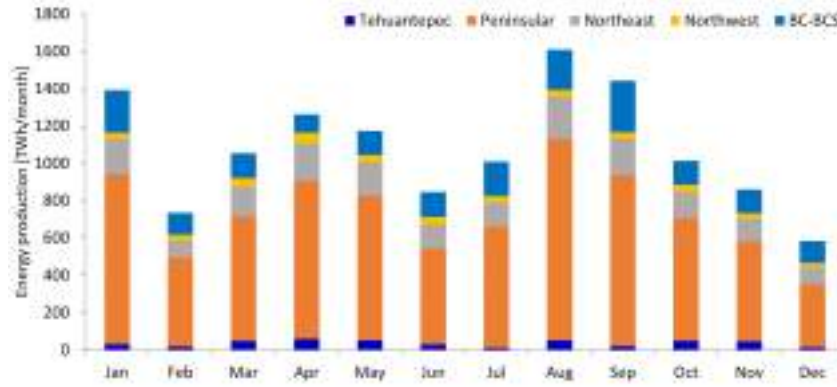


(a)
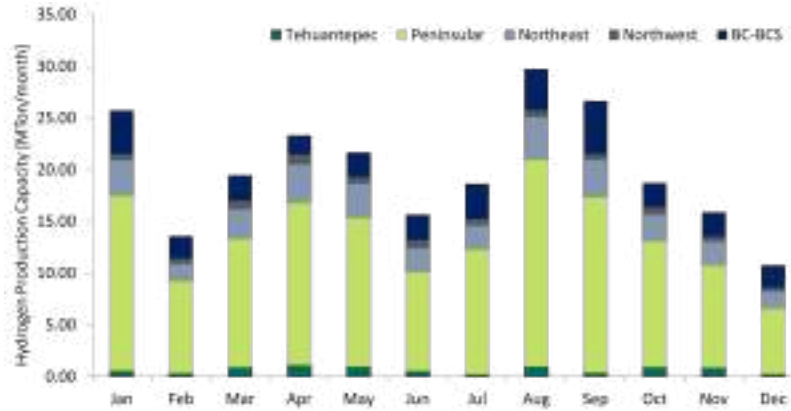


(b)

Figure 6.17: Offshore Wind Energy and Hydrogen Generation Monthly Profiles

## 6.2.3 Offshore Wind Hydrogen Assessment

As depicted in Figure 6.18, hydrogen production density ranges from 431.4 to 1049 Ton/km$^2$ per year, potentially yielding up to 217.33 MTon/year if fully utilized. This capacity could

cover 43 % of the global demand in 2022 (95 MTon) and contribute 41 % toward the global hydrogen production required to meet zero-emission targets (523 MTon/year) [123].
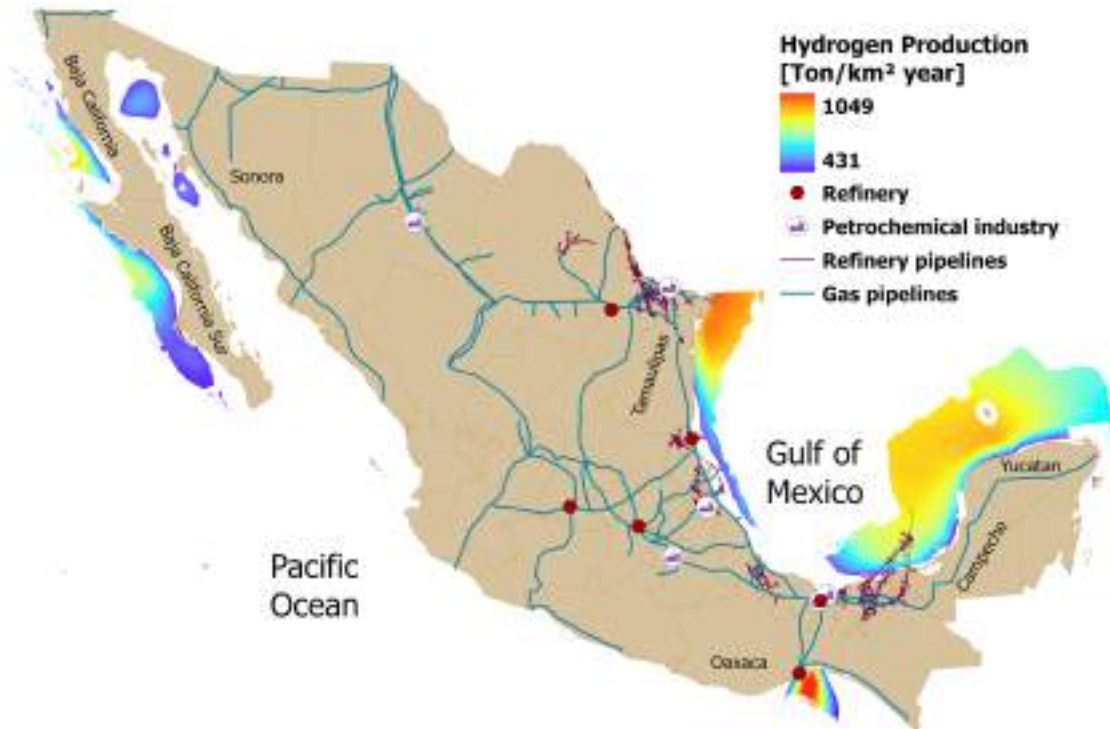


Figure 6.18: Hydrogen production potential from offshore wind energy.

Table 6.17 displays the total energy and hydrogen production by oceanic zone. The Peninsular region could contribute 63.7 % of hydrogen generation with 138 MTon/year, followed by the Northeast (32.79 MTon/year), BC-BCS (30.33 MTon/year), Tehuantepec (8.25 MTon/year), and Northwest (7.39 MTon/year). It is notable that despite the BC-BCS region having the second-largest area, its production is significantly lower than that of the Northeast, suggesting low capacity factors as indicated in [149].

Figure 6.17a depicts the national monthly average energy production, ranging from 590 TWh/month to 1,600 TWh/month. Peak months occurred in January, August, and September, whereas December experienced a 62 % reduction compared to August. Figure 6.17b illustrates the monthly contributions to H$_2$ production from different oceanic zones. Production fluctuated between 10 and 30 MTon/month, with the Peninsular region leading.

Table 6.17: Hydrogen production capacity and potential applications

| Oceanic Zone | AREA [km²] | Technical Energy Potential [TWh/year] | Hydrogen Production [Mton/year] | Potential use | Total H$_2$ demand [Mton/year] |
|---|---|---|---|---|---|
| Tehuantepec | 10,875 | 482.8 | 8.25 | Refinery and Transportation | 0.19 |
| Peninsular | 183,613 | 8,083.7 | 138.57 | Ammonia, Refinery and Transportation | 0.965 |
| Northeast | 41,918 | 1,913.0 | 32.79 | Ammonia, Refinery and Transportation | 0.517 |
| Northwest | 14,088 | 431.4 | 7.39 | Transportation | 0.12 |
| BC-BCS | 49,849 | 1,769.4 | 30.33 | Transportation | 0.25 |
| **Ntn'l** | **300,342** | **12,680.2** | **217.33** | | **2.042** |

Understanding these monthly variations is crucial for developing strategies to optimally utilize resources, facilitating informed decision-making, and enhancing the sustainability of hydrogen-based energy systems.

### Offshore wind hydrogen applications

While oceanic zones suitable for offshore wind hydrogen harvesting are present in both the Pacific Ocean and the Gulf of Mexico (GoM), the latter holds the greatest potential, constituting 78.8 % of the total capacity, as depicted in Figure 6.18. The GoM coastline, rich in oil and gas infrastructure, is well-aligned with hydrogen utilization in refinery and ammonia production, facilitating the decarbonization of energy and other sectors.

Priority applications for each oceanic region, based on proximity to onshore infrastructure (< 50 km), are delineated in Table 6.17. The BC-BCS and Northwest regions, distanced from gas and oil infrastructure, prioritize hydrogen for local applications such as light transportation, rural electrification, and salt mines, in contrast to the chemical industry focus in the southeast.

The estimated hydrogen demand, presented in Table 6.17 at 2.04 MTon/year, considers the geographic distribution of refineries and petrochemical plants along Mexican coasts. This encompasses a specific facility near the peninsular area with an ammonia output of 4.2 MTon/year. Additionally, hydrogen demand for the transportation sector in coastal states was assessed using the 2023 energy requirements of the registered vehicle fleet.
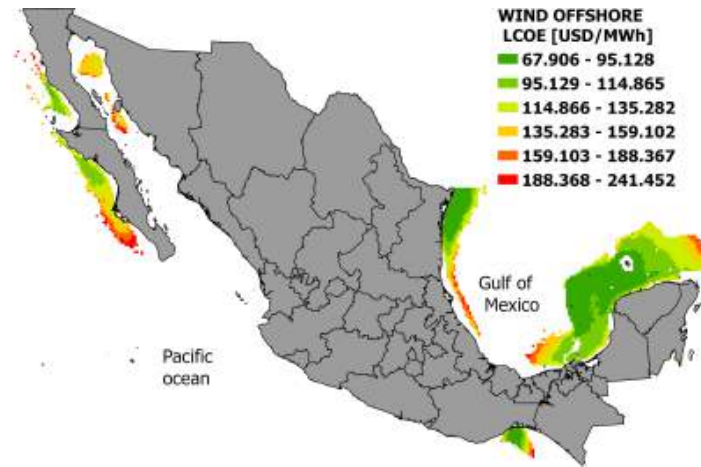
(a) Onshore H$_2$ Production



(b) Offshore H$_2$ Production
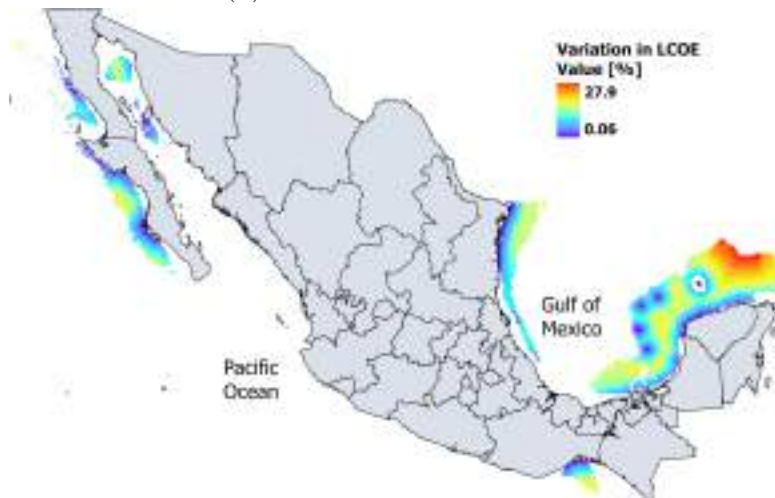


(c) LCOE percentage variation when the export cable is neglected from transmission cost.

Figure 6.19: LCOE values distribution for electricity and hydrogen transmission to shore
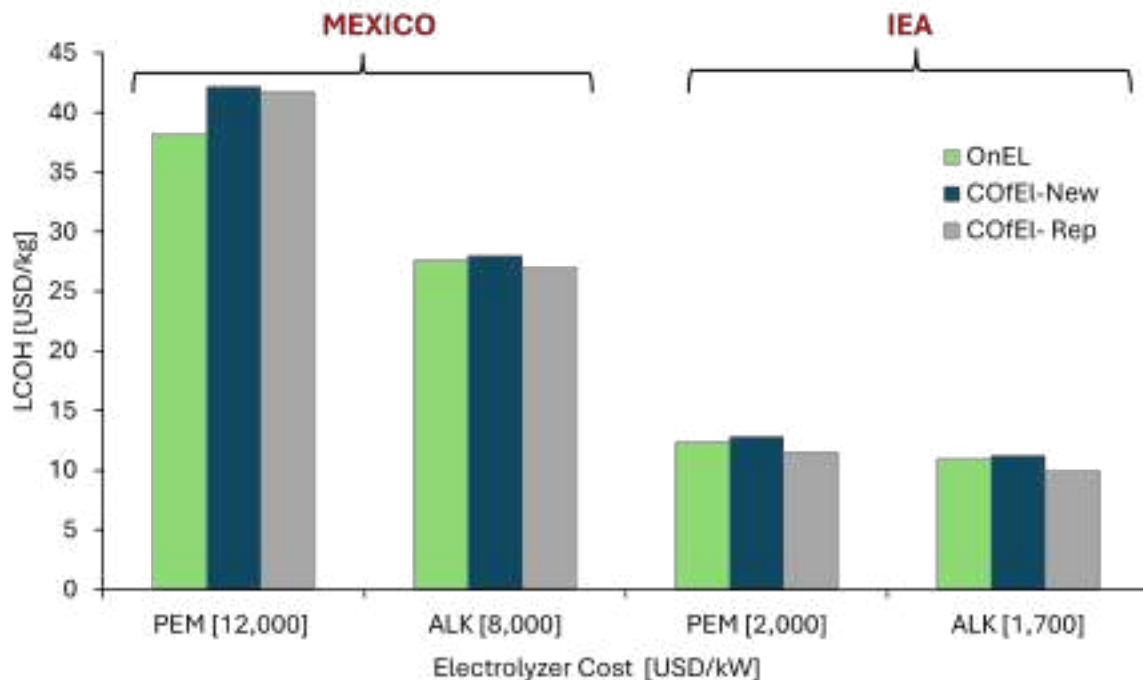
Figure 6.20: LCOH Values Across Various Electrolyzer Costs and Integration Topologies in International (IEA) and Mexican Contexts.

The Peninsular region, with the highest demand of 0.965 MTon/year, would need a 4.5 GW offshore wind plant, using only 0.45 % of its potential capacity. Conversely, the Northeast region would require 4.9 % of its available capacity to meet demand.

Nowadays Mexico produces 4.5 MTon of ammonia annually, resulting in a hydrogen demand of 0.8 MTon/year. If ammonia production were centralized at the six plants near the Gulf of Mexico, extrapolating from Cosoleacaque's production rates, hydrogen demand could escalate to 4.49 MTon/year. This elevated demand could potentially be accommodated by the Northeast or Peninsular regions, utilizing 13.69 % and 3.2 % of their respective potentials.

The study underlines the significant potential for offshore hydrogen generation, surpassing current requirements and enabling diverse applications. In addition to fulfilling existing demand, this capacity could facilitate hydrogen blending with natural gas via existing pipelines and enhance maritime industries by integrating hydrogen for aquaculture backup and port

energy supply.  These applications underscore the versatility and significance of offshore hydrogen in advancing energy and environmental objectives within marine environments.

## 6.2.4   Economic assessment (LCOH)

LCOH was assessed for both onshore and offshore production scenarios, alongside the LCOE. The findings reveal LCOE values for electricity transmission ranging between 67.9 and 241.5 USD/MWh (Figure 6.19a).  Excluding export cable costs, the LCOE for offshore hydrogen production spans from 65.1 to 214 USD/MWh (Figure 6.19b).  Particularly noteworthy are the observed reductions in LCOE, reaching up to 27.9 %, in regions where export cable costs are significantly influenced by distance.  This underscores substantial opportunities for integrating hydrogen production at increased distances from the shoreline (Figure 6.19c).

Onshore and centralized offshore hydrogen production scenarios were considered.  Given the extensive pipeline infrastructure in the oil and gas industry, offshore production was evaluated in two scenarios:  using new technology and repurposing existing infrastructure for hydrogen transport.  The findings indicate that the COfEL-Rep scenario is the most cost-effective, with reductions of 11 % and 8.5 % compared to new technology and onshore production, respectively.  Cost comparisons between electrolysis technologies showed that alkaline technology resulted in LCOH values of 10, 11.23, and 10.93 USD/kg for COfEL-Rep, COfEL-New, and OnEL, respectively, while PEM technology led to LCOH values of 11.53, 12.83, and 12.35 for the same scenarios (Figure 6.20).

As per IEA, electrolyzer costs ranging from 1,700 to 2,000 USD/kW could render hydrogen production from offshore sources internationally competitive, resulting in costs of approximately 12 USD/kg, akin to those associated with hydrogen derived from wind energy [123].  Nevertheless, the importation of electrolyzers may elevate the Levelized Cost of Hydrogen (LCOH) by 27 % [118], indicating the imperative for Mexico to align its electrolyzer pricing with international standards to ensure the economic viability of offshore hydrogen production.

Elevated importation costs for electrolyzers, spanning from 8,000 to 12,000 USD/kW, might result in production costs between 25 and 42 USD/kg for Proton Exchange Membrane (PEM) technology, thereby amplifying the LCOH to 2.4 to 3.5 times beyond international norms. Should the costs surpass 10,000 USD/kW, electricity transmission may become a more economically viable alternative. These cost dynamics underscore the necessity for Mexico to formulate robust public policies, regulate the importation market, and foster international collaborations to achieve cost competitiveness in hydrogen production.

With effective policy frameworks, strategic planning, and international partnerships, Mexico could align its LCOH with global benchmarks, as illustrated in Figure 6.21. Analysis indicates that in the Tehuantepec, Northeast, and Peninsular zones, hydrogen costs could potentially decrease below 9.6 and 11.3 USD/kg for alkaline and PEM technologies, respectively. Realizing a projected reduction of up to 3 USD/kg by 2050, as envisioned by the IEA, would enhance Mexico's competitiveness in the global hydrogen market, underscoring the significance of comprehensive policy measures and international cooperation in fostering sustainable hydrogen production.

## 6.2.5 Site selection assessment

The site selection analysis has revealed that Mexico has more suitable areas for hydrogen production than for electricity generation. Specifically, 40 % of the areas assessed for hydrogen harvesting have suitability indices above 0.63, indicating optimal conditions for hydrogen production (Figure 6.22b), compared to 34.8 % of areas suitable for electricity generation (Figure 6.22b). This demonstrates the enhanced potential of certain regions for hydrogen extraction over solely generating electricity. Moreover, regions like BC-BCS and Northwest, though less suitable for hydrogen production, could still be utilized for electricity generation, particularly to connect remote coastal areas currently far from the existing electric grid.

These findings are crucial as they provide insights into offshore resource distribution relative to proximity needs. By identifying areas with dual potential for hydrogen and electricity generation, strategic planning can be implemented to optimize resource allocation
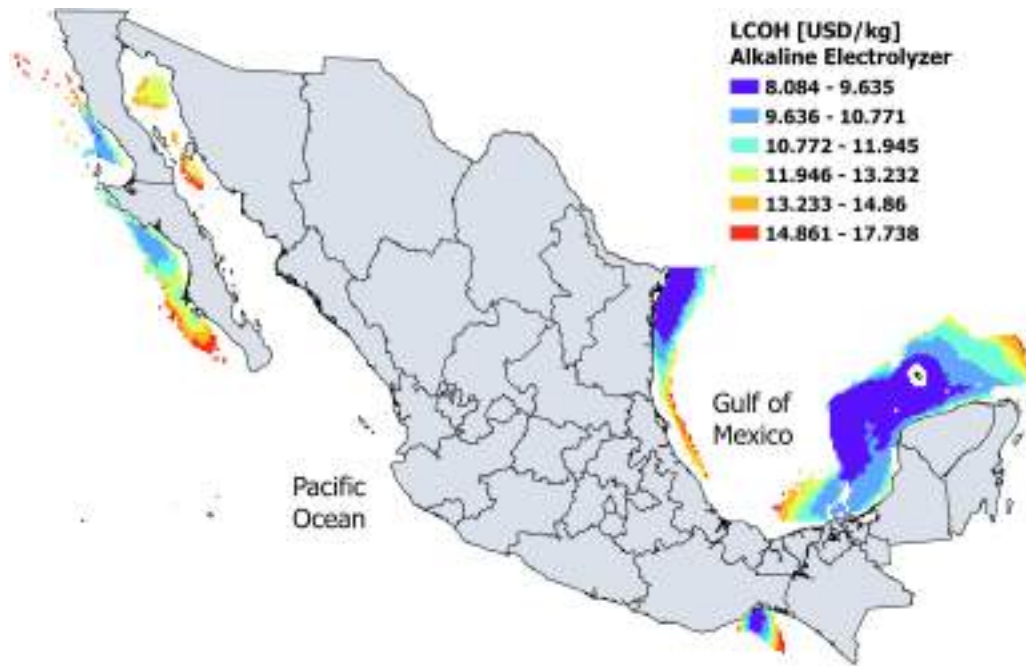
(a)
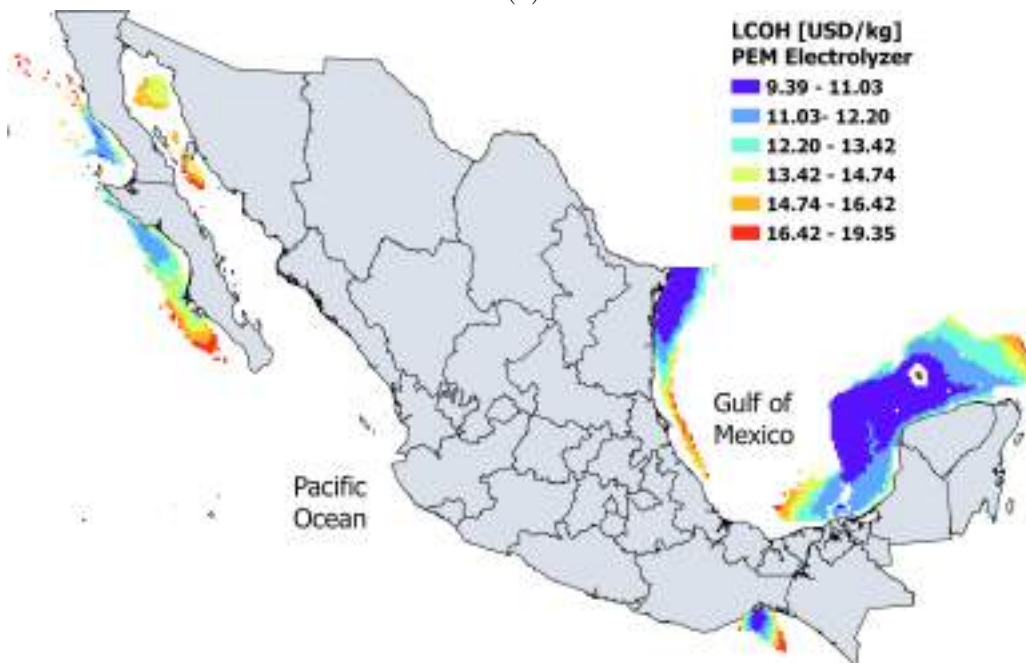


(b)

Figure 6.21: LCOH for offshore hydrogen production repurposing pipeline infrastructure and considering electrolyzer cost of 1,700 USD/kW (Alkaline) and 2,000 USD/kW (PEM)

and infrastructure development. This approach not only improves energy production efficiency but also integrates remote regions into the national energy network, enhancing energy accessibility and resilience across Mexico.

(a)



(b)
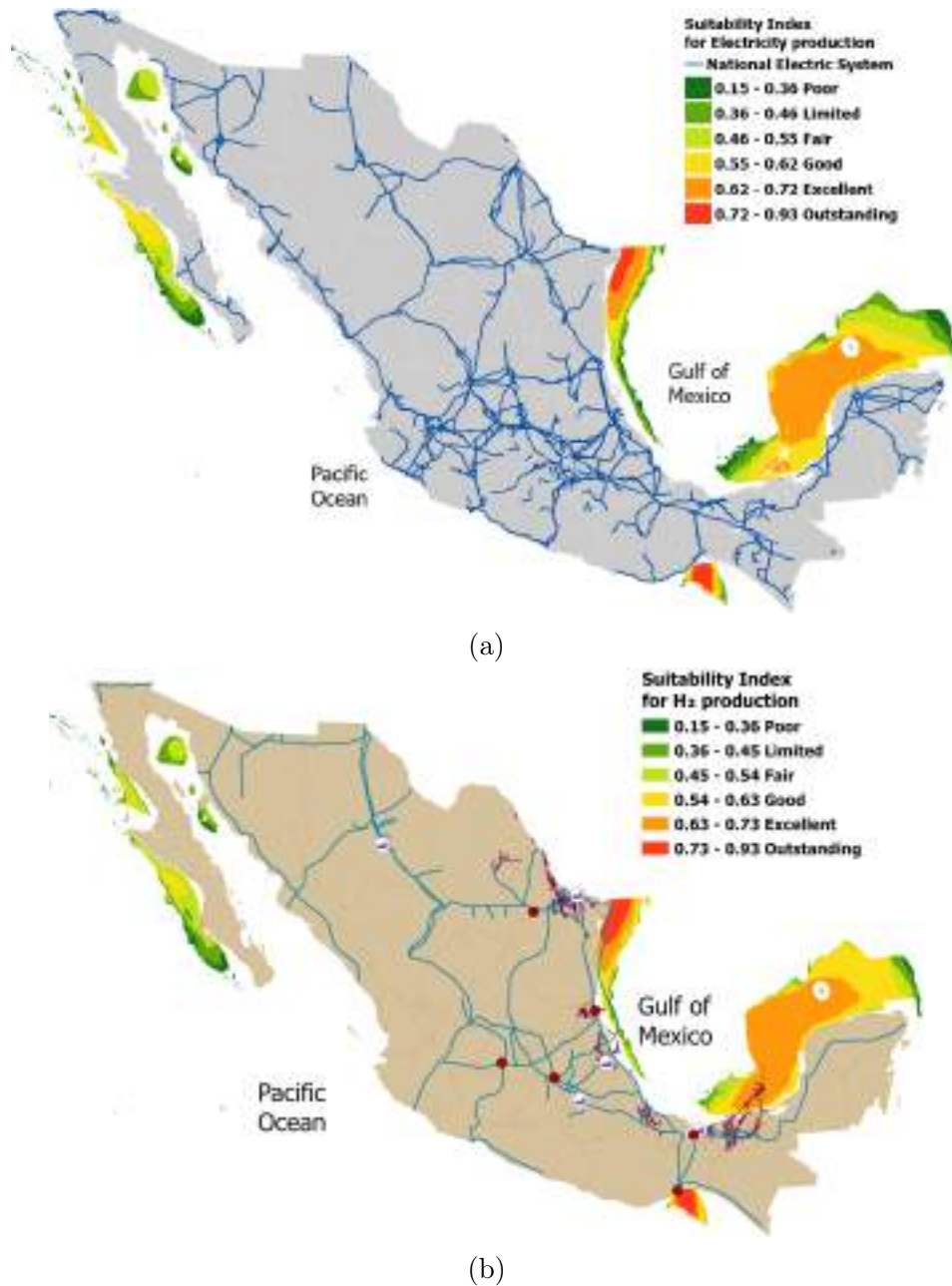
Figure 6.22: Suitabily Index for Electricity and Hydrogen Production.

## 6.2.6   Challenges for Offshore Wind Energy Utilization

IRENA [151] outlines a multi-stage process for the development of robust public policies facilitating the formulation of roadmaps and national strategies for energy technology deployment. This process initiates with an assessment of the technical and economic capabilities of power generation, followed by the identification of challenges hindering successful

deployment. Regarding offshore energy in Mexico, various technological and socio-political barriers have been identified, as elaborated below.

According to the International Renewable Energy Agency (IRENA) [151], the development of strong public policies enabling the creation of roadmaps and national strategies for the deployment of energy technology involves several stages, with its foundation lying in the understanding of the technical and economic capabilities for power generation, followed by identifying the challenges that need to be overcome for successful deployment. In the case of offshore energy in Mexico, some technological and socio-political barriers have been identified, which are discussed below.

1. Grid Integration: Offshore wind farms typically transmit energy at voltages exceeding 150 kV [152]. However, the Mexican coastal grid operates at a maximum of 163 kV, which is insufficient for consistent integration (Fig. 6.23). Hence, there is a critical need to enhance and expand grid capacity to 230 kV and 400 kV to facilitate offshore energy deployment.

2. Fossil Fuel-based Economy: Despite Mexico's commitment to the Paris Agreements, its energy economy remains heavily reliant on fossil fuel resources. This significantly hampers public policy orientation toward renewable energy integration, crucial for achieving decarbonization goals. In 2022, only 31.2 % of the total energy produced was from renewable sources [153].

3. Lack of Technology Development: While studies have utilized various wind turbine types with similar capacity factors [149, 120], [154] underscores the importance of sizing wind turbines based on local geographic capacities, presenting an opportunity for Mexico to venture into technological development. Designing turbines tailored to Mexico's wind resources could maximize energy extraction.

4. Risk for extreme weather: Hurricanes represent one of the most significant barriers that could limit the deployment of offshore wind energy. Several studies have been conducted to assess the risk posed by hurricanes of different categories to offshore wind

farms, particularly those situated in the Gulf of Mexico region of the United States ([155],[156]). It has been found that a Category 2 hurricane (45 m/s) would destroy approximately 6 % of the turbines, while a Category 3 hurricane (> 42.8 m/s) could potentially damage up to 46 % of the farm over its lifetime. As a consequence of these statistics, project planning must consider this parameter to consider the insurance cost and to identify the lowest-risk site. In [157], an assessment of the most suitable sites for offshore wind plants in Mexico was carried out, considering the risk of hurricanes, revealing that areas on the Pacific side are the most suitable. Furthermore, academia and industry are collaborating to develop stronger structures and technology to position the blades in alignment with the wind direction to mitigate risks [158]. On the other hand, although hurricanes are a risk for offshore wind farms, it has been identified that they could work as a potential means to mitigate destruction and save lives, as it has been demonstrated that offshore wind farms can soften hurricanes before they reach shore [159].

5. Social Engagement: Societal familiarity and acceptance of such technologies are crucial for their adoption. Initiatives aimed at enhancing public awareness and understanding are therefore imperative.

The recognition of decarbonization objectives by Mexico is pivotal in facilitating the transition towards the integration of renewable energy and maximizing its renewable resource potential. Establishing strong partnerships across government, academic institutions, and the industrial sector is essential for guiding the trajectory of technological advancements in this domain. Revealing Mexico's offshore energy potential has become imperative, given its strategic geographical positioning, which positions it as an indispensable nearshoring energy provider poised to support the expansion of North America.

## 6.3   Summary and Chapter Highlights

The analysis showed that Mexico possesses an offshore wind energy potential of 1609.7 GW, suggesting the theoretical capacity to produce approximately 12,688 TWh per year. This
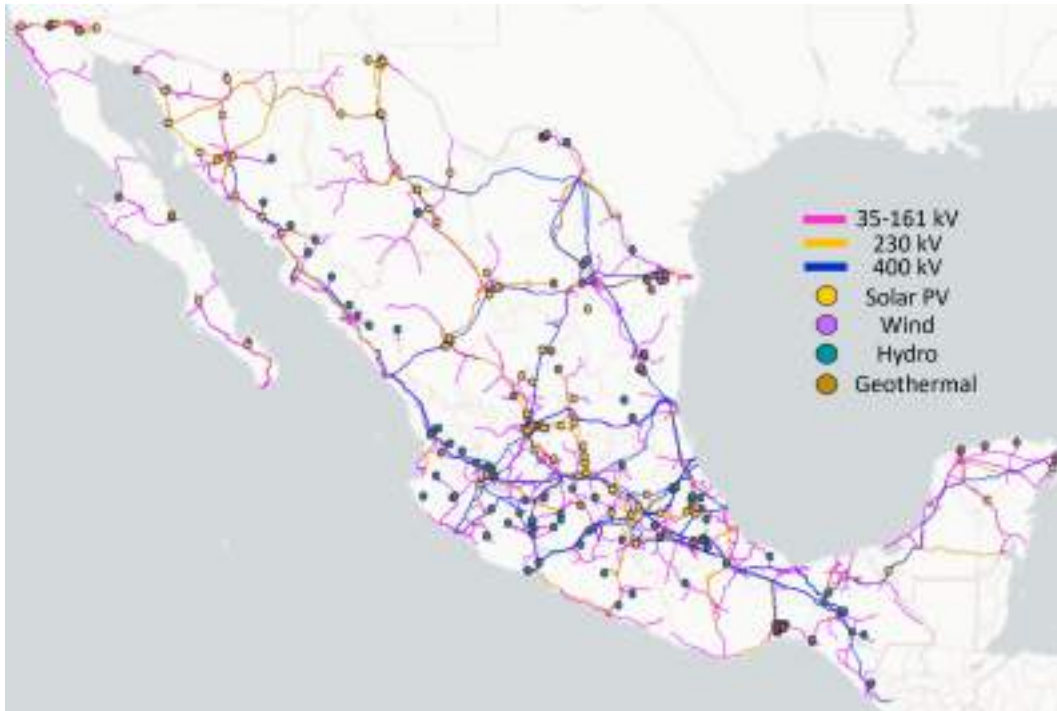
Figure 6.23: National Electric System of Mexico. Source: CONAHCYT [10].

substantial output significantly exceeds the nation's current energy demand by a factor of 33. Expanding on this potential, the study explores ancillary applications such as electrifying transportation infrastructures in nearby states, estimating that a mere 2.33 % of the extrapolated energy yield would be sufficient to meet these transportation needs.

Simultaneously, the investigation addresses the economic viability of offshore wind energy, primarily through the LCOE. It concludes that, on average, the LCOE for offshore wind stands at approximately 150 USD/MWh, indicating competitive parity with alternative energy sources within Mexico's energy portfolio. However, the inclusion of importation tariffs substantially increases the LCOE to 410 USD/MWh, highlighting a significant opportunity for Mexico to develop turbine technology tailored to its unique offshore conditions.

Challenges to the large-scale adoption of offshore wind energy in Mexico primarily revolve around the limitations of the existing electrical grid, necessitating significant upgrades beyond 230 kV capacities to accommodate potential scale-ups.

It was shown that Mexico possesses the capacity to annually generate up to 217.33 million tonnes of hydrogen, primarily from the Gulf of Mexico. This capacity positions Mexico as a key contributor to both domestic and global hydrogen demands, aligning with objectives for decarbonization.

Geographically, 40 % of the assessed offshore areas are deemed highly suitable for hydrogen production, owing to their proximity to existing infrastructure. This geographical advantage facilitates the seamless integration of hydrogen production into current energy systems, streamlining logistical operations.

Furthermore, the application of Geographic Information Systems (GIS) and Multi-Criteria Decision Making (MCDM) tools in site selection identifies areas suitable not only for hydrogen production but also for electricity generation. This dual capability allows for more strategic allocation of resources and infrastructure development, thereby enhancing the efficiency of Mexico's renewable energy sector.

# Chapter 7

# H$_2$ Micro scale Integration

Green hydrogen serves as an effective means of energy storage in microgrids, enabling the decoupling of energy production and consumption. During periods of excess renewable energy production, surplus electricity can be employed for electrolysis, producing green hydrogen for storage. Subsequently, when renewable energy generation is insufficient to meet demand, stored green hydrogen can be converted back to electricity through fuel cells or combustion, ensuring a continuous and reliable power supply.

The incorporation of green hydrogen across diverse applications not only mitigates environmental impacts but also contributes to economic sustainability. The reduction of greenhouse gas emissions associated with industrial activities and electrical systems aligns with global efforts to combat climate change. Moreover, the growth of the green hydrogen sector stimulates job creation and economic development, fostering a transition to a more sustainable and resilient energy landscape.

All the components in the MG (RES, energy storage system (ESS), and loads) have to work together to balance energy demand and supply at all times, as well as be electrically flexible on large shares of renewable electricity ensuring reliability to avoid energy mismatches (shortages and curtailment). Hence, it is crucial to optimally determine the energy dispatch and the capacity of each component since a poorly sized system always has a negative impact on investment costs and energy efficiency [160].

An energy management system (EMS) is required to effectively control and coordinate the energy flow of the system to satisfy the load, especially in isolated MGs such as remote villages and areas far from the grid. Researchers have made a great effort designing EMS for off-grid applications considering two approaches, rule-based (RB) and real-time optimization (RO). The RB approach estimates the component's operation status through decisions pre-defined flow chart while RO uses an optimization model designed for particular objectives to determine the power flow. Although RB approaches are simple and may not be cost effective, they are widely used due to the ease of practical implementation when compared to RO and hence they are studied in this work. [161].

The strategies used in RB EMS are load-following (LF) and cycle charging (CC). The main differences between LF and CC are the way in which the battery energy storage system (BESS) is charged and discharged and accordingly, the generator usage. In the LF mode, the RES has the priority to power the load and charge the battery and the generator only operates when RES does not satisfy the demand and is not allowed to charge the BESS. In addition, the BESS can discharge at low RE production as long as it has energy. However, these continuous charge and discharge cycle can lead to lower efficiency and reduced lifetime of the battery. On the other hand, in the CC strategy the generator operates at full capacity. Under periods of excess energy in this case, the BESS will be charged. However, the BESS can only be discharged when a specific SoC is reached. This leads to a non-optimal BESS usage but its lifetime is increased [161].

Despite numerous studies conducted on the development of energy management strategies for specific locations and scenarios, it remains essential to identify the impact of climatic conditions on energy demand and production, as well as on the sizing of isolated microgrids. The objectives of this study are as follows:

1. To analyze the influence of climate types on the sizing of isolated microgrids with a specific system, aiming to establish a comprehensive guideline on crucial considerations in energy storage (Hydrogen-Batteries).

2. To analyze the impact of sampling time on system sizing.
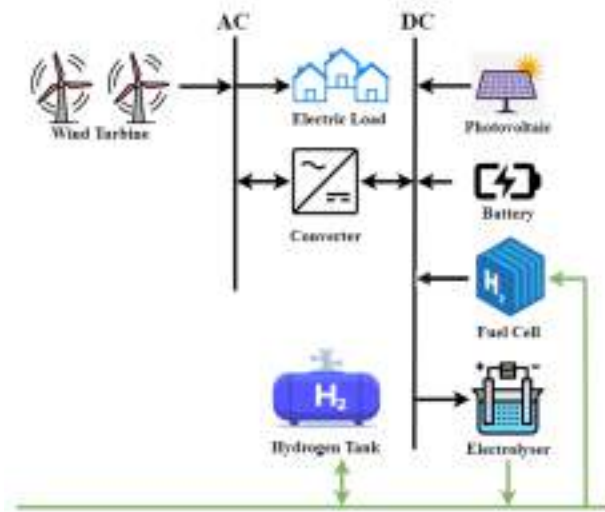


Figure 7.1: Microgrid system considered in this study

## 7.1 Methods and Materials

Figure 7.2 shows a diagram of the methodology developed in this work.

### 7.1.1 System analyzed

In this study, an isolated Wind-Solar PV-Battery-Hydrogen (Electrolyzer, Fuel cell (FC), and storage Tank) system is considered to meet a residential load profile of several locations between Canada, Mexico, and the United States. A schematic diagram of the microgrid is shown in Figure 7.1. PV array, FC, Electrolyzer, and batteries are connected to the DC bus, and a bi-directional converter (BDC) connects the DC and AC bus where the electric load and the wind turbine are attached.

### 7.1.2 Site selection

The locations chosen for the sizing of the microgrids were strategically selected based on two criteria: they were situated in regions where the Köppen classification could be directly corre-
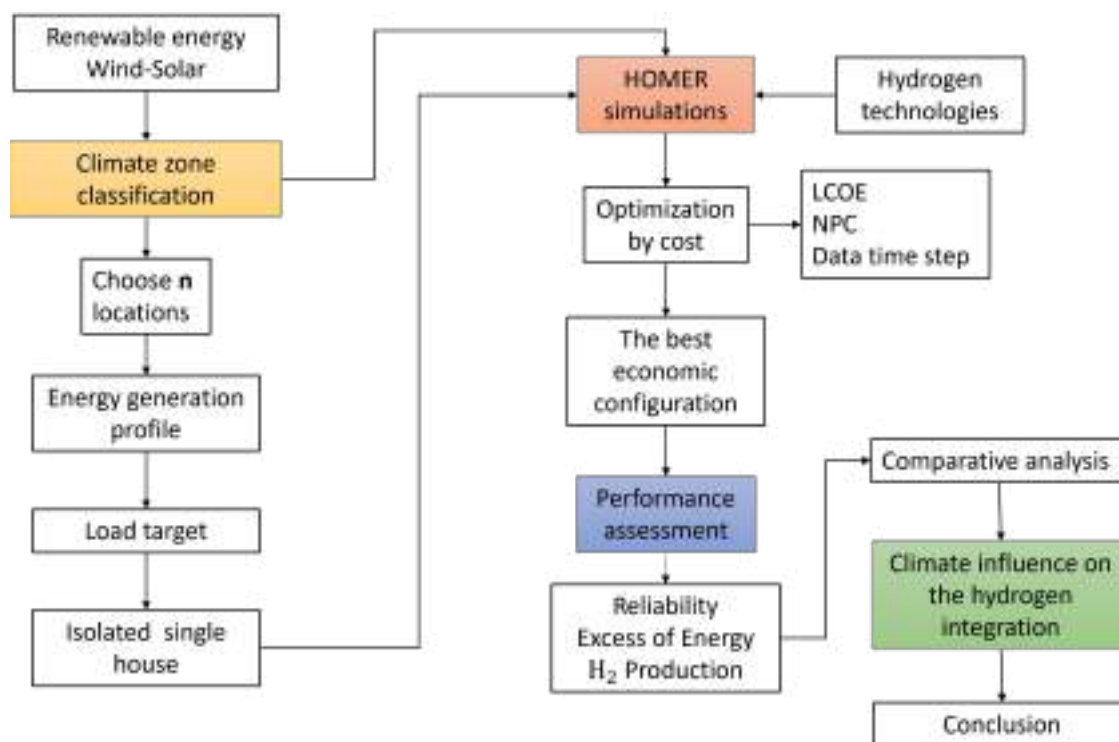
Figure 7.2: General Methodology

lated, and data on solar and wind resources, as well as energy demand, were readily available.

In this paper Köppen climate classification has been selected as reference for this analysis. This is a widely used system that categorizes climates based on vegetation, temperature, and precipitation patterns. It was developed by climatologist Wladimir Köppen and has been modified over time from the six climate types, 4 of them are found in North America: Tropical (A): Characterized by warm temperatures throughout the year, with high humidity and significant rainfall. Dry (B): Features arid and semi-arid climates with low precipitation and typically high temperatures. Temperate (C): Encompasses climates with distinct seasons, including mild to warm summers and cool to cold winters. Continental (D): Exhibits a greater temperature variation between seasons, with hot summers and cold winters [162].

Table 7.1 displays the list of selected locations for analysis, comprising 4 from the United States (climates B, C, and D), 2 from Mexico (climates A and C), and 1 location from Canada (D).

Table 7.1: Locations selected in this study

| Country | Location | Köppen Climate classification | Annual solar resource GHI [kWh/m day] | Annual wind resource @ 100m [m/s] |
|---|---|---|---|---|
| USA | Albany, Oregon | C | 4.03 | 8.97 |
| | Prescot, Arizona | B | 7.27 | 6.46 |
| | Rexburg, Idaho | D | 4.46 | 7.38 |
| | Jacksonville, Illinois | C | 4.17 | 7.84 |
| MEX | CDMX | C | 5.83 | 4.52 |
| | Cancun | A | 4.5 | 5.2 |
| CANADA | Ottawa | D | 3.67 | 7.04 |

### 7.1.3 Data acquisition

In this study, simulations were conducted utilizing measured data. Solar radiation and wind data were extracted from the meteorological databases of each respective country. Additionally, load profile data were obtained from various sources based on the country under investigation. For the United States, databases constructed by NREL were utilized, providing demand profiles corresponding to different climatic conditions [163]. In the case of Canada, data were derived from two prior experimental studies conducted by other researchers [164], [165].

Figure 7.4 illustrates the monthly profile of electric energy consumption for the selected locations. In most cases, two increments in demand are evident, one occurring during winter, particularly noticeable in the United States and Canada locations, and the other during summer due to heating and cooling requirements. However, for Mexico, the seasonal variation is not entirely apparent.

### 7.1.4 Evaluation parameters

To assess the performance of each EMS strategy, the numerical results of the simulations were condensed into four indicators for comparison. The first one is the Cumulative Energy along the year in kWh, which was calculated using equation 7.1 where $ET$ is the cumulative energy, $P_i$ is the power at hour $i$, $t_i$ is the time step in hours.

$$ET = \sum_{i=1}^{8760} P_i t_i \tag{7.1}$$
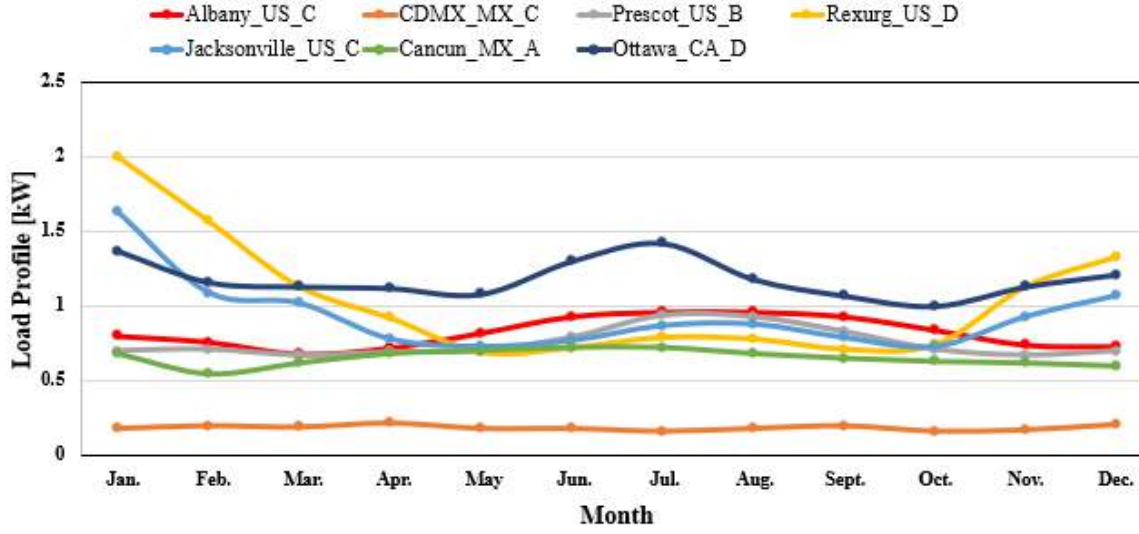
Figure 7.3: Effect of time step on sample number reduction and masking of instantaneous power values

The total mass of hydrogen produced by the electrolyzer in kg/h was computed according to equation 7.2. Where $E_{pvs}$ is the energy that comes from the PV panel array, $HHV_{H_2}$ is the Higher heating value of hydrogen (39.4 kWh/kg), and $eta_{elec}$ is the electrolyzer efficiency which was considered as 65 %.

$$M_{H_2} = \frac{\eta_{elec} E_{pvs}}{HHV_{H_2}} \tag{7.2}$$

The LCOE is defined as the average cost per kWh of the electrical energy produced by the HBRES during the project's lifetime. Therefore, to compute this value per year, the ratio between the annualized present cost of the system (Capital investment cost (CAPEX) and Operational Expenditures (OPEX) - that is the sum of Operation and maintenance (O&M) cost plus replacement cost) and the average of energy production is calculated in USD/kWh, according to equation 7.3 where $N$ is the project lifetime, and $I$ is the discount rate in %.

$$\text{LCOE} = \frac{\sum_{j=0}^{N}((\text{CAPEX} + \text{OPEX})(1+I)^{-j})}{\sum_{j=0}^{N}((ET)(1+i)^{-j})} \tag{7.3}$$

It is important to highlight that one of the parameters commonly used in the economic evaluation of energy projects is the Net Present Cost (NPC) which represents the present value of all costs the system will accumulate throughout its lifespan, subtracted by the

Table 7.2: Capital costs of system components

| Element | CAPEX DISTRIBUTED [USD/kW] | O&M DISTRIBUTED [USD/ kW-year] | REPLACEMENT COST [USD/ kW] |
|---|---|---|---|
| PV panel | 2286.98 | 26.98 | 250-1050 |
| BESS | 3034.7 | 75.86 | 3034.7 |
| FC | 2000 | 32.23 | 700 |
| PEM Electrolyzer | 1800 | 90 | 270 |
| Tank [USD/kg] | 1000 | — | 700-1000 |
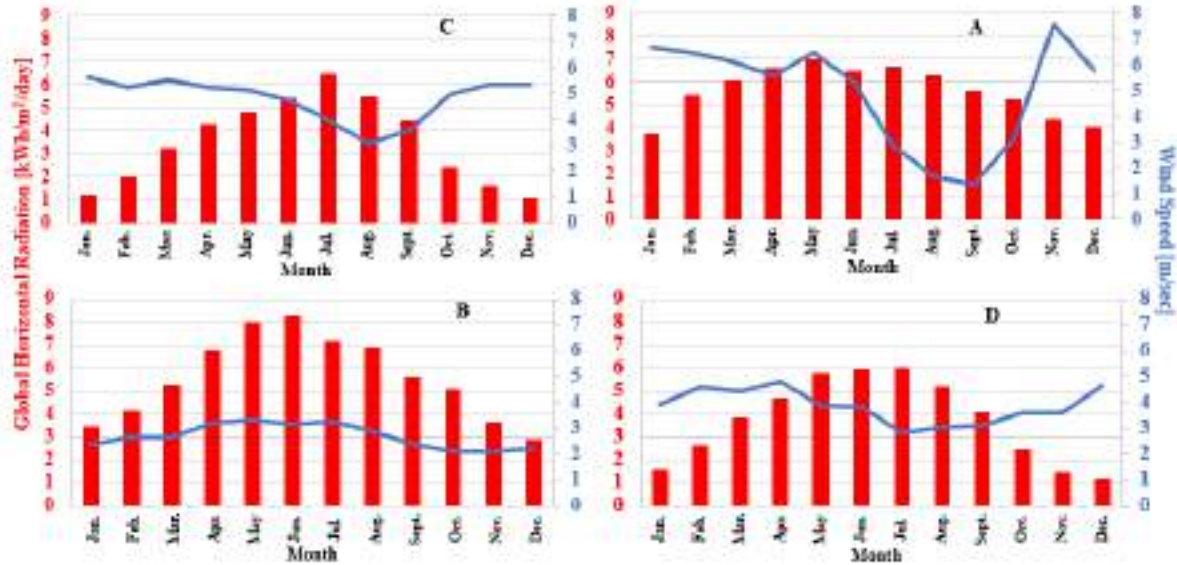


Figure 7.4: Wind Solar resources for each Köppen climate type

present value of all revenue it generates during the same period. This involves capital expenses, replacement costs as well as operation and maintenance costs.

## 7.1.5   Simulation conditions

The sizing of the MG was carried out by specifying a series of important parameters. In this work, the cost of a PEM electrolyzer that produces high-purity hydrogen to be fed into the fuel cell is taken into account (Table 7.2). The PV, BESS costs were taken from the cost list proposed by NREL [166], which includes costs at different scales (Utility and distributed). In this case, the costs corresponding to the distributed system category were used since, according to the Energy Information Administration (EIA) [167], installations with a capacity of at least 1MW are considered utility-scale and the studied system is smaller.
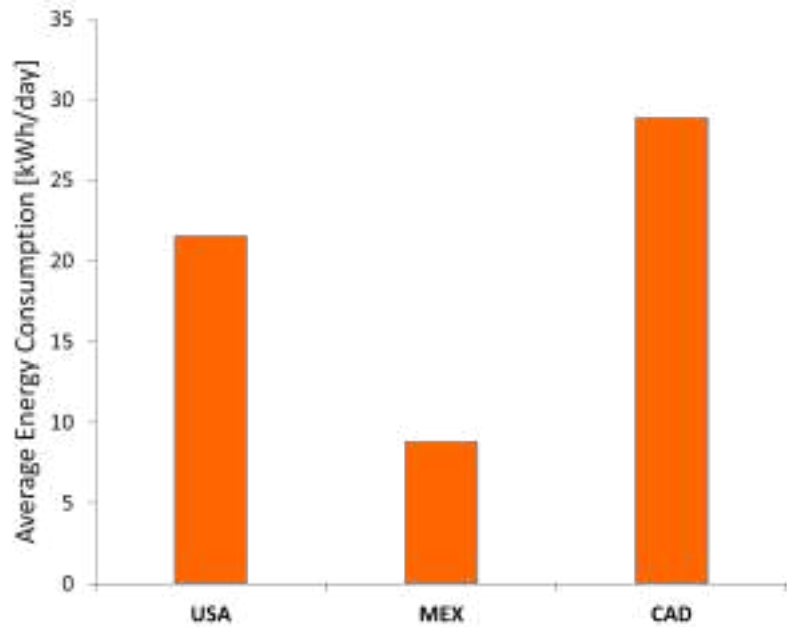
Figure 7.5: Average Energy Consumption per day

## 7.2    Results and Analysis

### 7.2.1    Effect of the time step on the microgrid sizing

The time step of data refers to the interval between consecutive data points used in simulations when sizing energy systems. The time step can significantly impact the accuracy and precision of the sizing process. Having Smaller time steps provides higher temporal resolution, allowing for a more detailed analysis of variations in energy generation, consumption, and storage. This can be particularly crucial for capturing rapid changes in renewable energy sources like solar and wind.

In Figure 7.7, the demanded power is depicted in terms of frequency at two distinct resolutions. At a 20-second interval, there are over a million data points, allowing the observation of frequency peaks for power levels that, upon averaging every 15 minutes, become imperceptible.
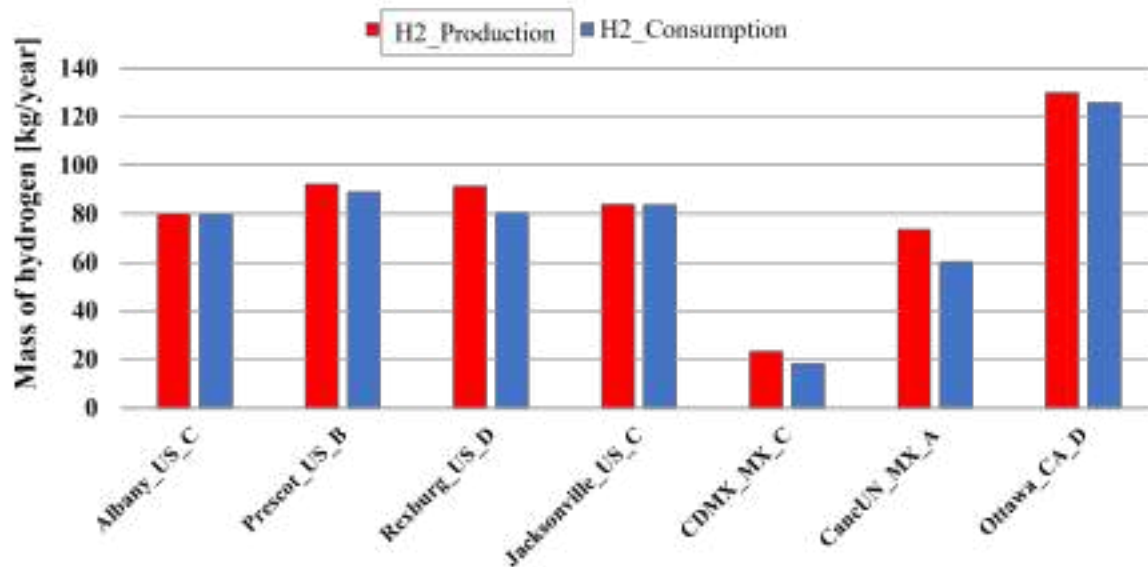
Figure 7.6: Total hydrogen production-consumption per location analyzed
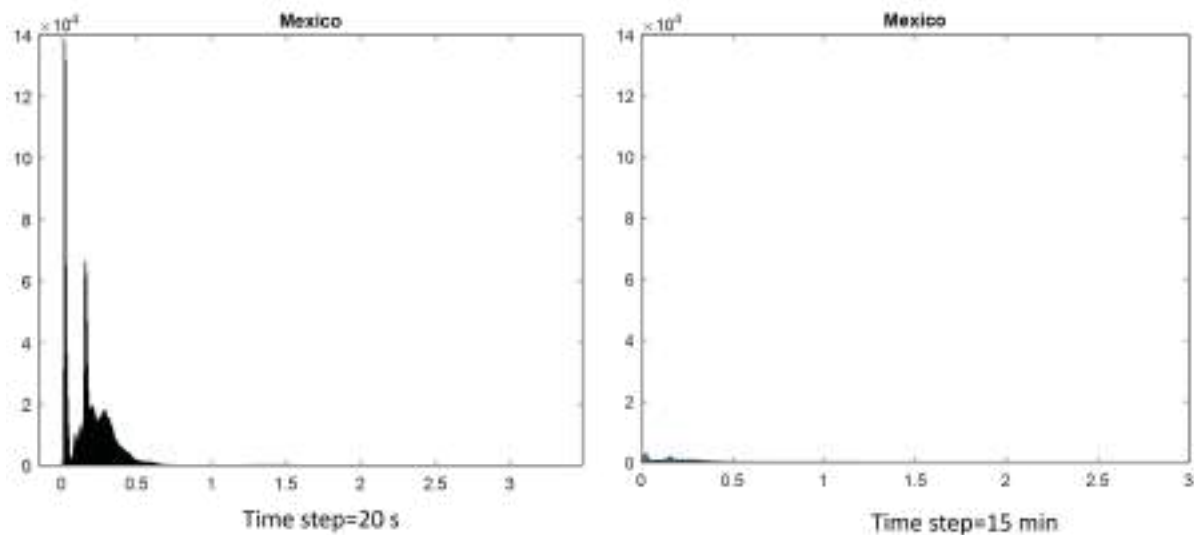


Figure 7.7: Effect of time step on sample number reduction and masking of instantaneous power values

Table 7.3: Microgrid component size for each location evaluated

| Location | Köppen Climate | PV [kW] | Wind Turbine [#] | FC [kW] | BESS [#] | Electrolyzer [kW] | Tank[kg] | Converter [kW] |
|---|---|---|---|---|---|---|---|---|
| Albany, US | C | 6 | 2 | 1 | 2 | 4 | 14 | 2.08 |
| Prescot, US | B | 5.6 | 1 | 1 | 2 | 3 | 12 | 1.56 |
| Rexburg, US | D | 12.3 | 9 | 3 | 1 | 7 | 15 | 4.53 |
| Jacksonville, US | B | 7.38 | 1 | 3 | 1 | 3 | 20 | 1.63 |
| CDMX, MX | C | 1.96 | 1 | 1 | 1 | 2 | 10 | 0.563 |
| Cancun, MX | A | 3.75 | 4 | 1 | 1 | 2 | 20 | 1.65 |
| Ottawa, CA | D | 14.4 | 3 | 2 | 9 | 5 | 20 | 5.64 |

## 7.2.2  Energy Capacity vs Energy demand evaluation

The energy demand for sizing a microgrid is not solely contingent upon the prevailing climate; the socio-economic aspect of the country is also a decisive factor. Figure 7.5 illustrates that Mexico exhibits the lowest energy consumption, with an annual average of 4.48 kWh/day, in contrast to the United States and Canada, where consumption ranges between 20 and 30 kWh/day. Nations endowed with greater resources tend to have increased access to energy-intensive amenities, whereas countries with limited resources predominantly utilize basic household appliances.

In Table 7.3, the sizing of a microgrid is presented, contingent upon both the climatic classification and energy demand. It is evident that in extreme climates such as D and B, characterized by either very cold or very hot conditions, larger energy systems are necessitated. Furthermore, in climates A and D, wind resources assume a pivotal role, mitigating the need for an excessively large photovoltaic system and consequently optimizing space utilization.

In climate type C, specifically in the case of Albany, Oregon, the system incorporates both wind and solar generation in all configurations. Across all scenarios, there is an energy surplus, with the minimum being 1.78 %. This implies that the storage system could potentially be expanded to enhance efficiency and perhaps reliability, albeit at a higher investment cost.

For locations like Mexico City and Prescott, HOMER indicates that sizing the system solely with photovoltaic systems is sufficient. The addition of wind turbines results in energy

surpluses due to the high solar resource in climate types B and C, rendering wind turbines unnecessary.

In cold climates such as Ottawa and Rexburg, the system is sized according to energy demand. As consumption significantly increases in winter, a surplus of energy is generated in summer, providing an opportunity for substantial hydrogen production. In such climates, seasonal energy storage would be highly advantageous, as the yearly energy surplus exceeds 40 %. Furthermore, energy management strategies such as Load Following (LF) could be implemented to avoid over-sizing with respect to the load.

In climate type A, the combination of solar and wind resources can be effectively utilized. Feasible systems with nearly negligible energy surplus were identified in these climates.

Additionally, it was found that in climate types B and C, over 65 % of the generated electrical energy comes from the photovoltaic system. In climate type D, the generation is obtained almost equally from both sources, with solar contributing 52 % and wind 48 % in some cases. In climate type A, 67 % of the energy is derived from wind sources, while solar resources contribute 32 %. These data are pivotal for making informed decisions when sizing a system.

In terms of hydrogen production, the climate in Mexico, combined with demand conditions, is highly conducive to hydrogen storage throughout the year. In the case of Prescott, the solar potential is remarkably high due to its classification as a climate type B. However, the substantial demand necessitates the system to produce sufficient hydrogen for nighttime utilization and to support the wind turbine, as depicted in Figure A.3. Similar occurrences are observed in other locations with climate types D and C and demands in the United States and Canada. In these cases, the system achieves self-sufficiency unless other applications of hydrogen are considered.

## 7.3    Summary and Highlights

Overall, the obtained results demonstrated the feasibility of constructing distributed systems (isolated microgrids) in all three North American countries, as the evaluated climates allow for self-sufficient systems. Concerning hydrogen production, Mexico exhibits significant potential due to lower energy demands and great solar and wind resources in climate A zones compared to Canada and the United States. This characteristic enables the storage of hydrogen for additional applications such as mobility, whereas the USA and CA two countries can only consume the produced hydrogen to meet their energy demands.

# Chapter 8

# Toward Hydrogen Road Map for Mexico

> In this chapter, a recapitulation of the results presented in the preceding chapters is provided to establish the foundations for a proposal of a hydrogen road map in Mexico.

The potential of hydrogen in decarbonizing the energy sector has been extensively researched and acknowledged within academic circles. It is widely accepted that hydrogen must be considered a significant contributor to achieving full decarbonization, accounting for approximately 11 % of emissions reductions. This assertion is supported by empirical evidence and modeling studies conducted by leading institutions in the field.

A notable observation made by IRENA is the global trend toward integrating hydrogen into national energy strategies. As of 2022, 66 countries were identified to have either established, are in the process of drafting, or have announced a national hydrogen strategy [11]. Mexico does not feature among these nations, as illustrated in Figure 8.1. This absence may be attributed to the historical orientation of Mexico's public policies toward fossil fuels.

However, the urgency of addressing climate change and the imperative to limit global warming to 1.5°C necessitates proactive measures on the part of Mexico. In alignment with international commitments and scientific consensus, Mexico must prioritize advancements in hydrogen technologies alongside other decarbonization strategies, including but not limited to renewables, energy efficiency improvements, and electrification initiatives.

Figure 8.1: Hydrogen strategies published or under development 2022 [11].

# 8.1 Strong Considerations for Hydrogen Policy Development.

Incorporating hydrogen into Mexico's energy matrix represents a pivotal step toward achieving its climate targets and fostering sustainable development. Furthermore, embracing hydrogen presents opportunities for economic diversification, technological innovation, and enhanced energy security. Therefore, Mexico must recalibrate its energy policies and track a trajectory that aligns with global efforts to mitigate climate change.

Globally, the integration of hydrogen faces three primary challenges: Infrastructure availability, policy, and institutional capacity. Infrastructure refers to the physical systems for hydrogen production, distribution, and utilization. The policy encompasses the regulatory frameworks and government initiatives that shape the hydrogen market and incentivise its adoption. Institutional capacity pertains to the organizational capabilities of public and

private entities involved in the hydrogen sector, including research institutions, industry associations, and governmental agencies (Figure 8.2).

Internationally, one of the most significant barriers is the high cost of hydrogen technology. While countries with established market control may perceive electrolyzers as expensive (1,700-2,000 USD/KW), the cost is even more pronounced for countries like Mexico due to additional importation expenses. This financial barrier delays widespread adoption and limits the scalability of hydrogen projects.

Moreover, the challenge of increasing hydrogen demand persists. Although various applications for hydrogen have been identified, including transportation, industrial processes, and energy storage, the lack of adequate infrastructure and the perceived difficulty of transitioning to low-carbon hydrogen contributes to keeping demand growth static. The economic viability of hydrogen as an alternative fuel source is contingent upon addressing these barriers.

In the case of Mexico, there exists a potential skills gap in the workforce required to support the hydrogen economy. Universities and educational institutions must adapt their curricula to incorporate hydrogen-related technologies and concepts, ensuring that future professionals are equipped with the requisite knowledge and expertise. Human resources play a crucial role in driving innovation and facilitating the integration of hydrogen technologies into existing systems.

Addressing these challenges necessitates a concerted effort from stakeholders across sectors. Collaboration between government entities, industry players, academic institutions, and civil society is essential to overcome barriers, stimulate investment, and foster the development of a sustainable hydrogen ecosystem. By tackling infrastructure constraints, implementing supportive policies, and building institutional capacity, countries can unlock the full potential of hydrogen as a clean energy solution.
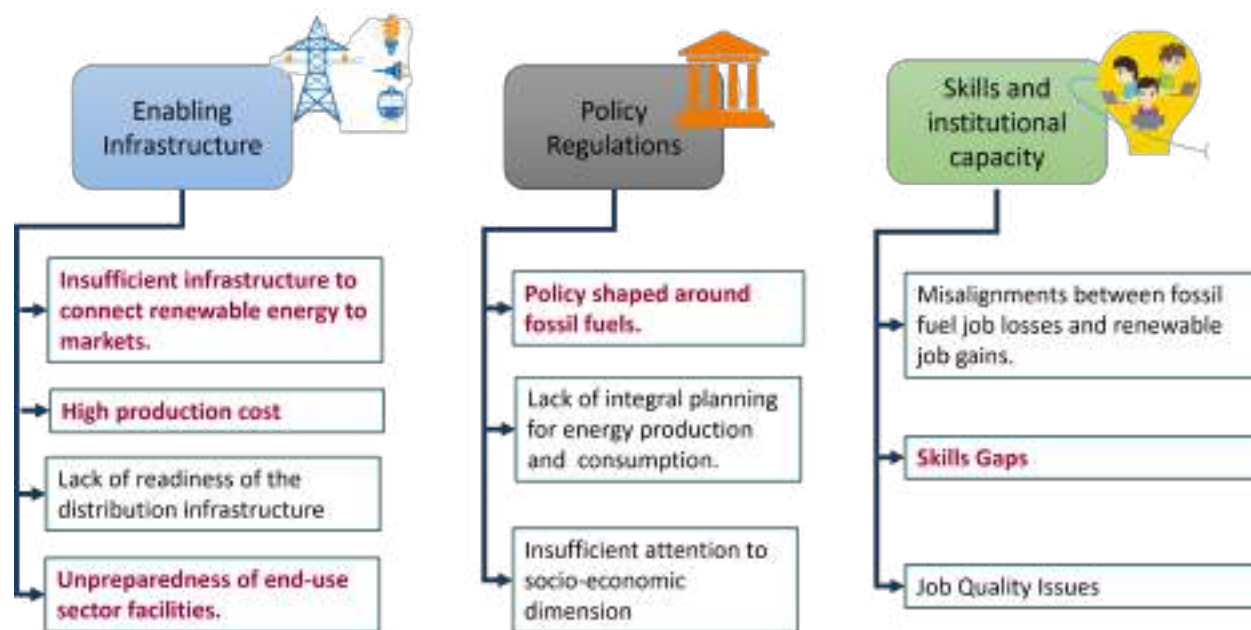
Figure 8.2: Key Hydrogen Integration Barriers.

According to IRENA, the formulation of robust public policies for hydrogen deployment relies on four fundamental pillars, delineated in Figure 8.3. These pillars serve as guiding principles for governments and stakeholders as they navigate the complexities of integrating hydrogen into their energy frameworks.

Hydrogen strategies outline the overarching vision and objectives for $H_2$ utilization within a country. However, to effectively implement these strategies, they must be supported by complementary elements such as road maps, vision statements, and research and development (R&D) programs.

The second pillar pertains to the identification of hydrogen priorities. Given that hydrogen serves as a complement to existing decarbonization strategies, it is imperative to delineate clear priorities to avoid potential conflicts or competition between initiatives. While certain applications, such as light transportation, may be viable candidates for hydrogen deployment, careful consideration must be given to avoid direct competition with alternative technologies, such as electric vehicles (EVs).
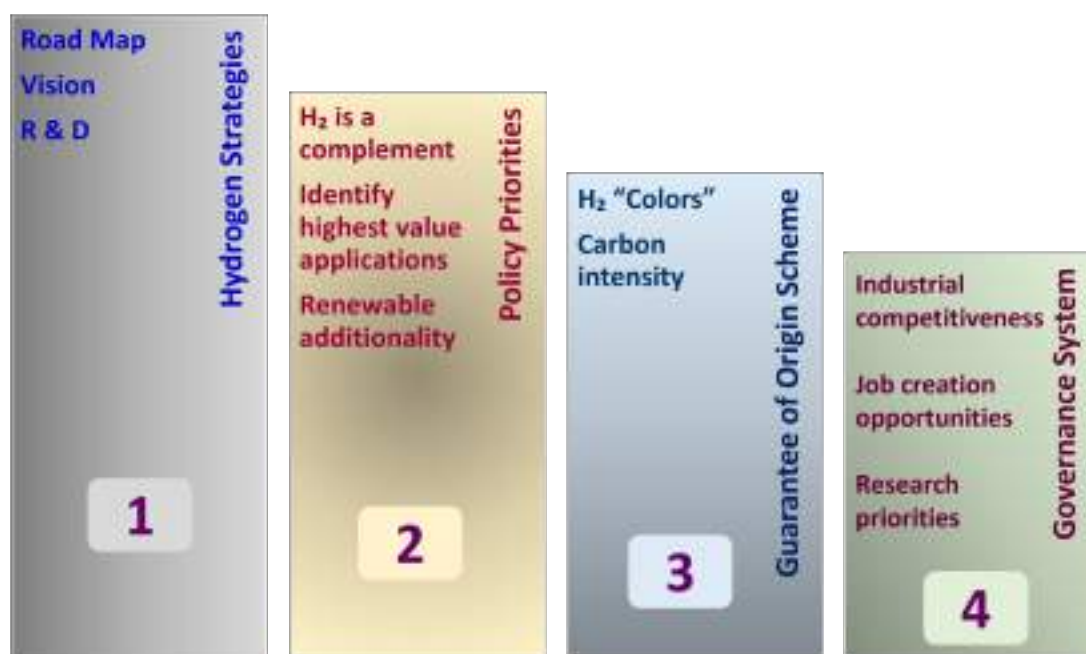
Figure 8.3: Pillars for developing public policies.

Furthermore, the intrinsic versatility of hydrogen necessitates a nuanced approach to its integration. Hydrogen should be directed towards applications that cannot be readily electrified, thereby maximizing its value proposition and leveraging renewable energy sources to achieve additional environmental benefits. In establishing a functioning hydrogen market, the establishment of a guarantee of origin mechanism is paramount. Given the diverse array of methods for hydrogen production, simply categorizing hydrogen by color is insufficient. Instead, rigorous measurements of hydrogen carbon intensity should be incorporated to ensure transparency and facilitate international trade.

Lastly, hydrogen public policy development must prioritize job creation and targeted research efforts to address specific national needs. By aligning hydrogen initiatives with broader socio-economic objectives, governments can maximize the socio-economic benefits of hydrogen deployment and foster inclusive growth.

In conclusion, the development of effective public policies for hydrogen deployment requires a multifaceted approach that considers technological, economic, and societal factors. By adhering to the principles outlined by IRENA and embracing a holistic perspective, countries can navigate the complexities of hydrogen integration and unlock its full potential as a key enabler of the transition to a sustainable energy future (Figure 8.4).
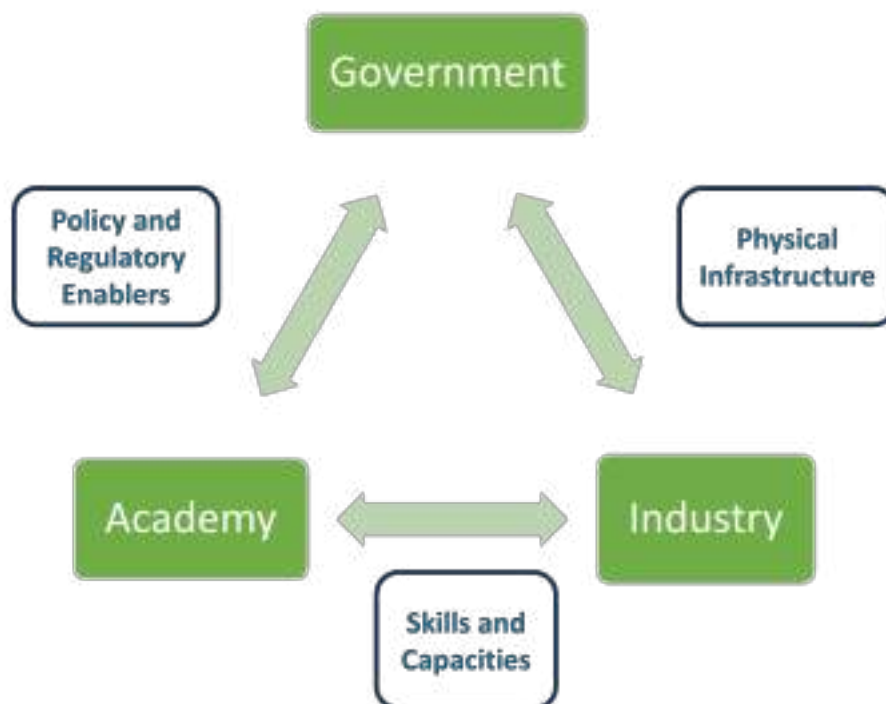


Figure 8.4: Suitable sites classification for renewable hydrogen product.

## 8.2   Worldwide Low-Carbon Hydrogen Production Projects

The IEA has established a comprehensive database to monitor hydrogen production projects globally since 2000, particularly those with energy or climate change mitigation objectives. This database encompasses projects intended to decrease the emissions related to hydrogen production for current applications and those aiming to employ hydrogen as an energy carrier or industrial feedstock in innovative applications that could serve as low-emission technological alternatives [168]. In addition, the database includes projects that are currently in the planning stages or under construction.

This data base is integrated by 1,996 low-carbon hydrogen production projects, with capacities typically in the megawatt (MW) range. Analysis of this extensive database indicates that in more than 50 % of these projects, the specific electrolysis technology employed is not disclosed. However, among those projects where the electrolysis technology is specified, it is observed that Proton Exchange Membrane (PEM) electrolysis is utilized in 345 projects, alkaline electrolysis in 254 projects, and Solid Oxide Electrolysis Cells (SOEC) in 48 projects. These three types of electrolysis technology have been implemented across the entire spectrum of end uses, highlighting their versatility and adaptability to various applications (Figure 8.5).

Moreover, the database reveals that 126 projects incorporate carbon capture when natural gas is used as the feedstock. This integration of carbon capture technology underscores the industry's commitment to reducing emissions and enhancing the sustainability of hydrogen production. The predominance of PEM electrolysis can be attributed to its efficiency and suitability for a range of applications, making it a preferred choice in the industry. The comprehensive data provided by the IEA underscores the critical role of electrolysis technologies in advancing low-carbon hydrogen production and highlights the ongoing efforts to develop and deploy sustainable energy solutions globally.

An analysis of the projects listed in the IEA database reveals a diverse array of end uses for hydrogen. The most prevalent application identified is hydrogen use in mobility, with 575 projects dedicated to this purpose. This is followed by industrial applications as a feedstock, encompassing 304 projects. In third place is the production of ammonia, with 296 projects. Electricity generation stands fourth, with 235 projects, while the injection of hydrogen into the natural gas grid is the focus of 164 projects (Figure 8.6).

Industrial $H_2$ utilization, such as feedstock, is crucial in chemical manufacturing and refining. Transitioning to low-carbon hydrogen can significantly reduce emissions in these hard-to-abate industries. The production of ammonia, also benefits from low-carbon hydrogen, potentially reducing the carbon footprint of the fertilizer industry.
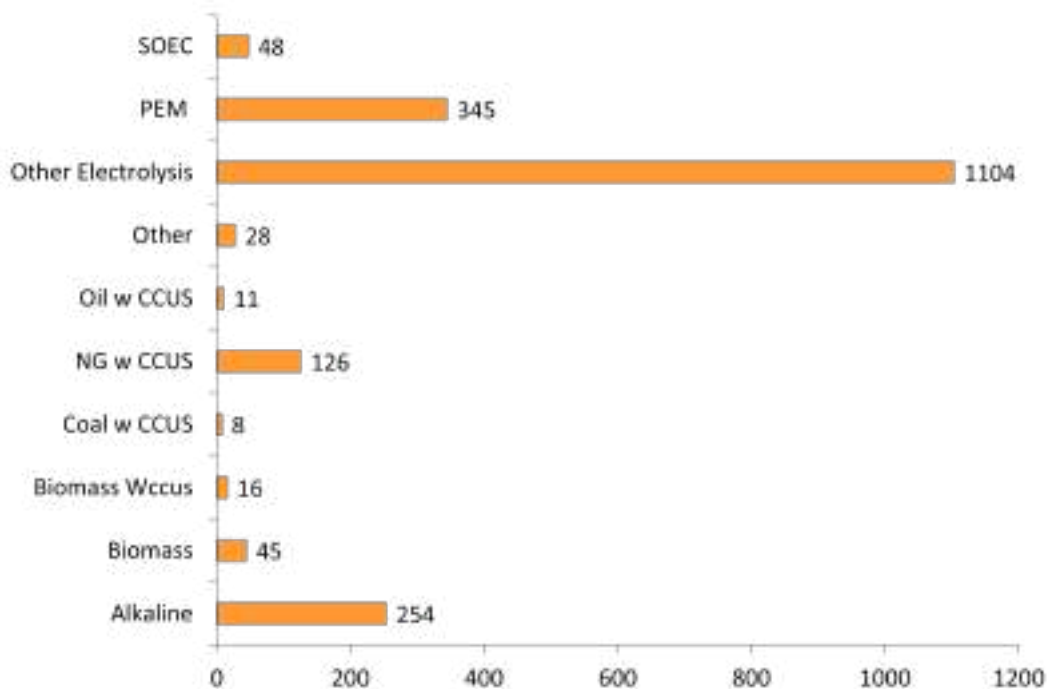
Figure 8.5: Hydrogen production technologies used in projects developed around the world.
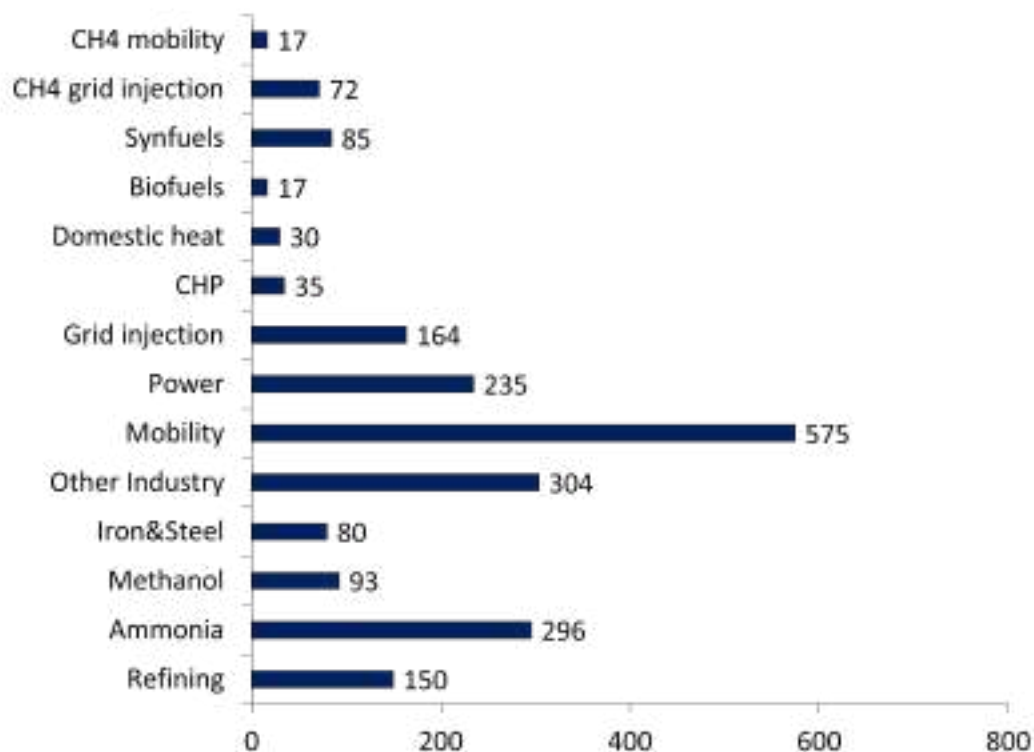


Figure 8.6: End use of hydrogen produced in the identified projects.

The generation of electricity through hydrogen can address the intermittency issues of renewable energy sources by providing a stable and flexible energy supply. Finally, injecting hydrogen into the natural gas grid helps in gradually decarbonizing existing gas infrastructure, facilitating a smoother transition to a low-carbon economy.

These prioritized uses reflect the sectors' readiness and potential impact on carbon emissions reduction. By focusing on these applications, significant progress can be made toward achieving global climate goals, underscoring the transformative potential of hydrogen in creating a sustainable energy future.

The analysis further identified that among the registered projects, 1,122 exclusively utilize pure renewable energy sources, while 184 projects rely solely on grid electricity. Additionally, 30 projects receive their energy supply from a combination of grid electricity and renewable sources (Figure 8.7a).

In addition, the results revealed that 310 projects use a combination of various renewable sources. Specifically, 245 projects are powered only for PV energy. Offshore and onshore wind energy are also significant contributors, with 112 and 122 projects, respectively, demonstrating nearly parallel development.

The predominant use of pure renewable energy in these projects highlights the industry's commitment to sustainability and the transition towards a low-carbon economy. The integration of multiple renewable sources in 310 projects indicates a strategic approach to enhance energy security and reliability (Figure 8.7b). The substantial number of projects utilizing solar PV energy reflects the maturity and decreasing costs of this technology, making it a favorable option for hydrogen production.
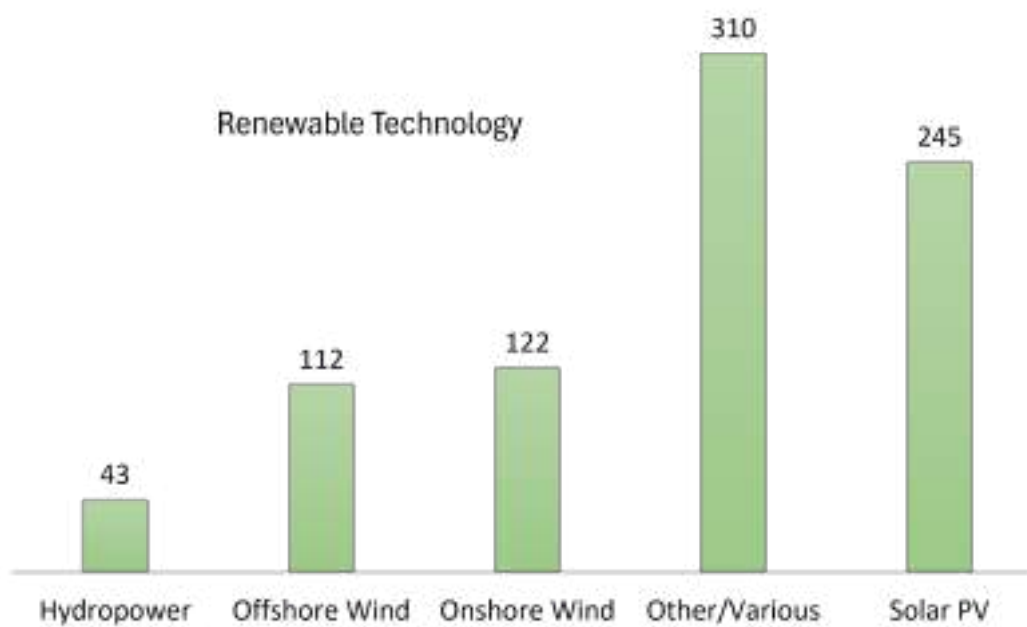
(a)
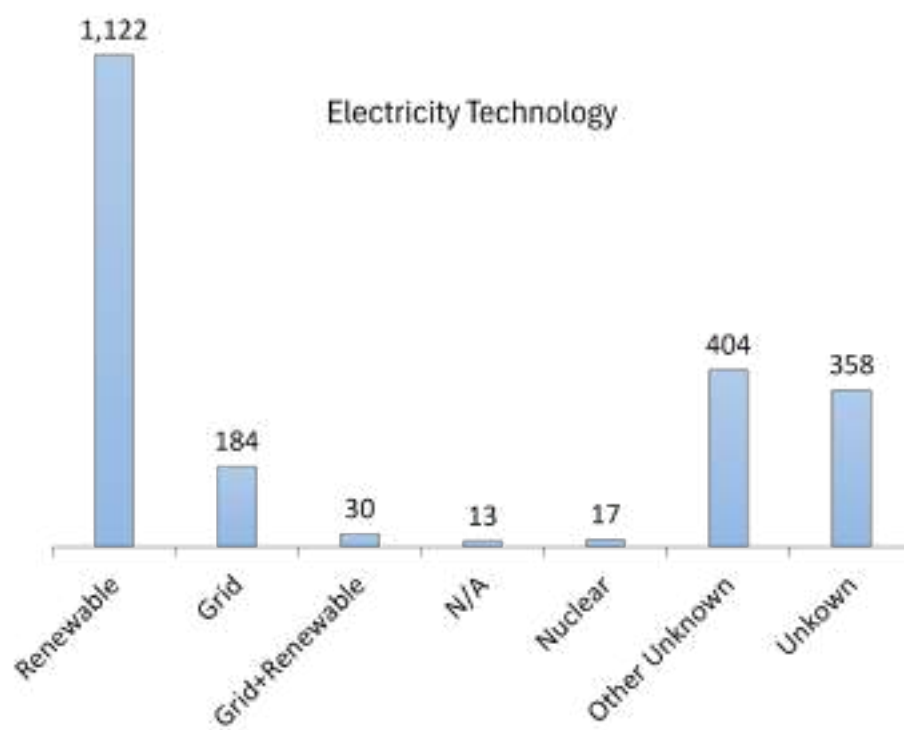


(b)

Figure 8.7: a) Renewable Technology used for $H_2$ production. b) Power source technologies used in hydrogen production projects.

## 8.2.1   Projects development in Mexico

Despite the fact that the IEA has not identified Mexico as a country with strong public policies on low-carbon hydrogen, it has identified nine projects, four of which will be dedicated to ammonia production and the rest to the generation of $H_2$ for refineries and power generation (Table 8.1). Additionally, it is observed that electrolysis is the dominant technology in these projects, which demonstrates evidence that Mexico is a key region for the implementation of this technology, thereby attracting the attention of foreign investors. However, caution must be exercised in these aspects because, while these projects will generate jobs, Mexican resources would be used for export to another country. It is necessary to achieve a balance in the development of these projects between national and foreign investors. Mexico is obligated to harness this potential in a way that does not compromise national sovereignty.

Although the Mexican government has not yet taken immediate action on the implementation of hydrogen projects, steps have been taken to lay the foundations for future policies and real projects development. In 2024, the creation of the "CONACYT National Hydrogen Technologies Laboratory" was approved, involving several institutions, with the National Polytechnic Institute leading this working group. The establishment of this laboratory will pave the way for investment in research aimed at deploying hydrogen technologies in the country, addressing issues related to the integration of this energy resource into power generation and its use in other processes.

Recently, the most significant action taken by the Mexican government, through the Ministry of Energy, is the creation of "Hydrogen guidelines". These document comprise a list of eleven points highlighting the lines of action for implementing $H_2$ in the energy matrix. However, they remain a collection of aspirations and ideas, with no clear goals or timelines for achieving them.

This nascent focus on hydrogen technologies positions Mexico at a critical juncture, where strategic action could transform the nation's energy landscape and bolster its sovereignty.

Table 8.1: Hydrogen Production Projects being developed in Mexico

| Project name | Status | H$_2$ Technology | Energy Source | Electricity Details | Product | End use | Announced size | Feasibility study | Capacity [N$^2$ H$_2$/h] | Capacity [kt H$_2$/y] |
|---|---|---|---|---|---|---|---|---|---|---|
| Energía Los Cabos | Feasibility study | PEM | Dedicated renewable | Solar PV | H$_2$ | Power | 25MW | 25 | 4807.692 | 3.75 |
| Dos Bocas refinery | Concept | NG w CCUS | — | | H$_2$ | Refining | | — | — | — |
| Delicias Solar | Feasibility study | Other Electrolysis | Dedicated renewable | Solar PV | H$_2$ | — | 35MW | 35 | 7777.778 | 6.06 |
| Dhamma Energy Guanajuato | Concept | Other Electrolysis | Dedicated renewable | Solar PV | H$_2$ | — | | — | — | — |
| Mexican Green Hydrogen Hub, phase 1 | Feasibility study | PEM | Dedicated renewable | Solar PV | Ammonia | Ammonia | 69MW | 69 | 13269.23 | 10.35 |
| Mexican Green Hydrogen Hub, phase 2 | Concept | PEM | Dedicated renewable | Solar PV | Ammonia | Ammonia | 343MW | 274 | 52692.31 | 41.08 |
| Hy2gen Yucatan project, 1 | Concept | ALK | Dedicated renewable | Others/Various | Ammonia | Ammonia | 160MW | 160 | 34782.61 | 27.11 |
| Hy2gen Yucatan project, 1 | Concept | PEM | Dedicated renewable | Others/Various | Ammonia | Ammonia | 40MW | 40 | 7692.308 | 5.99 |
| Hydrogen project - Oaxaca | Concept | Other Electrolysis | Other/Unknown | Unknown | H$_2$ | — | — | 0 | — | — |

Table 8.2: Summary of hydrogen production potential from the evaluated energy sources.

| Source | Energy [TWh/year] | H$_2$ [MTon/year] | LCOE [USD/kWh] | LCOH [USD/kg] PEM | ALK |
|---|---|---|---|---|---|
| Solar PV | 124,31 | 2,366.33 | 150 | 8.5 | 5.7 |
| Onshore Wind | 2,135.76 | 38.2 | 111 | 9.9 | 7.4 |
| Offshore Wind | 12,680.2 | 217.33 | 150 | 9.39 | 8.2 |

Table 8.3: Summary of hydrogen production potential from the evaluated energy sources.

| Suitability Class | H$_2$ Availability H$_2$ Production [Ton/km2] | H$_2$ Demand | Distance Petrochemical Plant [km] | Oil/Gas Pipekines [km] | Refinery [km] | Electric Grid [km] | Cities [km] |
|---|---|---|---|---|---|---|---|
| Alta | >4,000 | | 1.5-0.5 | 0.5-0.1 | 1.5-0.5 | 0.5-0.1 | 1.5-0.5 |
| Good | 3,500-4,000 | The demand | 3.0-1.5 | 1-0.5 | 3.0-1.5 | 1.5-0.5 | 3.0-1.5 |
| Moderate | 2,500-3,500 | is required | 5-3.0 | 2.5-1 | 5-3.0 | 2.5-1.5 | 5-3.0 |
| Low | 2,000-2,500 | and fixed for | 7.0-5.0 | 3.5-2.5 | 7.0-5.0 | 3.5-2.5 | 7.0-5.0 |
| Poor | 2,000 | each state | 7.0 | 3.5 | 7.0 | 3.5 | 7.0 |

## 8.3   Low-Carbon H$_2$ Applications Scenario in Mexico

The potential for hydrogen generation in Mexico from photovoltaic solar energy and onshore and offshore wind has been substantiated throughout this thesis. Table 8.2 provides a summary of the principal results obtained in the course of this study. Furthermore, it has been shown that this generation capacity could adequately meet the current and future demand for H$_2$ in Mexico and could even address the transportation sector. To substantiate this point, suitable sites for renewable hydrogen generation were examined.

The optimal sites for land-based solar-wind hydrogen production were determined by considering factors such as generation capacity and H$_2$ demand, distances to various points (such as the grid, petrochemical complexes, refineries, and pipelines), and constraints that allow the exclusion of geographic areas where renewable energy harvesting is not feasible. Table 8.3 lists all the factors considered.

Figure 8.8 shows the total hydrogen production map (solar-wind) after the indicated areas were excluded. It is noteworthy that only 42 % of the territory can harvest solar energy and only 20.5 % can harvest wind energy, resulting in a total of 62.5 % of the territory being usable for these purposes. This could produce up to 4,933 tons/km$^2$ of hydrogen per year.

After characterizing the hydrogen production potential in Mexico, the hydrogen demand scenario was calculated. This calculation was established based on three uses related to hard-to-decarbonize sectors (ammonia production, refining, and mobility) to approximate the consumption value, given that measured data for these applications are not yet available.

The demand aproximation for light vehicles was calculated based on the gasoline consumption per state reported by SENER, in a scenario where 30 % of this demand is met by hydrogen. For ammonia production and use in refineries, data established by PEMEX were considered, assuming only 30 % of the total consumption for refineries and 100 % for ammonia. Figure 8.9 shows the hydrogen demand, indicating that the states with the highest consumption are those where the country's refineries and petrochemical complexes are located.
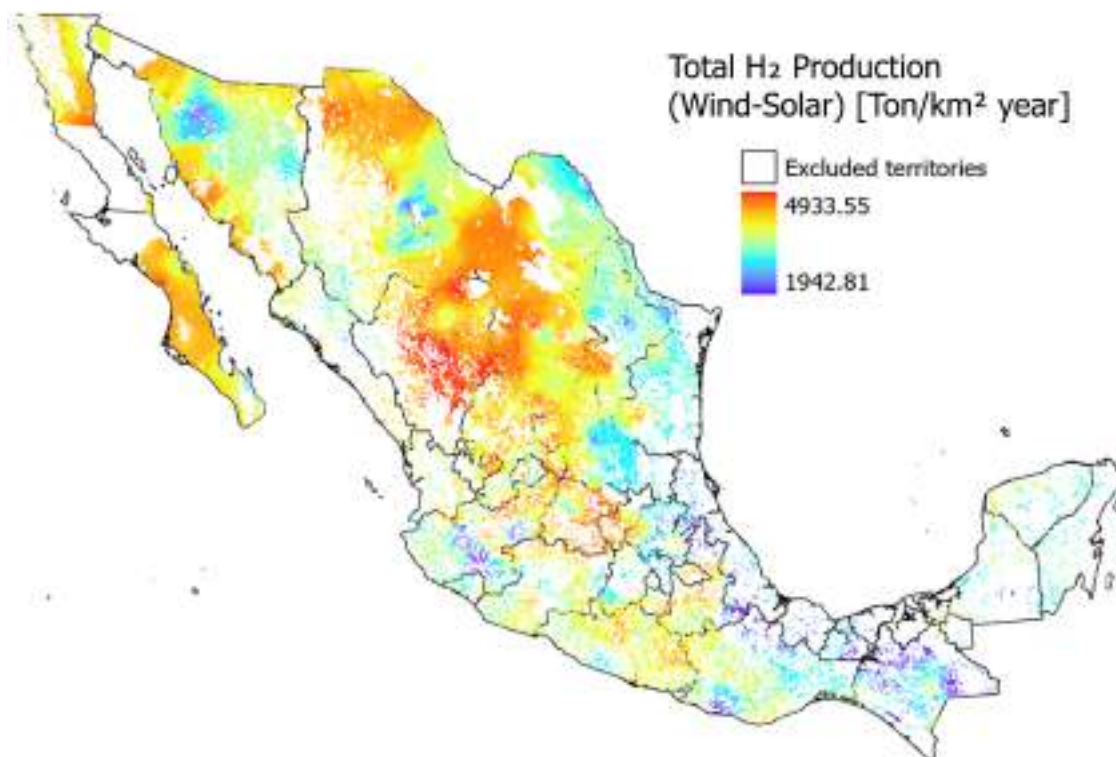


Figure 8.8: Total Wind-Solar Hydrogen Production Distribution in Mexico.

Figure 8.10 shows the sites where hydrogen production is feasible, classified according to their suitability in meeting the previously established optimal conditions. It is observed that, because the areas with the highest demand are in the eastern part of the country and

because most of the infrastructure is also located there, the best sites for hydrogen harvesting are in the eastern and northeastern regions of the country.
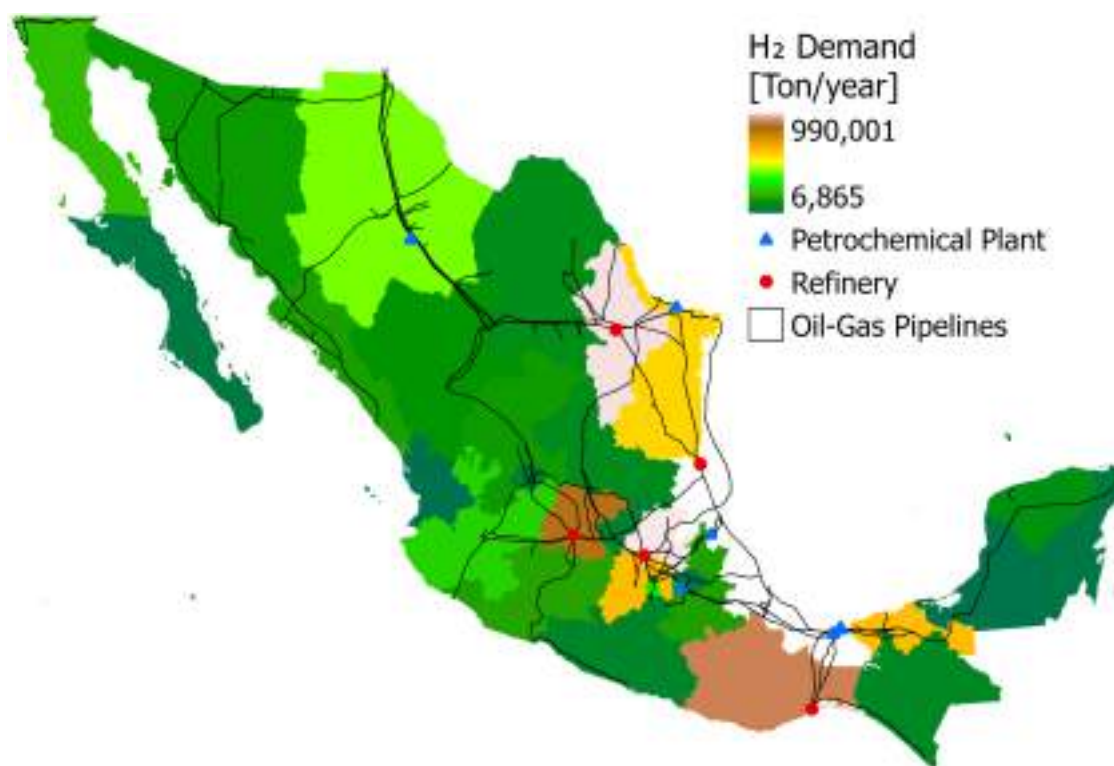


Figure 8.9: Hydrogen Demand scenario for Hard-to-abate applications.

## 8.4 Structure of the Hydrogen Roadmap for Mexico

It is evident that Mexico has significant potential for hydrogen production, focusing on solar and wind energy, as in the 1.5°C scenario, 70 % of energy should derive from these two sources. From the techno-economic evaluation, it was found that Mexico has significant potential expenditures for hydrogen production. In a centralized scenario, Mexico could produce up to 2,366 MTon/year, while in a decentralized one (10 % urban settlements), it could reach 9.39 MTon/year. Onshore wind could yield 154 MTon/year, and offshore wind 217.5 MTon/year.

These capacities could potentially meet the global demand for hydrogen (95 MTon/year). However, several factors delay hydrogen development in Mexico, If electrolyzer had the same
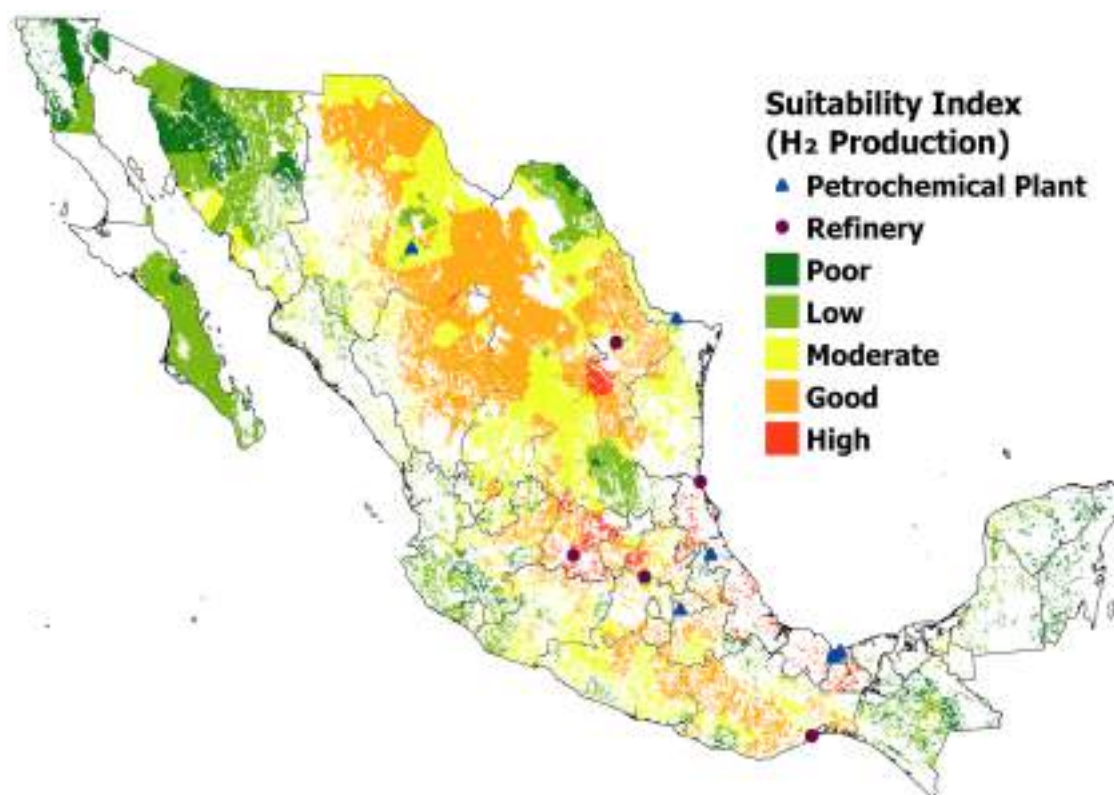
Figure 8.10: Optimal site selection for Wind-Solar Hydrogen Production

cost as in countries like the USA and China, the LCOH could be competitive internation-
ally. However, importing an electrolyzer to Mexico increases costs by 3.5 times [169]. Hence,
Mexico must establish public policies in two directions: promoting $H_2$ consumption through
incentives simultaneously setting market policies and reducing import taxes.

It should be noted that hydrogen should not compete with other decarbonization strate-
gies. Therefore, priority applications in Mexico should target heavy and light industries
to eliminate direct emissions from chemical processes. Mexico should consider policies to
increase ammonia and methanol production domestically.

Government, Industry and Academia must be integrated into a synergy scheme, as de-
picted in Figure 8.4, through the tools of the National Hydrogen Laboratory. The current
hydrogen consumption stands at less than 0.25 MTon/year. This consumption should be
increased through the creation of hydrogen demand to expand the decarbonization areas

while simultaneously intervening in the technology acquisition market.  Mexico must seek international alliances that enable it to obtain the technology at reasonable prices since México does not produce this technology making more difficult its deployment.

Based on the information collected thus far regarding the technical, economic, and political aspects of hydrogen, it is possible to establish the framework upon which the process of hydrogen integration in Mexico should be recommended, considering certain criteria.  Figure 8.11 presents a proposal for the deployment of $H_2$ in the form of a skeleton, which essentially requires the government, academia, and industry to fill in the details by establishing national figures, as these would be based on foundational policies.

Firstly, according to IRENA, the insertion and development of hydrogen must be carried out carefully, taking into account four criteria:

- Energy Efficiency: The processes of $H_2$ production and utilization must ensure logical energy exploitation.

- Emission Reduction:  This is the central variable that justifies the use of hydrogen. Priority uses and applications should align with areas where hydrogen's contribution is crucial and difficult to address through other decarbonization strategies.

-

- Education and Adaptation: The roadmap should be structured chronologically to allow society to become aware of, accept, and adapt to these technologies in a phased manner, starting with academia and industry, and finally the broader society.  Society should be the target sector in the development of hydrogen; it is crucial for the public to be familiar with the technical and safety aspects.  This familiarity will enable market development in a more personalized sector, such as the use of $H_2$ in microgrids.

Where to star?  Based on the evidence regarding the renewable potential and hydrogen generation, as well as the key utilization sectors, it is imperative that Mexico begins to work in two areas.  The first area involves robust programs for hydrogen technology research,

aimed at developing specialized human resources who can continue to address the challenges of this technology in materials, efficiency, storage, and markets.

Four priority research areas are suggested:

1. Exploration of offshore hydrogen production, given the proximity to existing gas and oil infrastructure.

2. Investigation into Mexico's manufacturing potential for electrolyzer assembly.

3. Hydrogen integration in the mobility sector.

4. Hydrogen integration in microgrids as storage system.

This effort must be accompanied by public policies that address the priority sector in Mexico, which is the industrial sector. It is essential to open up markets, and for this purpose, Mexico urgently needs to consider policies to incentivize international alliances. This should facilitate the regulation of import costs and establish agreements in industry, markets, technology, and human resources.

In conjunction, international alliances, combined with research and development, will enable the creation of necessary regulations and standards to ensure the safety and quality of hydrogen. It is essential to continue refining methods to guarantee the origin of hydrogen.

In terms of applications, the sequence outlined in the diagram of Figure 8.11 aims to meet the four basic criteria for generating the roadmap. It is urgent that Mexico begins to integrate carbon capture in conventional processes while simultaneously incorporating renewable hydrogen into these processes, with the primary goal of prioritizing emission reduction. Public policies should incentivize industrial processes where hydrogen is a raw material or where a value-added product, such as methanol or ammonia, is obtained. These sectors should be addressed within the next 10 years, considering Mexico's strong policy trend towards fossil fuels.
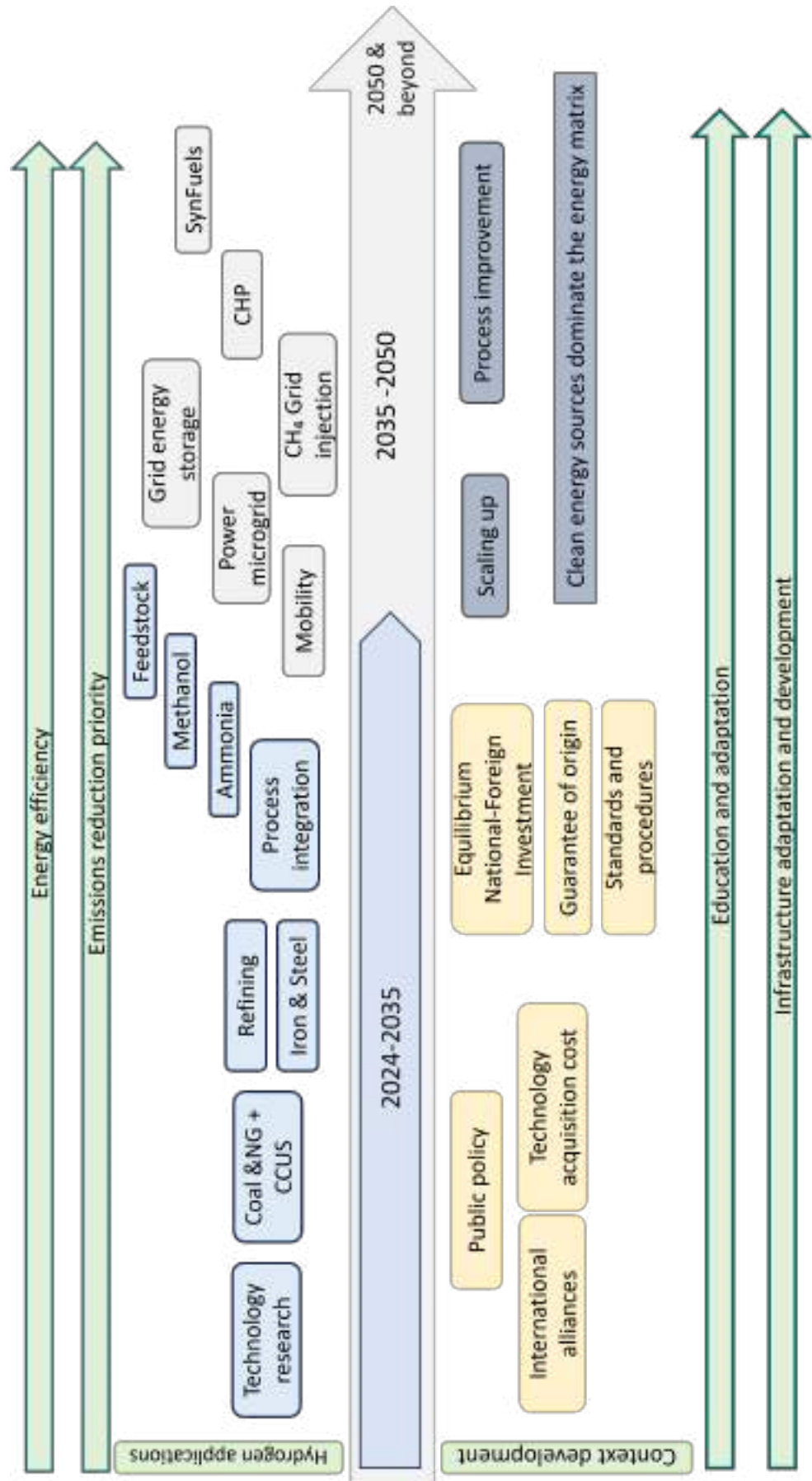
Figure 8.11: Analyzed vehicle technologies and energy production scenarios.

It is recommended that the goals for the implementation of hydrogen in electric mobility and microgrids be set for 2035, for two reasons. First, this timeline would allow for the deployment of transportation electrification through battery electric vehicles, which would more quickly address $CO_2$ emissions from transportation without entering into technological competition, as it is important to remember that the role of hydrogen is complementary. The second reason is that, by 2035, there would be more advanced knowledge of the technology, new infrastructure would have been developed, and society would have greater recognition of hydrogen as an energy source.

Upon reaching this point, it will be easier to consider the expansion and scaling of hydrogen use in generation turbines. After 2035, it is crucial that the national electric system has expanded and, more importantly, that its renewable capacity has increased.

# Conclusions

In this thesis, climatological data from meteorological stations were compiled, processed, and analyzed to evaluate Mexico's potential for large-scale hydrogen generation. The aim was to provide realistic information regarding the status of hydrogen in Mexico to lay the groundwork for a hydrogen roadmap in the country. The findings of this thesis can be summarized as follows:

1. Mexico exhibits immense potential for solar hydrogen generation, with a capacity of up to 2.366 MTon/year in a centralized scenario and 9.39 MTon/year in a decentralized scenario (urban settlements). This initial information suggests that Mexico could adequately cater to both large and small-scale applications, and even if the entirety of this potential were to be harnessed, less than 10% of the country's rainfall would be required for hydrogen production.

2. The onshore wind potential in Mexico is 14 times smaller than the solar potential but can serve as a perfect complement in areas where photovoltaic panels are not feasible. Additionally, significant potential was observed for offshore energy harvesting, presenting an opportunity for hydrogen production at sea and leveraging existing gas and oil infrastructure, primarily along the Gulf of Mexico coast.

3. In the microgrid scenario, Mexico stands out among the United States and Canada for having the greatest potential to integrate hydrogen at the microgrid level. The country's lower energy consumption and abundant energy resources represent a significant opportunity for small-scale hydrogen generation.

4. Mexico must pave the way for the development of public policies aimed at decarboniza-

tion, particularly in market regulation for technology acquisition. Currently, hydrogen generation costs in Mexico exceed 15 USD/kg due to high import costs. Failure to address this issue would hinder Mexico's international competitiveness.

5. The hydrogen roadmap in Mexico must consider technology costs and promote the production and consumption of low-carbon hydrogen. One of the major challenges is increasing hydrogen usage in Mexico, where national hydrogen consumption currently does not exceed 0.25 million tons per year. This demand must increase and be met with green hydrogen to facilitate participation in the decarbonization process.

# Bibliography

[1] O. S. Ibrahim, A. Singlitico, R. Proskovics, S. McDonagh, C. Desmond, and J. D. Murphy, "Dedicated large-scale floating offshore wind to hydrogen: Assessing design variables in proposed typologies," *Renewable and Sustainable Energy Reviews*, vol. 160, p. 112310, 2022. [Online]. Available: https://www.sciencedirect.com/science/article/pii/S1364032122002258

[2] A. Singlitico, J. Østergaard, and S. Chatzivasileiadis, "Onshore, offshore or in-turbine electrolysis? techno-economic overview of alternative integration designs for green hydrogen production into offshore wind power hubs," *Renewable and Sustainable Energy Transition*, vol. 1, p. 100005, 2021. [Online]. Available: https://www.sciencedirect.com/science/article/pii/S2667095X21000052

[3] A. Martinez and G. Iglesias, "Multi-parameter analysis and mapping of the levelised cost of energy from floating offshore wind in the mediterranean sea," *Energy Conversion and Management*, vol. 243, p. 114416, 2021.

[4] A. Myhr, C. Bjerkseter, A. Ågotnes, and T. A. Nygaard, "Levelised cost of energy for offshore floating wind turbines in a life cycle perspective," *Renewable Energy*, vol. 66, pp. 714–728, 2014. [Online]. Available: https://www.sciencedirect.com/science/article/pii/S0960148114000469

[5] IRENA, "World energy transitions outlook 2023," International Renewable Energy Agency, Tech. Rep., 2023. [Online]. Available: https://www.climate-transparency.org/g20-climate-performance/g20report2022

[6] DOE, "Department of energy hydrogen program plan," US

Energy department, Tech. Rep., 2020. [Online]. Available: https://www.hydrogen.energy.gov/docs/hydrogenprogramlibraries/pdfs/hydrogen-program-plan-2020.pdf

[7] IRENA, "Green hydrogen cost 2020," Tech. Rep., 2020. [Online]. Available: https://www.irena.org/publications/2020/Dec/Green-hydrogen-cost-reduction

[8] F. Onea, E. Rusu, and L. Rusu, "Assessment of the offshore wind energy potential in the romanian exclusive economic zone," *Journal of Marine Science and Engineering*, vol. 9, no. 5, 2021. [Online]. Available: https://www.mdpi.com/2077-1312/9/5/531

[9] J. Bosch, I. Staffell, and A. D. Hawkes, "Global levelised cost of electricity from offshore wind," *Energy*, vol. 189, p. 116357, 2019. [Online]. Available: https://www.sciencedirect.com/science/article/pii/S0360544219320523

[10] CONAHCYT, "Sistema eléctrico nacional," 2023, accessed = 2024-01-29. [Online]. Available: https://energia.conacyt.mx/planeas/electricidad/sistema-electrico-nacional

[11] IRENA, "Accelerating hydrogen deployment in the g7: Recommendations for the hydrogen action pact," 2022. [Online]. Available: https://www.irena.org/Publications/2022/Nov/Accelerating-hydrogen-deployment-in-the-G7

[12] ——, "Global hydrogen trade to meet the 1.5°c climate goal," International Renewable Energy Agency, Tech. Rep., 2022. [Online]. Available: https://www.climate-transparency.org/g20-climate-performance/g20report2022

[13] C. Transparency, "Climate transparency report 2022," Climate Transparency, Tech. Rep., 2022. [Online]. Available: https://www.climate-transparency.org/g20-climate-performance/g20report2022

[14] IRENA, "Geopolitics of the energy transition," International Renewable Energy Agency, Tech. Rep., 2024. [Online]. Available: https://www.gob.mx/sener/articulos/lineamientos-en-materia-de-hidrogeno

[15] IEA, "The future of hydrogen," International Energy Agency, Tech. Rep., 2019. [Online]. Available: https://www.iea.org/reports/the-future-of-hydrogen

[16] G. o. C. Ministery of energy, "National green hydrogen strategy chile, a clean energy provider for a carbon neutral planet," Ministery of energy, Tech. Rep., 2020. [Online]. Available: https://www.energypartnership.cl/newsroom/chile-hydrogen/

[17] O. o. F. E. DOE, "Hydrogen strategy: Enabling a low-carbon economy," US Department of Energy, Tech. Rep., 2020. [Online]. Available: https://www.energy.gov/fecm/downloads/hydrogen-strategy-enabling-low-carbon-economy

[18] E. Department of Industry, Science and A. G. Resources, "Australia's national hydrogen strategy," Tech. Rep., 2020. [Online]. Available: https://www.industry.gov.au/data-and-publications/australias-national-hydrogen-strategy

[19] G. Kakoulaki, I. Kougias, N. Taylor, F. Dolci, J. Moya, and A. Jäger-Waldau, "Green hydrogen in europe – a regional assessment: Substituting existing production with electrolysis powered by renewables," *Energy Conversion and Management*, vol. 228, p. 113649, 2021. [Online]. Available: https://www.sciencedirect.com/science/article/pii/S0196890420311766

[20] A. Sigal, E. Leiva, and C. Rodríguez, "Assessment of the potential for hydrogen production from renewable resources in argentina," *International Journal of Hydrogen Energy*, vol. 39, no. 16, pp. 8204–8214, 2014. [Online]. Available: https://www.sciencedirect.com/science/article/pii/S0360319914008490

[21] A. Gouareh, N. Settou, A. Khalfi, B. Recioui, B. Negrou, S. Rahmouni, and B. Dokkar, "Gis-based analysis of hydrogen production from geothermal electricity using co2 as working fluid in algeria," *International Journal of Hydrogen Energy*, vol. 40, no. 44, pp. 15 244–15 253, 2015, the 4th International Conference on Nuclear and Renewable Energy Resources (NURER2014), 26-29 October 2014, Antalya, Turkey. [Online]. Available: https://www.sciencedirect.com/science/article/pii/S0360319915012914

[22] F. Posso, J. Sánchez, J. Espinoza, and J. Siguencia, "Preliminary estimation of electrolytic hydrogen production potential from renewable energies in ecuador," *International Journal of Hydrogen Energy*, vol. 41, no. 4, pp. 2326–2344, 2016. [Online]. Available: https://www.sciencedirect.com/science/article/pii/S0360319915310624

[23] S. Rahmouni, B. Negrou, N. Settou, J. Dominguez, and A. Gouareh, "Prospects of hydrogen production potential from renewable resources in algeria," *International Journal of Hydrogen Energy*, vol. 42, no. 2, pp. 1383–1395, 2017. [Online]. Available: https://www.sciencedirect.com/science/article/pii/S0360319916307005

[24] A. Mraoui and S. Menia, "Renewable electrolytic hydrogen potential in algeria," *International Journal of Hydrogen Energy*, vol. 44, no. 49, pp. 26 863–26 873, 2019. [Online]. Available: https://www.sciencedirect.com/science/article/pii/S0360319919331489

[25] S. Kudria, I. Ivanchenko, B. Tuchynskyi, K. Petrenko, O. Karmazin, and O. Riepkin, "Resource potential for wind-hydrogen power in ukraine," *International Journal of Hydrogen Energy*, vol. 46, no. 1, pp. 157–168, 2021. [Online]. Available: https://www.sciencedirect.com/science/article/pii/S0360319920336818

[26] B. S. Thapa, B. Neupane, H. seong Yang, and Y.-H. Lee, "Green hydrogen potentials from surplus hydro energy in nepal," *International Journal of Hydrogen Energy*, vol. 46, no. 43, pp. 22 256–22 267, 2021. [Online]. Available: https://www.sciencedirect.com/science/article/pii/S0360319921014452

[27] G. Longoria, M. Lynch, and J. Curtis, "Green hydrogen for heating and its impact on the power system," *International Journal of Hydrogen Energy*, vol. 46, no. 53, pp. 26 725–26 740, 2021. [Online]. Available: https://www.sciencedirect.com/science/article/pii/S0360319921020231

[28] S. Uysal, M. F. Kaya, N. Demir, B. Hüner, R. U. Özcan, Ömer Nadir Erdem, and M. Yılmaz, "Investigation of hydrogen production potential from different natural water sources in turkey," *International Journal of Hydrogen Energy*, vol. 46, no. 61, pp. 31 097–31 107, 2021. [Online]. Available: https://www.sciencedirect.com/science/article/pii/S0360319921025970

[29] S. Rahmouni, N. Settou, B. Negrou, and A. Gouareh, "Gis-based method for future prospect of hydrogen demand in the algerian road transport sector," *International Journal of Hydrogen Energy*, vol. 41, no. 4, pp. 2128–2143, 2016. [Online]. Available: https://www.sciencedirect.com/science/article/pii/S0360319915309642

[30] D. Pyza, P. Gołda, and E. Sendek-Matysiak, "Use of hydrogen in public transport systems," *Journal of Cleaner Production*, vol. 335, p. 130247, 2022. [Online]. Available: https://www.sciencedirect.com/science/article/pii/S0959652621044127

[31] M. Genovese, D. Blekhman, M. Dray, and P. Fragiacomo, "Hydrogen station in situ back-to-back fueling data for design and modeling," *Journal of Cleaner Production*, vol. 329, p. 129737, 2021. [Online]. Available: https://www.sciencedirect.com/science/article/pii/S0959652621039135

[32] L. Zhou, F. Zhang, L. Wang, and Q. Zhang, "Flexible hydrogen production source for fuel cell vehicle to reduce emission pollution and costs under the multi-objective optimization framework," *Journal of Cleaner Production*, vol. 337, p. 130284, 2022. [Online]. Available: https://www.sciencedirect.com/science/article/pii/S0959652621044498

[33] M. Patel, S. Roy, A. P. Roskilly, and A. Smallbone, "The techno-economics potential of hydrogen interconnectors for electrical energy transmission and storage," *Journal of Cleaner Production*, vol. 335, p. 130045, 2022. [Online]. Available: https://www.sciencedirect.com/science/article/pii/S0959652621042116

[34] D. Mentis, S. Hermann, M. Howells, M. Welsch, and S. H. Siyal, "Assessing the technical wind energy potential in africa a gis-based approach," *Renewable Energy*, vol. 83, pp. 110–125, 2015. [Online]. Available: https://www.sciencedirect.com/science/article/pii/S0960148115002633

[35] D. Doljak, G. Stanojević, and D. Miljanović, "A gis-mcda based assessment for siting wind farms and estimation of the technical generation potential for wind power in serbia," *International Journal of Green Energy*, vol. 18, no. 4, pp. 363–380, 2021.

[36] F. González-Longatt, H. Medina, and J. Serrano González, "Spatial interpolation and orographic correction to estimate wind energy resource in venezuela," *Renewable and Sustainable Energy Reviews*, vol. 48, pp. 1–16, 2015. [Online]. Available: https://www.sciencedirect.com/science/article/pii/S1364032115001951

[37] Z. N. Ashrafi, M. Ghasemian, M. I. Shahrestani, E. Khodabandeh, and A. Sedaghat, "Evaluation of hydrogen production from harvesting wind energy at high altitudes in iran by three extrapolating weibull methods," *International Journal of Hydrogen Energy*, vol. 43, no. 6, pp. 3110–3132, 2018. [Online]. Available: https://www.sciencedirect.com/science/article/pii/S0360319917348759

[38] C. Morales-Ruvalcaba, O. Rodríguez-Hernández, O. Martínez-Alvarado, D. Drew, and E. Ramos, "Estimating wind speed and capacity factors in mexico using reanalysis data," *Energy for Sustainable Development*, vol. 58, pp. 158–166, 2020. [Online]. Available: https://www.sciencedirect.com/science/article/pii/S0973082620302878

[39] R. P. Gallardo, A. M. Ríos, and J. S. Ramírez, "Analysis of the solar and wind energetic complementarity in mexico," *Journal of Cleaner Production*, vol. 268, p. 122323, 2020. [Online]. Available: https://www.sciencedirect.com/science/article/pii/S0959652620323702

[40] IRENA, "Green hydrogen: A guide to policy making," Tech. Rep., 2020. [Online]. Available: https://www.irena.org/publications/2020/Dec/Green-hydrogen-cost-reduction

[41] E. Secretary of State for Business and I. Strategy, "Uk hydrogen strategy," 2021.

[42] O. o. F. E. DOE, "Road map to a us hydrogen economy," US Department of Energy, Tech. Rep., 2020. [Online]. Available: https://www.energy.gov/fecm/downloads/hydrogen-strategy-enabling-low-carbon-economy

[43] B. S. T. M. and H. J. S. E. M. C. P. D. H. P, "National hydrogen roadmap," 2018.

[44] F. Cells and H. . J. Undertaking, "Hydrogen roadmap europe," 2019.

[45] M. of Energy, "Uhoja de ruta del hidrógeno en colombia," 2018.

[46] R. de Guadalupe González Huerta and J. A. G. Rodríguez, "Política pública en méxico para la implementación del hidrógeno verde como vector energético," *Eficiencia Energética*, no. 32, pp. 31–40, 2021. [Online]. Available: https://www.fide.org.mx/wp-content/uploads/Revistas/eficiencia$_e$nergetica$_3$2.pdf

[47] M. L. Ávalos Rodríguez, J. J. Alvarado Flores, J. V. Alcaraz Vera, J. G. Rutiaga Quiñones, and J. E. Valencia, "The legal regulation of the h2 as a strategy for public policy in mexico from the consolidation of the national council of the hydrogen," *International Journal of Hydrogen Energy*, vol. 44, no. 24, pp. 12 303–12 308, 2019, xVII Mexican Hydrogen Society Congress Special Issue. [Online]. Available: https://www.sciencedirect.com/science/article/pii/S0360319918331434

[48] E. U. Peña Sánchez, S. D. Ryberg, H. U. Heinrichs, D. Stolten, and M. Robinius, "The potential of variable renewable energy sources in mexico: A temporally evaluated and geospatially constrained techno-economical assessment," *Energies*, vol. 14, no. 18, 2021. [Online]. Available: https://www.mdpi.com/1996-1073/14/18/577

[49] HINICIO, "Hidrógeno verde en méxico, el potencial de transformación. tomo 2: Integración de resultados y recomendaciones generales," Tech. Rep., 2021. [Online]. Available: https://www.energypartnership.mx/media-elements/

[50] ——, "Hidrógeno verde en méxico: el potencial de transformación. tomo vi: Análisis de la cadena de valor local y del potencial de exportación de hidrógeno verde," Tech. Rep., 2021. [Online]. Available: https://www.energypartnership.mx/media-elements/

[51] P. Pitchford, J. Jones, B. Glenn, G. Cook, L. Billman, and R. Adcock, *Photovoltaic fundamentals*, 9 1991. [Online]. Available: https://www.osti.gov/biblio/5137459

[52] B. Parida, S. Iniyan, and R. Goic, "A review of solar photovoltaic technologies," *Renewable and Sustainable Energy Reviews*, vol. 15, no. 3, pp. 1625–1636, 2011. [Online]. Available: https://www.sciencedirect.com/science/article/pii/S1364032110004016

[53] NREL. https://www.nrel.gov/research/re-photovoltaics.html.

[54] Office of Energy efficiency and Renewable energy. https://www.energy.gov/eere/solar/solar-photovoltaic-cell-basics.

[55] NREL, "Life cycle greenhouse gas emissions from solar photovoltaics," 2012. [Online]. Available: https://www.nrel.gov/docs/fy13osti/56487.pdf

[56] Office of Energy efficiency and Renewable energy. How do wind turbines work? [Online]. Available: https://www.energy.gov/eere/solar/solar-photovoltaic-cell-basics

[57] NREL. Wind research. [Online]. Available: https://www.nrel.gov/wind/

[58] A. Duffy, M. Hand, R. Wiser, E. Lantz, A. Dalla Riva, V. Berkhout, M. Stenkvist, D. Weir, and R. Lacal-Arántegui, "Land-based wind energy cost trends in germany, denmark, ireland, norway, sweden and the united states," *Applied Energy*, vol. 277, p. 114777, 2020. [Online]. Available: https://www.sciencedirect.com/science/article/pii/S0306261920302890

[59] "5 - wind power technology," in *Sustainable Fuel Technologies Handbook*, S. Dutta and C. Mustansar Hussain, Eds.  Academic Press, 2021, pp. 123–170. [Online]. Available: https://www.sciencedirect.com/science/article/pii/B9780128229897000068

[60] U. A., L. J., G. E., M. L., and S. P., "Photovoltaic hydrogen production with commercial alkaline electrolysers," Jul 2010.

[61] A. Yunez-Cano, R. de G. González-Huerta, M. Tufiño-Velázquez, R. Barbosa, and B. Escobar, "Solar-hydrogen hybrid system integrated to a sustainable house in mexico," *International Journal of Hydrogen Energy*, vol. 41, no. 43, pp. 19 539–19 545, 2016, the 5th Iberian Symposium on Hydrogen, Fuel Cells and Advanced Batteries (HYCELTEC 2015), 5-8 July 2015, Tenerife, Spain. [Online]. Available: https://www.sciencedirect.com/science/article/pii/S036031991630307X

[62] "Chapter 13 - hydrogen storage," in *Electrochemical Power Sources: Fundamentals, Systems, and Applications*, T. Smolinka and J. Garche, Eds.  Elsevier, 2022, pp. 455–486. [Online]. Available: https://www.sciencedirect.com/science/article/pii/B9780128194249000069

[63] Office of Energy efficiency and Renewable energy. Hydrogen production. [Online]. Available: https://www.energy.gov/eere/fuelcells/hydrogen-production

[64] "Sizing of a stand-alone microgrid considering electric power, cooling/heating, hydrogen loads and hydrogen storage degradation," *Applied Energy*, vol. 205, pp. 1244–1259, 2017. [Online]. Available: https://www.sciencedirect.com/science/article/pii/S0306261917311595

[65] in *Gis and Cartographic modeling.* Esri, 1990, p. 420. [Online]. Available: https://www.esri.com/en-us/esri-press/browse/gis-and-cartographic-modeling

[66] OQGIS. Datos vectoriales. [Online]. Available: https://docs.qgis.org

[67] ——. Datos raster. [Online]. Available: https://docs.qgis.org

[68] ——. Qgis - el sig líder de código abierto para escritorio. [Online]. Available: https://www.qgis.org/es/site/about/index.htmll

[69] ——. Arcgis online. [Online]. Available: https://www.esri.com/en-us/arcgis/products/arcgis-online/overview

[70] S. Touili, A. Alami Merrouni, Y. El Hassouani, A. illah Amrani, and S. Rachidi, "Analysis of the yield and production cost of large-scale electrolytic hydrogen from different solar technologies and under several moroccan climate zones," *International Journal of Hydrogen Energy*, vol. 45, no. 51, pp. 26 785–26 799, 2020. [Online]. Available: https://www.sciencedirect.com/science/article/pii/S0360319920326938

[71] F. I. Gallardo, A. Monforti Ferrario, M. Lamagna, E. Bocci, D. Astiaso Garcia, and T. E. Baeza-Jeria, "A techno-economic analysis of solar hydrogen production by electrolysis in the north of chile and the case of exportation from atacama desert to japan," *International Journal of Hydrogen Energy*, vol. 46, no. 26, pp. 13 709–13 728, 2021, european Fuel Cell Conference and Exhibition 2019. [Online]. Available: https://www.sciencedirect.com/science/article/pii/S0360319920325842

[72] World Meteorological Organization, *Guide to Meteorological Instruments and Methods of Observation (2014 edition updated in 2017)*. Geneva: WMO, 2017.

[73] C. A. Cervantes-Ortiz, I. Cervantes, and R. E. Cervantes-Camacho, "The effect of parameters and irradiance estimation techniques on pv potential quantification: The case of mexico," *Sustainable Energy Technologies and Assessments*, vol. 45, p. 101131, 2021. [Online]. Available: https://www.sciencedirect.com/science/article/pii/S2213138821001417

[74] D. Messaoudi, N. Settou, B. Negrou, and B. Settou, "Gis based multi-criteria decision making for solar hydrogen production sites selection in algeria," *International Journal of Hydrogen Energy*, vol. 44, no. 60, pp. 31 808–31 831, 2019. [Online]. Available: https://www.sciencedirect.com/science/article/pii/S036031991933887X

[75] M. Minutillo, A. Perna, A. Forcina, S. Di Micco, and E. Jannelli, "Analyzing the levelized cost of hydrogen in refueling stations with on-site hydrogen production via water electrolysis in the italian scenario," *International Journal of Hydrogen Energy*, vol. 46, no. 26, pp. 13 667–13 677, 2021, european Fuel Cell Conference and Exhibition 2019. [Online]. Available: https://www.sciencedirect.com/science/article/pii/S0360319920343160

[76] S. Touili, A. Alami Merrouni, A. Azouzoute, Y. El Hassouani, and A. illah Amrani, "A technical and economical assessment of hydrogen production potential from solar energy in morocco," *International Journal of Hydrogen Energy*, vol. 43, no. 51, pp. 22 777–22 796, 2018. [Online]. Available: https://www.sciencedirect.com/science/article/pii/S0360319918333639

[77] O. Schmidt, A. Gambhir, I. Staffell, A. Hawkes, J. Nelson, and S. Few, "Future cost and performance of water electrolysis: An expert elicitation study," *International Journal of Hydrogen Energy*, vol. 42, no. 52, pp. 30 470–30 492, 2017. [Online]. Available: https://www.sciencedirect.com/science/article/pii/S0360319917339435

[78] A. Mostafaeipour, H. Rezayat, and M. Rezaei, "A thorough investigation of solar-powered hydrogen potential and accurate location planning for big cities: A case study," *International Journal of Hydrogen Energy*, vol. 45, no. 56, pp. 31 599–31 611, 2020. [Online]. Available: https://www.sciencedirect.com/science/article/pii/S0360319920332389

[79] V. Franzitta, D. Curto, D. Rao, and A. Viola, "Hydrogen production from sea wave for alternative energy vehicles for public transport in trapani (italy)," *Energies*, vol. 9, no. 10, 2016. [Online]. Available: https://www.mdpi.com/1996-1073/9/10/850

[80] D. Groppi, L. de Santoli, F. Cumo, and D. Astiaso Garcia, "A gis-based model to assess buildings energy consumption and usable solar energy potential in urban areas," *Sustainable Cities and Society*, vol. 40, pp. 546–558, 2018. [Online]. Available: https://www.sciencedirect.com/science/article/pii/S2210670718301902

[81] B. Kılkıs and S. Kılkıs, "Hydrogen economy model for nearly net-zero cities with exergy rationale and energy-water nexus," *Energies*, vol. 11, no. 5, 2018. [Online]. Available: https://www.mdpi.com/1996-1073/11/5/1226

[82] INEGI, "Uso de suelo y vegetacion," Tech. Rep., 2018. [Online]. Available: https://www.inegi.org.mx/temas/usosuelo/

[83] ——, "Producto interno bruto por entidad federativa 2021," Tech. Rep., 2021.

[84] PEMEX, "Prospectiva de petróleo crudo y petrolíferos 2018-2032," Tech. Rep., 2018. [Online]. Available: https://www.gob.mx/sener/documentos/prospectivas-del-sector-energetico

[85] CONUEE, "Lista de combustibles y sus poderes calorÍficos 2021," Tech. Rep., 2021. [Online]. Available: www.gob.mx/attachment/file/Lista Combustibles 2021 26 feb 2021

[86] HINICIO, "Hidrógeno verde en méxico, el potencial de transformación. tomo 1: Contexto nacional e internacional del hidrógeno verde," Tech. Rep., october 2021. [Online]. Available: https://www.energypartnership.mx/media-elements/

[87] INEGI, "Cuentame de mexico, poblacion," Tech. Rep., 2021. [Online]. Available: http://cuentame.inegi.org.mx

[88] INECC, "Inventario nacional de emisiones de gases y compuestos de efecto invernadero 1990-2015," Tech. Rep., 2018. [Online]. Available: https://www.gob.mx/inecc/

[89] ANIQ, "Anuario estadÍstico de la industria quÍmcia," Tech. Rep., 2020. [Online]. Available: https://aniq.org.mx/webpublico/notas/anuarioestadisticoiq.asp

[90] Sofia G. Simoes and Justina Catarino and Ana Picado and Tiago F. Lopes and Santino di Berardino and Filipa Amorim and Francisco Gírio and C.M. Rangel and Teresa Ponce de Leão, "Water availability and water usage solutions for electrolysis in hydrogen

production," *Journal of Cleaner Production*, vol. 315, p. 128124, 2021. [Online]. Available: https://www.sciencedirect.com/science/article/pii/S0959652621023428

[91] Beswick, Rebecca R. and Oliveira, Alexandra M. and Yan, Yushan, "Does the green hydrogen economy have a water problem?" *ACS Energy Letters*, vol. 6, no. 9, pp. 3167–3169, 2021.

[92] Khan, M. A. and Al-Attas, Tareq and Roy, Soumyabrata and Rahman, Muhammad M. and Ghaffour, Noreddine and Thangadurai, Venkataraman and Larter, Stephen and Hu, Jinguang and Ajayan, Pulickel M. and Kibria, Md Gola, "Seawater electrolysis for hydrogen production: a solution looking for a problem?" *Energy Environ. Sci.*, vol. 14, pp. 4831–4839, 2021. [Online]. Available: http://dx.doi.org/10.1039/D1EE00870F

[93] Hodges, Aaron and Hoang, Anh Linh and Tsekouras, George and Wagner, Klaudia and Lee, Chong-Yong and Swiegers, Gerhard F. and Wallace, Gordon G, "A high-performance capillary-fed electrolysis cell promises more cost-competitive renewable hydrogen," *Nature Communications*, vol. 13, p. 128124, 2022.

[94] M. Carrasco-Díaz, D. Rivas, M. Orozco-Contreras, and O. Sánchez-Montante, "An assessment of wind power potential along the coast of tamaulipas, northeastern mexico," *Renewable Energy*, vol. 78, pp. 295–305, 2015. [Online]. Available: https://www.sciencedirect.com/science/article/pii/S0960148115000142

[95] Q. Hernández-Escobedo, F. Manzano-Agugliaro, and A. Zapata-Sierra, "The wind power of mexico," *Renewable and Sustainable Energy Reviews*, vol. 14, no. 9, pp. 2830–2840, 2010. [Online]. Available: https://www.sciencedirect.com/science/article/pii/S1364032110001991

[96] Q. Hernandez-Escobedo, F. Manzano-Agugliaro, J. A. Gazquez-Parra, and A. Zapata-Sierra, "Is the wind a periodical phenomenon? the case of mexico," *Renewable and Sustainable Energy Reviews*, vol. 15, no. 1, pp. 721–728, 2011. [Online]. Available: https://www.sciencedirect.com/science/article/pii/S1364032110003102

[97] Q. Hernández-Escobedo, R. Saldaña-Flores, E. Rodríguez-García, and F. Manzano-Agugliaro, "Wind energy resource in northern mexico," *Renewable and Sus-*

*tainable Energy Reviews*, vol. 32, pp. 890–914, 2014. [Online]. Available: https://www.sciencedirect.com/science/article/pii/S1364032114000549

[98] J. Olauson, "Era5: The new champion of wind power modelling?" *Renewable Energy*, vol. 126, pp. 322–331, 2018. [Online]. Available: https://www.sciencedirect.com/science/article/pii/S0960148118303677

[99] G. Gualtieri, "Reliability of era5 reanalysis data for wind resource assessment: A comparison against tall towers," *Energies*, vol. 14, no. 14, 2021. [Online]. Available: https://www.mdpi.com/1996-1073/14/14/4169

[100] N. N. Davis, J. Badger, A. N. Hahmann, B. O. Hansen, N. G. Mortensen, M. Kelly, X. G. Larsén, B. T. Olsen, R. Floors, G. Lizcano, P. Casso, O. Lacave, A. Bosch, I. Bauwens, O. J. Knight, A. P. van Loon, R. Fox, T. Parvanyan, S. B. K. Hansen, D. Heathfield, M. Onninen, and R. Drummond, "The global wind atlas: A high-resolution dataset of climatologies and associated web-based application," *Bulletin of the American Meteorological Society*, vol. 104, no. 8, pp. E1507 – E1525, 2023. [Online]. Available: https://journals.ametsoc.org/view/journals/bams/104/8/BAMS-D-21-0075.1.xml

[101] A. Hahmann, A. Peña Diaz, and J. C. Hansen, "Wrf mesoscale pre-run for the wind atlas of mexico," Tech. Rep., 2016. [Online]. Available: https://backend.orbit.dtu.dk/ws/portalfiles/portal

[102] H. Villanuavea, A. Peña, and C. Jens, "Wind atlas for mexico (wam) observational wind atlas," Tech. Rep., 2021. [Online]. Available: https://orbit.dtu.dk/en/publications/wind-atlas-for-mexico-wam-observational-wind-atlas

[103] V. Magar, A. Peña, A. N. Hahmann, D. A. Pacheco-Rojas, L. S. García-Hernández, and M. S. Gross, "Wind energy and the energy transition: Challenges and opportunities for mexico," *Sustainability*, vol. 15, no. 6, 2023. [Online]. Available: https://www.mdpi.com/2071-1050/15/6/5496

[104] SENER, "Atlas nacional de zonas con alto potential de energías limpias," Tech. Rep., 2023.

[Online]. Available: https://www.gob.mx/sener/articulos/atlas-nacional-de-zonas-con-alto-potencial-de-energias-limpias

[105] X. Chen, X. Ye, X. Xiong, Y. Zhang, and Y. Li, "Improving the accuracy of wind speed spatial interpolation: A pre-processing algorithm for wind speed dynamic time warping interpolation," *Energy*, vol. 295, p. 130876, 2024. [Online]. Available: https://www.sciencedirect.com/science/article/pii/S0360544224006480

[106] S. Van Ackere, G. Van Eetvelde, D. Schillebeeckx, E. Papa, K. Van Wyngene, and L. Vandevelde, "Wind resource mapping using landscape roughness and spatial interpolation methods," *Energies*, vol. 8, no. 8, pp. 8682–8703, 2015. [Online]. Available: https://www.mdpi.com/1996-1073/8/8/8682

[107] M. Keskin, A. O. Dogru, F. B. Balcik, C. Goksel, N. Ulugtekin, and S. Sozen, "Comparing spatial interpolation methods for mapping meteorological data in turkey," in *Energy Systems and Management*, A. N. Bilge, A. Ö. Toy, and M. E. Günay, Eds. Cham: Springer International Publishing, 2015, pp. 33–42.

[108] D. Duplyakin, S. Zisman, C. Phillips, and H. Tinnesand, "Bias characterization, vertical interpolation, and horizontal interpolation for distributed wind siting using mesoscale wind resource estimates," NREL, Tech. Rep., 2021.

[109] H. Saleh, A. Abou El-Azm Aly, and S. Abdel-Hady, "Assessment of different methods used to estimate weibull distribution parameters for wind speed in zafarana wind farm, suez gulf, egypt," *Energy*, vol. 44, no. 1, pp. 710–719, 2012, integration and Energy System Engineering, European Symposium on Computer-Aided Process Engineering 2011. [Online]. Available: https://www.sciencedirect.com/science/article/pii/S036054421200401X

[110] S. A. Akdağ and A. Dinler, "A new method to estimate weibull parameters for wind energy applications," *Energy Conversion and Management*, vol. 50, no. 7, pp. 1761–1766, 2009. [Online]. Available: https://www.sciencedirect.com/science/article/pii/S0196890409000934

[111] J. A. Guarienti, A. Kaufmann Almeida, A. Menegati Neto, A. R. de Oliveira Ferreira, J. P. Ottonelli, and I. Kaufmann de Almeida, "Performance analysis of numerical methods

for determining weibull distribution parameters applied to wind speed in mato grosso do sul, brazil," *Sustainable Energy Technologies and Assessments*, vol. 42, p. 100854, 2020. [Online]. Available: https://www.sciencedirect.com/science/article/pii/S2213138820312819

[112] S. Kang, A. Khanjari, S. You, and J.-H. Lee, "Comparison of different statistical methods used to estimate weibull parameters for wind speed contribution in nearby an offshore site, republic of korea," *Energy Reports*, vol. 7, pp. 7358–7373, 2021. [Online]. Available: https://www.sciencedirect.com/science/article/pii/S2352484721010969

[113] D. Kang, K. Ko, and J. Huh, "Comparative study of different methods for estimating weibull parameters: A case study on jeju island, south korea," *Energies*, vol. 11, no. 2, 2018. [Online]. Available: https://www.mdpi.com/1996-1073/11/2/356

[114] L. F. de Assis Tavares, M. Shadman, L. P. de Freitas Assad, C. Silva, L. Landau, and S. F. Estefen, "Assessment of the offshore wind technical potential for the brazilian southeast and south regions," *Energy*, vol. 196, p. 117097, 2020. [Online]. Available: https://www.sciencedirect.com/science/article/pii/S0360544220302048

[115] O. Nematollahi, P. Alamdari, M. Jahangiri, A. Sedaghat, and A. A. Alemrajabi, "A techno-economical assessment of solar/wind resources and hydrogen production: A case study with gis maps," *Energy*, vol. 175, pp. 914–930, 2019. [Online]. Available: https://www.sciencedirect.com/science/article/pii/S0360544219305419

[116] A. Ulazia, J. Sáenz, G. Ibarra-Berastegi, S. J. González-Rojí, and S. Carreno-Madinabeitia, "Global estimations of wind energy potential considering seasonal air density changes," *Energy*, vol. 187, p. 115938, 2019. [Online]. Available: https://www.sciencedirect.com/science/article/pii/S0360544219316226

[117] SENER, "Programa para el desarrollo del sistema eléctrico nacional 2021 a 2035," Seceretaría de energía, Tech. Rep., 2022. [Online]. Available: https://www.gob.mx/cenace/documentos/programa-para-el-desarrollo-del-sistema-electrico-nacional-276178

[118] V. Juárez-Casildo, I. Cervantes, C. A. Cervantes-Ortiz, and R. de G. González-Huerta, "Key aspects in quantifying massive solar hydrogen production: Energy intermittence, water availability and electrolyzer technology," *Journal of Cleaner Production*, vol. 371, p. 133550, 2022. [Online]. Available: https://www.sciencedirect.com/science/article/pii/S0959652622031298

[119] H. Hersbach, B. Bell, P. Berrisford, G. Biavati, A. Horányi, J. M. Sabater, J. Nicolas, C. Peubey, R. Radu, I. Rozum, D. Schepers, A. Simmons, C. Soci, D. Dee, and J.-N. Thépaut, "Era5 hourly data on single levels from 1940 to present," *Copernicus Climate Change Service (C3S) Climate Data Store (CDS)*, 2023.

[120] D. Canul-Reyes, O. Rodríguez-Hernández, and A. Jarquin-Laguna, "Potential zones for offshore wind power development in the gulf of mexico using reanalyses data and capacity factor seasonal analysis," *Energy for Sustainable Development*, vol. 68, pp. 211–219, 2022. [Online]. Available: https://www.sciencedirect.com/science/article/pii/S0973082622000424

[121] INEGI, "Geography and environment," 2023. [Online]. Available: https://en.www.inegi.org.mx/temas/relieve/submarino/

[122] A. Rogeau, J. Vieubled, M. de Coatpont, P. Affonso Nobrega, G. Erbs, and R. Girard, "Techno-economic evaluation and resource assessment of hydrogen production through offshore wind farms: A european perspective," *Renewable and Sustainable Energy Reviews*, vol. 187, p. 113699, 2023. [Online]. Available: https://www.sciencedirect.com/science/article/pii/S1364032123005567

[123] IEA, "Global hydrogen review 2023," International Energy Agency, Tech. Rep., 2023.

[124] P. Kotek, B. T. Tóth, and A. Selei, "Designing a future-proof gas and hydrogen infrastructure for europe – a modelling-based approach," *Energy Policy*, vol. 180, p. 113641, 2023. [Online]. Available: https://www.sciencedirect.com/science/article/pii/S0301421523002264

[125] Q. V. Dinh, V. N. Dinh, H. Mosadeghi, P. H. Todesco Pereira, and P. G. Leahy, "A geospatial method for estimating the levelised cost of hydrogen production from offshore wind," *International Journal of Hydrogen Energy*, vol. 48, no. 40, pp. 15 000–15 013, 2023. [Online]. Available: https://www.sciencedirect.com/science/article/pii/S0360319923000174

[126] T. R. Lucas, A. F. Ferreira, R. Santos Pereira, and M. Alves, "Hydrogen production from the windfloat atlantic offshore wind farm: A techno-economic analysis," *Applied Energy*, vol. 310, p. 118481, 2022. [Online]. Available: https://www.sciencedirect.com/science/article/pii/S0306261921017037

[127] M. Newborough and G. Cooley, "Green hydrogen: water use implications and opportunities," *Fuel Cells Bulletin*, vol. 2021, no. 12, pp. 12–15, 2021.

[128] S. Cavazzi and A. Dutton, "An offshore wind energy geographic information system (owe-gis) for assessment of the uk's offshore wind energy potential," *Renewable Energy*, vol. 87, pp. 212–228, 2016. [Online]. Available: https://www.sciencedirect.com/science/article/pii/S0960148115303001

[129] L. Castro-Santos, D. Silva, A. R. Bento, N. Salvação, and C. Guedes Soares, "Economic feasibility of floating offshore wind farms in portugal," *Ocean Engineering*, vol. 207, p. 107393, 2020. [Online]. Available: https://www.sciencedirect.com/science/article/pii/S0029801820304224

[130] A. Martinez and G. Iglesias, "Site selection of floating offshore wind through the levelised cost of energy: A case study in ireland," *Energy Conversion and Management*, vol. 266, p. 115802, 2022.

[131] ——, "Mapping of the levelised cost of energy for floating offshore wind in the european atlantic," *Renewable and Sustainable Energy Reviews*, vol. 154, p. 111889, 2022. [Online]. Available: https://www.sciencedirect.com/science/article/pii/S1364032121011564

[132] T. Stehly and P. Duffy, "2021 cost of wind energy review," NREL, Tech. Rep., 2022.

[133] T. Stehly, P. Duffy, and D. M. Hernando, "2022 cost of wind energy review," NREL, Tech. Rep., 2023.

[134] B. Associates, "Wind farm cost-guide to an offshore wind farm," 2021. [Online]. Available: https://guidetoanoffshorewindfarm.com/wind-farm-costs

[135] X. Wu, Y. Hu, Y. Li, J. Yang, L. Duan, T. Wang, T. Adcock, Z. Jiang, Z. Gao, Z. Lin, A. Borthwick, and S. Liao, "Foundations of offshore wind turbines: A review," *Renewable and Sustainable Energy Reviews*, vol. 104, pp. 379–393, 2019. [Online]. Available: https://www.sciencedirect.com/science/article/pii/S1364032119300127

[136] C. Bjerkseter and A. Ägotnes, "Levelised cost of energy for offshore floating wind turbine concepts," 2013.

[137] D. Hdidouan and I. Staffell, "The impact of climate change on the levelised cost of wind energy," *Renewable Energy*, vol. 101, pp. 575–592, 2017. [Online]. Available: https://www.sciencedirect.com/science/article/pii/S0960148116307856

[138] S. V. Arun Kumar, G. Nagababu, R. Sharma, and R. Kumar, "Synergetic use of multiple scatterometers for offshore wind energy potential assessment," *Ocean Engineering*, vol. 196, p. 106745, 2020. [Online]. Available: https://www.sciencedirect.com/science/article/pii/S0029801819308534

[139] M. Abdel-Basset, A. Gamal, R. K. Chakrabortty, and M. Ryan, "A new hybrid multi-criteria decision-making approach for location selection of sustainable offshore wind energy stations: A case study," *Journal of Cleaner Production*, vol. 280, p. 124462, 2021. [Online]. Available: https://www.sciencedirect.com/science/article/pii/S0959652620345066

[140] I. C. Gil-García, A. Ramos-Escudero, M. García-Cascales, H. Dagher, and A. Molina-García, "Fuzzy gis-based mcdm solution for the optimal offshore wind site selection: The gulf of maine case," *Renewable Energy*, vol. 183, pp. 130–147, 2022. [Online]. Available: https://www.sciencedirect.com/science/article/pii/S0960148121015172

[141] M. Taoufik and A. Fekri, "Gis-based multi-criteria analysis of offshore wind farm development in morocco," *Energy Conversion and Management: X*, vol. 11, p. 100103, 2021. [Online]. Available: https://www.sciencedirect.com/science/article/pii/S2590174521000283

[142] T. L. Saaty, "What is the analytic hierarchy process?" in *Mathematical Models for Decision Support*, G. Mitra, H. J. Greenberg, F. A. Lootsma, M. J. Rijkaert, and H. J. Zimmermann, Eds. Berlin, Heidelberg: Springer Berlin Heidelberg, 1988, pp. 109–121.

[143] S. Moradi, H. Yousefi, Y. Noorollahi, and D. Rosso, "Multi-criteria decision support system for wind farm site selection and sensitivity analysis: Case study of alborz province, iran," *Energy Strategy Reviews*, vol. 29, p. 100478, 2020. [Online]. Available: https://www.sciencedirect.com/science/article/pii/S2211467X20300328

[144] A. Vinhoza and R. Schaeffer, "Brazil's offshore wind energy potential assessment based on a spatial multi-criteria decision analysis," *Renewable and Sustainable Energy Reviews*, vol. 146, p. 111185, 2021. [Online]. Available: https://www.sciencedirect.com/science/article/pii/S1364032121004731

[145] "Gis-based multi-criteria decision analysis for site selection of hybrid offshore wind and wave energy systems in greece," *Renewable and Sustainable Energy Reviews*, vol. 73, pp. 745–757, 2017.

[146] G. Di Lullo, T. Giwa, A. Okunlola, M. Davis, T. Mehedi, A. Oni, and A. Kumar, "Large-scale long-distance land-based hydrogen transportation systems: A comparative techno-economic and greenhouse gas emission assessment," *International Journal of Hydrogen Energy*, vol. 47, no. 83, pp. 35 293–35 319, 2022. [Online]. Available: https://www.sciencedirect.com/science/article/pii/S036031992203659X

[147] T. L. Saaty and L. T. Tran, "On the invalidity of fuzzifying numerical judgments in the analytic hierarchy process," *Mathematical and Computer Modelling*, vol. 46, no. 7, pp. 962–975, 2007, decision Making with the Analytic Hierarchy Process and the Analytic Network Process. [Online]. Available: https://www.sciencedirect.com/science/article/pii/S0895717707000787

[148] R. Williams and F. Zhao, "Global offshore wind report 2023," Global Wind Energy Council, Tech. Rep., 2023.

[149] J. P. Arenas-López and M. Badaoui, "Analysis of the offshore wind resource and its economic assessment in two zones of mexico," *Sustainable Energy Technologies and Assessments*, vol. 52, p. 101997, 2022. [Online]. Available: https://www.sciencedirect.com/science/article/pii/S2213138822000492

[150] Comision Reguladora de Energia, "Tarifas de electricidad vigentes," 2023, accessed = 2024-01-26. [Online]. Available: https://www.gob.mx/cre/articulos/consulta-las-memorias-de-calculo-de-las-tarifas-electricas?state=published

[151] IRENA, "Green hydrogen: A guide to policy making," International Renewable Energy Agency, Tech. Rep., 2020.

[152] Iberdrola, "What is offshore wind energy," 2023, accessed = 2024-02-13. [Online]. Available: https://www.iberdrola.com/sustainability/how-does-offshore-wind-energy-work

[153] SENER, "Programa para el desarrollo del sistema eléctrico nacional 2021 a 2035," Seceretaría de energía, Tech. Rep., 2021. [Online]. Available: https://www.gob.mx/cenace/documentos/programa-para-el-desarrollo-del-sistema-electrico-nacional-276178

[154] D. G. Caglayan, D. S. Ryberg, H. Heinrichs, J. Linßen, D. Stolten, and M. Robinius, "The techno-economic potential of offshore wind energy with optimized future turbine designs in europe," *Applied Energy*, vol. 255, p. 113794, 2019. [Online]. Available: https://www.sciencedirect.com/science/article/pii/S0306261919314813

[155] S. T. Hallowell, A. T. Myers, S. R. Arwade, W. Pang, P. Rawal, E. M. Hines, J. F. Hajjar, C. Qiao, V. Valamanesh, K. Wei, W. Carswell, and C. M. Fontana, "Hurricane risk assessment of offshore wind turbines," *Renewable Energy*, vol. 125, pp. 234–249, 2018. [Online]. Available: https://www.sciencedirect.com/science/article/pii/S0960148118302349

[156] S. Rose, P. Jaramillo, M. J. Small, I. Grossmann, and J. Apt, "Quantifying the hurricane risk to offshore wind turbines," *Proceedings of the National Academy of Sciences*, vol. 109, no. 9, pp. 3247–3252, 2012. [Online]. Available: https://www.pnas.org/doi/abs/10.1073/pnas.1111769109

[157] K. L. Mattu, H. C. Bloomfield, S. Thomas, O. Martínez-Alvarado, and O. Rodríguez-Hernández, "The impact of tropical cyclones on potential offshore wind farms," *Energy for Sustainable Development*, vol. 68, pp. 29–39, 2022. [Online]. Available: https://www.sciencedirect.com/science/article/pii/S0973082622000278

[158] EERE, "Wind turbines in extreme weather: Solutions for hurricane resiliency," 2018, accessed = 2024-02-13. [Online]. Available: https://www.energy.gov/eere/articles/wind-turbines-extreme-weather-solutions-hurricaneresiliency

[159] M. Z. Jacobson, C. L. Archer, and W. Kempton, "Taming hurricanes with arrays of offshore wind turbines," *Nature Climate Change*, vol. 4, pp. 195–200, 2014.

[160] Y. He, S. Guo, P. Dong, Y. Zhang, J. Huang, and J. Zhou, "A state-of-the-art review and bibliometric analysis on the sizing optimization of off-grid hybrid renewable energy systems," *Renewable and Sustainable Energy Reviews*, vol. 183, p. 113476, 2023.

[161] M. A. Hossain, M. R. Islam, M. A. Hossain, and M. Hossain, "Control strategy review for hydrogen-renewable energy power system," *Journal of Energy Storage*, vol. 72, p. 108170, 2023.

[162] H. E. Beck, N. E. Zimmermann, T. R. McVicar, N. Vergopolan, A. Berg, and E. F. Wood, "Present and future köppen-geiger climate classification maps at 1-km resolution," vol. 5, 2018.

[163] NREL, "Resstock highly granular modeling of the u.s. housing stoc," 2023. [Online]. Available: https://resstock.nrel.gov/

[164] N. Saldanha and I. Beausoleil-Morrison, "Measured end-use electric load profiles for 12 canadian houses at high temporal resolution," *Energy and Buildings*, vol. 49, pp. 519–530, 2012. [Online]. Available: https://www.sciencedirect.com/science/article/pii/S0378778812001429

[165] M. Aydinalp Koksal, I. H. Rowlands, and P. Parker, "Energy, cost, and emission end-use profiles of homes: An ontario (canada) case study," *Applied Energy*, vol. 142, pp. 303–316, 2015. [Online]. Available: https://www.sciencedirect.com/science/article/pii/S0306261914013348

[166] NREL, "Annual technology baseline," 2023. [Online]. Available: https://atb.nrel.gov/electricity/2023/utility-scale$_b$attery$_s$torage

[167] EIA, "Annual technology baseline," 2023. [Online]. Available: https://www.eia.gov/tools/faqs/faq.php?id=427t=8

[168] IEA, "Hydrogen production and infrastructure projects database," International Energy Agency, Tech. Rep., 2023. [Online]. Available: https://www.iea.org/data-and-statistics/data-product/hydrogen-production-and-infrastructure-projects-database

[169] Horizon, "Horizon alkaline electrolizer price," 2024. [Online]. Available: https://www.horizonfuelcell.com/electrolyser

[170] IRENA, "Hydrogen overview," 2022. [Online]. Available: https://www.irena.org/Energy-Transition/Technology/Hydrogen

[171] ——, "Quality intraestructure for smart mini-grids," 2020. [Online]. Available: https://www.irena.org/publications/2020/Dec/Quality-infrastructure-for-smart-mini-grids

[172] M. B. Abdelghany, A. Al-Durra, and F. Gao, "A coordinated optimal operation of a grid-connected wind-solar microgrid incorporating hybrid energy storage management systems," *IEEE Transactions on Sustainable Energy*, vol. 15, no. 1, pp. 39–51, 2024.

[173] F. Garcia-Torres, C. Bordons, J. Tobajas, R. Real-Calvo, I. Santiago, and S. Grieu, "Stochastic optimization of microgrids with hybrid energy storage systems for grid flexibility services considering energy forecast uncertainties," *IEEE Transactions on Power Systems*, vol. 36, no. 6, pp. 5537–5547, 2021.

[174] L. Valverde, C. Bordons, and F. Rosa, "Integration of fuel cell technologies in renewable-energy-based microgrids optimizing operational costs and durability," *IEEE Transactions on Industrial Electronics*, vol. 63, no. 1, pp. 167–177, 2016.

[175] T. A. Fagundes, G. H. F. Fuzato, P. G. B. Ferreira, M. Biczkowski, and R. Q. Machado, "Fuzzy controller for energy management and soc equalization in dc microgrids powered by fuel cell and energy storage units," *IEEE Journal of Emerging and Selected Topics in Industrial Electronics*, vol. 3, no. 1, pp. 90–100, 2022.

[176] M. Jafari, Z. Malekjamshidi, J. Zhu, and M.-H. Khooban, "A novel predictive fuzzy logic-based energy management system for grid-connected and off-grid operation of residential smart microgrids," *IEEE Journal of Emerging and Selected Topics in Power Electronics*, vol. 8, no. 2, pp. 1391–1404, 2020.

[177] M. Ramesh and R. P. Saini, "Dispatch strategies based performance analysis of a hybrid renewable energy system for a remote rural area in india," *Journal of Cleaner Production*, vol. 259, p. 120697, 2020.

[178] F. H. Jufri, D. R. Aryani, I. Garniwa, and B. Sudiarto, "Optimal battery energy storage dispatch strategy for small-scale isolated hybrid renewable energy system with different load profile patterns," *Energies*, vol. 14, no. 11, 2021.

[179] "Techno-economic analysis of both on-grid and off-grid hybrid energy system with sensitivity analysis for an educational institution," *Energy Conversion and Management*, vol. 239, p. 114188, 2021.

[180] H. Pro, "Homer pro 3.16," 2023. [Online]. Available: https://support.ul-renewables.com/homer-manuals-pro/index.html

# Appendix A

# Techno-Economic Considerations for Optimal Sizing of Isolated Hydrogen-Battery-Solar Powered Microgrids

**Abstract**

Hydrogen and Battery Energy Storage Systems (BESS) are being widely integrated in microgrids with renewable energy storage systems. However, factors such as control strategies, capital costs, system efficiency and operation constraints have an impact on the planning of microgirds and system sizing. The effect of controller strategies, battery technologies on the system performance was studied and a sensitivity analysis has also been carried out for the system for two types of loads: single house and residential. It was found that cycle charging proved to be more effective for single house while for a residential community the load following strategy was more effetive. Also, in terms of battery chemistry Lithium Ion Nickel Managanese Cobalt Oxide (Li-Ion NMC) battery had the longest lifetime. The sensitivity analysis showed that capital cost for hydrogen electrolyzer and the solar reserve capacity had the most impact on the system sizing.

   Key Words: fuel cell, hydrogen, electrolyzer,renewable energy, microgrids

# A.1   Introduction

According to the International Renewable Energy Agency's (IRENA) 2050 energy transformation road map, renewable energy (RE), energy efficiency, direct electrification, and hydrogen are the could cover about 80% of the necessary emission reductions to achieve the goals established by the Paris agreements [170]. The application of these strategies implies, among other major concerns, the electrical grid transformation into small energy-distributed systems such as microgrids (MG) [171].

All the distributed energy resources (DER) in the MG (RE sources (RES), energy storage system (ESS) and loads) have to work together to balance energy demand and supply at all times. Also, the MG system should be resilient to renewable generation variability in order to ensure reliability and avoid energy mismatches. Hence, it is crucial to optimally determine the energy dispatch and the capacity of each DER since a poorly sized system always has a negative impact on investment costs and energy efficiency [160].

An energy management system (EMS) is required to coordinate effectively the system's energy flow to satisfy the load, especially in isolated MGs such as remote locations. Researchers have made a great effort designing EMS for off-grid applications considering two approaches: rule-based (RB) and optimization. Optimization based EMS have been explored in [172, 173, 174] while Fuzzy Logic Controllers have been used in [175, 176]. The RB approach estimates the component's operation status through decisions made using a predefined flowchart while optimization techniques require developing a cost model designed for particular objectives to determine the power flow. Although RB approaches are simple and may not be cost effective, they are widely used due to the ease of practical implementation and hence they are studied in this work.

The strategies used in RB EMS are Load Following (LF) and Cycle Charging (CC). In the LF mode, the RES has the priority to power the load and charge the battery and the generator only operates when RES does not satisfy the demand and is not allowed to charge

the BESS. In addition, the BESS can discharge at low RE production as long as it has energy. However, these continuous charge and discharge cycle can lead to lower efficiency and reduced lifetime of the battery. On the other hand, in the CC strategy, the generator operates at full capacity. Under periods of excess energy in this case, the BESS will be charged. However, the BESS can only be discharged when a specific SoC is reached. This leads to a non-optimal BESS usage but its lifetime is increased [161].

Both control strategies are widely used in systems that include several energy generation technologies their effect on MG planning has been evaluated by several authors. In [177], the impact of LF, CC, and combined dispatch were evaluated on two system configurations (PV-Hydro-Battery and PV-Wind-Hydro-GE-Battery) for Li-ion and Lead Acid Battery using HOMER Pro$^{\text{TM}}$. Jufri et al. [178], proposed an optimal control dispatch for BESS based on the drawbacks of LF, CC, and CD. The objective was to minimize the Levelized Cost of Energy (LCOE) while maximizing the renewable energy penetration. In [179], authors evaluated the techno-economic performance of grid-connected and off-grid systems for a school using CC and LF.

Although the performance of LF and CC EMS have been extensively studied in MG with BESS, the impact of including hydrogen on the performance of these strategies is still not clear. In this paper, we aim to compare the performance of the LF and CC control strategies on a single house and a residential community, the impact of battery technology on the system design and costs, and a sensitivity analysis of the techno-economic parameters for the LCOE.

## A.2   Methodology

In this study, an isolated Solar Photovoltaic (PV)-Battery-Hydrogen (Electrolyzer, Fuel cell (FC), and Hydrogen Tank) system is considered to meet a residential load profile located in southern Ontario, Canada. The typical monthly Global Horizontal Irradiation (GHI) profile for the area is shown in Fig. A.1. The PV-Battery-Hydrogen system (PBHS) is shown in
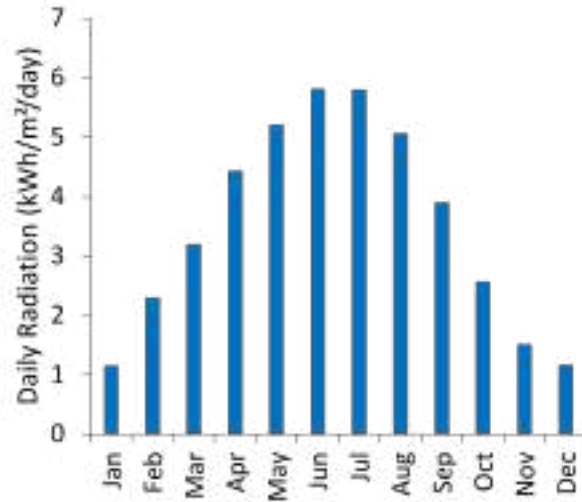
Figure A.1: Global Horizontal Irradiation Profile

Fig. A.2. The PV array and FC are connected to the DC bus through DC-DC converters. In HOMER Pro$^{TM}$, the PV and FC System is modeled as a black box as highlighted in Fig. A.2. The electrolyzer and BESS are connected to the DC bus. A bi-directional converter (BDC) connects the DC and AC bus where the electric load is attached.

HOMER Pro$^{TM}$ is one of the most widely used software tools for optimal sizing of MGs and energy systems, since PBHS are usually evaluated in terms of its economic viability. This tool sizes the PBHS with the aim of meeting the load and minimizing the system cost. However, in doing so, there could be a scenario where the winning system architecture in terms of cost produces excess energy (EE) that cannot be managed by the storage system and is thus sent to the ground, causing the system to be inefficient. Therefore, in this work, in addition to having systems with the lowest cost, an additional filter of $EE = 0$ has been added as shown in the methodology diagram presented in Fig. A.3.

This analysis considers consumption profiles at two scales: individual homes and residential community (a set of 10 houses) (Fig. A.4) [180]. To achieve this, a comparative analysis was conducted in terms of hydrogen production and storage efficiency. Subsequently, at the community level, the best EMS was selected to examine how the system behaves when considering three different types of batteries. Finally, a sensitivity analysis was performed
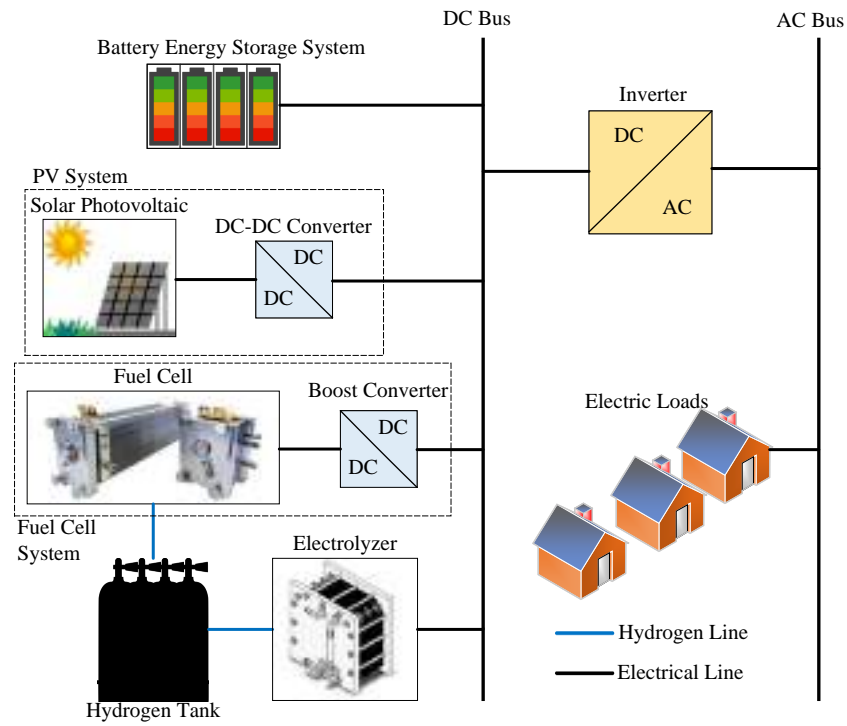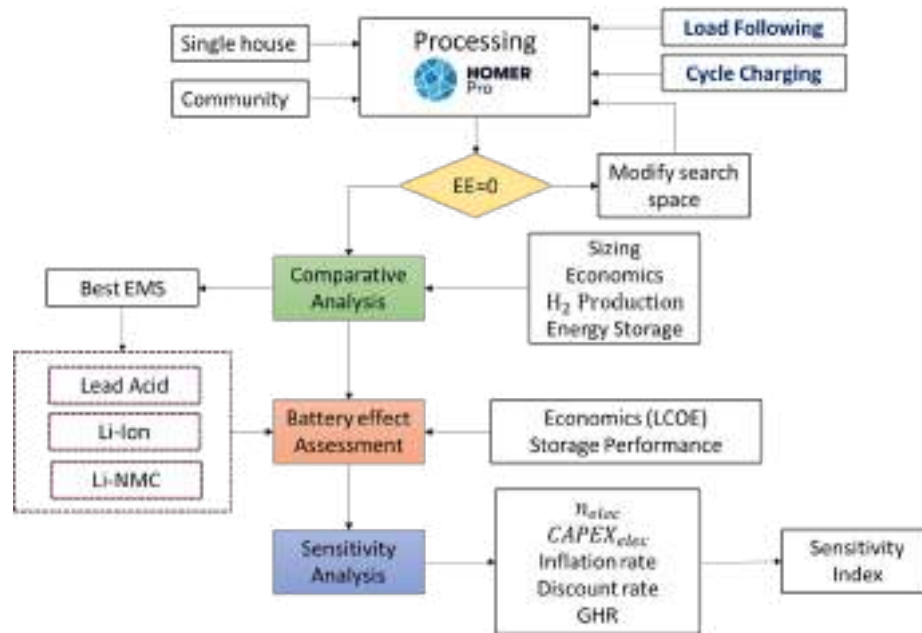
Figure A.2: System Model



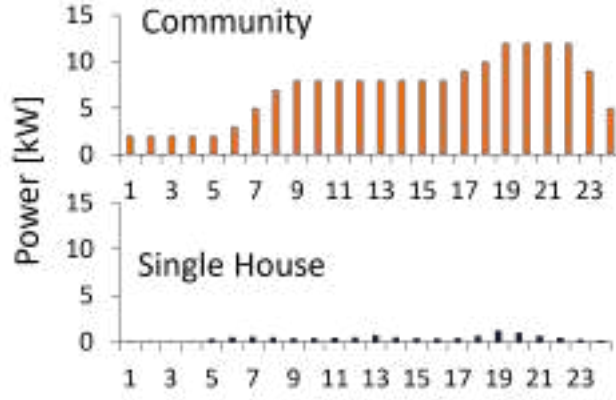Figure A.3: Methodology to identify the Winning System

Figure A.4: Load Profiles

to assess the effect of economic factors such as capital cost, inflation rate and the discount rate on the LCOE that the system would generate. Additionally, the impact of electrolyzer efficiency ($\eta_{elec}$) and the solar resource was also evaluated.

## A.2.1 Evaluation Parameters

To assess the performance of each EMS strategy, the numerical results of the simulations were condensed into four indicators for comparison. The first one is the Cumulative Energy along the year in kWh, which was calculated using equation A.1 where $ET$ is the cumulative energy, $P_i$ is the power at hour $i$, $t_i$ is the time step in hours.

$$\text{ET} = \sum_{i=1}^{8760} P_i t_i \tag{A.1}$$

ESS efficiency ($\eta_{Storage}$) is the relationship between the energy output from the BESS-FC ($E_{FC} + E_{BESS,discharge}$) and the energy input to the storage system (BESS charging ($E_{BESS,charge}$) and electrolyzer consumption ($E_{Elec}$)). The efficiency is calculated using equation A.2.

$$\eta_{Storage} = \frac{E_{FC} + E_{BESS,discharge}}{E_{Elec} + E_{BESS,charge}} \tag{A.2}$$

The total mass of hydrogen produced by the electrolyzer in kg/h was computed according to equation A.3. Where $E_{pvs}$ is the energy that comes from the PV panel array, $HHV_{H_2}$ is

the Higher Heating Value of hydrogen (39.4 kWh/kg), and $eta_{elec}$ is the electrolyzer efficiency which was considered as 65%.

$$M_{H_2} = \frac{\eta_{elec} E_{pvs}}{HHV_{H_2}} \tag{A.3}$$

The LCOE is defined as the average cost per kWh of the electrical energy produced by the PBHS during the project's lifetime. Therefore, to compute this value per year, the ratio between the annualized present cost of the system (Capital investment cost (CAPEX) and Operational Expenditures (OPEX) - that is the sum of Operation and Maintenance (O&M) cost plus Replacement cost) and the average of energy production is calculated in USD/kWh, according to equation A.4 where $N$ is the project lifetime, and $I$ is the discount rate in %.

$$\text{LCOE} = \frac{\sum_{j=0}^{N}((\text{CAPEX} + \text{OPEX})(1 + I)^{-j})}{\sum_{j=0}^{N}((ET)(1 + i)^{-j})} \tag{A.4}$$

It is important to highlight that one of the parameters commonly used in the economic evaluation of energy projects is the Net Present Cost (NPC) which represents the present value of all costs the system will accumulate throughout its lifespan, subtracted by the present value of all revenue it generates during the same period. This involves capital expenses, replacement costs as well as O&M costs.

## A.2.2 Economic considerations

The sizing of the MG was carried out by specifying a series of important parameters. These include the cost of a PEM electrolyzer that produces high-purity hydrogen to be fed into the fuel cell (Table A.1), The PV, BESS costs from the cost list proposed by NREL [166] (which includes costs at different scales: Utility and distributed). In this case, the costs corresponding to the distributed system category were used since, according to the Energy Information Administration (EIA) [167], installations with a capacity of at least 1 MW are considered utility scale and the system under consideration is a smaller scale.

---

[1]Applies to Hydrogen Storage Tank

Table A.1: Capital Costs for DERs

| DER | Capital Cost (USD/kW) (USD/kg) [1] | O&M Cost (USD/kW-yr) (USD/yr) [1] | Replacement Cost (USD/kW) (USD/kg) [1] |
|---|---|---|---|
| PV | 2286.98 | 26.98 | 250-1050 |
| BESS | 3034.7 | 75.86 | 3034.7 |
| Fuel Cell | 2000 | 32.23 | 700 |
| PEM Electrolyzer | 1800 | 90 | 270 |
| Hydrogen Storage Tank | 1000 | 30 | 700-1000 |

## A.2.3  Simulation conditions

For the control strategies evaluated, an hourly time step was used. For the project, a discount rate of 8% and an inflation rate of 2% was used. Additionally, the operating reserve (defined as the amount of excess energy that should be available at all times for unforeseen circumstances) was set to 10% of the load. Finally, as the system is a stand-alone system, an allowance was made for outages where the system need not meet the maximum load for up to 10 days (corresponding to 3% of the year).

It should be noted that, in the case of batteries, HOMER Pro™ establishes storage models that assume a flat discharge curve because the supply voltage remains mostly constant during the discharge cycle [180]. These models are generically named to group certain types of batteries, such as Lead Acid and Li-Ion. Additionally, HOMER™has other specialized models that allow simulating technologies with specific materials, such as Lithium-Nickel-Manganese-Cobalt (NMC), which, according to NREL [166], is a more suitable battery type for stationary applications.

## A.2.4  Sensitivity Analysis (Sensitivity Index)

In order to reveal the sensitivity of some parameters in the LCOE, the sensitivity index (SI) was used, which is given by

$$\text{SI} = [max_\gamma - min_\gamma(x)]/max_\gamma(x) \tag{A.5}$$

where $\gamma$ accounts for the parameter varied and $x$ for the output variable to be evaluated.

Sensitivity indexes for the Gas Heat Rate (GHR), Discount Rate, Inflation rate, $\eta_{elec}$ and $CAPEX_{elc}$ were computed in this work.
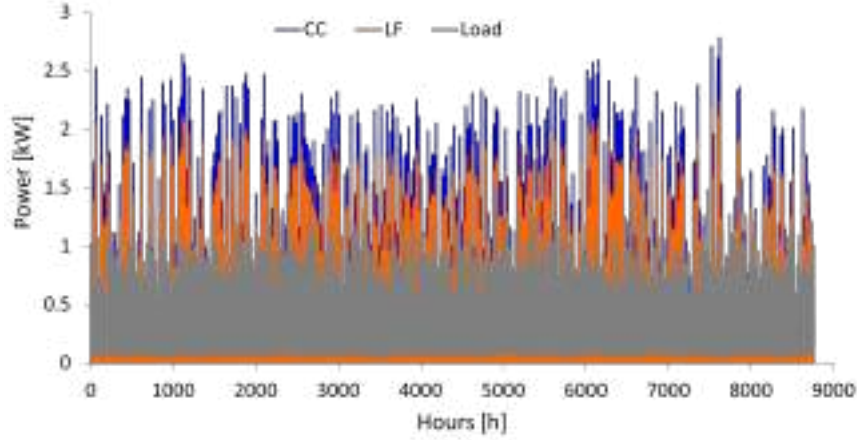


Figure A.5: Renewable Energy Production Profile for Single House

## A.3 Results and Discussion

In this section, the results for the performance evaluation of LF and CC EMS strategies is described. Subsequently, a discussion is conducted on the comparison of the different battery technologies used. Finally, the sensitivity analysis for this system is presented.

### A.3.1 Energy Management System

The performance of the EMS (CC and LF) was evaluated at two scales: Single House and a Residential Community. Using HOMER Pro$^{\text{TM}}$ makes it possible to analyze several feasible configurations in terms of cost and power balance. Within that group of possible solutions, the most economic system along with satisfying the $EE = 0$ constraint are selected for a single house and a residential community as shown in Fig. A.6 and Fig. A.7 respectively.

For a single house, it is observed that CC sizes the photovoltaic (PV) system 19% larger than LF and only requires one battery, while LF requires two. The hydrogen system is the same size in both cases. These dimensions imply that CC will generate more energy

throughout the year due to its larger installed capacity, thus requiring less BESS capacity and allowing more hydrogen production. LF, on the other hand, produces less energy, making it more likely to instantly require greater BESS capacity.

Table A.2 displays the performance of the EMS in terms of the comparison parameters defined in the previous section. In terms of storage efficiency, LF outperforms with 71.34%, while CC resulted in 48.87%. On the other hand, using CC would yield hydrogen production almost double that of LF (improving seasonal storage as shown in Fig A.8). However, the BESS's lifetime is reduced by almost 50% when CC is employed. As observed, in some parameters such as Cumulative Energy, $H_2$ production and LCOE, CC has a better performance than LF. Nevertheless, LF increases the battery lifetime which is favorable when Lead Acid technology is used.

According to [178], LF control strategy is typically suitable for systems in which the power generated by the PV system during the day exceeds the load demand. On the other hand, the CC algorithm is appropriate for optimizing the dispatched power in systems where the power generated by the PV system during the day is lower than the required demand for similar periods. This is one of the main reason why CC over sizes the system making it more reliable but at the same time more expensive. The NPC for CC is USD 94,859 and USD 94,350 when LF is used. Overall, it is possible to say both techniques could work appropriately at the given conditions and the user can choose between LF and CC depending on the objective.

For the residential community, the EMSs exhibited a different performance compared to what was found on a small scale, probably due to a change in the load profile. Firstly, LF generates the costliest system with a NPC $1.13M, while CC's NPC is $1.10M. Additionally, LF has higher energy production throughout the year and also requires a larger BESS with 45 batteries, unlike CC, which only requires 10 batteries and the hydrogen system has the same size for both cases. However, LF produces more hydrogen with lower storage efficiency. This seems to be due to the fact that at both scales, when there is higher hydrogen pro-
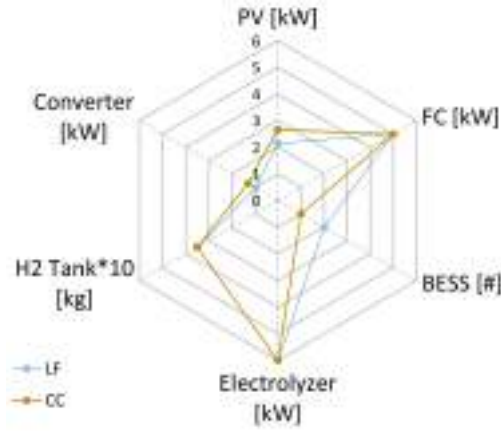
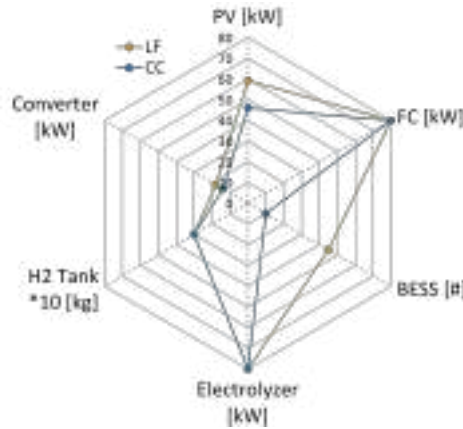Figure A.6: PBHS Configuration for one single house



Figure A.7: PBHS Configuration for Residential Community

duction, storage efficiency decreases due to all the energy transformation stages that must be considered. According to Table A.2, in several parameters, CC performs better than LF, however, LF always improves the capacity of the storage system increasing the lifetime of the battery and harnessing the advantages of seasonal storing of $H_2$ as it is shown in Fig. A.8.

## A.3.2    Battery Chemistry

To compare the impact of battery type on the sizing and capacity of the PBHS, the load profile of the residential community along with the LF control strategy was used. Three types of batteries were evaluated: Lead Acid (1 kWh), Lithium Ion (1 kWh), and Nickel Manganese Cobalt (NMC) (4 kWh). Table A.3 demonstrates the significant advantage of high-capacity batteries in terms of volume, as generic Lithium Ion batteries would require

Table A.2: EMS Performance based on Evaluation Parameters

| Parameter | Control strategy | Single house | Community |
|---|---|---|---|
| Total Energy [$kwhYear$] | LF | 4,315.00 | 100,502.00 |
| | CC | 5,153.00 | 92,342.00 |
| Energy Storage efficiency [%] | LF | 71.34 | 40.00 |
| | CC | 48.87 | 54.10 |
| LCOE [$USD/kWh$] | LF | 2.38 | 1.47 |
| | CC | 2.42 | 1.42 |
| Capacity Shortage [%] | LF | 0.82 | 0.90 |
| | CC | 0.66 | 0.59 |
| H2 Production[$kg/year$] | LF | 16.80 | 604.00 |
| | CC | 30.10 | 476.00 |
| BS autonomy [$h$] | LF | 3.39 | 3.93 |
| | CC | 1.70 | 0.87 |
| BS expected life [$year$] | LF | 5.65 | 5.84 |
| | CC | 2.72 | 3.02 |
| FC Operation life [$year$] | LF | 11.00 | 13.40 |
| | CC | 12.00 | 9.60 |
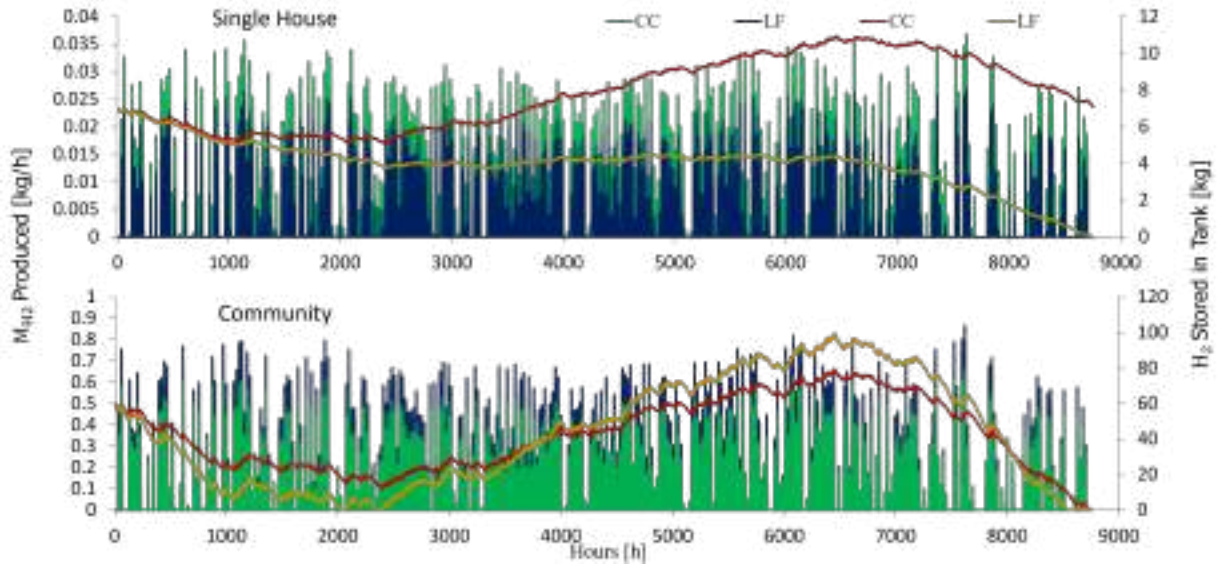


Figure A.8: Annual Hydrogen Production for both Loads and EMS strategies

Table A.3: Effect of the Battery Chemistry on the Capacity Size of the PBHS

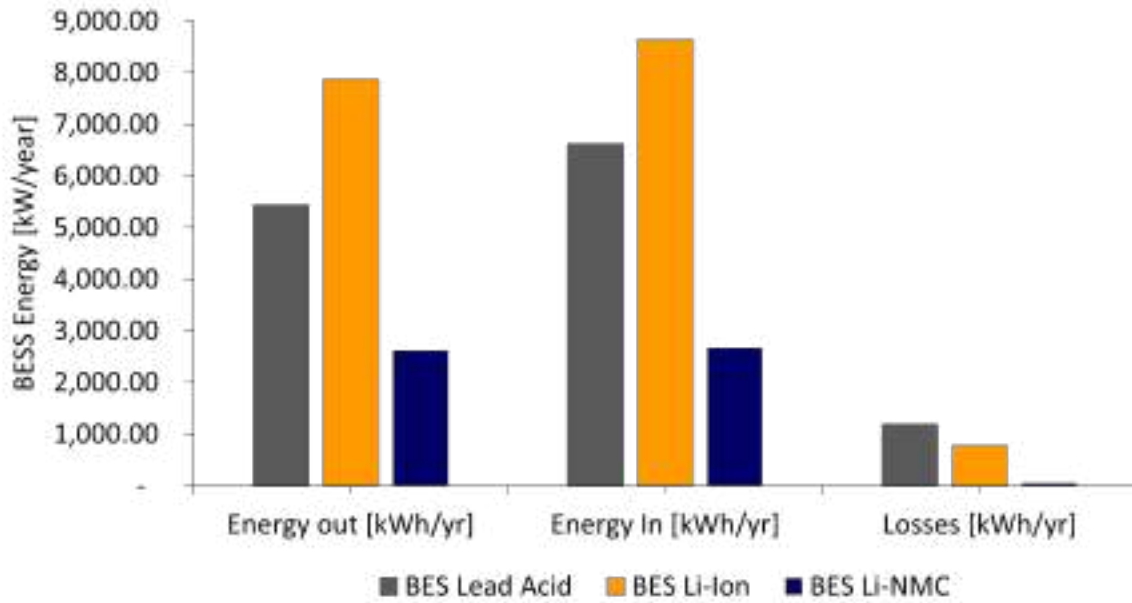| Parameter | Lead-Acid | Li-Ion | Li-NMC |
|---|---|---|---|
| PV | 49.60 | 58.40 | 56.10 |
| FC | 80.00 | 80.00 | 80.00 |
| Battery | 44.00 | 40.00 | 2.00 |
| Electrolyzer | 80.00 | 80.00 | 80.00 |
| H2 Tank *10 | 30.00 | 30.00 | 30.00 |
| Converter | 14.10 | 16.30 | 14.30 |



Figure A.9: Annual BESS Performance

more than 40 units, while NMC would only need 2 batteries. On the other hand, Table A.4 shows the differences induced by the battery type in the system's key characteristics. It is observed that, despite NMC being a costly technology, over the useful life of the system, the total project cost is only 3% higher compared to Lead Acid batteries. This is due to the long useful life of NMC.

It is observed that a high-capacity battery such as Li-NMC is specified, and HOMER Pro$^{TM}$ sizes the system with only two batteries inducing limited autonomy time. Sacrificing this parameter may be of little relevance since the hydrogen system is available. Figure A.9 shows the total energy received and delivered by the batteries over the year. In terms of the energy received by the BESS, energy losses are 17%, 8.89%, and 1.8% for Lead Acid, Lithium

Ion, and Li-NMC, respectively. It should be noticed that by considering the complete project lifetime, the CAPEX of the PBHS using Li-NMC is only 2% different from the one that uses Lead Acid technology.

Table A.4: Impact of Battery Chemistry on the Techno-Economic Variables

| Variable | Lead Acid | Li-Ion | Li-NMC |
|---|---|---|---|
| NPC [MUSD] | 1.10 | 1.11 | 1.13 |
| CAPEX [USD] | 745,525.00 | 778,186.00 | 760,553.00 |
| LCOE [USD/kWh] | 1.43 | 1.44 | 1.47 |
| $M_{H_2}$ [kg/year] | 437.00 | 560.00 | 617.00 |
| Autonomy [h] | 5.25 | 4.16 | 1.31 |
| Expected Life [year] | 6.80 | 14.30 | 20.00 |

Another important parameter to consider regarding the effect of the battery type is the hydrogen production. In Table A.4, it is observed that perhaps the technology with the highest synergy between BESS and hydrogen is the model given by the generic Lithium Ion batteries. Besides storing the most energy throughout the year with 4.16 hours of autonomy, they allow hydrogen generation only 10% less than NMC, with a production of 560 kg/year.

## A.3.3 Sensitivity analysis

One of the most representative parameters in sizing PBHS is the cost of produced energy. To comprehensively analyze the impact of technical and economic factors, the LCOE is considered. LCOE depends on both economic and technological factors. Therefore, to assess the impact of these factors on LCOE, a sensitivity analysis was conducted considering the electrolyzer's CAPEX, discount rate, and inflation rate as economic variables, and the GHR and electrolyzer efficiency as technical variables.

The sensitivity analysis evaluation was conducted according to equation A.5. Results are shown in Table A.5. Among the economic parameters, the one with the most significant impact is the electrolyzer's CAPEX, accounting for 28%, followed by the interest rate at 12%. This indicates that the cost of the technology is essentially the limiting factor for the deployment of such systems. Regarding the technical parameters, solar resource availability

Table A.5: Sensitivity Analysis for the Considered MG System

| Parameter | Sensitivity Index [%] |
|---|---|
| GHR [$kWh/m^2day$] | 7.57 |
| Discount Rate [%] | 12.72 |
| Inflation [%] | 14.96 |
| $\eta_{elec}$ | 2.73 |
| CAPEX$_{elec}$ | 28 |

has the greatest impact at 7.57%, whereas the electrolyzer efficiency has a lower impact at only 2.73%.

## A.4 Conclusions

Renewable Energy, Hydrogen Storage and BESS systems are widely being considered for MGs. In this study it was found that the LF strategy was more efficient compared to CC strategy. Also, the CC increases the size compared to the LF strategy. In terms of battery chemistry, although NMC have a higher cost, the battery lifetime is increased. Also, a sensitivity analysis showed that the capital cost for hydrogen electrolyzer and the solar reserve capacity had the most impact on the system sizing.

The results show that in off-grid areas, we can have a reliable MG with zero emissions. The work done can also be used as a benchmark for using optimization algorithms that are used in planning and operation studies for MGs. Furthermore, the research work can be done to integrate electric vehicles (EV) and fuel cell vehicles (FCV) in the remote MG. Further studies can also include using hydrogen technology for combined heat and power (CHP) integration with the MG.

# Appendix B

# Design and Control of a Maximum Power Point Tracking System for a Fuel-Cell-Battery Hybrid Electric Vehicle

In this appendix, the results obtained during the research stay at Ontario Tech University in Canada are presented. This involves a comparative analysis of maximum power point control methods applied to a fuel cell vehicle.

**Abstract** Both fuel cells (FC) and battery energy storage systems (BESS) have wide applications in electric vehicles (EV). Combining the two technologies (FC and BESS) to form a hybrid EV provides the combined advantages of both technologies which improved response to transients, clean energy source, increased efficiency and increased autonomy. In this study, using maximum power point tracking (MPPT) to control the FC output and its impact on the overall power train is investigated.

Key words: fuel cells, hybrid electric vehicles, battery energy storage, powertrain design, electric vehicles

# B.1  Introduction

Hydrogen, with its significant potential, serves as a versatile and efficient means to store and distribute clean energy across several economic sectors such as transportation (Electric vehicles (EV)) at different scales. Designing fuel cell (FC) systems with battery energy storage systems (BESS) creates a hybrid system that is efficient and has increased range.

As such, several energy management strategies (EMS) to optimize the power sharing between the FC and the battery have been implemented. In [1], the authors have used a non-linear model predictive (MPC) method for real time energy management. Similarly, model-based reinforcement learning and model-free reinforcement learning techniques were used for developing the EMS for the FC - battery EV (FCBEV) in [2]. In addition an ultracapacitor was added to the FCBEV and the impact of the EMS to find the best trade-off between the number of start up/shut down cycles and the hydrogen consumption in [3]. The EMS investigated included fixed-set point operation, charge-balancing and predictive energy management. A fuzzy logic control approach was used in [4] to implement the controller for a FCBEV.

A power sharing algorithm that operates the FC at its minimum operation set point to avoid multiple start up/shutdown sequences and using the battery power for additional power is proposed in [5]. The algorithm is used to control a dual input inverter that drives the electrical motor. A hierarchical rule based and cost optimization algorithm is used to compare the performance of a single stack FC and a multiple stack FC in [6]. An overview of integrating FC with BESS for marine vessels has been presented in [8]. Additional power sharing schemes for the EMS have also been researched in [8] and [9].

In order to integrate the FC with the electric powertrain, A DC/DC boost converter is typically necessary to increase the voltage of the FC to those required by the system. During operation, it is important to control the FC power output. Therefore, a controller is required to govern the duty cycle and the power flow between the load and the FC.

Among the several control techniques implemented, the Maximum Power Point Tracking (MPPT) method is one of the most commonly used. According to [10], there are four types of MPPT techniques. However, Incremental Conductance (IC) and Perturbation and Observation (P&O) are the most widely used MPPT techniques. Several authors have implemented these techniques for stationary and mobile FC applications. In [11], authors implemented the P&O algorithm to control the FC output power for a refrigeration cycle load profile. A Fuzzy Logic Maximum Power Point Tracking (MPPT) control technique was used in [12] to sustain the operation of a FC at a specific efficiency point, considering variations in the system temperature. The authors in [13] combined the P&O MPPT method with the current reference generator to develop a FC System which includes the DC-DC Boost Converter while incremental resistance technique was used in [14] to improve the performance of the FC.

Although MPPT techniques have been widely implemented and evaluated in FC-converters systems, proving to be simple and effective, the feasibility of implementing them in an electric vehicle system under a driving profile is still not clear. Therefore, the objectives in this research study was to present the impact of a drive cycle on the performance of P&O and IC MPPT control algorithm for the FC in the FCBEV.

## B.2   System Model

The FC-Battery System for the EV is shown in Figure B.1. The FC is connected to a DC-DC Boost converter while the battery is connected to a bidirectional converter (BDC). THe BDC implements the controls for the battery charging and discharging. Both the systems are fed into a permanent magnet DC Motor (PMDC).

### B.2.1   Driving Profile

To test the MPPT control techniques in the system, the Worldwide Harmonised Light Vehicle Test Procedure (WLTP) driving profile was used since it has served to quantify the fuel consumption, $CO_2$ emissions, and pollutant emissions of passenger cars and vans (Figure B.2).
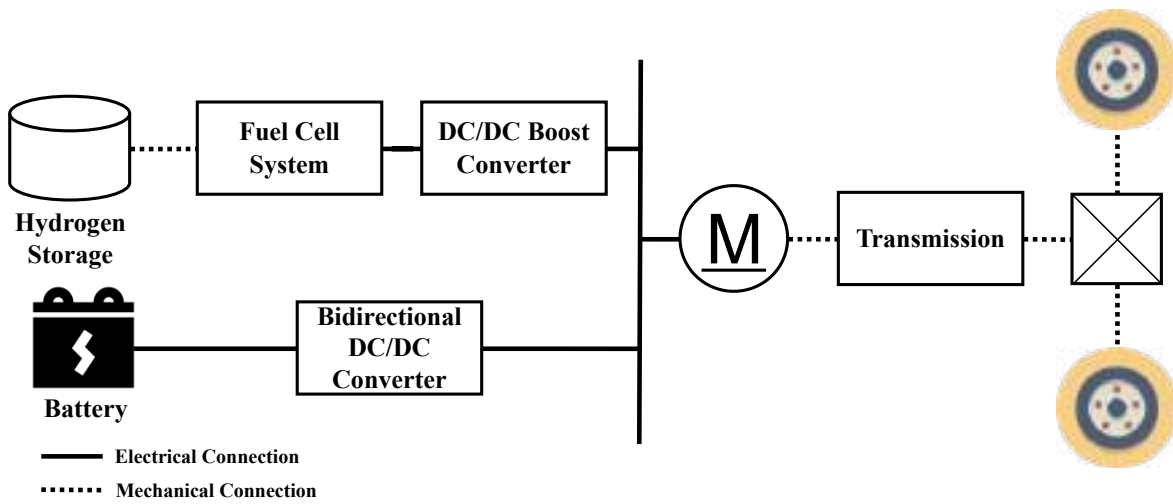
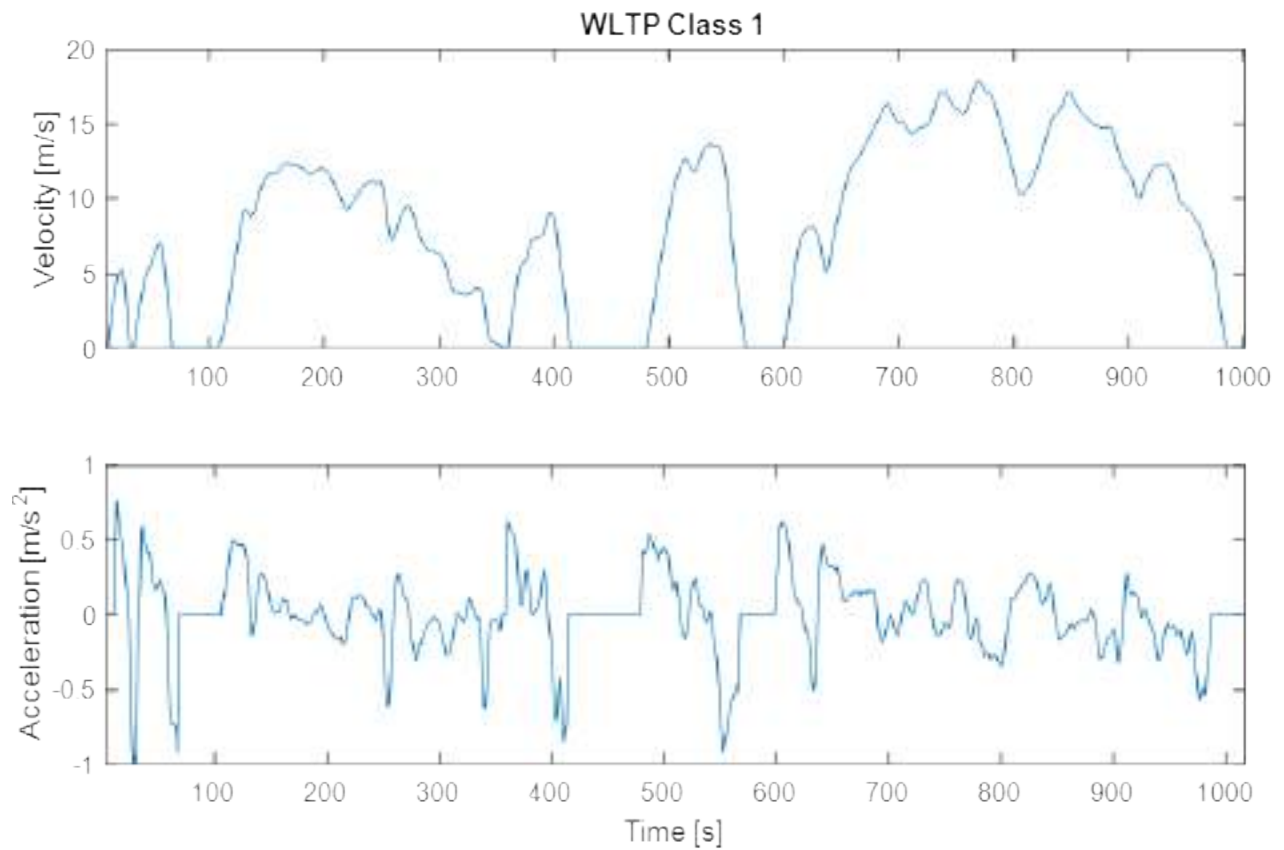Figure B.1: System Under Consideration



Figure B.2: The driving profile used to evaluate the performance of the developed control in this study.
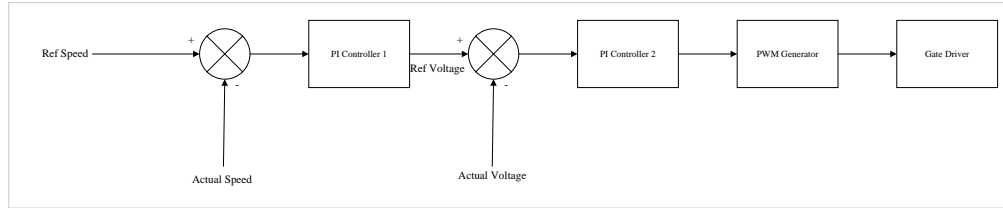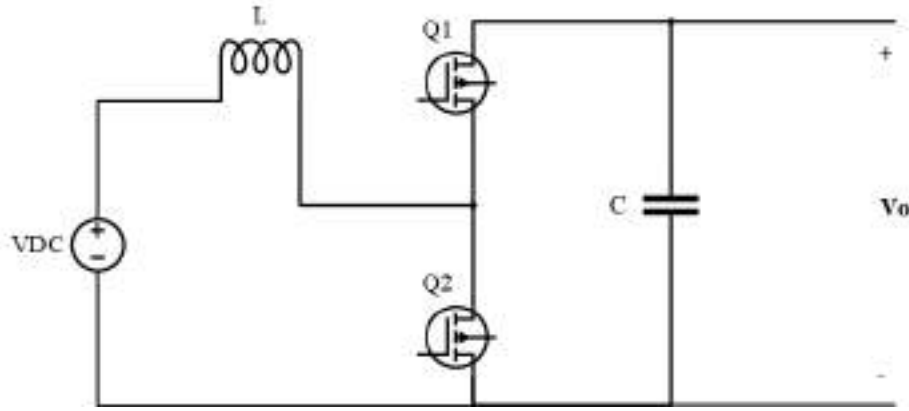
Figure B.3: The BDC Control System



Figure B.4: BDC Circuit Diagram

## B.2.2  Battery and BDC

For preliminary simulations in this study, a BESS system with a BDC and PMDC was developed. The BESS was rated at 60 V, 400 Ah and the PMDC was a 5 HP, 480 V system, 1750 rpm. The circuit for the BDC is shown in Figure B.4 below. The parameters for the BDC are shown in Table B.1.

The control for the BDC is determined using two proportional-integral (PI) controllers as shown in Figure B.3. The first PI controller is used to determine the voltage reference according the difference between the reference speed and the actual speed of the motor. The inner loop then is used to generate the switching signals for the BDC in order to control the DC bus voltage. The gains for the PI controllers are shown in Table B.2.

Table B.1: Bidirectional Converter Parameters

| Parameters | General Time of Use |
|---|---|
| Input Voltage (V) | 60 |
| Output Voltage (V) | 240 |
| Switching Frequency (kHz) | 10 |
| Inductor (uH) | 10 |
| Capacitor (mF) | 10 |

Table B.2: PI Controllers Gains

| | Proportional Gain | Integral Gain |
|---|---|---|
| **Controller 1** | 1 | 0.8 |
| **Controller 2** | 0.007 | 0.1 |

## B.2.3   Fuel Cell - DC Boost Converter System

For this investigation, the power curve of a commercial 45-kW FC has been derived from the datasheet [15], and the MATLAB FC Stack module has been utilized to implement the control techniques. The V-I curve was modeled according to Equations (B.1) - (B.2) where $V_{FC}$ is the output voltage of the FC, Enerst is the Nerst voltage, $V_{act}$ is the actuation losses, $V_{ohmic}$ represents the ohmic losses and $V_{conc}$ stands for the concentration losses, $E_{cell}$ is the voltage across one FC, R is the ideal gas constant, T is the temperature, F is Faraday's constant, $I_{FC}$ is the FC current, $\alpha$ is the transfer coefficient, $i_0$ is the current exchange density, $R_{int}$ is the internal resistance of the FC. Accordingly, the FC voltage and power curves as a current function are shown in Figure B.5.

$$V_{FC} = E_{nerst} - V_{act} - V_{ohmic} - V_{conc} \tag{B.1}$$

$$V_{FC} = E_{cell} - \frac{RT}{2\alpha F} ln \frac{I_{FC}}{i_0} - \frac{RT}{2F} \ln \left( 1 - \frac{I_{FC}}{i_L} \right) - I_{FC} R_{int} \tag{B.2}$$
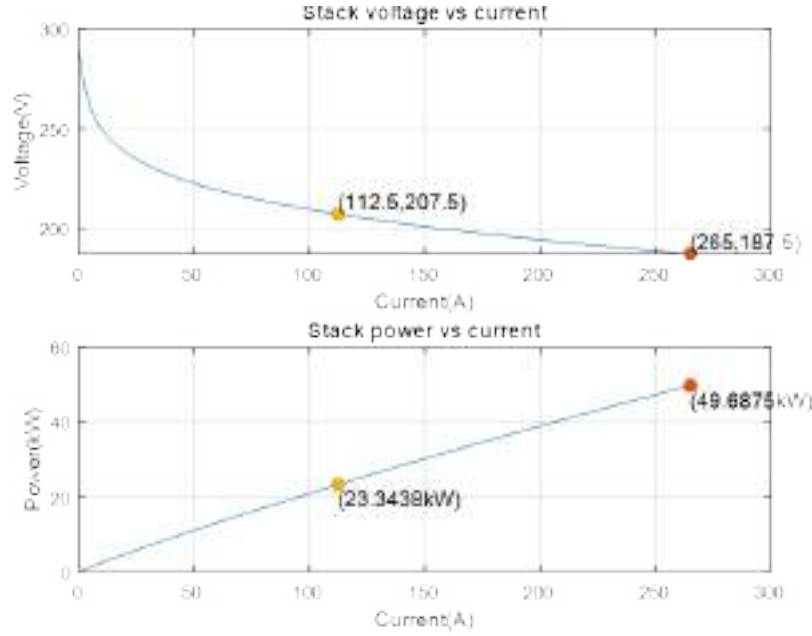
Figure B.5: characteristic curves of the 45-kW PEM Fuel Cell.

The FC efficiency during the simulation time established by the driving profile was calculated through Equation B.3.

$$\eta_{FCstack} = \frac{\int_{t_{initial}}^{t_{final}} V_{FC}(t) \times I_{FC}(t)dt}{\int_{t_{initial}}^{t_{final}} M_{H_2}(t) \times LHV dt} \tag{B.3}$$

where LHV is the lower heating value of hydrogen (considered as 33.32 kWh/kg), $M_{H_2}$ and $M_{H_2}$ was computed through the FC MATLAB/Simulink$^{TM}$model.

For the 45 kW PEMFC, it was necessary to calculate a DC-DC Boost Converter to adjust the cell's output voltage to 480 V. Using the relationship between the output voltage and input voltage as shown in Equation B.4 where $V_o$ is the average output voltage, $V_S$ is the input voltage and D is the duty cycle of the PWM signal passed to the switch. Accordingly, the inductor and capacitor were calculated using equations B.5 and B.6 where $R$ is the load resistance, $\Delta V_o$ is the acceptable voltage ripple for the system. Accordingly, the parameters for the boost converter are shown in Table B.3.

$$\frac{V_O}{V_S} = \frac{1}{1-D} \tag{B.4}$$

Table B.3: Converter Parameters

| Boost Converter parameters | Value |
|---|---|
| Input voltage range $VS$ | 190-300 V |
| Output voltage $V_o$ | 480 V |
| Maximum power $P_{omax}$ | 45 kW |
| Current ripple $\Delta I_L$ | 25 |
| Voltage ripple $\Delta V_L$ | 5 V |
| Switching frequency $f_{sw}$ | 50 kHz |
| Load range $R$ | $230 - 5.12$ $\Omega$ |
| Inductor $L$ | 115.2 $\mu H$ |
| Capacitor $C$ | 112.5 $\mu F$ |

$$i_L(t) = \frac{1}{L} \int_0^{DT} v_L(t)\, dt \qquad (B.5)$$

$$v_C(t) = \frac{1}{C} \int_0^{DT} i_C(t)\, dt \qquad (B.6)$$

## B.2.4 Maximum Power Point Tracking Algorithm

The two algorithms P&O and IC were implemented to control the Boost Converter of the FC System. Based on the actual power measurements, the MPPT algorithm will generate the voltage reference which will then be used to generate the duty cycle of the Boost Converter. The algorithm is shown in Figure B.6. The IC algorithm will generate the voltage reference according to the resistance value and then the duty cycle will be generated for the boost converter switching cycle as shown in Figure B.7.

## B.2.5 Vehicle Control System

Figure B.8 presents the controller between the FC and the DC-DC converter. The output voltage and current of the FC serve as the input variables for the P&O and IC controllers. The algorithms were programmed into a MATLAB function in which at each time step, an error in the FC is calculated (eFC), through the difference between the input and output
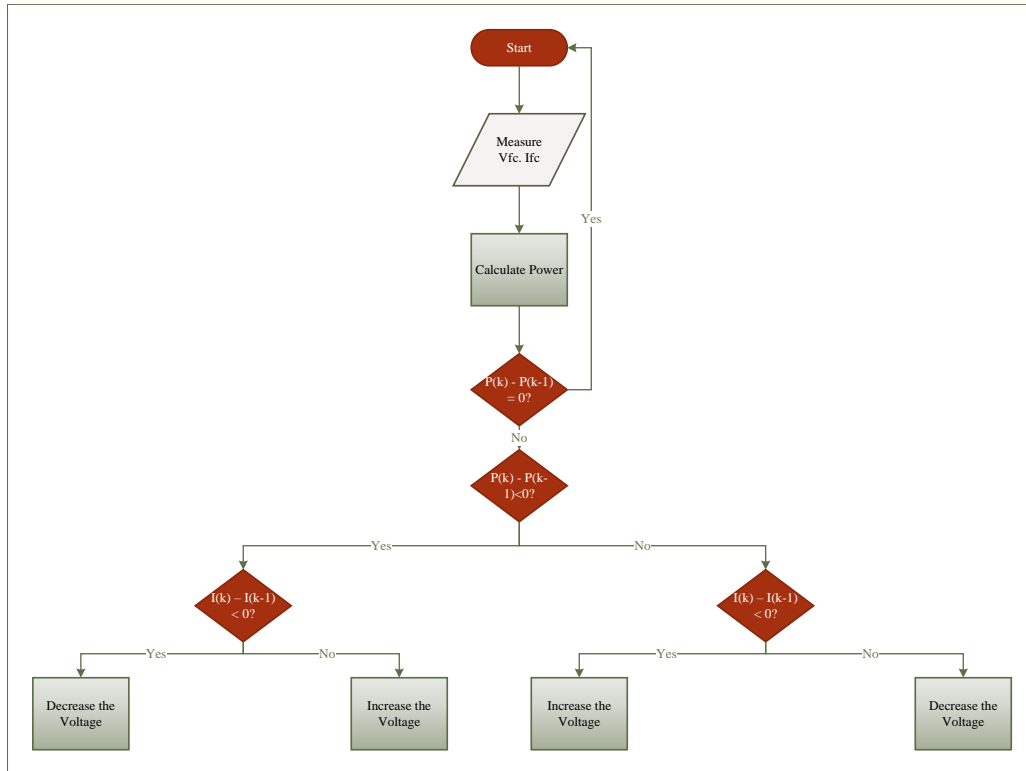
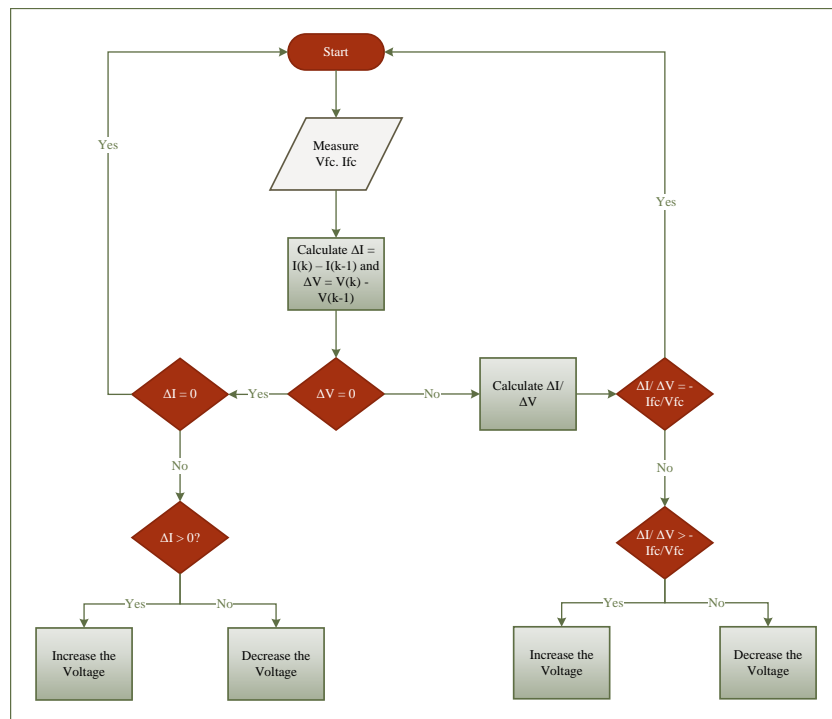Figure B.6: P&O Algorithm for the FC



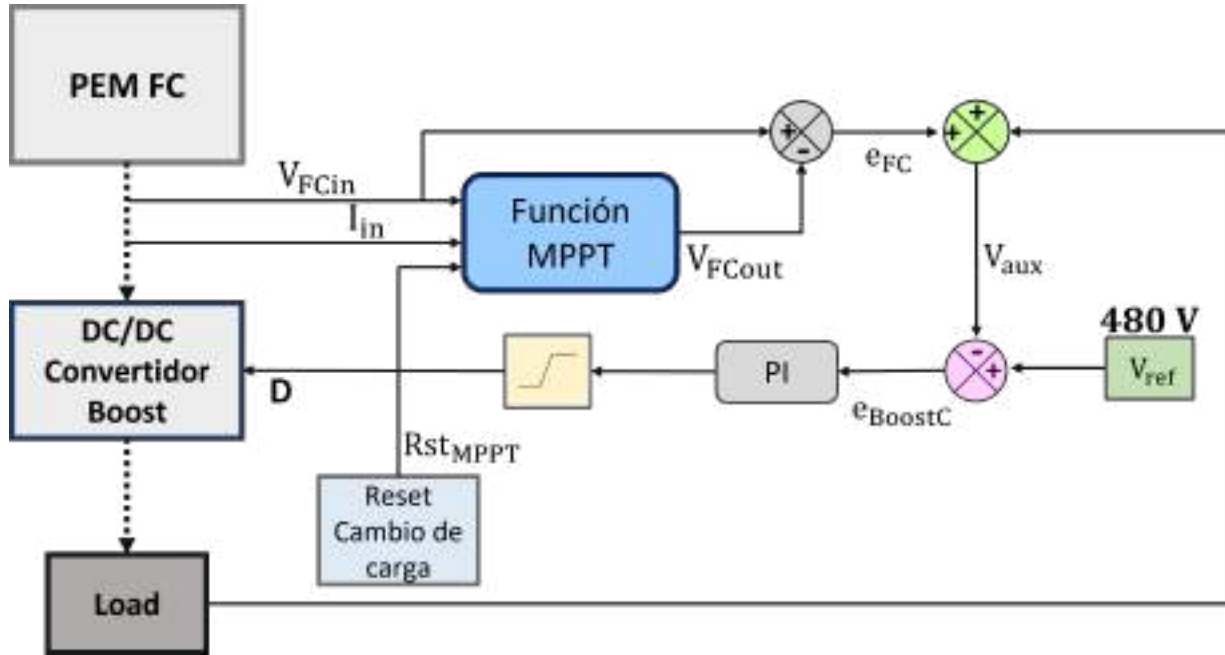Figure B.7: IC algorithm for the FC

Figure B.8: Control System Block Diagram

voltage $e_{FC} = V_{FCin}$ - $V_{FCout}$. $e_{FC}$ is then added to the output voltage of the converter to produce an auxiliary voltage ($V_{aux}$). This result is compared with the reference voltage ($V_{ref}$), generating an error related to the converter $e_{BoostC}= V_{ref}$ - $V_{aux}$. The value of $e_{BoostC}$ was then fed into the Proportional-Integral (PI) controller to produce the converter's duty cycle. The control performance was evaluated by simulating a demand profile along the power curve of the FC at each second. To ensure that the controller traces the path to the maximum power point according to the load, a function was implemented to reset ($Rst_{MPPT}$) the Maximum Power Point Tracking (MPPT) each time the energy demand changes.

## B.3  Simulation Results

A comparative analysis was conducted to evaluate the performance of two MPPT control techniques (P&O and IC) for an FCBEV. The developed control strategy focused on the FC-DC Boost Converter subsystem to regulate the DC bus voltage at 480 V under a WLTP class 1 driving profile.
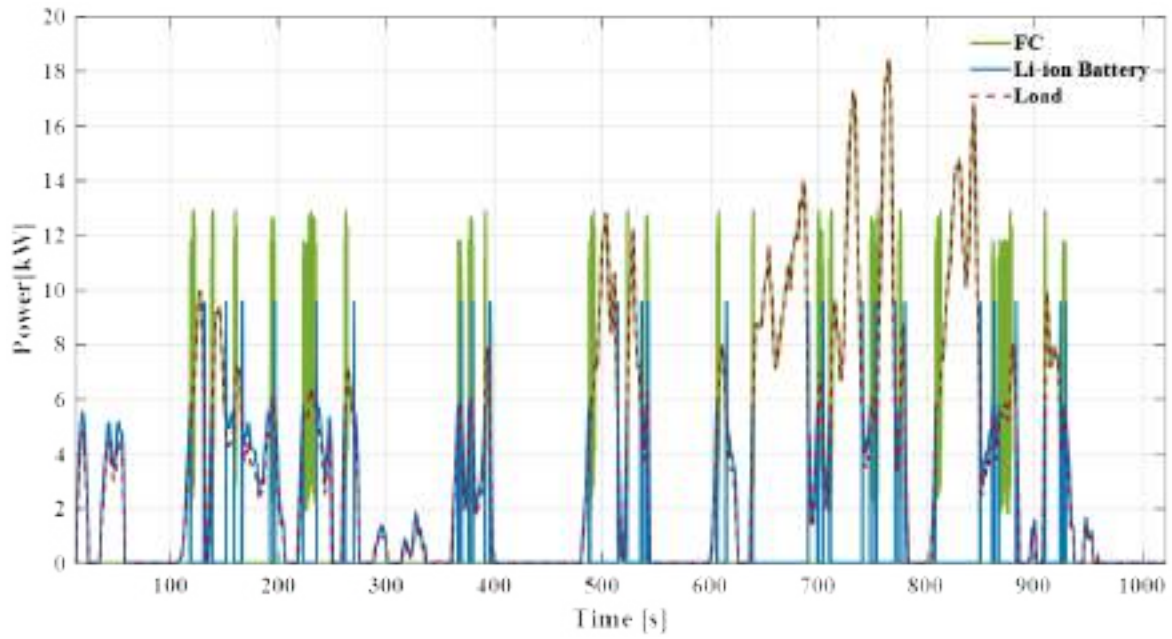
(a) P&O
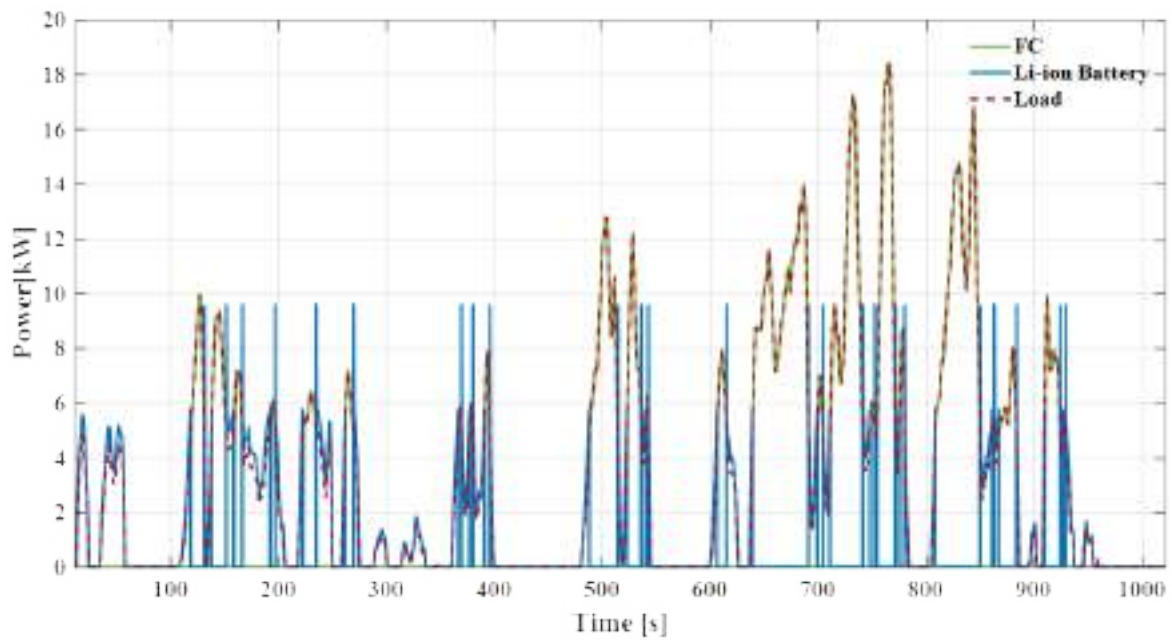


(b) IC

Figure B.9: Battery and Fuel cell system operation following the WLTP class 1 driving profile.

## B.3.1 MPPT controller performance

The simulated power train is dominantly fed by the FC. This means that power demands lower than 5 kW were covered by the battery avoiding the FC operating in the activation zone of the power curve.

In Figure B.9, the battery and the FC operation under the power demand for the P&O and IC controllers are depicted. It is observed that the demand peaks, corresponding to speeds greater than 10 m/s, are covered by the FC, while the battery handles the rest. These results provide an initial insight into the performance of both controllers since the IC method allows the FC to follow the load according to the demand. However, P&0 produces disturbances while trying to satisfy the load.

In Figure B.10a, the voltage and current of the FC and the DC bus are shown throughout the simulation time for the two control methods. Specifically, in the voltage graph, the behavior of the controllers is observed. When the FC is activated, the controllers manage to bring the voltage at the output of the converter to 480 V, whereas when the battery is activated, the voltage settles at 516 V, which is within a 10% tolerance. This is because only a PI controller was used for the battery subsystem.

Despite both controllers reaching the reference voltage value, when the FC is activated, P&O exhibits sharp oscillations reaching up to 600 V before stabilizing, whereas IC, with each power change, presents a downward peak (440V) followed by stabilization. In the seconds 220, 500, and 860, it is possible to observe that due to the oscillations generated by the P&O algorithm, it takes longer to reach the set point.

In Figure B.11a, a zoom-in at 260 seconds is shown, where it can be observed in detail that while IC stabilizes the voltage in 0.01 seconds while P&O takes 2.5 seconds to stabilize. This is likely due to the nature of the algorithm. Although P&O keeps the system perturbed to bring it to the maximum power point, when there is a sudden change in demand, it must
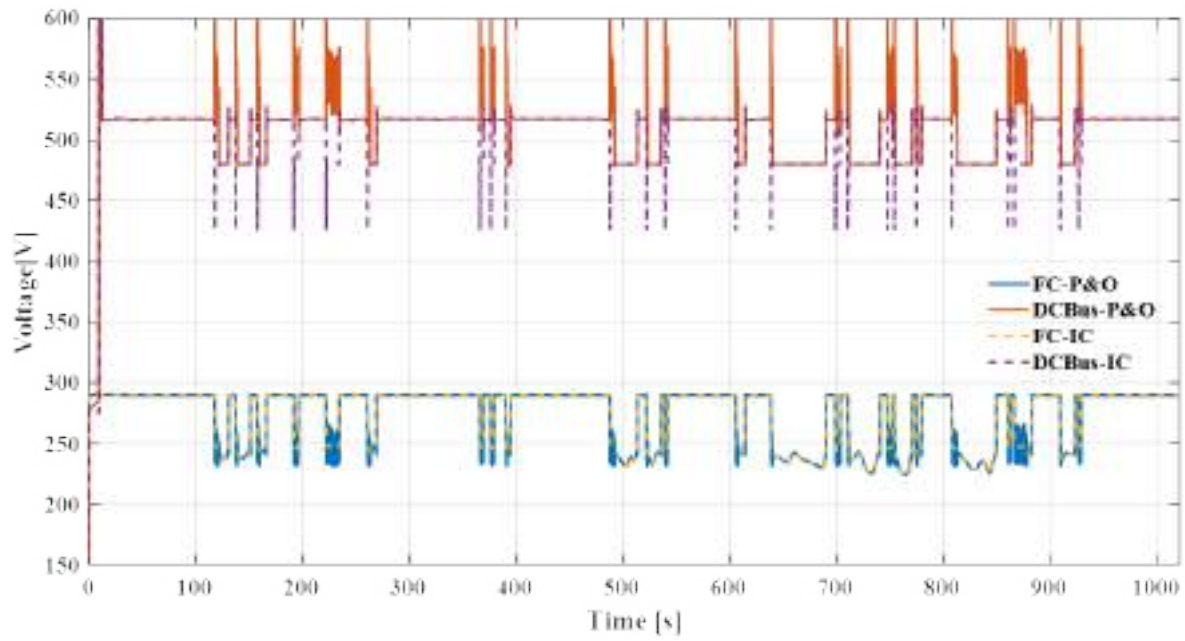
(a)
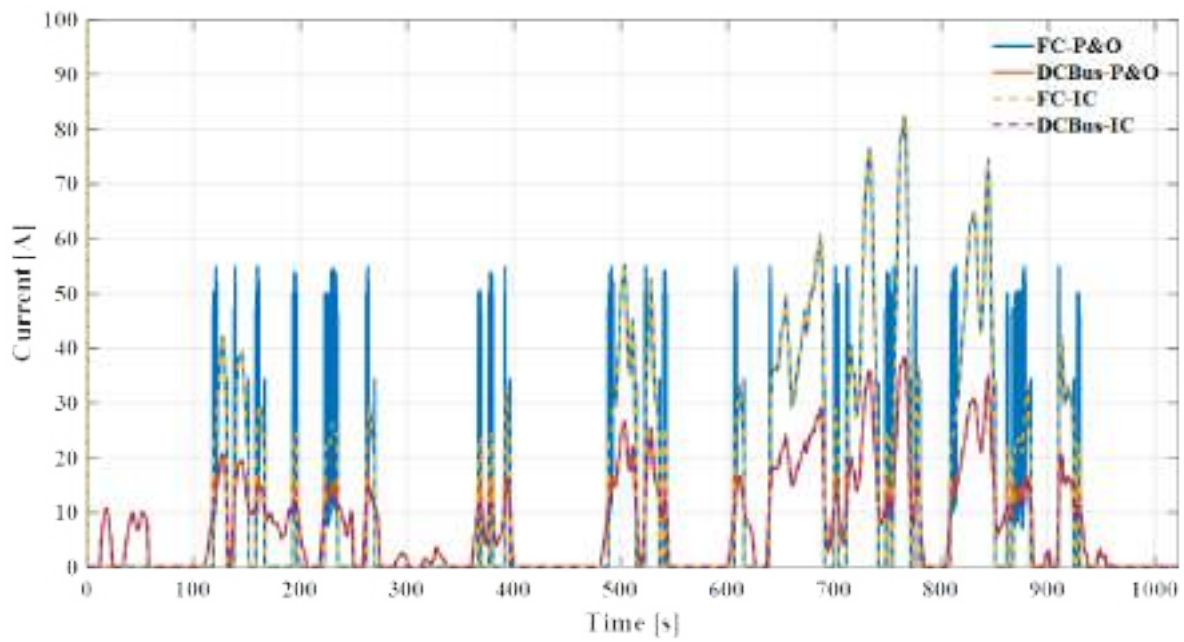


(b)

Figure B.10: Electric performance of the Fuel Cell and DC-Bus (480V)

locate the new operating point. This process of searching and perturbation causes the signal to bounce as shown in Figure B.11b. Therefore, it can be stated that P&O, despite being a very practical algorithm, is not able to follow the energy demand dynamics established by a driving profile, while IC shows better performance.
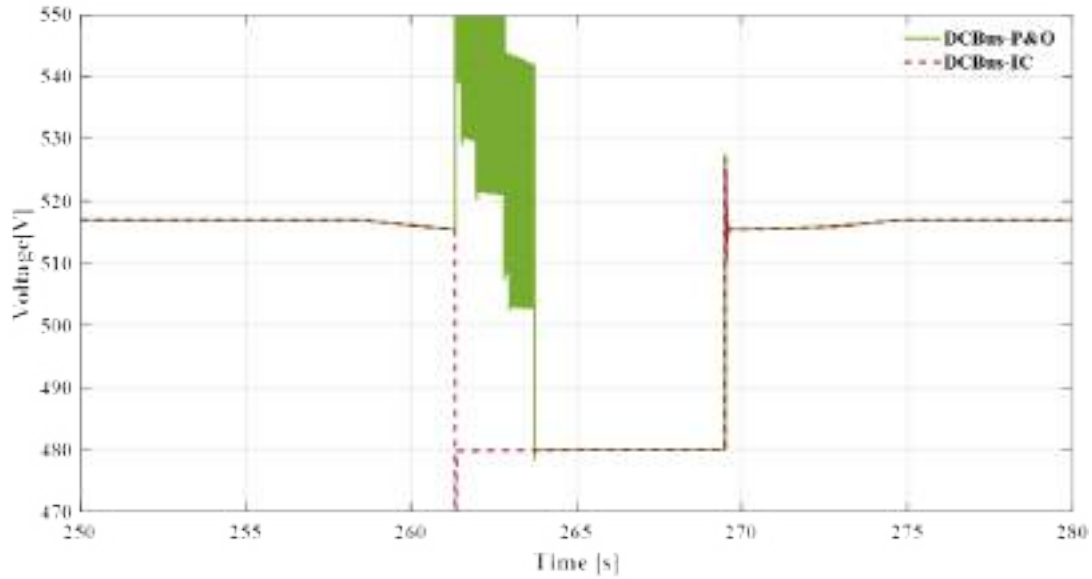


(a) Comparison of stabilization at 480V (zoom in)
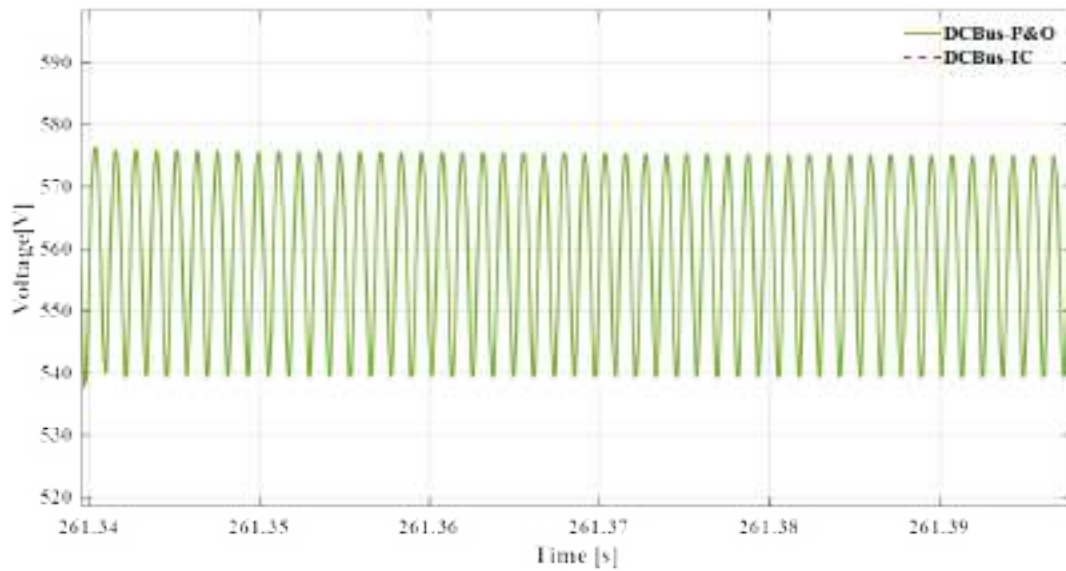


(b) P&O signal jitter during stabilization (zoom in)

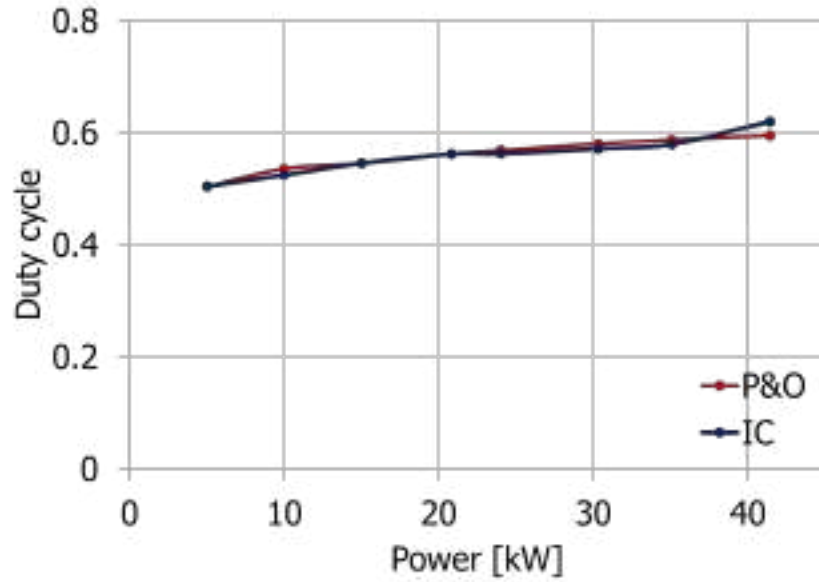Figure B.11: FC MPPT P&O and IC controllers behavior

Figure B.12: DC-Boost Converter designed (Duty Cycle behavior.)

## B.3.2    Fuel Cell Efficiency

The FC efficiency was calculated according to Equation B.3 for the entire simulation time. Based on the measured hydrogen flow, the FC efficiency was 58% for IC and 53.2% for P&O. These results could be an indirect explanation that IC can control the FC very well even when it is operating close to the activation zone (cell start-up, see Figure B.5), which is not the case with P&O. The disturbances shown on the current and voltage of the FC in Figures B.10 and B.10a correspond to values close to this zone. These drastic increases in current imply higher hydrogen consumption and therefore lower efficiency.

## B.3.3    Converter behaviour

Additionally, in Figure B.12, the behavior of the converter designed for the 45 kW FC is shown. This converter was evaluated across the entire power range of the FC. It was found that for both controllers, the duty cycle exhibits a linear behavior. Despite sudden changes in the demanded power, the duty cycle remained between 0.5 and 0.62, indicating proper operation under the evaluated driving profile.

# B.4  Conclusion

From the results presented in the earlier sections, we saw that using MPPT algorithms for controlling the FC converter, we can control the DC bus voltage as well as effectively meet the power demand. It was seen that the P&O MPPT algorithm has a higher steady state error and more oscillations in the system. These results show that the MPPT algorithms can be applied to FC for EV applications. The results presented here will be then integrated with an BESS and DC Motor completing the Power train for the EV. Also teh EMS for the overall control can be looked at in the paper.

# Bibliography

[1] D. F. Pereira, F. D. C. Lopes, and E. H. Watanabe, "Nonlinear Model Predictive Control for the Energy Management of Fuel Cell Hybrid Electric Vehicles in Real Time," IEEE Transactions on Industrial Electronics, vol. 68, no. 4, pp. 3213–3223, Apr. 2021, doi: 10.1109/TIE.2020.2979528.

[2] H. Lee and S. W. Cha, "Energy Management Strategy of Fuel Cell Electric Vehicles Using Model-Based Reinforcement Learning with Data-Driven Model Update," IEEE Access, vol. 9, pp. 59244–59254, 2021, doi: 10.1109/ACCESS.2021.3072903.

[3] A. Ferrara and C. Hametner, "Impact of Energy Management Strategies on Hydrogen Consumption and Start-Up/Shut-Down Cycles in Fuel Cell-Ultracapacitor-Battery Vehicles," IEEE Trans Veh Technol, vol. 71, no. 6, pp. 5692–5703, Jun. 2022, doi: 10.1109/TVT.2021.3127582.

[4] S. George and T. Rajeev, "Fuzzy Based Hybrid Control Topology for Fuel Cell and Battery Powered EV," 2022 IEEE 2nd International Conference on Sustainable Energy and Future Electric Transportation, SeFeT 2022, 2022, doi: 10.1109/SE-FET55524.2022.9909199.

[5] M. Pathmanathan, S. Semsar, C. Viana, and P. W. Lehn, "Power Sharing Control Algorithm for Direct Integration of Fuel Cells in a Dual-Inverter Electric Vehicle Drivetrain," IEEE Transactions on Transportation Electrification, vol. 8, no. 2, pp. 2490–2500, Jun. 2022, doi: 10.1109/TTE.2022.3143092.

[6] M. Moghadari, M. Kandidayeni, L. Boulon, and H. Chaoui, "Operating Cost Comparison of a Single-Stack and a Multi-Stack Hybrid Fuel Cell Vehicle Through an Online

Hierarchical Strategy," IEEE Trans Veh Technol, vol. 72, no. 1, pp. 267–279, Jan. 2023, doi: 10.1109/TVT.2022.3205879.

[7] A. Haxhiu, A. Abdelhakim, S. Kanerva, and J. Bogen, "Electric Power Integration Schemes of the Hybrid Fuel Cells and Batteries-Fed Marine Vessels - An Overview," IEEE Transactions on Transportation Electrification, vol. 8, no. 2, pp. 1885–1905, Jun. 2022, doi: 10.1109/TTE.2021.3126100.

[8] A. Meshginqalam and J. Bauman, "Integrated Convex Speed Planning and Energy Management for Autonomous Fuel Cell Hybrid Electric Vehicles," IEEE Transactions on Transportation Electrification, vol. 9, no. 1, pp. 1072–1086, Mar. 2023, doi: 10.1109/TTE.2022.3200013.

[9] S. K. Das and J. Kim, "Evaluation of Power Sharing Mechanism of a PEM Fuel Cell-Battery Powered Electric Vehicle," 2023 4th International Conference on Clean and Green Energy Engineering, CGEE 2023, pp. 112–118, 2023, doi: 10.1109/CGEE59468.2023.10351891.

[10] S. George, N. Sehgal, K. P. S. Rana, and V. Kumar, "A comprehensive review on modelling and maximum power point tracking of PEMFC," Cleaner Energy Systems, vol. 3, p. 100031, Dec. 2022, doi: 10.1016/J.CLES.2022.100031.

[11] F. Segura, F. J. Vivas, J. M. Andújar, and M. Martínez, "Hydrogen-powered refrigeration system for environmentally friendly transport and delivery in the food supply chain," Appl Energy, vol. 338, p. 120945, May 2023, doi: 10.1016/J.APENERGY.2023.120945.

[12] T. Hai, A. K. Alazzawi, J. Zhou, and H. Farajian, "Performance improvement of PEM fuel cell power system using fuzzy logic controller-based MPPT technique to extract the maximum power under various conditions," Int J Hydrogen Energy, vol. 48, no. 11, pp. 4430–4445, Feb. 2023, doi: 10.1016/J.IJHYDENE.2022.10.103.

[13] M. Derbeli, O. Barambones, M. Y. Silaa, and C. Napole, "Real-Time Implementation of a New MPPT Control Method for a DC-DC Boost Converter Used in a PEM Fuel

Cell Power System," Actuators 2020, Vol. 9, Page 105, vol. 9, no. 4, p. 105, Oct. 2020, doi: 10.3390/ACT9040105.

[14] H. Rezk and A. Fathy, "Performance Improvement of PEM Fuel Cell Using Variable Step-Size Incremental Resistance MPPT Technique," Sustainability 2020, Vol. 12, Page 5601, vol. 12, no. 14, p. 5601, Jul. 2020, doi: 10.3390/SU12145601.

[15] "Fuel Cell Engines - Nuvera." Accessed: Dec. 17, 2023. [Online]. Available: https://www.nuvera.com/solutions/fuel-cell-engines/